

Integrating Sustainability into High Performance Polyurethanes and Engineering

Polymers

by

Jose Ignacio Sintas

A Dissertation Presented in Partial Fulfillment
of the Requirements for the Degree
Doctor of Philosophy

Approved March 2024 by the
Graduate Supervisory Committee:

Timothy E. Long, Chair
Caitlin S. Sample
Kailong Jin

ARIZONA STATE UNIVERSITY

May 2024

ABSTRACT

Engineering polymers are critical for contemporary high-performance applications where toughness, thermal stability, and density are at a premium. These materials often demand high-energy processing conditions or highly reactive monomers that hold negative impacts on human and environmental health. Thus, this work serves to remediate the negative impacts of engineering polymer synthesis by addressing toxicity and processing at the monomer level, while maintaining or exceeding previous thermomechanical and stimuli-responsive performance. Polyurethanes (PUs) represent a class of engineering polymers that possess highly modular properties due to the diverse monomer selection available for their synthesis. The efficient reaction between isocyanates and hydroxyls impart stellar properties and flexible processing modalities, however recent scrutiny regarding the toxicity of the isocyanate precursors has driven the search for non-isocyanate polyurethane (NIPU) pathways. The advancement of bis-carbonylimidazolidone (BCI) monomers for the synthesis of NIPU thermoplastics and foams is thoroughly investigated in this work. Remarkably, a novel decarboxylation pathway for BCI monomers controlled by catalyst loading enabled in-situ CO₂ generation during crosslinking with trifunctional amines, and resulted in a facile synthetic route for NIPU foams. Further explorations into catalyst considerations revealed Dabco[®] 33-LV as a suitable mechanism for controlling reaction times and careful selection of surfactant concentration provided control over pore size and geometry. This led to a library of flexible and rigid NIPU foams that displayed a wide range of thermomechanical properties. Furthermore, sequestration of the imidazole byproduct through an efficient Michael reaction identified maleimide and acrylate additives as a viable pathway to eliminate post-processing steps resulting in NIPU foam

synthesis that is amenable to current industrial standards. This route held advantages over the isocyanate route, as condensate removal drove molecular weight increase and ultimately achieved the first reported phase separation behavior of a NIPU thermoplastic containing a poly(ethylene glycol) soft segment. Furthermore, sustainable considerations for engineering polymers were explored with the introduction of a novel cyclobutane bisimide monomer that readily installs into various polymeric systems. Direct installation of this monomer, CBDA-AP-I, into a polysulfone backbone enabled controlled photo-cleavage, while further hydroxy ethyl functionalization allowed for incorporation into PU systems for photo-cleavable high-performance adhesive applications.

DEDICATION

This work is dedicated to my parents, Maria Graciela Barolli and Jose Antonio Sintas, for giving me the opportunity to pursue my passions and for their unconditional, unwavering support.

ACKNOWLEDGMENTS

I would like to gratefully acknowledge my parents Maria and Jose for their guidance throughout my personal and professional development. Thank you both for being the foundation I built my life upon. You both immersed me in science from my conception, spurring my interest and comfort within the field. I would also like to thank my little brother and sister, Adrian and Andrea Sintas, for pushing me to be a big brother you can both look up to. I also acknowledge my undergraduate inorganic chemistry professor, Joseph Templeton. Your insane class forced me to visit your office hours, where we grew close and you pushed me to pursue undergraduate research with Gerald Meyer. I am eternally grateful to Gerald for accepting me into his lab, where his passion for raising undergraduate students immersed me in an environment that greatly contributed to my scientific development. Alongside Gerald, I must acknowledge my two undergraduate mentors, Andrew Maurer and Eric Piechota. They devoted countless hours of their time in an effort to teach me how to think like a scientist, how to analyze scientific papers, and how to be skeptical and inquisitive when needed. All while putting up with my nonsense. I also thank my committee members, Caitlin Sample and Kailong Jin for guiding me throughout my graduate journey with compassion. I must also offer my sincerest thanks to Timothy Long, who accepted me into his research group where I not only learned polymer chemistry, but also furthered my professional development. Aside from my education, he showed me compassion in times of trial and pushed me past limits I thought were unbreakable (although that was not always fun). At the beginning of my graduate journey, he told me “these are going to be the best years of your life”, which, understandably, I did not believe. However, through his research group and those surrounding it, I can no longer argue that

statement. My mentors Josh Wolfgang and Emily Wilts remain good friends of mine, and I thank them for being role models during my early years in the lab; Josh taught me to clean my hood and Emily taught me how to conduct pointed research. I would also like to thank all the friends I made during my years in Arizona, especially Rose Snyder for keeping me sane during trying times, my lab mates Boer Liu and Jared Nettles for all the fun times we shared together, the ASU gym for being my temple, Charlotte Barker (and Austin) for being very dependable neighbors, Kyle Williamson for being my best friend throughout my life, Ben Clary for his emotional support, and the rest of the Long research group for creating a positive atmosphere for my Ph.D. journey. I must also acknowledge the immense support I received from my undergraduate contemporaries, especially Jake Evans, who I look up to as a chemist and friend. He is a model researcher and I learned a lot from him (we also directed our graduate school complaints to each other). Lastly, I would like to state how lucky I am to have met and lived with Cody Weyhrich, James Brown, and Ren Bean. Our years of shared hardships made us brothers who supported and challenged each other, resulting in remarkable personal and professional growth shrouded in, perhaps too many, good memories.

TABLE OF CONTENTS

	Page
LIST OF TABLES	xiii
LIST OF FIGURES	xiv
CHAPTER	
1 INTRODUCTION TO MONOMER DESIGN AND STRUCTURE- PROPERTY RELATIONSHIPS FOR ENGINEERING POLYMERS	1
1.1 Engineering Polymers	1
1.2 General Structure-Property Relationships	1
1.3 Polyurethanes.....	1
1.4 Polyimides and Maleimides	1
1.5 References.....	1
2 REVIEW OF POLYURETHANES FOR BIOMEDICAL APPLICATIONS: A STRUCTURE-PROPERTY ANALYSIS OF IN-VIVO DEGRADATION AND FAILURE	9
2.1 Abstract.....	9
2.2 Introduction.....	9
2.3 Synthesis and Compositions of Polyurethanes	11
2.4 Oxidation and Chain Scission Events	14
2.5 Bacterial Biofilm Formation	19
2.6 Encrustation	23
2.7 Hydrolytic and Enzymatic Degradation of PUs	25
2.8 Conclusions and Outlook.....	28

CHAPTER	Page
2.9 References.....	30
3 CARBAMATE THERMAL DECARBOXYLATION FOR THE DESIGN OF NON-ISOCYANATE POLYURETHANE FOAMS	42
3.1 Abstract.....	42
3.2 Introduction.....	43
3.3 Experimental/Methods	47
3.3.1 Instruments	47
3.3.2 Materials	48
3.3.3 Synthesis of 1,4-butyl(bis-carbonylimidazolide) (BBCI), 1b, and 1,4- cyclohexanedimethyl(bis-carbonylimidazolide) (CHDMBCI), 1a.....	48
3.3.4 Synthesis of 4,4'-diphenylmethane(bis-carbonylimidazolide) (BCIF)	49
3.3.5 Synthesis of Polyurethane Foams	50
3.4 Results and Discussion.....	51
3.5 Conclusions.....	63
3.6 Acknowledgements	63

CHAPTER	Page
3.7 Funding	64
3.8 References.....	64
3.9 Supporting Information	66
4 NON-ISOCYANATE POLYURETHANE SEGMENTED COPOLYMERS	
FROM BIS-CARBONYLIMIDAZOLIDES	74
4.1 Abstract.....	74
4.2 Introduction.....	75
4.3 Experimental Section	77
4.3.1 Instruments	77
4.3.2 SAXS/WAXS Measurements	78
4.3.3 Materials	79
4.3.4 Synthesis of 1,4-Butyl(bis-carbonylimidazolide) (BBCI)	80
4.3.5 Synthesis of Phase Separated NIPUS	81
4.4 Results and Discussion.....	81
4.5 Conclusions.....	90
4.6 Acknowledgements	91
4.7 Funding	91
4.8 References.....	91
4.9 Supporting Information	98
5 DIVALENT IMIDAZOLIUM IONIC LIQUIDS FROM BIS-	
CARBONYLIMIDAZOLIDE MONOMERS	105
5.1 Abstract.....	105

CHAPTER	Page
5.2 Introduction.....	105
5.3 Materials	107
5.4 Synthesis of BBCI	108
5.5 Synthesis of BBCI IL	108
5.6 Synthesis of Imidazolium Ionenenes	109
5.7 Analytical Methods	109
5.8 Results and Discussion.....	110
5.9 Conclusions.....	121
5.10 Acknowledgements	121
5.11 Funding	121
5.12 References.....	122
5.13 Supporting Information	126
6 MICHAEL ACCEPTORS AS REACTIVE FILLERS IN BIS- CARBONYLIMIDAZOLIDE-DERIVED NON-ISOCYANATE POLYURETHANE FOAMS	129
6.1 Abstract.....	129
6.2 Introduction.....	130
6.3 Experimental and Methods	133
6.3.1 Instruments	133
6.3.2 Materials	134

CHAPTER	Page
6.3.3 Synthesis of 1,4-Butyl(bis-carbonylimidazolide) (BBCI) and 4,8-Bis(hydroxymethyl)tricyclo[5.2.1.0 ^{2,6}]decane(bis-carbonylimidazolide) (TCDBCI)	135
6.3.4 Synthesis of Non-Isocyanate Polyurethane Foams	135
6.3.5 Synthesis of Foams Containing Michael Acceptor Additives	136
6.4 Results and Discussion	137
6.5 Conclusions	146
6.6 Acknowledgements	147
6.7 Funding	147
6.8 References	148
7 A NOVEL CYCLOBUTANE BISIMIDE MONOMER FOR PHOTO-CLEAVABLE POLYURETHANE SYNTHESIS	154
7.1 Abstract	154
7.2 Introduction	154
7.3 Materials and Methods	157
7.3.1 Materials	157
7.3.2 Instruments	157
7.3.3 Chemical and Thermal Synthesis of CBDA-AP-I	158
7.3.4 Synthesis of CBDA-AP-I-HE	159
7.3.5 Synthesis of CBDA-AP-I-HE PU	159
7.4 Results and Discussion	160

CHAPTER	Page
7.5 Conclusions.....	167
7.6 Acknowledgements	168
7.7 Funding	168
7.8 References.....	168
7.9 Supporting Information	173
8 PHOTO-RESPONSIVE CYCLOBUTANE BISIMIDE-CONTAINING POLYSULFONES CAPABLE OF LIGHT-MEDIATED DEPOLYMERIZATION.....	176
8.1 Introduction.....	176
8.2 Materials and Methods	178
8.2.1 Materials	178
8.2.2 Instruments	179
8.2.3 Synthesis of CBDA-AP-I.....	180
8.2.4 Synthesis of Phenol-Terminated PSU 1, 2, and 3	180
8.3 Results and Discussion.....	181
8.4 Conclusions.....	190
8.5 Acknowledgements	191
8.6 Funding	191
8.7 References.....	191
8.8 Supporting Information	8
9 FUTURE WORK	197

CHAPTER	Page
9.1 Injection Molding of Non-Isocyanate Polyurethane Structural Foam Composites	197
9.2 Enhanced Phase Separation of Non-Isocyanate Polyurethane Thermoplastic Elastomers.....	202
9.3 High-Performance Cyclobutane Bisimide-Containing Polyesters.....	206
9.4 Coumarin-Containing Photo-Reversible Polymeric Systems	207
9.5 References.....	209
10 SUMMARY AND CONCLUSIONS.....	213
REFERENCES	219
APPENDIX	
A PUBLISHED PORTIONS	246
B PERMISSIONS	248

LIST OF TABLES

Table	Page
2.1 Polyurethane Soft Segment Compositions	14
3.1 Thermomechanical Properties of BCI Foams	57
S4.1 Tabulated Raw SAXS Data	103
5.1 VFT Parameters for BBCI IL	115
5.2 Thermal Properties of BBCI Ionenex	119
8.1 SEC Analysis of PSU 1, 2, and 3 after Irradiation	189

LIST OF FIGURES

Figure	Page
2.1 Synthetic Scheme for the Synthesis of Polyurethanes	13
2.2 Production of Reactive Oxygen Species	16
2.3 Mechanism for Radical Chain Scission of Polyethers	17
2.4 Graphical Depiction of Biofilm Formation	20
2.5 Ureteral Stent Encrustation	24
3.1 Polymerization of BCI Monomers	52
3.2 Decarboxylation Mechanism for BCI Monomers	53
3.3 CO ₂ Generation Profiles for BCI Monomers	53
3.4 Catalyst Effects on NIPU Foam Curing	55
3.5 TGA Confirms Imidazole Removal	56
3.6 BCI Monomers Control NIPU Foam T _g	59
3.7 SEM of Closed Cell BCCI-T-403 Foam	60
3.8 Surfactant Controls Cell Architecture	61
3.9 BCCI-TADE Foam Displays Closed Cell Architecture	62
S3.1 ¹ H NMR of BCCI	67
S3.2 ¹ H NMR of CHDMBCI	68
S3.3 CO ₂ Generation During BCI Foam Curing	69
S3.4 Synthesis of BCI Monomers	69
S3.5 ATR-FTIR Confirms NIPU Structure	69
S3.6 TGA Shows Imidazole Removal	70
S3.7 TMA Ramp of BCI Foams Elucidates CTE	71

Figure	Page
S3.8 DSC of BCI Foams	71
S3.9 T-403 Incorporation effects on T_g	72
S3.10 DSC of BBCI-T-403 Foams	72
S3.11 SEM of Open-Cell T-403 Foams	73
S3.12 SEM of Closed-Cell Foam	73
4.1 Synthesis of NIPU Segmented Copolymers	82
4.2 DMA of Synthesized NIPUs	85
4.3 DSC of Synthesized NIPUs	86
4.4 FTIR of Hydrogen-Bonded and Free Carbonyls	87
4.5 SAXS of all NIPUs	89
4.6 AFM of 60 wt. % HS NIPU	90
S4.1 ATR-FTIR Confirms NIPU Structure	98
S4.2 Water Uptake of all NIPUs	99
S4.3 AFM of 40 and 80 wt. % HS NIPUs	99
S4.4 $\tan \delta$ of all NIPU Samples	100
S4.5 WAXS Regime of all NIPU Samples	100
S4.6 2D Scattering of 40 wt. % HS Sample	101
S4.7 2D Scattering of 60 wt. % HS Sample	101
S4.8 2D Scattering of 80 wt. % HS Sample	101
S4.9 Lorentzian Peak Fitting for SAXS Regime	102
5.1 Synthetic Scheme for BBCI IL	110
5.2 In-Situ FTIR Confirms BBCI IL Synthesis	110

Figure	Page
5.3 Weight Loss Profiles for BBCI and BBCI IL	112
5.4 In-Situ FTIR Reveals Decreased Reactivity of BBCI IL	114
5.5 Temperature Dependence of Ionic Conductivity	114
5.6 Static Permativity Data for BBCI IL	116
5.7 Synthesis of BBCI Ionenenes	117
5.8 DSC of BBCI Ionenenes	118
S5.1 ¹³ C NMR of BBCI IL	125
S5.2 MO Diagram for BBCI IL	125
S5.3 TGA-SA Reveals Water Uptake of BBCI IL	126
S5.4 ¹ H NMR of BBCI IL	126
S5.5 DSC of BBCI IL	127
S5.6 CO ₂ Production of BBCI IL	127
6.1 General Scheme for the Synthesis of BCI NIPUs	131
6.2 Synthesis of TCDBCI	137
6.3 Summary of TCDBCI NIPU Foam Thermal Properties	139
6.4 Reaction Scheme for Imidazole Addition to Michael Acceptor	140
6.5 In-Situ FTIR of Imidazole Addition onto BDDA	141
6.6 BCI Foam containing BDDA Additive	142
6.7 TGA Highlights Imidazole Sequestration	143
6.8 Sequestration of Imidazole in Structural Foams	145
7.1 Synthesis of CBDA-AP-I	159
7.2 Synthesis of CBDA-AP-I-HE	159

Figure	Page
7.3 Synthesis of CBDA-AP-I-HE PU	159
7.4 Rheology of CBDA-AP-I-HE PU	159
7.5 DMA of CBDA-AP-I-HE PU after Irradiation	159
7.6 Tensile of CBDA-AP-I-HE PU after Irradiation	159
7.7 ¹ H NMR of Irradiated CBDA-AP-I-HE PU	159
S7.1 ¹ H NMR of CBDA-AP-I.....	172
S7.2 ¹ H NMR of CBDA-AP-I-HE	172
S7.3 ¹ H NMR of CBDA-AP	173
S7.4 ATR-FTIR of CBDA-AP Imidization	173
S7.5 Step-Wise Isothermal TGA of CBDA-AP	174
8.1 Synthesis of PSU 1, 2, and 3	181
8.2 PSU End Group Analysis by ¹ H NMR	182
8.3 FTIR of PSU 1, 2, and 3	183
8.4 TGA of PSU 1, 2, and 3	185
8.5 DSC Analysis of PSU 1, 2, and 3	186
8.6 DMA Analysis of PSU 1, 2, and 3	188
S8.1 ¹ H NMR of CBDA-AP-I	195
9.1 Synthesis of Rigid BCI Monomers	197
9.2 Synthesis of TCDBCI-TADE Rigid NIPU Foam	198
9.3 Molded Structural NIPU Foam	199
9.4 Microscopy of Molded NIPU Foams	200
9.5 Synthesis and ¹ H NMR of CBBCI	202

Figure	Page
9.6 Decarboxylation Profile of CBBCI	203
9.7 Proposed Synthesis of PDMS-CBBCI NIPU	204
9.8 Synthesis of CBDA-AP-I-HE	205
9.9 Synthesis of Photo-Cleavable Polyester	206
9.10 Proposed Synthesis of 7-Hydroxy Coumarin Monomer	207
9.11 Proposed Synthetic Pathway for Hydroxyethyl Functionalized Coumarin	208

CHAPTER 1

INTRODUCTION TO MONOMER DESIGN AND STRUCTURE-PROPERTY RELATIONSHIPS FOR ENGINEERING POLYMERS

1.1 Engineering Polymers

Innovations in the early 20th century produced a new class of synthetic material that, unknowingly, changed the scope of material science in unprecedented ways. The manifestation of polymer chemistry by Hermann Staudinger nucleated interest in lightweight, tunable, and cheap materials, that by the 1950's, would achieve global demand.¹ Polymers undergo careful evaluation over what properties they offer for any given application, the most important of which is cost. Thus, the prevalence of polymers derived from abundant petroleum sources that polymerize readily gave rise to “commodity polymers”.² These macromolecules, which are capable of facile control over color, texture, shape, and longevity revolutionized society, allowing for a higher quality of life for a growing population. Cheap alternatives to wooden or metal material choices and unique properties resulted in the production and consumption of commodity plastics on a global scale, namely poly(ethylene terephthalate) (PET) water bottles, poly(ethylene) (PE) and poly(propylene) (PP) packaging, and poly(vinyl chloride) (PVC) building materials. However, the human thirst for innovation demanded soft materials with outstanding properties unachievable by commodity plastics. Innovations in the energy, aerospace, and infrastructure industries rely on lightweight polymers with carefully programmed macroscopic properties. Insufficient glass transition temperatures (T_g s), inadequate mechanical or adhesion properties, or insufficient biological tolerances disqualifies commodity polymers from use in higher value applications. Polymers that possess higher

value properties often require control over chemical composition that target specific applications and are referred to as “engineering polymers”.

Engineering polymers require more expensive monomers for production and additional processing considerations compared to commodity polymers, resulting in increased cost. Likewise, engineering polymers are often heavily formulated for their application. One such example is polyurethanes (PUs), a class of polymers produced at a large scale with a wide scope of applications.³ They maintain large temperature windows of consistent thermomechanical performance due to their phase separated nature, useful for construction or structural uses. Other engineering polymers include poly(amide)s for their toughness and wear resistance, poly(carbonate)s for their optical clarity and impact resistance, or certain poly(ester)s for their chemical resistance. Due to this diverse range of thermomechanical properties, engineering polymers find prolific use in automotive, aerospace, electronics, construction, and biomedical industries. Most notably, however, is the constant improvement engineering polymers undergo. A lack of economic incentives and high demand for existing commodity plastics limits their rate of innovation; why improve a cheap plastic if it sells well? Engineering polymers exist at the forefront of next-generation technologies that require highly tailored properties for advancing to market. Due to this and higher per-pound revenue, engineering polymers benefit from constant research and innovation, and is thus a major focus throughout this dissertation.

1.2 General Structure-Property Relationships

It is important to note that the chemical structure of compositional monomers drive the macroscale properties polymers achieve. Inevitably molecular weight, molecular weight distribution, topology, and processing further dictate thermomechanical behavior, however

the chemical structure of the monomer remains the largest contributor. Simple Van der Waals forces, permanent dipole interactions, pi-stacking, hydrogen bonding, and steric repulsion interactions that occur between small molecules multiply tens to thousands of times in polymers to create unique macroscale properties dependent on the specific chemical composition. Understanding of these interactions in small molecules allows for informed monomer decisions when targeting specific properties and is a common theme throughout all chapters in this document. For example, hydrogen bonding is a relatively strong intermolecular force, with bond energies ranging from 1-40 kcal mol⁻¹ in polymeric materials.⁴ On the small molecule scale, this interaction enables compounds with low molecular weight, such as water, to exist as a liquid at room temperature. When replicated over hundreds of repeating units, hydrogen bonding now enables increased rigidity and modulus at elevated temperatures, higher T_gs, and increased toughness.⁵ Drawing comparisons between polyesters and nylons furthers this point. Two chemically equivalent backbones, differing only in the hydrogen bonding amide nitrogen yield two different sets of thermomechanical properties.

High degrees of polymerization enable this phenomenon of additive intermolecular interactions. Additionally, intramolecular attributes including bond distance and conformational freedom also affect polymer properties. Poly(dimethylsiloxane) exemplifies this as the long Si-O bond allows for increased conformational freedom leading to an incredibly low T_g (-125 °C). Polyimides comprise the other end of this spectrum, where the cyclic nature of the repeating unit heavily prohibits long range movement leading to T_gs in excess of 400 °C. The understanding of polymer structure property relationships is invaluable during monomer design, both synthetically and

analytically. Common industrial requirements pertain to continuous use temperature, modulus/adhesive values, T_g , dielectric properties, toughness, or any number of specialty criterion. Outlining a comprehensive list of common structure-property interactions is beyond the scope of this work, however general principles remain constant. T_g , characterized by long-range segmental backbone movement, is often controlled through the steric considerations of the comprising monomer. For example, a linear backbone will likely have a lower T_g than a backbone of similar chemical structure containing cyclic or bulky substituents. Likewise, the introduction of stronger intermolecular forces such as charge transfer or hydrogen bonding will further increase T_g . The impacts of hydrogen bonding on water uptake or charge transfer complexes on dielectric relaxation is also important to consider when designing a polymer for a targeted application. Throughout this dissertation, the concept of structure-property relationships is used to target monomer structures to achieve thermomechanical properties necessary for a selected application.

1.3 Polyurethanes

Polyurethanes (PUs) encompass a highly modular class of engineering polymers, capable of adapting to a broad range of thermomechanical performance parameters. Their incredible versatility and robust synthetic methods encourage their use in many specialty applications where good adhesive strength, toughness, wide thermal operating window, and adaptive processing is required. In 1937, Otto Bayer patented the efficient polyaddition reaction between isocyanates and hydroxyl functionalities, which exothermically form urethane (carbamate) linkages to afford PUs.⁶ This novel polymerization method enabled the production of an ever-expanding library of PU chemical structures that were popularized by the 1960's.⁷ There exists near infinite combinations of various isocyanates

and alcohols all of various molecular weights and chemical structures. Logically, the structure of the chosen isocyanates, polyols, and chain extenders dictate the thermomechanical properties of the resulting PU. The section of the PU backbone comprised of the small molecule alcohol (chain extender) and isocyanate is denoted the hard segment (HS) and imparts mechanical and thermal stability to the resultant PU. Increasing the content of HS in a PU results in a more rigid material, however decreases its adhesion and toughness properties. Dimeric hydrogen bonding between HS units and rigid chemical structures imparts macroscale structural integrity and an ultimate T_g value approaching 100 °C. Conversely, the oligomeric polyol section of the PU is labeled the soft segment (SS). This portion of the PU backbone exists well above the T_g during use, imparting for damping, toughness, and low temperature performance properties. The covalently bound HS provides the SS with the structural integrity needed to prevent material failure during use, but still allows the PU to leverage the useful properties the SS provides.

Monomer functionality and stoichiometry enable control over topology, which is often formulated to control physical properties. This broad description of PU formulation highlights the versatility and potential for this polymer. Notably, this chemistry adapts to multiple synthetic procedures that commonly include one-shot extrusion, two-step chain extension, spray coating, slabstock foams, and molded foams.⁸⁻¹⁰ Controlling the functionality of the isocyanate or polyol used, either a thermoplastic or thermoset PU can be formed. The thermal and creep stability of thermoset PUs allows their use for construction, coating, or foam applications. Conversely, thermoplastic PUs are amenable

to extrusion or injection molding, allowing for facile processing into consumer goods. Both topologies are leveraged in this work to cover a large scope of application spaces.

1.4 Polyimides and Maleimides

Unlike PUs, polyimides and maleimides target high temperature or extreme environments. The addition of an amine functionality to an anhydride, followed by imidization and the liberation of water affords the imide moiety. While the imide functional group boasts exceptional thermal and chemical resistance, the amic acid intermediate displays chemical instability, resulting in a dynamic nature and deconstruction under certain environments. Solvent choice, namely *n*-methyl-2-pyrrolidone, or neutralization of the amic acid with a base effectively increases the stability of amic acids, which is advantageous for processing.¹¹ Namely, conversion to the imide largely prohibits additional thermal processing of poly(imide) (PI) materials due to their possession of a T_g above their degradation temperature.¹² Due to this, PIs commercially present in 2-dimensional form factors such as films and are used for dielectric, shielding, and lining applications. Recent advancements in PI processing technology remedies this to an extent, however.^{13, 14}

The imide linkage in this work, namely chapters 7 and 8, focuses on their ability to photochemically cleave under select UV irradiation wavelengths. The unique electronics of aromatic cyclobutane bisimide linkages allow for formation of two maleimide moieties after irradiation with 254 nm light, a phenomenon that enables a class of thermally stable, photo-processable polymers for semiconductor or encapsulating applications.¹⁵ The resulting maleimide is capable of further reactivity, i.e., radical polymerization or a dimerization back to the cyclobutane bisimide functional group.

1.5 References

1. Staudinger, H., Über Polymerisation. *Berichte der deutschen chemischen Gesellschaft (A and B Series)* **1920**, 53 (6), 1073-1085.
2. Andrady, A. L.; Neal, M. A., Applications and societal benefits of plastics. *Philos Trans R Soc Lond B Biol Sci* **2009**, 364 (1526), 1977-84.
3. Szycher, M., *Szycher's Handbook of Polyurethanes, First Edition*. Taylor & Francis: 1999.
4. Hydrogen Bonding in Polymeric Materials. In *Hydrogen Bonding in Polymeric Materials*, 2018; pp 1-8.
5. Paul C. Painter, M. M. C., *Fundamentals of Polymer Science* Second ed.; CRC Press LLC: 1997.
6. Bayer, O. A Process for the Production of Polyurethanes and Polyureas. 1937.
7. Prisacariu, C., *Polyurethane Elastomers: From Morphology to Mechanical Aspects*. Springer Vienna: 2011.
8. Kaushiva, B. D.; McCartney, S. R.; Rossmly, G. R.; Wilkes, G. L., Surfactant level influences on structure and properties of flexible slabstock polyurethane foams. *Polymer* **2000**, 41 (1), 285-310.
9. Hyun, M. E.; Kim, S. C., A study on the reactive extrusion process of polyurethane. *Polymer Engineering & Science* **1988**, 28 (11), 743-757.
10. Yilgör, I.; Yilgör, E.; Wilkes, G. L., Critical parameters in designing segmented polyurethanes and their effect on morphology and properties: A comprehensive review. *Polymer* **2015**, 58, A1-A36.

11. Stoffel, N. C.; Kramer, E. J.; Volksen, W.; Russell, T. P., Solvent and isomer effects on the imidization of pyromellitic dianhydride-oxydianiline-based poly(amic ethyl ester)s. *Polymer* **1993**, *34* (21), 4524-4530.
12. Hergenrother, P., The Use, design, synthesis, and properties of high performance/high temperature polymers: An overview, high perform. *High Performance Polymers* **2003**, *15*, 3-45.
13. Hegde, M.; Meenakshisundaram, V.; Chartrain, N.; Sekhar, S.; Tafti, D.; Williams, C. B.; Long, T. E., 3D Printing All-Aromatic Polyimides using Mask-Projection Stereolithography: Processing the Nonprocessable. *Advanced Materials* **2017**, *29* (31), 1701240.
14. Arrington, C. B.; Hegde, M.; Meenakshisundaram, V.; Dennis, J. M.; Williams, C. B.; Long, T. E., Supramolecular Salts for Additive Manufacturing of Polyimides. *ACS Applied Materials & Interfaces* **2021**, *13* (40), 48061-48070.
15. June, S. M.; Suga, T.; Heath, W. H.; Long, T. E.; Lin, Q.; Puligadda, R., Photo-Reactive Polyimides and Poly(siloxane imide)s as Reversible Polymeric Interfaces. *The Journal of Adhesion* **2010**, *86* (10), 1012-1028.

CHAPTER 2

REVIEW OF POLYURETHANES FOR BIOMEDICAL APPLICATIONS: A STRUCTURE-PROPERTY ANALYSIS OF IN-VIVO DEGRADATION AND FAILURE

2.1 Abstract

Optimal biocompatibility and tunable mechanical properties render polyurethanes (PUs) a common choice for biomedical device construction. However, the degradation of these materials when exposed to biological conditions compromises performance and leads material failure. Prevalent mechanisms for PU degradation in biologically relevant conditions include hydrolysis, oxidation, enzymatic attack, and bacteria aggregation. As degradation progresses throughout the device, symptoms including inflammation and tissue damage appear, however severe damage occurs once the device reaches complete failure. The body contains diverse environments with varying organisms, pH, and oxidative species concentration that each drive a unique degradation pathway. The extent of PU degradation depends on several factors, including the chemical composition of the PU, the location of the device, and the patient's physiological environment. Hydrolytic and oxidative degradation modes are explored This review discusses the various environments and degradation pathways for PUs in the human body and the complex relationship between PU device chemical structure, device environment, and degradation modalities.

2.2 Introduction

Good mechanical properties, chemical resistance, biocompatibility, and versatility in chemical composition render Polyurethanes (PUs) an ideal polymer for diverse applications. These applications include construction, foams, electrical insulation, tires, footwear, paints, adhesives, and medical devices.¹⁻³ The wide range of uses stems from the diversity in chemical composition of the polymer, leading to tunable structure-property relationships.^{4, 5} Many of the desirable properties PUs possess result from the thermomechanical characteristics of the hard segment (HS) and soft segment (SS). The ratios of HS to SS, selected isocyanate, and molecular weight of each component determine thermomechanical performance.⁵⁻⁷ The characteristic urethane (carbamate) linkage connects SSs with HSs, yielding thermoplastic or elastomeric PUs amenable to melt processing or crosslinked thermosets that are chemical and creep resistant. Low modulus SSs allow for good flexibility, low temperature performance, and tear resistance while high modulus HSs afford good mechanical properties and structural integrity. Soft and hard segment chemistries enable properties tailored to specific applications and subsequently direct the predominant degradation modality. Previous reviews serve to discuss the structure property relationships that inform on PU material choices for additional applications, however this review serves to explore the relationship between chemical structure, physical properties, and degradation vulnerabilities for biomedical use.⁸⁻¹² While PUs undergo different decomposition pathways when exposed to different stimuli including heat, shear, or strain, this review focuses on medical uses of polyurethanes and the degradation pathways that lead to the end of device lifecycle. These degradation pathways include hydrolysis, oxidation, immune attack, and surface fouling. In the biomedical field, PUs comprise ureteral stents, catheters, vascular devices, artificial heart

valves, pacemaker leads, and scaffolds for tissues or bones.¹³⁻¹⁹ The assorted environments inhabited by PUs fulfilling these roles each favor their own degradation pathway. Once implanted, all medical devices begin their contact with the body as they operate, ultimately leading to degradation. The aqueous environment of urine, coupled with a large relative bacteria and mineral presence results in ureteral stents to primarily undergo surface fouling through biofilm formation and encrustation. Pacemaker leads, however, are in constant contact with various metal impurities, facilitating metal ion oxidation (MOI). Heavy contact with blood leads to oxidation events due to reactive oxygen species (ROS) present or degradation facilitated by enzymatic breakdown or macrophage attack. Throughout this review, the different degradation methods are discussed along with explored solutions.

Several polyurethane medical devices decompose by design, acting as temporary tissue scaffolds for embolic wound healing.^{16, 20-23} These PUs are designed to degrade over time as they are replaced by living tissue, however this review defines degradation as any process that results in the discontinued use or non-intended damage of the PU device. Surface fouling, chemical and mechanical testing, and molecular weight analysis evaluate the degradation of the bulk material. Characterized weight loss profiles, size exclusion chromatography (SEC) traces, modulus values, and FTIR spectrums allow for the quantitative characterization of degraded medical devices and elucidates degradation susceptibilities.

2.3 Synthesis and Compositions of Polyurethanes

Polyurethane medical devices require melt processability for large scale manufacturing and flexibility for patient comfort or to achieve their intended use. Because of this, most medical grade polyurethanes are elastomers, denoted polyurethane elastomers. Commercially, the reaction between a diisocyanate (R-NCO) and a polyol yields a polymer linked together by carbamate bonds, commonly referred to as urethane linkages and is shown in **Figure 2.1**.²⁴ Polyurethanes derive their names from this linking moiety. Additionally, chain extenders offer a route towards achieving the PU's final mechanical properties. The polyol is flexible, creating the SS, and the diisocyanate or macro diisocyanate and chain extenders comprise the HS. Ether, ester, aliphatic, polydimethylsiloxane (PDMS), carbonate, or a combination thereof encompass common polyols, displayed in **Table 2.1**.²⁵ The diversity of available SS components gives rise to a host of mechanical properties and various preferred degradation pathways. In fact, most degradation modes initiate in the soft segment of the polyurethane due to a decreased kinetic barrier for access. This indicates that the different chemical properties of these SS polyols determine the primary degradation mode of the final PU. PU HS chemistry is tailored for modulus, elasticity, and toughness. Discussed in this review, these different chemical linkers give the final medical PU resistances to different stresses, however, introduce different weaknesses as well. These changes allow the tuning of different SS backbones for different biomedical applications, i.e., PDMS for increased elasticity or PTMO for increased hydrophilicity.

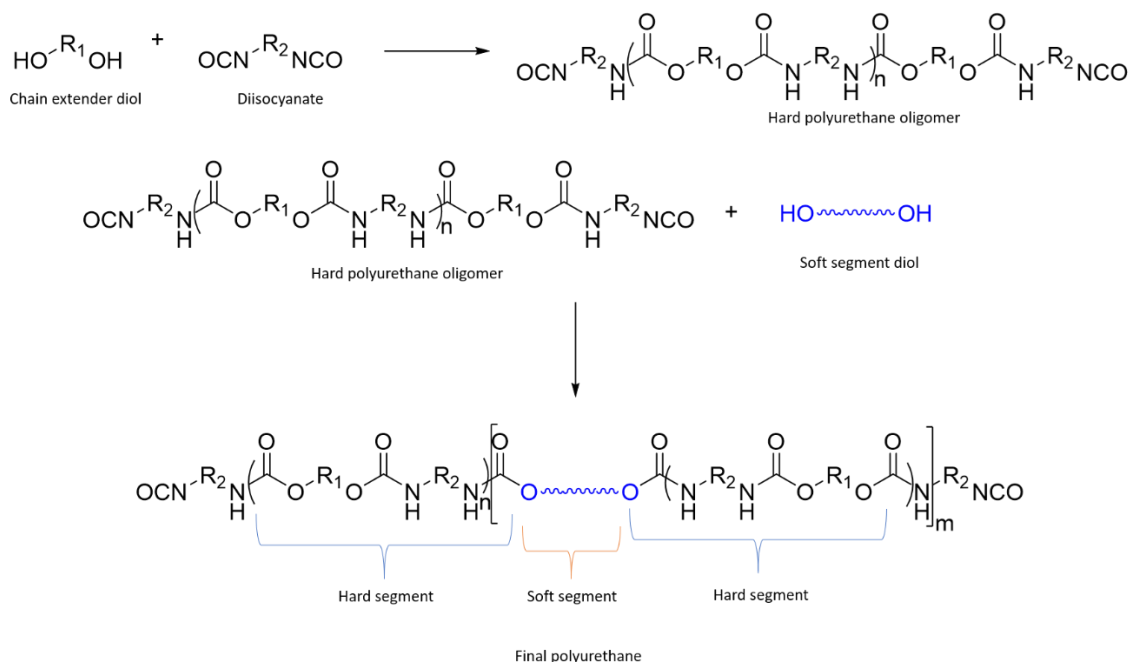


Figure 2.1 Model synthetic scheme of a segmented PU elastomer. Reaction conditions, catalyst selection, and solvent use vary depending on the processing method.

There exists a wide range of diisocyanates available for polyurethane synthesis. The most common of these include methylenebis(phenyl isocyanate) (MDI), toluene diisocyanate (TDI), and hexamethylene diisocyanate (HDI). In the realm of biomedical polymers, MDI is the diisocyanate of choice for most applications.²⁶ This isocyanate imparts good mechanical properties, i.e., toughness, into the final PU while limiting crystallinity in the hard segment. Preventing the crystallization of the hard segment is beneficial, as maintaining high toughness values prevents PU tearing in-vivo. Likewise, the symmetry and bulkiness of MDI compared to TDI allows for better phase separation in the final PU, resulting in superior elastomeric properties.²⁷ This aromatic isocyanate,

however, increases susceptibility to oxidation events, requiring the introduction of stabilizers into the final formulation.²⁸


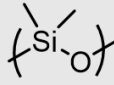
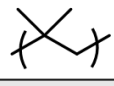
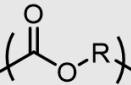
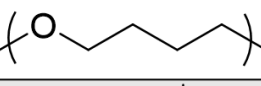
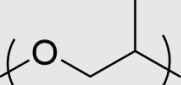
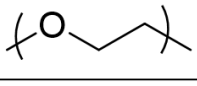
Increasing Polarity	Soft Segment	Structure	T _g °C
Least  Most	Polydimethylsiloxane (PDMS)		-123
	Polyisobutylene (PIB)		-73
	Polyester		Variable
	Polytetramethylene oxide (PTMO)		-83
	Polypropylene glycol (PPG)		-73
	Polyethylene Oxide (PEO)		-40

Table 2.1: There are several classes of PU elastomers, each providing different physical and chemical characteristics that are suitable for different applications.²⁹

2.4 Oxidation and Chain Scission Events

Oxidation remains a prevalent degradation pathway for many polymers, including polyurethanes often leading to embrittlement and increasing susceptibility to stress

fractures or tears after prolonged use. The human body regularly produces reactive oxygen species (ROS) through a wide range of catalytic mechanisms and serve to govern cells for the preservation of homeostasis, leading to both constructive and destructive mechanisms in the body.³⁰ The formation of ROS in the body additionally catalyzes the oxidative degradation of implanted polymers.³¹ Several enzymatic and redox processes produce ROS, subjecting polymer chains to radicals that react to cause chain scission and crosslinking. Chain scission refers to the cleaving of polymer chains at random positions along the backbone, reducing molecular weight. Conversely, crosslinking events join two individual chains to form one molecule, increasing the overall molecular weight.

In a study by Korotkova et al., it was found that the concentration of HO[•] radicals in the blood serum of a healthy individual is 340 μM, highlighting the constant oxidative stress some implanted materials experience.³² The mechanism for ROS formation involves a one electron reaction of elemental oxygen to form an anionic radical that then interacts with enzymes or metal ions to form peroxide or nitroxide species. These intermediates further react forming the reactive species shown in **Figure 2.2**. Susceptibility to oxidative attack correlates with ROS concentration and is patient specific.

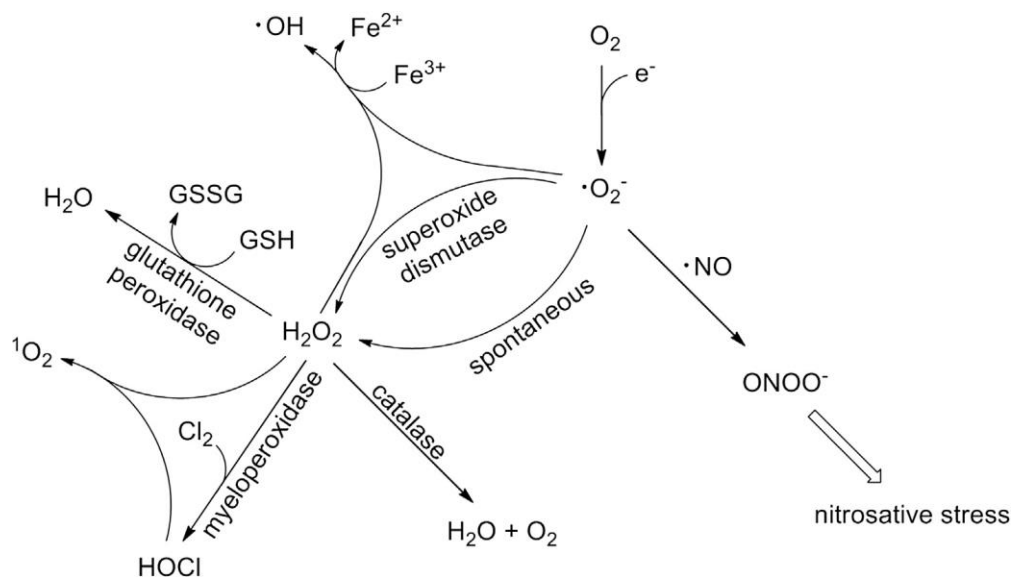


Figure 2.2 Diatomic oxygen degrades under different conditions into several ROS. Peroxides are the most common products from these oxidation reactions leading to crosslinking and chain scission along the polymer backbone.³¹

Figure 2.3 highlights a model mechanism that initiates ether-based urethane oxidative degradation through chain scission. It should be noted that the radicals formed can couple with other chains, resulting in a crosslinking event or further propagate the oxidation of other chains. Due to the good hydrolytic stability of polyether urethanes, oxidative degradation prevails in these systems, leading to an increase in molecular weight within the aqueous environment of the human body. These findings indicate that oxidative degradation in polymers through ROS results in a higher degree of crosslinking than chain scission.^{33,34}

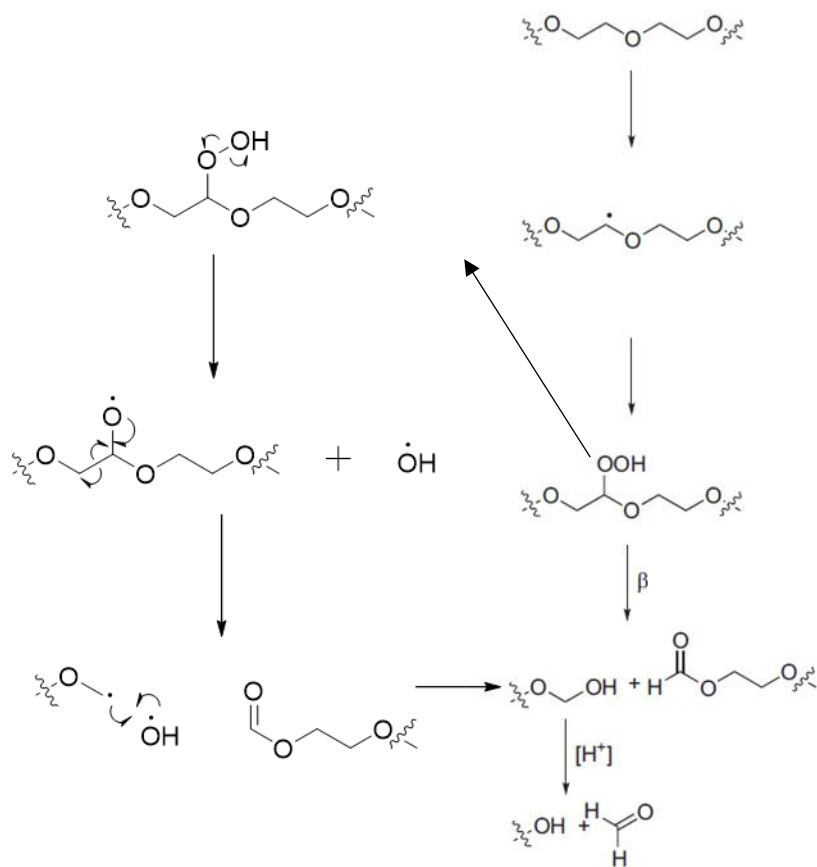


Figure 2.3 An ethylene glycol derived backbone subjected to oxidative stress undergoes chain scission, generating formaldehyde as a byproduct. This serves as one example of an oxidative reaction, as radical chemistry allows for a host of different intermediates and products. Adapted from (10).

Metal ions present another source of oxidative degradation for both long- and short-term implanted PUs. Several studies demonstrate the effects of different trace metal ions on polyurethane stability in the body, with different levels of stability correlated with different soft segments.³⁵⁻⁴⁰ Metal ion oxidation (MIO) is especially important to consider when polyurethanes are used for insulation or guide wire purposes, often found in cardiac

pacemaker leads or stent reinforcers. PUs remain a prominent choice for this application due to capability to tolerate hysteresis loads that the cardiac system produces, while resisting deformation.⁴¹ While the metals used for these applications are not inherently reactive, they contain trace amounts of residual metal cations, including cobalt, silver, nickel, chromium, molybdenum, iron, titanium, and platinum.³⁹ These trace metals readily catalyze the oxidation of polyurethanes. Stokes et al. demonstrated that polyether urethanes are especially susceptible to MIO, as the polyether components have interactions with metal ions similar to that of a crown ether.³⁸ The coiling of the oligomeric ether segments in the PU backbone around the metal introduces localized sites of internal stress. Continued stress residing in the polymer results in increased susceptibility to stress cracking. In particular, cobalt displays a potent oxidative effect on polyether urethanes. When studied in the context of pacemaker leads, cobalt exposures led to wire insulation failure similar to that of H₂O₂, requiring device explantation.^{39 42}

The prevalence of oxidative degradation in implanted PUs prompted the blending of antioxidants within the PU matrix. Polyether urethane, Pellethane[®], stents often incorporate Irganox[®] 1076 (a common antioxidant).³⁹ These antioxidants, incorporated at low weight percent concentrations (often less than 5%), effectively limit oxidation for PU based materials. Another common antioxidant is Santowhite[®], and when incorporated at 2.2 wt % showed extended oxidation protection out to 12 months, demonstrating no crosslinking or chain scission when compared to untreated samples.⁴³ However, a known issue with blending antioxidants into the polymer matrix is the phenomenon of blooming. The blended additive leaching out to the material surface characterizes blooming. The leached additive crystallizes, causing a reduction in homogeneity that reduces

effectiveness. A study conducted by Nouman et al. highlighted significant blooming during cold storage of samples (causing crystallization of the Ingranox 1076) or during sterilization, where high temperatures melt the additive resulting in antioxidant inhomogeneity after phase separation.⁴⁴ Studies incorporating PDMS soft segments were conducted to overcome this blooming phenomenon. The high resistance to stress cracking in highly oxidative environments render PDMS a promising soft segment for bypassing antioxidant addition. Ward et al. showed that incorporating PDMS into the SS of a PU at 35 wt % leads to a large decrease in oxidative events.³⁷ Incorporating PDMS also leads to less stress cracking events in the material due to increased oxidative resistance.⁴⁵ As previously mentioned, SS chemistry selection helps remediate certain degradation modes, however introduces new susceptibilities as well. PDMS SSs display decreased hydrolytic stabilities and increased surface fouling tendencies without additional functionalities.⁴⁶⁻⁴⁹

2.5 Bacterial Biofilm Formation

Biologically active implantation sites impart additional stresses onto certain non-surgically implanted medical devices, i.e., catheters and stents. A prevalent example of such a site is PU stents located in the urinary tract. Long-term exposure to biological fluids leads to biofilm formation, defined by bacterial colonization on the device surface that conglomerates to form a film encased in a protective mucoid glycocalyx.⁵⁰ Biofilms allow the persistence of bacteria that boast increased resistance to antibiotics and heightened ability to develop resistances.⁵¹ Bacteria in biofilms orient in an organized matrix, affording increased stability that leads to enhanced antibiotic resistance. Biofilm formation

leads to infections and encrustation, requiring antibiotics and immediate device removal, which proves fatal if not addressed.^{52, 53}

The first step in biofilm fouling enables the formation of a conditioning layer on the polymer surface.⁵⁴ This conditioning layer develops as proteins and extra cellular matrix coat the surface through a dynamic adsorption-desorption process.⁵¹ Proteins interact with the device surface and begin to denature in reversible steps. Each step involves a conformational change in the protein, liberating water and/or other proteins bound to the surface. Each displacement contains a discrete energetic cost that drives rate of this process.⁵⁵ These steps are reversible, as proteins constantly compete with water and other proteins for positioning on the polymer surface. However, once the protein undergoes enough conformational changes, it denatures completely and adsorbs onto the surface irreversibly. The denatured proteins then provide an ideal surface for bacteria interaction. **Figure 2.4** visualizes the different biofilm formation stages, beginning with protein adsorption followed by bacterial attachment, growth, and release.

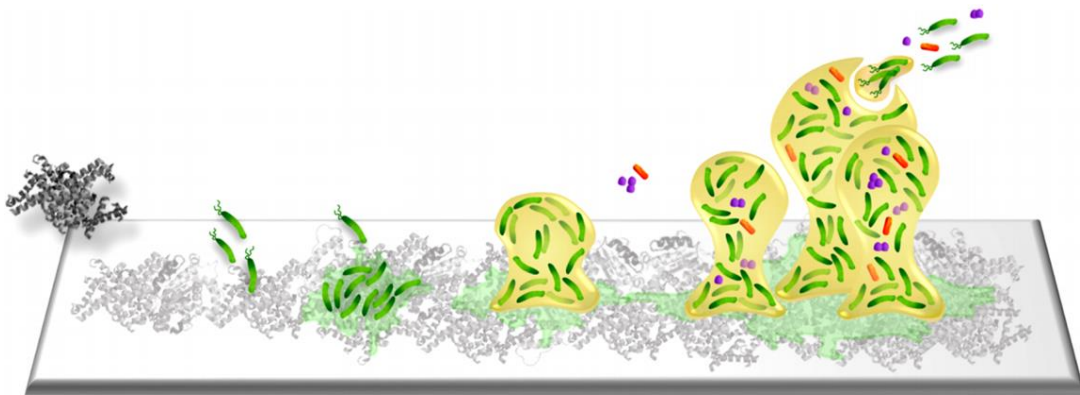


Figure 2.4 Biofilm formation begins with the formation of a conditioning layer composed of denatured proteins. This is then followed by bacterial attachment and colonization.

When enough bacteria attach to the surface, they are released into the body causing infection and biofilm propagation.²⁵

The bacterial lattice formed in a biofilm still allows nutrients to diffuse rendering biofilms capable of sustaining bacteria life and reproduction. The sessile bacteria break off from the main lattice and colonize other parts of the implant or begin an infection at the implant site. Once a biofilm forms, it is difficult to remediate with antibiotics, resulting in device removal (explantation) accompanied by discomfort, medical costs, and occasional mortality.⁵⁰ Due to this, the best method to combat biofilm formation is to prevent it.

When considering the different types of polymer based biomedical materials, polyurethanes exhibit the largest resistance to biofilm formation.⁵⁶ While better at resisting encrustation, silicon based implants generally possess problems with biofilm formation due to their lack of hydrophilic properties. Whitesides et al. demonstrated the importance of hydrophilicity in the realm of protein repulsion, with surface bound water molecules directing protein adsorption.⁵⁷ Hydrophilic polymers, including polyether urethanes are relevant in environments where biofilm formation is common, such as the urinary tract. These hydrophilic polymers interact favorably with water molecules in the body, increasing the energetic barrier a protein needs to overcome to bind to the surface. This energetic barrier relates directly to displacing the tightly bound water molecules and presents the best method to combat biofilm formation. Likewise, altering the surface energy of the PU through post-processing methods also serves to reduce formation.

Several attempts exist to control protein-surface interactions, and still command considerable research interest. The most widely studied method of protein resistance is

increasing hydrophilicity, however studies have also explored increasing the steric hinderance or roughness of the surface to discourage bacterial attachment.^{58, 59} The theory behind this technique involves increasing the favorability of the surface's interaction with water. This leads to a greater energy barrier for protein adsorption onto the surface, due to the increased difficulty the protein has in displacing surface water molecules.⁶⁰ An additional emerging solution for biofilm formation is the development of novel coatings on PU medical devices. Coating technologies tackle this issue by creating a surface that is not energetically favorable for protein adsorption, contains antibacterial properties, or possesses some controlled degradation pathway that expels fouled surfaces.

Diamonlike carbon (DLC) received substantial attention due to the favorable biological compatibility it possesses. Remarkably, Laube et. al. demonstrated the efficacy of this coating on patients who experience severe stent encrustation and biofilm formation.⁶¹ These patients possessed urinary tract conditions that encouraged development of surface fouling conditions. DLC coatings, applied through a plasma vapor deposition process, resulted in complete remediation of the fouling issue across a 2,467-day trial. Additionally, patients and physicians reported excellent handling and a facile insertion process. Further surface functionalization with copper provides an enhanced antibacterial effect.⁶² Controlled release of antibiotics incorporated into the device surface also acts as a pathway for biofilm remediation. Wang et. al. synthesized a multi-layer polymeric film composed of a poly(acrylic acid)/poly(ethylenimine) copolymer that contained the antibiotic gentamicin.⁶³ The steady release of gentamicin produced a zone of inhibition along the polymeric surface, preventing biofilm formation.

2.6 Encrustation

PUs, along with many other polymeric implants, display a susceptibility to a phenomenon known as encrustation. Generically, encrustation is the result of mineral deposition onto the device surface that, over time, can result in infection and stent obstruction requiring multiple operations for removal that can be costly or even deadly.⁶⁴ ⁶⁵ This phenomenon is most common in urinary applications, as ideal mineral concentrations and pH values create an environment where mineral deposition can occur. Because of this, encrustation remains a concern when designing polymer based ureteral stents or urinary catheters as can be seen in **Figure 2.5**. The main factors that influence encrustation are indwelling time and the patient's predisposition to kidney stone formation (urolithiasis).^{50, 66} Additional considerations include pH, diet, and mineral diversity.



Figure 2.5 Example of severe encrustation on a polyurethane ureteral stent. These stents require surgical removal, a costly and dangerous procedure for the patient.⁶⁷

Biofilm formation helps aid the growth of an encrustation layer. The presence of different bacteria in the urinary tract introduces several environmental factors that reduce mineral solubility, increasing rates of encrustation. In uninfected urine, calcium oxalate is the primary substance in the encrusted layer, however, bacteria that cause the release of urase result in a higher composition of struvite (magnesium ammonium phosphate and calcium phosphate).⁶⁸ As bacteria release urase, urea in the urine decomposes into ammonia which augments local pH. This increase in pH lowers the solubility of different minerals and facilitates encrustation.⁶⁹ Because of this, biofilm regulation is one of necessary steps to regulating encrustation on polymer based biomedical devices.

Currently, polyurethane based stents and catheters display a higher rate of encrustation than silicon-based stents. This results from the hydrophobic nature of the silicon stents providing poor surface properties for mineral accumulation. Silicon based polymers are ideal for maximizing encrustation resistance, however polymer stiffness is an important factor in certain somatic applications.⁷⁰⁻⁷² One such application is ureteral stents, an application where encrustation is a prevalent issue. Ureteral stents are implanted in the ureter to encourage urine draining from the kidneys to the bladder. This urine draining relies on the mechanical integrity of the stent, which is impacted by the stent material chosen. Silicon based stents, which show increased encrustation resistance compared to polyurethane based stents, have increased compressibility that can impact urine draining. Incorporating an interpenetrating polymer network (IPN) into the stent design mitigates this issue, allowing for increased mechanical properties with a blend in surface properties. Jones et al. showed when polymethylmethacrylate (PMMA) was utilized in an IPN, a 648 % increase in ultimate tensile strength and a 1000% increase in the storage modulus can be achieved at the cost of a 631% decrease in elongation at break and an increase in the glass transition temperature of almost 100 °C.⁶⁸ While the increase in modulus and tensile strength is important for ensuring device integrity, stiffer devices can cause patient discomfort and difficulty during insertion. An increase in the T_g of the material to above body temperature also decreased the flexibility of the device *in vivo* and result in patient discomfort.

2.7 Hydrolytic and Enzyme Degradation of PUs

While the urethane linkage itself is hydrolytically stable at a range of common body pH's, the soft segment has potential for hydrolytic degradation, the severity of which is dependent on chemical composition. Of the common soft segment constituents, the most vulnerable to hydrolytic cleavage is the ester-based soft segment. The hydrolytically unstable nature of polyester urethanes resulted in their discontinued use in the 1960's.³⁵ They have since been replaced by polyether, polycarbonate, and PDMS urethanes, whose relatively higher hydrolytic stability allows for long implantation times. Polyether urethanes are considered hydrolytically stable, however they undergo hydrolysis at the carbamate linkage under certain conditions. Chaffin et al. studied the hydrolysis of polyether and PDMS urethanes and showed that polyether urethanes display chain scission after one year at room temperature in a buffered water solution at pH 7.⁷³ The activation energy for the hydrolysis of the carbamate bond was found to be approximately 90 kJ mol⁻¹. When the study was repeated with a PDMS based urethane, similar results were found, but chain scission happened on the PDMS backbone instead, suggesting an increased hydrolytic instability when selecting a PDMS SS. Stokes et al. showed that adding carbonate backbone segments also increased hydrolytic resistance.³⁵ Mathur et al. showed that hydrolysis was mitigated by incorporating PDMS segments into the polymer SS at shorter time scales.²⁵ Including this hydrophobic group onto the backbone reduces the water uptake of the material and therefore reduces the rate of hydrolysis. Altogether, PDMS modified backbones are more susceptible to hydrolysis, however their lack of water uptake limits hydrolysis of the bulk material resulting in primarily surface degradation.

Enzymatic degradation is an additional concern for biomedical polyurethanes. Enzymes and macrophages both lead to the breakdown of polyurethanes via catalytic hydrolysis or oxidation. To explore this, a proteolytic enzyme known as Papain was investigated for its ability to degrade polyether urethanes and PDMS urethanes as shown by Cooper et al.⁷⁴ The study concluded through X-ray photoelectron spectroscopic data that the urethane linkage is susceptible to enzymatic degradation resulting in chain scission. The same experiment using a PDMS-based PU concluded that those polyurethanes degrade via lipid sorption due to the oleophilic nature of the PDMS-based backbone.

While macrophages do not register polymers as foreign materials, they identify polymer surfaces that have been fouled with protein adsorption.⁷⁵ Macrophages then expose the material surface to acidic, basic, and oxidative stresses. Acidic environments are particularly devastating to polyether and polycarbonate urethanes, resulting in an increase of hydrolysis and subsequent chain scission. Developing a resistance to the oxidative and hydrolytic stresses that enzymes and macrophages exert onto a polymer is not trivial and developing a material resistant to all of the aforementioned conditions could be expensive and not viable commercially. The most effective pathway to prevent this form of degradation is to decrease the material's interactions with proteins, as denatured proteins on the surface of the material are recognized by the body and become subject to attack. Increasing the hydrophobic content in the stent material helps mitigate hydrolytic cleavage. This can be done by increasing the aliphatic content or by introducing PDMS into the backbone.⁷⁶ While polyester urethanes are no longer used in devices that require long indwelling times, they have found an important role in the realm of polyurethane tissue

scaffolds, where controlled degradation is needed. Because of this, tissue scaffolds comprised of lactic acid or caprolactones are common.^{16, 18}

2.8 Conclusions and Outlooks

Despite the aforementioned degradation pathways, polyurethanes remain at the forefront of biomedical innovation. Their good mechanical properties and biocompatibility, coupled with the versatility in soft and hard segment composition, endow PUs with the potential for numerous medical applications. It is the versatility in polyurethane composition where new advancements reside. Tailoring the soft and hard segments for specific environments in the body allow for prolonged device lifetime and custom applications.

One of the biggest knowledge gaps in understanding and preventing polyurethane degradation *in vivo* are the different degradation mechanisms, including intermediates of the different degradation pathways. A good understanding of the chemical and biological interactions polymer chains have in the body will elucidate discrete steps in the degradation process that can then be the target of new synthetic endeavors. Information regarding polymer chain conformation at the various polymer-somatic interfaces, polymer-protein hydrogen bonding and interaction energies, and transition metal containing intermediates would help guide research involving polyurethane degradation *in vivo*. Figuring out these pathways, either by *in situ* IR experiments, or controlled experiments can unlock new understandings of degradation pathways and ways to prevent them.

In the realm of encrustation, studies have conflicting results on the best material to prevent it. Most sources agree that silicon-based devices have the best resistance to encrustation, but have weaker mechanical properties than PU devices. Different synthetic advancements remedy these problems, however. Polymer interpenetrating networks have been studied to reinforce polyurethane based polymers, and an IPN composed of PU structural components with a silicon-based polymer incorporated could lead to a favorable mix of both encrustation and biofilm resistance. Another possibility is utilizing a copolymer of a medical grade polyurethane with a silicon based soft segment that could lead to a synergy that increases resistance to biofilm and encrustation resistance.

Although new materials are being explored to mitigate encrustation, some critical factors are patient diet and genetic predispositions. This makes encrustation a unique type of degradation, where research could be focused on patient habits and increased doctor-patient interaction. Patients with urolithiasis or a urinary tract infection are going to have a higher risk of encrustation, and can benefit from a diet change such as an increase in citrated drinks as shown by Broomfield et al.⁶⁷ Since bacterial infections catalyze encrustation, endeavors that aim to protect against biofilms will work in tandem to mitigate encrustation. New advancements in biofilm mitigation include understanding the effect of surface morphology and domain size on polymer-bacteria interactions as well as what effect covalently attaching antibiotics or proteins will have on polymer-bacteria interactions.

Hydrolytic degradation of PUs in the body has been largely remedied with the decreased use of polyester based soft segments in polyurethanes. Polyether and polycarbonate polyurethanes show excellent hydrolytic stability both *in vivo* and *in vitro*,

closely followed by PDMS based polyurethanes. Aliphatic polyurethanes have also been explored *in vivo*, showing similar biological responses to that of polyether urethanes and suffering from less hydrolytic cleavage.⁷⁷ More investigation is required to determine biofilm and encrustation effects on these aliphatic substrates. Taking advantage of hydrolytic degradation is also an option when exploring polyester urethanes for tissue scaffold applications. In environments where oxidative degradation is most common, incorporating a PDMS soft segment helps mitigate chain scission and crosslinking events as shown by Ward et al.^{37, 78} Future work going into covalently attaching antioxidants to the backbone of polyurethane chains could result in less antioxidant blooming or leaching out into the patient.

Specific tailoring of polyurethane structures is currently hindered by limited synthetic methods that are available on an industrial scale. New chemistries allow the synthesis of polyurethanes with controlled structures that can be used to target specific degradation pathways. Shifting polyurethane synthesis away from the isocyanate route towards carbamate chemistry will result in a greener approach to polyurethane synthesis and a safer end polymer. Moving to an activated carbamate monomer for PU synthesis will broaden the scope of available chemicals to incorporate into the backbone, as isocyanate-based monomers are limited by the cost of production and availability. A larger library of chemicals to incorporate into the end polyurethane device will allow chemists to have greater control of the final structure-property relationships of the constitutive polymer.

2.9 References

1. Akindoyo, J. O.; Beg, M. D. H.; Ghazali, S.; Islam, M. R.; Jeyaratnam, N.; Yuvaraj, A. R., Polyurethane types, synthesis and applications – a review. *RSC Advances* **2016**, *6* (115), 114453-114482.
2. Xie, F.; Zhang, T.; Bryant, P.; Kurusingal, V.; Colwell, J. M.; Laycock, B., Degradation and stabilization of polyurethane elastomers. *Progress in Polymer Science* **2019**, *90*, 211-268.
3. Gama, N. V.; Ferreira, A.; Barros-Timmons, A., Polyurethane Foams: Past, Present, and Future. *Materials* **2018**, *11* (10), 1841.
4. Delebecq, E.; Pascault, J.-P.; Boutevin, B.; Ganachaud, F., On the Versatility of Urethane/Urea Bonds: Reversibility, Blocked Isocyanate, and Non-isocyanate Polyurethane. *Chemical Reviews* **2013**, *113* (1), 80-118.
5. Yilgör, I.; Yilgör, E.; Wilkes, G. L., Critical parameters in designing segmented polyurethanes and their effect on morphology and properties: A comprehensive review. *Polymer* **2015**, *58*, A1-A36.
6. Abouzahr, S.; Wilkes, G. L.; Ophir, Z., Structure-property behaviour of segmented polyether-MDI-butanediol based urethanes: effect of composition ratio. *Polymer* **1982**, *23* (7), 1077-1086.
7. Aneja, A.; Wilkes, G. L., A systematic series of ‘model’ PTMO based segmented polyurethanes reinvestigated using atomic force microscopy. *Polymer* **2003**, *44* (23), 7221-7228.
8. Rusu, L.-C.; Ardelean, L. C.; Jitariu, A.-A.; Miu, C. A.; Streian, C. G., An Insight into the Structural Diversity and Clinical Applicability of Polyurethanes in Biomedicine. *Polymers* **2020**, *12* (5), 1197.

9. Joseph, J.; Patel, R. M.; Wenham, A.; Smith, J. R., Biomedical applications of polyurethane materials and coatings. *Transactions of the IMF* **2018**, *96* (3), 121-129.
10. Wendels, S.; Avérous, L., Biobased polyurethanes for biomedical applications. *Bioactive Materials* **2021**, *6* (4), 1083-1106.
11. Griesser, H. J., Degradation of polyurethanes in biomedical applications—A review. *Polymer Degradation and Stability* **1991**, *33* (3), 329-354.
12. Król, P., Synthesis methods, chemical structures and phase structures of linear polyurethanes. Properties and applications of linear polyurethanes in polyurethane elastomers, copolymers and ionomers. *Progress in Materials Science* **2007**, *52* (6), 915-1015.
13. Polymers as Ureteral Stents. *Journal of Endourology* **2010**, *24* (2), 191-198.
14. Gunatillake, P. A.; Martin, D. J.; Meijjs, G. F.; McCarthy, S. J.; Adhikari, R., Designing Biostable Polyurethane Elastomers for Biomedical Implants. *Australian Journal of Chemistry* **2003**, *56* (6), 545-557.
15. Zawadzak, E.; Bil, M.; Ryszkowska, J.; Nazhat, S. N.; Cho, J.; Bretcanu, O.; Roether, J. A.; Boccaccini, A. R., Polyurethane foams electrophoretically coated with carbon nanotubes for tissue engineering scaffolds. *Biomed Mater* **2009**, *4* (1), 015008.
16. Singhal, P.; Small, W.; Cosgriff-Hernandez, E.; Maitland, D. J.; Wilson, T. S., Low density biodegradable shape memory polyurethane foams for embolic biomedical applications. *Acta Biomaterialia* **2014**, *10* (1), 67-76.
17. Adhikari, R.; Gunatillake, P. A.; Griffiths, I.; Tatai, L.; Wickramaratna, M.; Houshyar, S.; Moore, T.; Mayadunne, R. T. M.; Field, J.; McGee, M.; Carbone, T.,

Biodegradable injectable polyurethanes: Synthesis and evaluation for orthopaedic applications. *Biomaterials* **2008**, *29* (28), 3762-3770.

18. Guelcher, S.; Srinivasan, A.; Hafeman, A.; Gallagher, K.; Doctor, J.; Khetan, S.; McBride, S.; Hollinger, J., Synthesis, in vitro degradation, and mechanical properties of two-component poly(ester urethane)urea scaffolds: effects of water and polyol composition. *Tissue Eng* **2007**, *13* (9), 2321-33.

19. Zdrahala, R. J.; Zdrahala, I. J., Biomedical Applications of Polyurethanes: A Review of Past Promises, Present Realities, and a Vibrant Future. *Journal of Biomaterials Applications* **1999**, *14* (1), 67-90.

20. Synthesis, In Vitro Degradation, and Mechanical Properties of Two-Component Poly(Ester Urethane)Urea Scaffolds: Effects of Water and Polyol Composition. *Tissue Engineering* **2007**, *13* (9), 2321-2333.

21. Lyu, S.; Untereker, D., Degradability of Polymers for Implantable Biomedical Devices. *International Journal of Molecular Sciences* **2009**, *10* (9), 4033-4065.

22. Sobczak, M., Biodegradable Polyurethane Elastomers for Biomedical Applications – Synthesis Methods and Properties. *Polymer-Plastics Technology and Engineering* **2015**, *54* (2), 155-172.

23. Pedersen, D. D.; Kim, S.; Wagner, W. R., Biodegradable polyurethane scaffolds in regenerative medicine: Clinical translation review. *Journal of Biomedical Materials Research Part A* **2022**, *110* (8), 1460-1487.

24. Szycher, M., *Szycher's Handbook of Polyurethanes, First Edition*. Taylor & Francis: 1999.

25. Mathur, A. B.; Collier, T. O.; Kao, W. J.; Wiggins, M.; Schubert, M. A.; Hiltner, A.; Anderson, J. M., In vivo biocompatibility and biostability of modified polyurethanes. *J Biomed Mater Res* **1997**, *36* (2), 246-57.
26. NIOSH Publication No. 2008-109.
[\(https://www.cdc.gov/niosh/topics/isocyanates/default.html#:~:text=The%20most%20commonly%20used%20diisocyanates,and%20isophorone%20diisocyanate%20\(IPDI\)\)](https://www.cdc.gov/niosh/topics/isocyanates/default.html#:~:text=The%20most%20commonly%20used%20diisocyanates,and%20isophorone%20diisocyanate%20(IPDI))
(accessed 09/07/2020).
27. Seefried Jr, C. G.; Koleske, J. V.; Critchfield, F. E., Thermoplastic urethane elastomers. II. Effects of variations in hard-segment concentration. *Journal of Applied Polymer Science* **1975**, *19* (9), 2503-2513.
28. Allan, D.; Daly, J. H.; Liggat, J. J., Oxidative and non-oxidative degradation of a TDI-based polyurethane foam: Volatile product and condensed phase characterisation by FTIR and solid state ¹³C NMR spectroscopy. *Polymer Degradation and Stability* **2019**, *161*, 57-73.
29. Juan V. Cauich-Rodríguez, L. H. C.-C., Fernando Hernandez-Sánchez and José M. Cervantes-Uc, Degradation of Polyurethanes for Cardiovascular Applications. *Advances in Biomaterials Science and Biomedical Applications*, Rosario Pignatello, IntechOpen **2013**, 51-82.
30. Bardaweel, S. K.; Gul, M.; Alzweiri, M.; Ishaqat, A.; HA, A. L.; Bashatwah, R. M., Reactive Oxygen Species: the Dual Role in Physiological and Pathological Conditions of the Human Body. *Eurasian J Med* **2018**, *50* (3), 193-201.
31. Ulbricht, J.; Jordan, R.; Luxenhofer, R., On the biodegradability of polyethylene glycol, polypeptoids and poly(2-oxazoline)s. *Biomaterials* **2014**, *35* (17), 4848-4861.

32. Korotkova, E. I.; Misini, B.; Dorozhko, E. V.; Bukkel, M. V.; Plotnikov, E. V.; Linert, W., Study of OH● Radicals in Human Serum Blood of Healthy Individuals and Those with Pathological Schizophrenia. *International Journal of Molecular Sciences* **2011**, *12* (1), 401-409.
33. Stevenson, J. S.; Kusy, R. P., Structural degradation of polyurethane-based elastomeric modules. *Journal of Materials Science: Materials in Medicine* **1995**, *6* (7), 377-384.
34. Anderson, J. M.; Hiltner, A.; Wiggins, M. J.; Schubert, M. A.; Collier, T. O.; Kao, W. J.; Mathur, A. B., Recent advances in biomedical polyurethane biostability and biodegradation. *Polymer International* **1998**, *46* (3), 163-171.
35. Stokes, K.; McVenes, R.; Anderson, J. M., Polyurethane Elastomer Biostability. *Journal of Biomaterials Applications* **1995**, *9* (4), 321-354.
36. Zweifel, H., *Stabilization of Polymeric Materials*. 1 ed.; Springer-Verlag Berlin Heidelberg: 1998; p 219.
37. Ward, B.; Anderson, J.; Ebert, M.; McVenes, R.; Stokes, K., In vivo biostability of polysiloxane polyether polyurethanes: Resistance to metal ion oxidation. *Journal of Biomedical Materials Research Part A* **2006**, *77A* (2), 380-389.
38. Stokes, K.; Urbanski, P.; Upton, J., The in vivo auto-oxidation of polyether polyurethane by metal ions. *Journal of Biomaterials Science, Polymer Edition* **1989**, *1* (3), 207-230.
39. Wiggins, M. J.; Wilkoff, B.; Anderson, J. M.; Hiltner, A., Biodegradation of polyether polyurethane inner insulation in bipolar pacemaker leads. *Journal of Biomedical Materials Research* **2001**, *58* (3), 302-307.

40. Stokes, K.; Coury, A.; Urbanski, P., Autooxidative Degradation of Implanted Polyether Polyurethane Devices. *Journal of Biomaterials Applications* **1986**, *1* (3), 411-448.
41. Navas-Gómez, K.; Valero, M. F., Why Polyurethanes Have Been Used in the Manufacture and Design of Cardiovascular Devices: A Systematic Review. *Materials* **2020**, *13* (15), 3250.
42. Meijs, G. F.; McCarthy, S. J.; Rizzardo, E.; Chen, Y.-C.; Chatelier, R. C.; Brandwood, A.; Schindhelm, K., Degradation of medical-grade polyurethane elastomers: The effect of hydrogen peroxide in vitro. *Journal of Biomedical Materials Research* **1993**, *27* (3), 345-356.
43. Christenson, E. M.; Anderson, J. M.; Hiltner, A., Antioxidant inhibition of poly(carbonate urethane) in vivo biodegradation. *Journal of Biomedical Materials Research Part A* **2006**, *76A* (3), 480-490.
44. Nouman, M.; Saunier, J.; Jubeli, E.; Marlière, C.; Yagoubi, N., Impact of sterilization and oxidation processes on the additive blooming observed on the surface of polyurethane. *European Polymer Journal* **2017**, *90*, 37-53.
45. Gallagher, G.; Padsalgikar, A.; Tkatchouk, E.; Jenney, C.; Iacob, C.; Runt, J., Environmental stress cracking performance of polyether and PDMS-based polyurethanes in an in vitro oxidation model. *Journal of Biomedical Materials Research Part B: Applied Biomaterials* **2017**, *105* (6), 1544-1558.
46. Ducom, G.; Laubie, B.; Ohannessian, A.; Chottier, C.; Germain, P.; Chatain, V., Hydrolysis of polydimethylsiloxane fluids in controlled aqueous solutions. *Water Science and Technology* **2013**, *68* (4), 813-820.

47. Wu, H.; Dai, T.; Ao, W.; Shao, S.; Li, Z.; Luo, F.; Li, J.; Zhao, D.; Lan, W.; Zhang, H.; Tan, H., The role of segmental mixing on the mechanical properties and oxidative stability of polydimethylsiloxane-based polyetherurethane. *Polymer* **2022**, *261*, 125401.
48. Tang, L.; Long, X.; He, X.; Ding, M.; Zhao, D.; Luo, F.; Li, J.; Li, Z.; Tan, H.; Zhang, H., Improved in vivo stability of silicon-containing polyurethane by fluorocarbon side chain modulation of the surface structure. *Journal of Materials Chemistry B* **2021**, *9* (14), 3210-3223.
49. Kim, S.; Ye, S.-h.; Adamo, A.; Orizondo, R. A.; Jo, J.; Cho, S. K.; Wagner, W. R., A biostable, anti-fouling zwitterionic polyurethane-urea based on PDMS for use in blood-contacting medical devices. *Journal of Materials Chemistry B* **2020**, *8* (36), 8305-8314.
50. KEANE, P. F.; BONNER, M. C.; JOHNSTON, S. R.; ZAFAR, A.; GORMAN, S. P., Characterization of biofilm and encrustation on ureteric stents in vivo. *British Journal of Urology* **1994**, *73* (6), 687-691.
51. Kram, W.; Buchholz, N.; Hakenberg, O. W., Ureteral stent encrustation. Pathophysiology. *Arch Esp Urol* **2016**, *69* (8), 485-493.
52. Scotland, K. B.; Lo, J.; Grgic, T.; Lange, D., Ureteral stent-associated infection and sepsis: pathogenesis and prevention: a review. *Biofouling* **2019**, *35* (1), 117-127.
53. Vladkova, T. G.; Staneva, A. D.; Gospodinova, D. N., Surface engineered biomaterials and ureteral stents inhibiting biofilm formation and encrustation. *Surface and Coatings Technology* **2020**, *404*, 126424.

54. Lange, D.; Bidnur, S.; Hoag, N.; Chew, B. H., Ureteral stent-associated complications—where we are and where we are going. *Nature Reviews Urology* **2015**, *12* (1), 17-25.
55. Penna, M. J.; Mijajlovic, M.; Tamerler, C.; Biggs, M. J., Molecular-level understanding of the adsorption mechanism of a graphite-binding peptide at the water/graphite interface. *Soft Matter* **2015**, *11* (26), 5192-5203.
56. Zander, Z. K.; Becker, M. L., Antimicrobial and Antifouling Strategies for Polymeric Medical Devices. *ACS Macro Letters* **2018**, *7* (1), 16-25.
57. Ostuni, E.; Chapman, R. G.; Holmlin, R. E.; Takayama, S.; Whitesides, G. M., A Survey of Structure–Property Relationships of Surfaces that Resist the Adsorption of Protein. *Langmuir* **2001**, *17* (18), 5605-5620.
58. MacKintosh, E. E.; Patel, J. D.; Marchant, R. E.; Anderson, J. M., Effects of biomaterial surface chemistry on the adhesion and biofilm formation of *Staphylococcus epidermidis* in vitro. *Journal of Biomedical Materials Research Part A* **2006**, *78A* (4), 836-842.
59. TIESZER, C.; REID, G.; DENSTEDT, J., CONDITIONING FILM DEPOSITION ON URETERAL STENTS AFTER IMPLANTATION. *Journal of Urology* **1998**, *160* (3 Part 1), 876-881.
60. Zhang, H.; Chiao, M., Anti-fouling Coatings of Poly(dimethylsiloxane) Devices for Biological and Biomedical Applications. *Journal of Medical and Biological Engineering* **2015**, *35* (2), 143-155.

61. Laube, N.; Kleinen, L.; Bradenahl, J.; Meissner, A., Diamond-Like Carbon Coatings on Ureteral Stents—A New Strategy for Decreasing the Formation of Crystalline Bacterial Biofilms? *Journal of Urology* **2007**, *177* (5), 1923-1927.
62. Kram, W.; Rebl, H.; de la Cruz, J. E.; Haag, A.; Renner, J.; Epting, T.; Springer, A.; Soria, F.; Wienecke, M.; Hakenberg, O. W., Interactive Effects of Copper-Doped Urological Implants with Tissue in the Urinary Tract for the Inhibition of Cell Adhesion and Encrustation in the Animal Model Rat. *Polymers* **2022**, *14* (16), 3324.
63. Wang, B.; Jin, T.; Xu, Q.; Liu, H.; Ye, Z.; Chen, H., Direct Loading and Tunable Release of Antibiotics from Polyelectrolyte Multilayers To Reduce Bacterial Adhesion and Biofilm Formation. *Bioconjugate Chemistry* **2016**, *27* (5), 1305-1313.
64. Dirk Lange, K. S., *The Role of Bacteria in Urology*. Springer International Publishing, 2019; p 193.
65. Tomer, N.; Garden, E.; Small, A.; Palese, M., Ureteral Stent Encrustation: Epidemiology, Pathophysiology, Management and Current Technology. *Journal of Urology* **2021**, *205* (1), 68-77.
66. Grases, F.; Söhnel, O.; Costa-Bauzá, A.; Ramis, M.; Wang, Z., Study on concretions developed around urinary catheters and mechanisms of renal calculi development. *Nephron* **2001**, *88* (4), 320-8.
67. Broomfield, R. J.; Morgan, S. D.; Khan, A.; Stickler, D. J., Crystalline bacterial biofilm formation on urinary catheters by urease-producing urinary tract pathogens: a simple method of control. *J Med Microbiol* **2009**, *58* (Pt 10), 1367-1375.
68. Jones, D. S.; Bonner, M. C.; Gorman, S. P.; Akay, M.; Keane, P. F., Sequential polyurethane–poly(methylmethacrylate) interpenetrating polymer networks as ureteral

biomaterials: mechanical properties and comparative resistance to urinary encrustation. *Journal of Materials Science: Materials in Medicine* **1997**, 8 (11), 713-717.

69. McBane, J. E.; Santerre, J. P.; Labow, R. S., The interaction between hydrolytic and oxidative pathways in macrophage-mediated polyurethane degradation. *Journal of Biomedical Materials Research Part A* **2007**, 82A (4), 984-994.

70. Barghouthy, Y.; Wiseman, O.; Ventimiglia, E.; Letendre, J.; Cloutier, J.; Daudon, M.; Kleinclauss, F.; Doizi, S.; Corrales, M.; Traxer, O., Silicone-hydrocoated ureteral stents encrustation and biofilm formation after 3-week dwell time: results of a prospective randomized multicenter clinical study. *World J Urol* **2021**, 39 (9), 3623-3629.

71. Mathias, S.; Wiseman, O., Silicone vs. Polyurethane Stent: The Final Countdown. *J Clin Med* **2022**, 11 (10).

72. Gadzhiev, N.; Gorelov, D.; Malkhasyan, V.; Akopyan, G.; Harchelava, R.; Mazurenko, D.; Kosmala, C.; Okhunov, Z.; Petrov, S., Comparison of silicone versus polyurethane ureteral stents: a prospective controlled study. *BMC Urology* **2020**, 20 (1), 10.

73. Chaffin, K. A.; Chen, X.; McNamara, L.; Bates, F. S.; Hillmyer, M. A., Polyether Urethane Hydrolytic Stability after Exposure to Deoxygenated Water. *Macromolecules* **2014**, 47 (15), 5220-5226.

74. Takahara, A.; Hergenrother, R. W.; Coury, A. J.; Cooper, S. L., Effect of soft segment chemistry on the biostability of segmented polyurethanes. II. In vitro hydrolytic degradation and lipod sorption. *Journal of Biomedical Materials Research* **1992**, 26 (6), 801-818.

75. Sheikh, Z.; Brooks, P. J.; Barzilay, O.; Fine, N.; Glogauer, M., Macrophages, Foreign Body Giant Cells and Their Response to Implantable Biomaterials. *Materials* **2015**, 8 (9), 5671-5701.
76. Stefanović, I. S.; Špírková, M.; Poręba, R.; Steinhart, M.; Ostojić, S.; Tešević, V.; Pergal, M. V., Study of the Properties of Urethane–Siloxane Copolymers Based on Poly(propylene oxide)-b-poly(dimethylsiloxane)-b-poly(propylene oxide) Soft Segments. *Industrial & Engineering Chemistry Research* **2016**, 55 (14), 3960-3973.
77. Jayabalan, M.; Shunmuga Kumar, N.; Rathinam, K.; Kumari, T. V., In vivo biocompatibility of an aliphatic crosslinked polyurethane in rabbit. *Journal of Biomedical Materials Research* **1991**, 25 (12), 1431-1442.
78. Ward, R.; Anderson, J.; McVenes, R.; Stokes, K., In vivo biostability of polysiloxane polyether polyurethanes: Resistance to biologic oxidation and stress cracking. *Journal of Biomedical Materials Research Part A* **2006**, 77A (3), 580-589.

CHAPTER 3

CARBAMATE THERMAL DECARBOXYLATION FOR THE DESIGN OF NON-ISOCYANATE POLYURETHANE FOAMS

3.1 Abstract

Polyurethane foams remain at the forefront of cushioning, insulation, packaging, and structural applications. Risk of exposure to isocyanate-containing precursors during foaming operations directly contributes to the regulation of isocyanates, thus prompting investigations into non-isocyanate alternatives. This work presents non-isocyanate polyurethanes (NIPUs) that are readily prepared from carbonyldiimidazole (CDI) derived monomers for efficient synthetic methods that strive to adhere to the principles of green chemistry. Various bis-carbonylimidazolide (BCI) monomers undergo β -hydrogen elimination at temperatures exceeding 140 °C, which liberates a carbamic acid that subsequently decarboxylates. Decarboxylation provides an *in situ* blowing agent, and carbon dioxide is capable of producing a microcellular foam with concurrent crosslinking. BCI difunctional monomers in presence of trifunctional crosslinking agents enabled the synthesis of both rigid and flexible NIPU foams, and the addition of conventional surfactants and catalysts allowed for precise control over pore structure. Thermomechanical analysis elucidated foam glass transition temperatures ranging from 0 to 120 °C and coefficients of thermal expansion on the order of 10^{-6} mm/mm °C. Scanning electron microscopy enabled characterization of pore size and foam structure. Optimized catalyst and surfactant levels enabled a range of flexible and rigid foam compositions. Fundamental structure-property-processing relationships were established for novel BCI-derived NIPU foams to reliably predict performance.

3.2 Introduction

Polyurethane (PU) foams are ubiquitous for porous material applications due to versatile mechanical performance and structural diversity.¹⁻⁴ Their low density, thermal conductivity, and extensive vibrational damping encourage insulation, padding, and weight reduction applications.⁵⁻⁸ Although enabling chemical structure-property relationships exist for PU foams, their mechanical properties are derived from cell size and structure, density, and fill gas.⁹⁻¹¹ Closed-cell foams are ideal for structural and insulation applications, while an open-cell structure allows for flexible foams, typically found in padding. In addition to common additives, i.e., catalysts and flame retardants, surfactants dictate pore formation and structure. Specialized foams utilize tailored fill gasses, e.g., pentane or chlorofluorocarbons, to fine tune thermal conductivity and decrease reaction exotherms during foam manufacturing.¹² PUs possess excellent mechanical strength, elongation at break, compositional modularity, abrasion resistance, and performance retention over extended temperature ranges due to nano-scale phase separation.¹³⁻¹⁵ The combination of these highly desirable properties and modularity enables their use in the furniture, insulation, biomedical, transportation, and clothing industries. From a sustainability standpoint, foams enable multi-faceted impact from material light weighting, decreased polymer consumption, and energy-saving insulation.¹⁶ Their crosslinked nature allows for minimal aging or creep, allowing increased service life for long term applications.

Conventional synthesis of PUs and PU foams take advantage of the rapid reaction of isocyanates and diols with differing chemical compositions and functionalities.¹⁷

Commercial PUs involve a tailored mixture of isocyanates, polymeric isocyanates, diols, oligomeric polyols, and other additives to tune final properties. Dimeric hydrogen bonding occurs between urethane-containing hard segments, further bolstering thermomechanical properties. Soft segments commonly include polyols, typically low glass transition temperature polyethers, and low concentrations of urethane linkages. These hard and soft segments undergo nano-phase separation, resulting in a multi-phase morphology with covalently bound low and high T_g segments, i.e., a soft phase for elasticity and a hard phase for structural integrity.¹⁴ During foam manufacturing, the addition of water in tandem with isocyanates produces an amine and CO_2 from the decarboxylation of an unstable carbamic acid intermediate. The released CO_2 generates micron-scale pores that are stabilized with surfactants, resulting in a microcellular structure in the final PU thermoset.¹⁸ The versatile and highly reactive nature of the isocyanate functional group enables this multifaceted reaction sequence and leads to a commercially viable manufacturing process. However, the inherent toxicity of the isocyanate group leads to allergic reactions or asthma upon mild, consistent contact, while more significant exposures are potentially fatal. This toxicity drives the search for alternative chemistries and hence the long-standing attention to NIPU foams.¹⁹

While safer synthetic pathways are a principle of green chemistry, foams themselves exemplify several aspects of sustainability. Porous structures enable lightweight alternatives to traditional materials, while reducing material consumption. Useful for aerospace applications where lower density is paramount, lightweight materials offer avenues for decreased material consumption if applied to other fields. For example, vehicle weight is directly correlated to fuel consumption in the automotive industry.²⁰

Various economic analyses indicate that the prevalence of lightweight vehicles will increase over time, resulting from increased fuel prices and greenhouse gas regulation. Thus, high performance foams remain a contemporary subject for investigation and are a central avenue for increased global sustainability.^{21, 22} Additional examples for energy saving applications include materials for insulation to increase energy efficiency while lowering costs. PU foams offer substantial benefits to sustainability; however, the research community continues the search for greener synthetic pathways.

The most prevalent non-isocyanate polyurethane (NIPU) synthetic method is the cyclic carbonate route.²³ Dicyclic carbonates react with diamines to form linear polyurethanes with pendant secondary and primary hydroxyl groups adjacent to the carbamate. Past NIPU foam formulations involved these cyclic carbonates, producing residual hydroxyl groups along the polyurethane backbone, which resulted in a loss of desirable properties.²⁴ The presence of these groups increases water uptake, mitigating weight reduction and resulting in plasticization.²⁵ Moreover, the pendant hydroxyl group compromises the hydrogen bonding interactions, thus negatively influencing the formation of a well-defined multi-phase morphology. In addition, the carbonate-amine reaction requires a catalyst to compensate for slow reaction kinetics and produces flammable H₂ gas during the foaming process.²⁶ Other processes remedy the off-gassing of H₂, however they require addition of thiols to produce CO₂ and require reaction times up to 4 h for curing.²⁷ Our previous work demonstrated the synthesis of NIPU using carbonyldiimidazole (CDI) functionalized bis-carbonylimidazolide (BCI) monomers.²⁸ This BCI pathway exhibited greater versatility compared to previous NIPU pathways due to increased compositional diversity compared to cyclic carbonate and isocyanate

approaches.²⁹⁻³² BCI monomers provided an isocyanate-free pathway to a highly versatile platform for the future synthesis of polyurethanes. Furthermore, BCI monomers offer the benefits of an expansive selection of commercial diols, thus providing a wide range of achievable polymer properties. For example, the versatility of CDI functionalization enabled the unprecedented synthesis of 1,4-cyclohexanedimethanol-derived BCI monomer to investigate the structure-property effects of rigid BCI monomers on the thermal performance of synthesized foams (**Scheme S3.1**). Room temperature reaction conditions, high yields, low-cost diols, and simple workup allowed for large-scale synthesis of these monomers.

Linear PUs from the BCI approach displayed thermal and mechanical properties comparable to conventional PUs, but earlier literature omitted crosslinked polyurethanes. This manuscript demonstrates that BCI monomers react with multifunctional amines to provide crosslinked porous foams, thus introducing a non-isocyanate route for PU foam manufacturing. The novelty of this approach leverages *in situ* CO₂ generation through an elimination mechanism in the absence of additional catalyst. The inherent solvent- and isocyanate-free nature of this synthetic method proves desirable, as safer reagents and the absence of solvent align with several principles of green chemistry.³³ Thermal analysis of these foams revealed T_g tunability through assorted BCI and triamine monomers. Our research results herein explore the effects of catalysts and surfactants on foam curing time, cell structure, and foam density. A fundamental understanding of BCI chemistry enables fine tuning of final foam properties and a deeper understanding of structure-property relationships for crosslinked NIPU foams with potential impact on many emerging technologies.

3.3 Experimental/Methods

3.3.1 Instruments

^1H and ^{13}C nuclear magnetic resonance (NMR) spectroscopy utilized a Varian Unity 400 spectrometer functioning at 399.87 MHz and 23 °C (solution concentration of 10 mg mL⁻¹). A Mel-Temp 1101D digital melting point apparatus operating at 5 °C min⁻¹ provided melting points for BCI monomers. A ThermoFisher Scientific Nicolet iS5 FTIR spectrometer iD7 ATR, with a diamond cell, confirmed PU foam structure after 32 scans. A TA Instruments Discovery Series TGA 5500 facilitated thermogravimetric analysis (TGA) by utilizing a heating rate of 10 °C min⁻¹ from 25 – 800 °C with a steady nitrogen purge. The $T_{d, 5\%}$, or temperature where 5% of the original sample mass is lost, stands as an indicator for sample thermal stability. Stepwise isothermal TGA followed by ramping from 25 – 800 °C at 10 °C min⁻¹ until the weight change was > 0.1 % min⁻¹, and the TGA would isotherm until the weight change was < 0.05 % min⁻¹. A TA Instruments Discovery Series DSC 2500 with heat/cool/heat cycles of 10 °C min⁻¹, 10 °C min⁻¹, and 10 °C min⁻¹, respectively, provided differential scanning calorimetry (DSC) data where the sample was under a nitrogen environment throughout the experiment. DSC provided the glass transition temperatures from the midpoint of the endothermic transition in the 2nd heat. A TA instruments TMA Q400 temperature ramp, operating at a rate of 5 °C min⁻¹ in air from -20 – 150 °C, provided coefficient of thermal expansion (CTE) and T_g of PU foams. A JEOL JSM IT500HR or JEOL 6300 scanning electron microscope coupled with a Cressington sputter coater 208HR using an Au/Pd conductive layer provided micrographs of PU foams. The 30 nm Au/Pd layer allowed for high-resolution images at 10x, 25x, 100x, and 500x magnification, and the secondary electron detector maintained 15.0 kV for all

images. A Gas Lab CM-0177, S8 CO₂ sensor kit enabled the detection of CO₂ released from the reaction.

3.3.2 Materials

1,4-butanediol (>99.0%), 1,1'-carbonyldiimidazole (CDI) (>97.0%), 4,4'-methylenedianiline (MDA) (>97.0%), 1,4-cyclohexanedimethanol (CHDM) (mixture of isomers, 99%), Dabco[®] 33LV, and dibutyltin dilaurate (95%) were purchased from Sigma Aldrich and stored in a desiccator under reduced pressure. 4,4'-dihydroxydiphenylmethane (BPF) (>99.0%), was purchased from TCI and used as received. 4-(4-aminophenoxy) benzene-1,3-diamine, or triaminodiphenylether, (TADE) (97%) was provided by SABIC and stored in a desiccator under reduced pressure. Jeffamine[®] T-403 polyetheramine was provided by Huntsman and had a number-average molecular weight of 440 g mol⁻¹. The Jeffamine[®] was dried at 60 °C under reduced pressure prior to use. Dabco[®] DC193 was provided by Honeywell NSC and used as received. Ethyl acetate (> 99.5%, ACS grade), acetone (99.6% ACS reagent), and methanol (>99.8%, ACS grade) were purchased from Fisher Scientific and used as received. Nitrogen gas (99.999% UHP-T) was purchased from Praxair Distribution. Deuterated chloroform (CDCl₃) was purchased from Cambridge Isotope Laboratories, Inc.

3.3.3 Synthesis of 1,4-butyl(bis-carbonylimidazolide) (BBCI), 1b, and 1,4-cyclohexanedimethyl(bis-carbonylimidazolide) (CHDMBCI), 1a.

Synthesis followed from our previous literature (Scheme S1).²⁸ 1,4-butanediol (27.04 g, 0.3 mol) was added to a three-necked, 1 L round-bottomed flask outfitted with a magnetic stir bar, nitrogen inlet, nitrogen outlet, and rubber septa. The butanediol was dissolved in ethyl acetate (600 mL) at 25 °C for 10 min under a nitrogen purge. 1,1'-

Carbonyldiimidazole (CDI) (121.61 g, 0.7 mol) was added to the flask in partitions to allow for even mixing and to reduce the propensity for cyclization.³⁹ The initial ~60 g of CDI dissolved readily in the solvent, producing a transparent and colorless solution. CDI solution saturation and product formation resulted in a turbid, white slurry. An additional 60 mL of ethyl acetate was added to ensure reagents were well mixed. The reaction was allowed to proceed for ~2 h prior to filtration using a fritted funnel. The white powder was washed twice with ethyl acetate to remove byproducts (500 mL total) and dried at 60 °C and ~25 in-Hg for 18 h. The final isolated yield was > 90% with a melting point range of 138-140 °C. ¹H NMR (CDCl₃, δ, Figure S1) 8.13-8.14 (t, 2H, 3), 7.41-7.42 (t, 2H, 2), 7.07-7.08 (m, 2H, 1), 4.47-4.51 (t, 4H, 5) 1.95-2.00 (m, 4H, 6). The synthesis for **1a** followed the same procedure as above and provided a yield >80% with a melting point range of 170-174 °C and was also a white powder. The mixture of *cis* and *trans* isomers presents multiple peaks in NMR, specifically the splitting at 4.3 ppm and 1.6 ppm. ¹H NMR (CDCl₃, δ, Figure S2) 8.12-8.14 (t, 2H, 3), 7.41-7.42 (t, 2H, 2), 7.07-7.08 (m, 2H, 1), 4.25-4.37 (d, 4H, 4) 1.11-2.11 (m, 10H, 5-7).

3.3.4 Synthesis of 4,4'-diphenylmethane(bis-carbonylimidazolide) (BCIF)

Due to the increased solubility of the BCIF monomer, reaction conditions deviated from **1a** and **1b**. BPF (10 g, 0.05 mol) was added to a three-necked, 1 L round-bottomed flask outfitted with a magnetic stir bar, nitrogen inlet, nitrogen outlet, and a rubber septum. The BPF was dissolved in 250 mL of ethyl acetate and purged. CDI (20.27 g, 0.125 mol) was dissolved and the reaction was allowed to proceed for 2 h for full conversion. The reaction mixture was evaporated using a rotary evaporator and the solids were collected and dissolved in 20 mL of acetone. The dissolved mixture was then precipitated into

reverse osmosis purified water and allowed to stir for 15 min. The solid was filtered on a fritted funnel then dried in a vacuum oven for 6 h at 25 °C under vacuum (~25 in-Hg). The temperature was then augmented to 60 °C and dried for an additional 18 h. The final yield was > 85% and melting point range of 125-127 °C. ¹H NMR (CDCl₃, δ, Figure S1) 8.21-8.22 (t, 2H), 7.48-7.49 (t, 2H), 7.19-7.20 (d, 4H) 7.12-7.15 (d, 4H), 7.06-7.12 (t, 2H), 3.95-4.01 (s, 2H).

3.3.5 Synthesis of Polyurethane Foams

1a and **1b** were used to synthesize PU foams with varied T_gs by incorporating aromatic amines according to **Figure 3.1**. BBCI (5.00 g, 18.0 mmol) was added to a 50 mL single-neck round bottomed flask with a stir bar and a twin connecting hose joint to allow for nitrogen flow over the flask. The flask was purged with nitrogen for 5-10 min before lowering the flask into an oil bath at 160 °C to melt the monomer. Once the BBCI was in the melt (<5 min), the T-403 (5.17 g, 11.7 mmol) was quickly added to the reaction with a syringe. The reaction proceeded for 1-2 min before curing. The final product was yellow in color and soft to the touch. The foam was placed in a 250 mL jar with enough methanol to cover the foam and was submerged for 18 h to extract the imidazole byproduct. The foams were then placed in an oven at 80 °C for 16 h before applying reduced pressure for an additional 18 h. This process was repeated for all the MDA-containing foams where MDA was added in molar ratios of 0:100, 20:80, 40:60, and 60:40 mol:mol, MDA:T-403; however, the 60:40 product never reached gelation for the BBCI-based foams. MDA was added immediately prior to the addition of the T-403, after the BBCI was molten. CHDMBCI-based PU foams were synthesized in an identical fashion, but the reaction

temperature was increased to 180 °C to accommodate the higher melting point of the monomer, and the reactions proceeded for 3-5 min before curing.

An aromatic triamine was utilized to further increase the T_g of the PU foams, shown in **Figure 3.2**. Following the same procedure, BBCI (1.88 g, 6.7 mmol) and TADE (0.95 g, 4.4 mmol) were added to a 50 mL single-neck round bottomed flask with a stir bar and a twin connecting hose joint to allow for nitrogen flow over the flask. The flask was purged with nitrogen for 5-10 min before lowering the flask into an oil bath at 160 °C to melt the monomers. Once the reagents were in the melt, the reaction cured in <3 min. This process was repeated for the T-403-containing foams where T-403 was added in molar ratios of 100:0, 90:10, 80:20, 70:30, and 60:40 mol:mol, TADE:T-403. A low concentration, 0.8 wt. %, of Dabco[®] DC193 was added to select PU foams to elucidate the effect on cell structure and overall homogeneity. The surfactant was added with the BCI monomer prior to the addition of the amines and surfactant-containing foams were not used for thermal characterization.

3.4 Results and Discussion

The reaction of difunctional BCI monomers with aliphatic or aromatic triamines results in a crosslinked NIPU, as depicted in **Figure 3.1**. The polycondensation reaction, which liberates imidazole, between **1b** and T-403 (a polypropylene based triamine) at 25 °C in an organic solvent (e.g., chloroform) showcased crosslinking efficacy with the observation of organogels. Performing these reactions at elevated temperatures in the bulk

resulted in spontaneous decarboxylation of the BCI monomer and subsequent network formation to generate a porous microcellular structure.

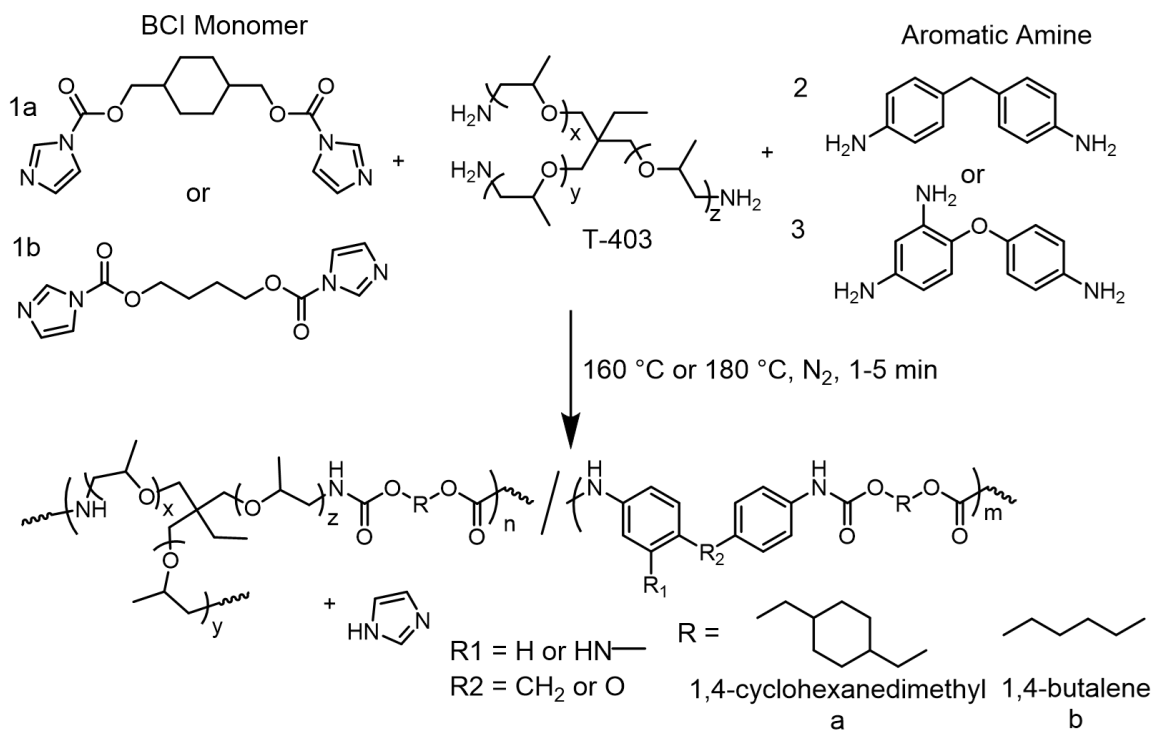


Figure 3.1. Polymerization of BCI monomers (**1a** or **1b**) with T-403 ($x + y + z \sim 5-6$) and aromatic amines, MDA (**2**) or TADE (**3**), produced PU foams with varied T_g s.

Spontaneous foaming during BCI crosslinking was not reported earlier, and thus efforts followed to identify a plausible mechanism for gas generation. A CO₂ detector together with stepwise TGA analysis confirmed that off-gassing and subsequent foaming resulted from *in situ* CO₂ generation. Elucidating the mechanism for decarboxylation promised avenues for future tailoring of foam density. A β -hydrogen elimination reaction, as depicted in **Figure 3.2**, was plausible to produce a terminal alkene and carbamic acid, leading to facile CO₂ production. Similar decomposition pathways for carbamate linkages are present in earlier polyurethane literature, commonly termed dissociation reactions, that predominantly occurred at high temperature, basic conditions.^{17, 34, 35} Foaming conditions

used for BCI NIPU foams emulate these decomposition conditions, further justifying this proposed mechanism, displayed in Figure S3. The presence of base enables elimination and proton transfer while high temperatures encouraged entropically driven CO₂ generation. A BPF-derived BCI monomer, which lacks abstractable β -hydrogens, served as a control to validate this theory. Heating this monomer in with the presence of a CO₂ detector enabled the quantification of decarboxylation. **Figure 3.3** displays CO₂ generation for an aliphatic BCI monomer with abstractable β -hydrogens and the aromatic BCIF monomer that is not amenable to decarboxylation. As predicted, the aromatic monomer did not decarboxylate, thus supporting the decarboxylation mechanism as shown in **Figure 3.2**. Additionally, FTIR spectroscopy displays the appearance of a carbon-carbon double bond absorbance in the spectrum of a BCCI-T-403 foam (Figure S4). This further suggests the formation of a vinyl group during decarboxylation.

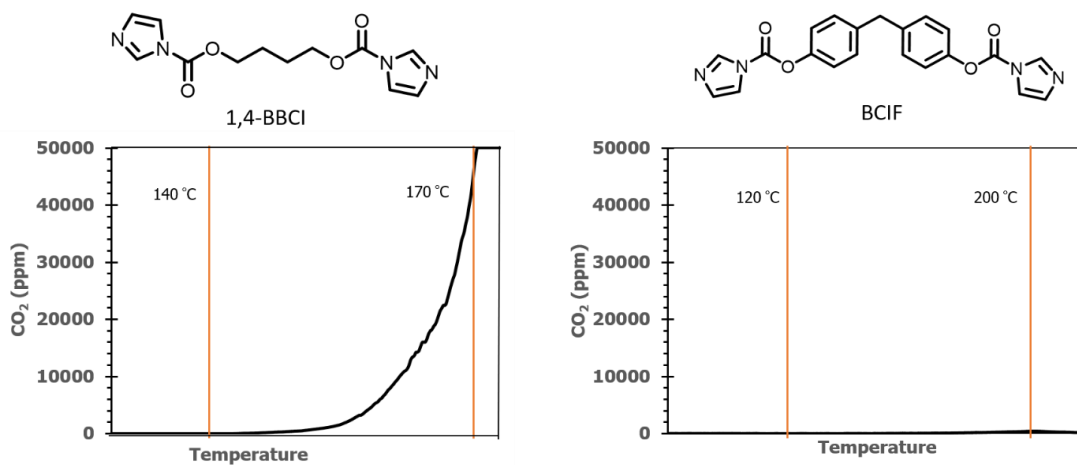


Figure 3.3 Comparison of CO₂ generation profiles for an aliphatic and aromatic BCI monomer. The lack of CO₂ generation in aromatic BCI monomers suggests a mechanistic importance of the β -hydrogen, through a β -hydrogen elimination pathway.

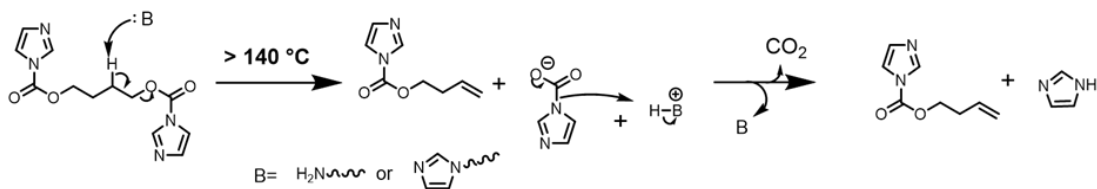


Figure 3.2 Proposed decarboxylation mechanism for BCI monomers after exposure to elevated temperature. Addition of an amine accelerated CO_2 production while crosslinking.

Cure times are also a critical consideration when designing a foaming platform. Molds for final foam parts range in size and complexity, often requiring different cure times for different applications. Traditional catalysts for PU foams vary and include different organic and inorganic compounds, i.e., 1,4-diazabicyclo[2.2.2]octane (DABCO) and dibutyltin dilaurate (DBTDL).^{14, 36} A combination of catalysts is typically employed to optimize reaction kinetics and foam formation, although tin-based catalysts are currently under scrutiny.^{37, 38} A BBCI-T-403 homopolymer synthesized with varying amounts of an organotin or tertiary amine catalyst elucidated the degree of kinetic control available to BCI monomers. Foams with varying amounts of catalyst quantified the effect of catalyst loading on reaction times. Catalyst was added dropwise, with 1 drop = 50 μL , on a 2 g reaction scale and cure times were noted when the foam structure prohibited stirring. The DBTDL catalyst decreased reaction kinetics, likely from free amines complexing with the tin center or displacing the lauryl groups through an amidation reaction, however the exact mechanism is still under investigation. DABCO, however, effectively catalyzed the BCI-amine transcarbamoylation reaction. An optimal concentration of 3-4 drops of DABCO boasted the most potent catalytic effects, with higher concentrations of catalyst resulting in increased reaction times. This significant increase in reaction times at higher DABCO loadings is likely due to competition between the tertiary and primary amine for

electrophilic carbonyl addition.^{39, 40} Overall, DABCO presented an effective pathway for both tuning reactivity and ensuring precursor stability for BCI foams, displayed in **figure 3.4**.

3.4.

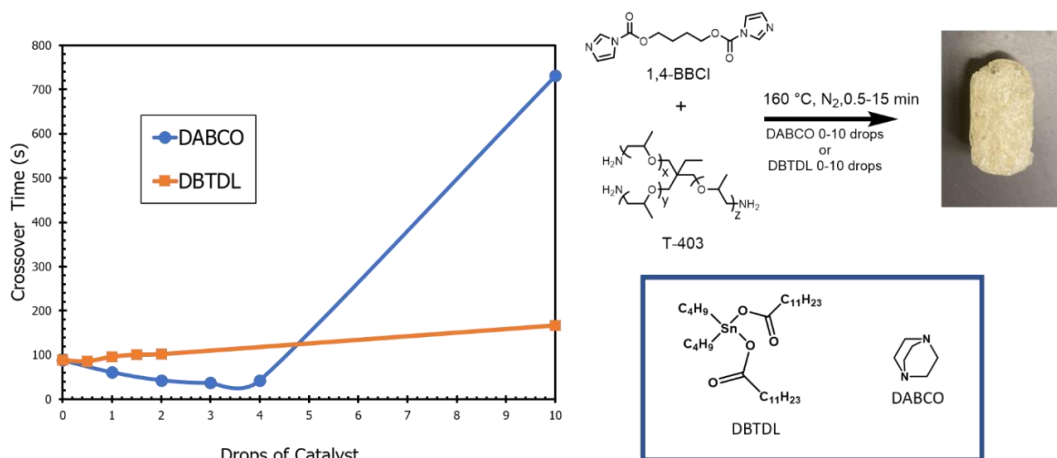


Figure 3.4 The organic tertiary amine (DABCO 33-LV) catalytically promoted the amine addition to a BCI monomer. DBTDL, a traditional PU catalyst, is not effective at promoting this reaction with identical reaction conditions. Both catalysts display elongated reaction times at increased catalyst loading. A drop of catalyst was quantified as a volume of 50 μL dispensed from a micropipette.

The polycondensation reaction of BCI monomers with various multifunctional amines liberated imidazole as a low molar mass condensate. This condensate did not pose a problem, as imidazole is readily soluble in numerous organic and aqueous solvents and sublimates above 90 $^{\circ}\text{C}$ with reduced pressure resulting in a facile recovery. A stepwise isothermal TGA of the foam product before (red curve) and after (blue curve) extraction with methanol and subsequent drying confirmed that a low level of imidazole remained in the foam after reaction, as shown in **Figure 3.5**. A temperature ramp experiment also illustrated the effect of extraction on PU foams (Figure S5). Solvent extraction

quantitatively removed residual imidazole and low molecular weight, soluble, oligomers, providing a ~ 100 °C increase in $T_{d,5\%}$.

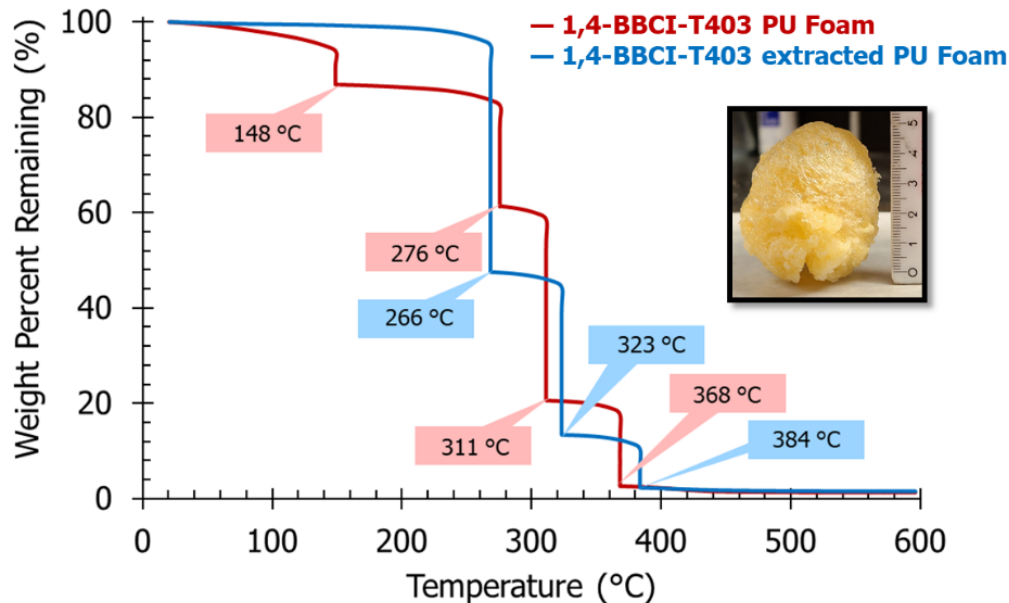


Figure 3.5. Stepwise isothermal TGA demonstrated complete removal of imidazole byproduct after solvent extraction.

BCI functionality enabled the synthesis of a library of NIPUs with diverse compositions. Backbone rigidity, hydrogen bonding, and crosslink density drove key structure-property relationships within this series. Thermomechanical analysis (TMA) and DSC probed thermal transitions for foams as synthesized in **Figure 3.1**. Temperature ramps also revealed coefficients of thermal expansion, and thermogravimetric analysis allowed for weight loss profiles (Figure S3.6). **Table 3.1** summarizes these findings, allowing for an in-depth comparison. Incorporating either a cyclohexyl (1a) or a butyl (1b) BCI monomer and a two-part amine reagent containing varying ratios of either MDA and T-403 or TADE and T-403 enabled decoupling of backbone chemistry effects for thorough investigation.

Homopolymer foams of chemical composition, 1a-T-403, 1b-T-403, 1a-TADE, and 1b-TADE were synthesized for comparison. The consistent urethane structures garnered from BCI chemistry served as controls and isolated the effects of butyl, cyclohexyl, phenyl, and ether groups on thermal performance. As expected, units that impart restricted rotation give rise to higher glass transition temperatures, while more mobile groups decrease T_g (as shown in Figure S7-S9). Aromatic foams containing difunctional MDA linkages display lower T_g s compared to aromatic, trifunctional TADE foams, which exemplify the effects of crosslink density on thermal performance.

Composition	Monomer	(mol:mol)	CTE TMA (mm/mm °C)	T_g DSC (°C)	T_g TMA (°C)	$T_d, 5%$ (°C)	$T_d, 10%$ (°C)
MDA:T-403	BBCI	0:100	29×10^{-6}	-3	3	239	282
		20:80	72×10^{-6}	12	15	227	260
		40:60	105×10^{-6}	24	26	225	250
		60:40	N/A	N/A	N/A	N/A	N/A
	CHDMBCI	0:100	68×10^{-6}	23	30	270	303
		20:80	80×10^{-6}	35	38	234	281
		40:60	71×10^{-6}	54	52	225	272
		60:40	46×10^{-6}	65	55	248	274
TADE:T-403	BBCI	100:0	48×10^{-6}	91	88	230	244
		90:10	58×10^{-6}	86	82	222	243
		80:20	65×10^{-6}	62	65	200	231
		70:30	70×10^{-6}	46	53	208	238
		60:40	77×10^{-6}	52	52	214	244

	CHDMBCI	100:0	53×10^{-6}	126	111	221	267
		90:10	44×10^{-6}	114	99	235	267
		80:20	49×10^{-6}	89	95	191	253
		70:30	52×10^{-6}	82	85	236	276
		60:40	49×10^{-6}	61	62	186	238

Table 1: Thermomechanical properties of synthesized BCI foams acquired from TMA, DSC, and TGA.

BCI foams comprised of aromatic amines displayed increased closed-cell content with incorporation of a silicon-based surfactant, as discussed later using scanning electron microscopy. As expected, the incorporation of aromatic amines increased the T_g and impacted foam structure. This linear, predictable increase as shown in **Figure 3.6** displays tunable properties. In addition, **Figure 3.6** demonstrates this trend is also valid for difunctional rigid monomers. Poor structural integrity of the 60 mol% BBCI:MDA foam prohibited mechanical testing. The dark appearance of TADE-based foams presumably arises from the color of the TADE monomer.

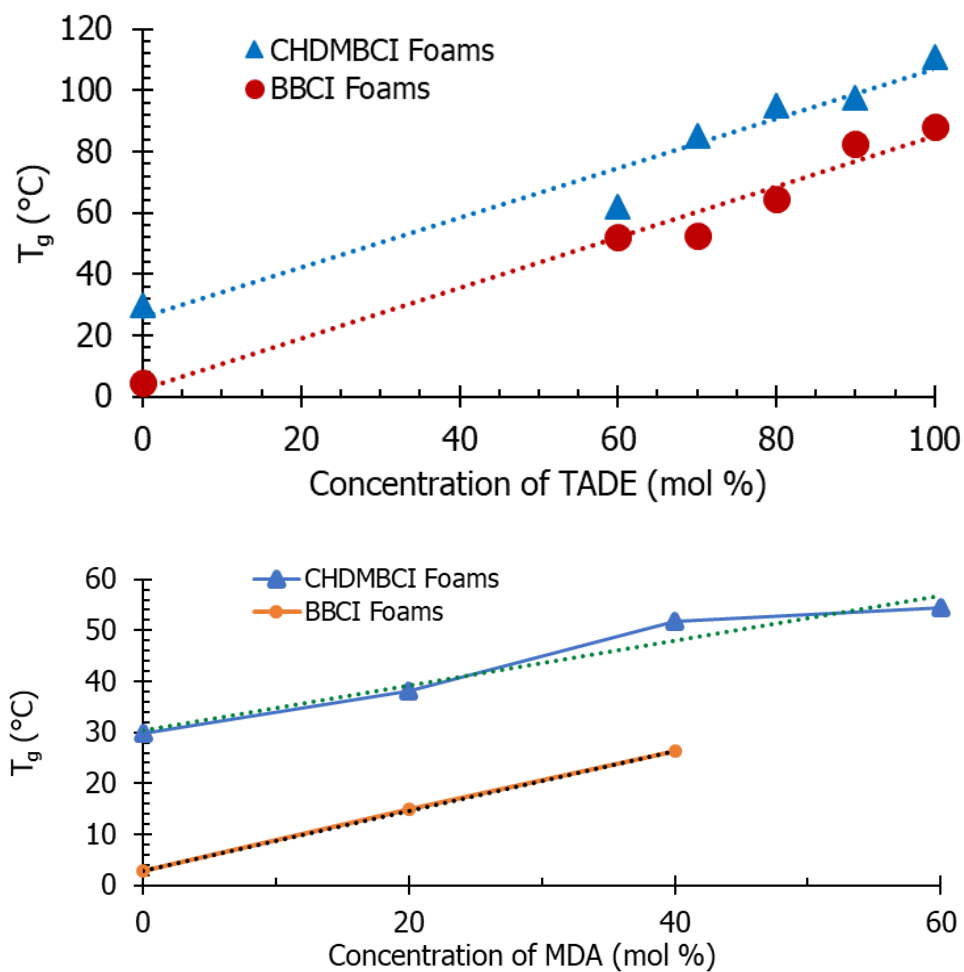


Figure 3.6 TMA elucidated an increase in T_g with an increase in the concentration of the trifunctional aromatic amine, TADE, and difunctional aromatic amine, MDA, in PU foams. Mol. % calculations were calculated with respect to moles of BCI and amine functional groups.

Foam thermal properties arise from both chemical composition and microscale foam structure. Thus, it is imperative to understand the microscale structure of BCI foams to enable performance tunability. Scanning electron microscopy (SEM) provided micron-scale features of the PU foams (**Figures 3.7-3.9** and S3.10 and S3.11). Micrographs of the BBCI-MDA:T-403 0:100, BBCI-TADE:T-403 100:0, and CHDMBCI-TADE:T-403 100:0 PU foams, with and without surfactant, enabled visualization of foam structures. Neat BBCI:T-403 homopolymer foams displayed partially closed cells with uneven pore distributions, as illustrated in **Figure 3.7**. The absence of surfactant results in low pore stability, which explains the abnormal pore distribution.

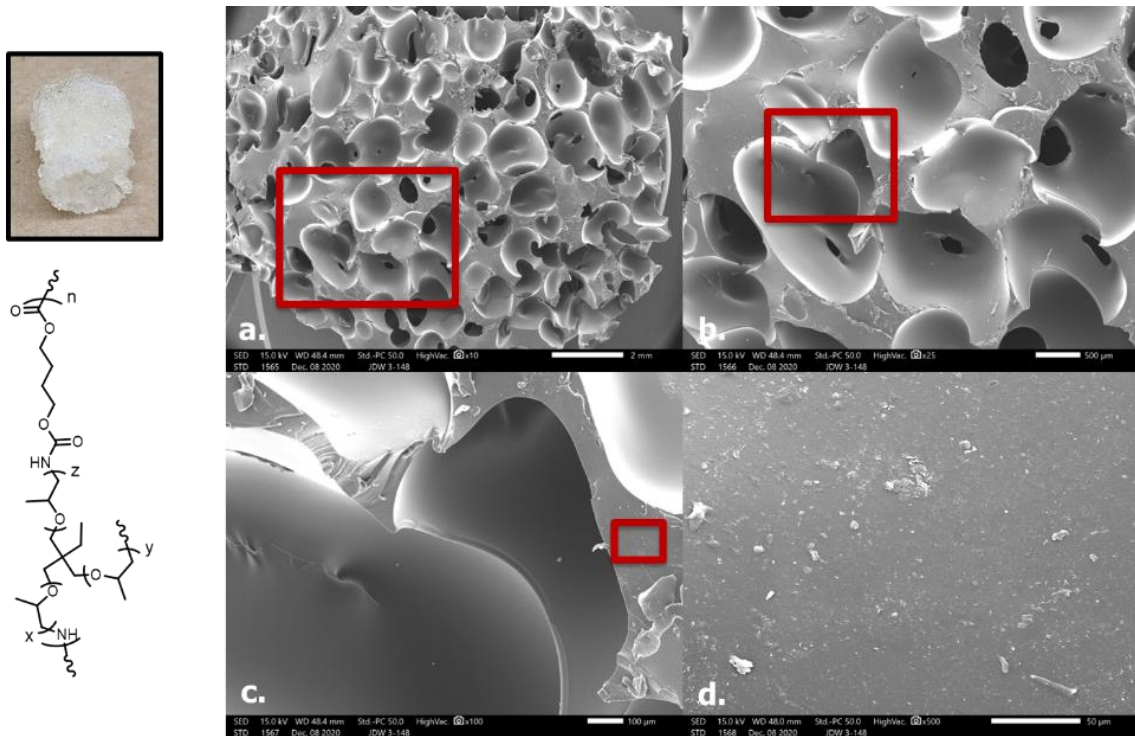


Figure 3.7. SEM of BBCI-MDA:T-403 0:100 indicated a closed-cell or partially open-cell system.

Closed-cells impart better insulating properties compared to open-cells, which are more frequently used in vibrational damping and cushioning applications. Cell structures were on the order of $\sim 500 \mu\text{m}$ and $\sim 1000 \mu\text{m}$ for the BBCI-MDA:T-403 0:100 and BBCI-

TADE:T-403 100:0, respectively. Holes were evident in cell walls for each of the samples, which was consistent with an open-cell character, however, closed-cell structure dominated. The addition of surfactant significantly changed the appearance, density, texture, and cellular structure of the foams, as shown in **Figure 3.8**.

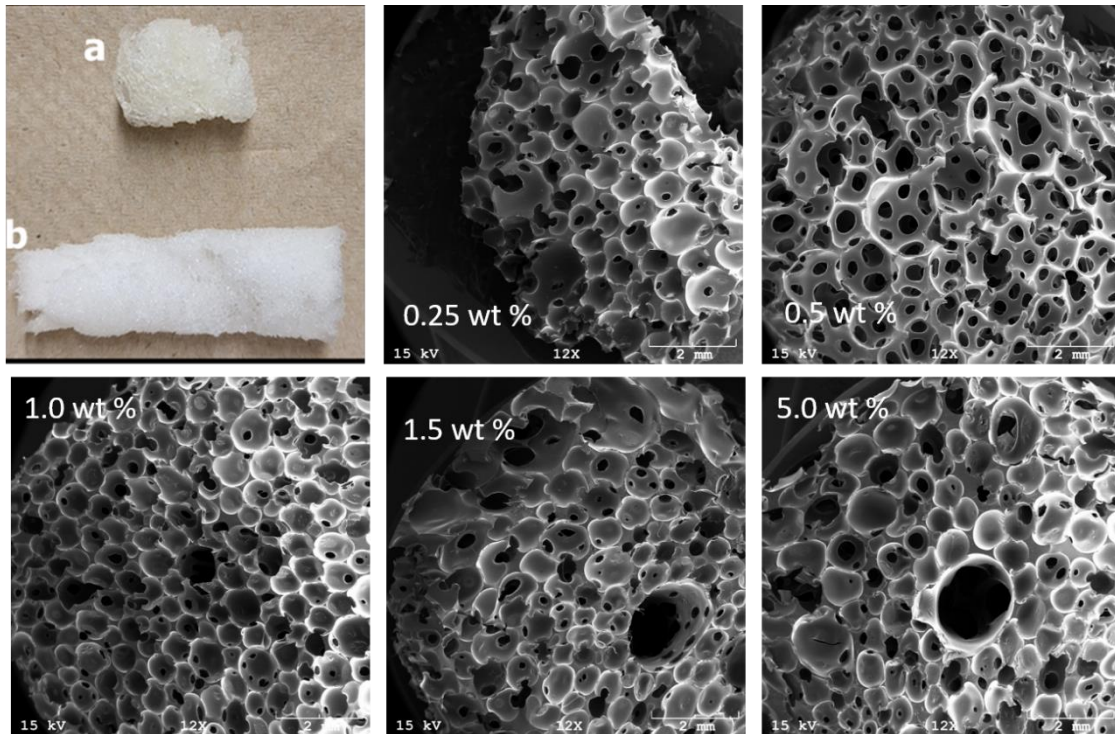


Figure 3.8 Controlling surface energy through surfactant addition (Dabco[®] DC193) in the BBCI-T-403 homopolymer foam results in an array of possible foam structures ranging from open to closed cell. Foam density is also affected with less surfactant loading (a) providing a denser foam than (b).

Silicon-ether copolymer surfactants represent a widely accepted standard for rigid foam applications.¹² Altering the siloxane:ether ratio in these surfactants impart great versatility for tuning surface tension. Consequentially, their tunability allows siloxane-ether surfactants to achieve a diverse range of pore structures. **Figure 3.9** displays the effect of 0.8 wt. % Dabco[®] DC193 (a siloxane-ether surfactant) loading on the final pore structure of a CHDMBCI:TADE homopolymer foam. During foam crosslinking, the surfactant lowers the surface energy of the polymer matrix and allows for stabilization of growing pores.⁴¹ This uniform stabilization results in a well-defined cell structure and more isotropic foam properties. DSC confirmed that surfactant loading did not influence the T_g of the final foam.

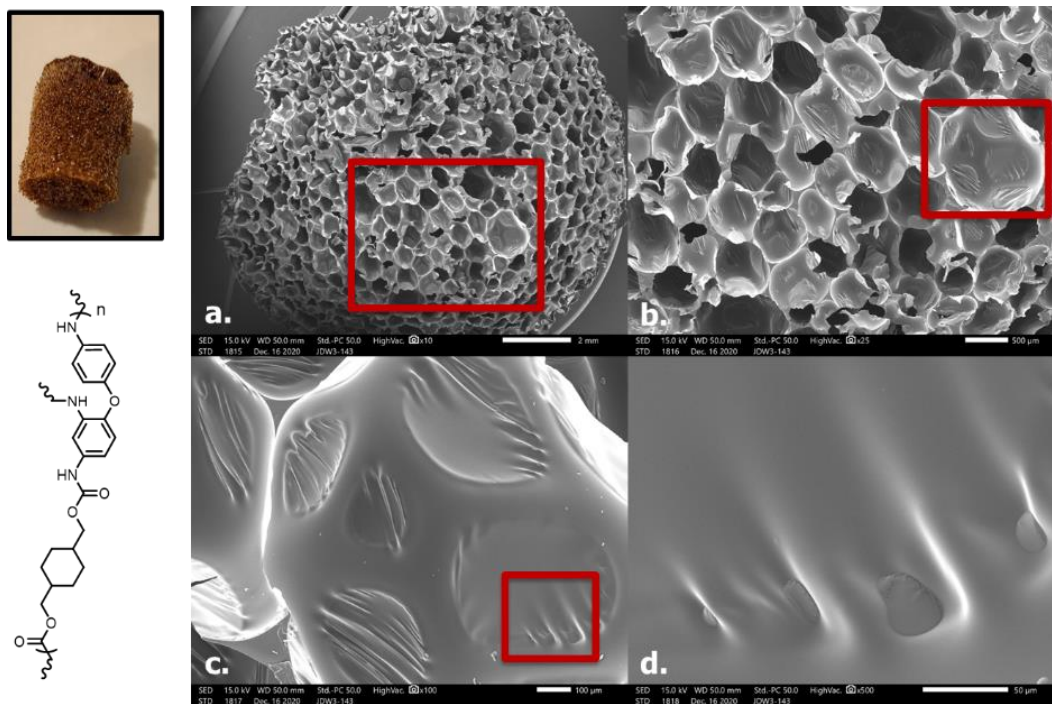


Figure 3.9. SEM of BBCI-TADE:T-403 100:0 indicated a fully closed-cell system after addition of 0.8 wt. % Dabco[®] DC193 surfactant.

3.5 Conclusions

This manuscript established a novel synthetic methodology for isocyanate-free foaming of polyurethane structures. A thermal decarboxylation mechanism of bis-carbonylimidazolide monomers for *in situ* blowing resulted from the BCI monomer β -hydride elimination to produce CO₂ and imidazole. CO₂ was captured in the polymer melt with the aid of a surfactant to achieve a final foamed structure. Two series of foams with varied concentrations of aromatic di- and triamines, in concert with an aliphatic triamine, enabled predictable tailoring of thermal properties. The increase in MDA or TADE incorporation yielded foams with higher T_gs and more rigid structures, which were confirmed with consistent DSC and TMA results. SEM indicated that the process described herein provided closed-cell foams, except when adding a surfactant into the low-T_g system. A simple solvent extraction removed low molar mass byproducts; however, further work will investigate pathways for their *in situ* capture and retention in the final foam. Investigations of BCI foam catalysis revealed DABCO as an avenue for tuning BCI reactivity and flowability in molding applications. Overall, BCI functional monomers introduce a new synthetic methodology for non-isocyanate polyurethanes that is impactful for both thermoplastics and thermosets. BCI foams show predictable cure times, T_g, and porosity control, which suggests potential impact for a multitude of traditional and emerging polyurethane foam applications.

3.6 Acknowledgements

The authors would like to thank Honeywell Federal Manufacturing & Technologies LLC for financial support (AWD00036877) and helpful discussions. The authors would also like to thank SABIC (Dr. Roy Odle) for providing TADE monomer for high T_g foams.

3.7 Funding

This work was funded by Honeywell FM&T.

3.8 References

1. H. M. C. C. Somarathna, S. N. Raman, D. Mohotti, A. A. Mutalib and K. H. Badri, *Construction and Building Materials*, 2018, **190**, 995-1014.
2. N. V. Gama, A. Ferreira and A. Barros-Timmons, *Materials*, 2018, **11**, 1841.
3. P. Singhal, W. Small, E. Cosgriff-Hernandez, D. J. Maitland and T. S. Wilson, *Acta Biomaterialia*, 2014, **10**, 67-76.
4. F.-L. Jin, M. Zhao, M. Park and S.-J. Park, *Polymers*, 2019, **11**, 953.
5. J.-W. Wu, W.-F. Sung and H.-S. Chu, *International Journal of Heat and Mass Transfer*, 1999, **42**, 2211-2217.
6. H. Zhang, W.-Z. Fang, Y.-M. Li and W.-Q. Tao, *Applied Thermal Engineering*, 2017, **115**, 528-538.
7. F. M. Casati, R. M. Herrington, R. Broos and Y. Miyazaki, *Journal of Cellular Plastics*, 1998, **34**, 430-466.
8. T. Khan, V. Acar, M. R. Aydin, B. Hülägü, H. Akbulut and M. Ö. Seydibeyoğlu, *Polymer Composites*, 2020, **41**, 2355-2400.
9. G. F. Smits, *Journal of Thermal Insulation and Building Envelopes*, 1994, **17**, 309-329.
10. M. Thirumal, D. Khastgir, N. K. Singha, B. S. Manjunath and Y. P. Naik, *Journal of Applied Polymer Science*, 2008, **108**, 1810-1817.
11. M. Thirumal, N. K. Singha, D. Khastgir, B. S. Manjunath and Y. P. Naik, *Journal of Applied Polymer Science*, 2010, **116**, 2260-2268.
12. R. Hansen, *Journal of Polymer Science Part A: Polymer Chemistry*, 1993, **31**, 1344-1344.
13. J. P. Sheth, S. Unal, E. Yilgor, I. Yilgor, F. L. Beyer, T. E. Long and G. L. Wilkes, *Polymer*, 2005, **46**, 10180-10190.
14. I. Yilgör, E. Yilgör and G. L. Wilkes, *Polymer*, 2015, **58**, A1-A36.
15. A. Aneja and G. L. Wilkes, *Polymer*, 2003, **44**, 7221-7228.
16. E. Burgaz, *Polyurethane Insulation Foams for Energy and Sustainability*, Springer Cham, 2019.
17. E. Delebecq, J.-P. Pascault, B. Boutevin and F. Ganachaud, *Chemical Reviews*, 2013, **113**, 80-118.
18. V. S. Daniel Klempner, *Handbook of Polymeric Foams and Foam Technology* Hanser Gardner Publications Inc. , Cincinnati, Ohio, 2nd edn., 2004.

19. H. Khatoon, S. Iqbal, M. Irfan, A. Darda and N. K. Rawat, *Progress in Organic Coatings*, 2021, **154**, 106124.
20. J. W. McAuley, *Environmental Science & Technology*, 2003, **37**, 5414-5416.
21. A. T. Mayyas, A. Qattawi, A. R. Mayyas and M. Omar, *Journal of Cleaner Production*, 2013, **40**, 177-189.
22. M. Fadzil, A. B. Abdullah, Z. Samad, F. Yusof and Y. H. P. Manurung, in *Design for Sustainability*, eds. S. M. Sapuan and M. R. Mansor, Elsevier, 2021, DOI: <https://doi.org/10.1016/B978-0-12-819482-9.00006-X>, pp. 435-463.
23. H. Blattmann, M. Fleischer, M. Bähr and R. Mülhaupt, *Macromolecular Rapid Communications*, 2014, **35**, 1238-1254.
24. E. K. Leitsch, G. Beniah, K. Liu, T. Lan, W. H. Heath, K. A. Scheidt and J. M. Torkelson, *ACS Macro Letters*, 2016, **5**, 424-429.
25. Y.-J. Yu, K. Hearon, T. S. Wilson and D. J. Maitland, *Smart Materials and Structures*, 2011, **20**, 085010.
26. H. Blattmann, M. Lauth and R. Mülhaupt, *Macromolecular Materials and Engineering*, 2016, **301**, 944-952.
27. F. Monie, B. Grignard, J.-M. Thomassin, R. Mereau, T. Tassaing, C. Jerome and C. Detrembleur, *Angewandte Chemie International Edition*, 2020, **59**, 17033-17041.
28. J. D. Wolfgang, B. T. White and T. E. Long, *Macromolecular Rapid Communications*, 2021, **42**, 2100163.
29. E. B. Anderson and T. E. Long, *Polymer*, 2010, **51**, 2447-2454.
30. R. Gao, M. Zhang, S.-W. Wang, R. B. Moore, R. H. Colby and T. E. Long, *Macromolecular Chemistry and Physics*, 2013, **214**, 1027-1036.
31. K. Zhang, A. M. Nelson, S. J. Talley, M. Chen, E. Margareta, A. G. Hudson, R. B. Moore and T. E. Long, *Green Chemistry*, 2016, **18**, 4667-4681.
32. J. M. Dennis, L. I. Steinberg, A. M. Pekkanen, J. Maiz, M. Hegde, A. J. Müller and T. E. Long, *Green Chemistry*, 2018, **20**, 243-249.
33. R. A. Sheldon, *Chemical Society Reviews*, 2012, **41**, 1437-1451.
34. M. Ravey and E. M. Pearce, *Journal of Applied Polymer Science*, 1997, **63**, 47-74.
35. N. Yoshitake and M. Furukawa, *Journal of Analytical and Applied Pyrolysis*, 1995, **33**, 269-281.
36. J. O. Akindoyo, M. D. H. Beg, S. Ghazali, M. R. Islam, N. Jeyaratnam and A. R. Yuvaraj, *RSC Advances*, 2016, **6**, 114453-114482.
37. F. A. Milton, M. G. Lacerda, S. B. P. Sinoti, P. G. Mesquita, D. Prakasan, M. S. Coelho, C. L. de Lima, A. G. Martini, G. T. Pazzine, M. d. F. Borin, A. A. Amato and F. d. A. R. Neves, *Frontiers in Pharmacology*, 2017, **8**.
38. S. Zhang, L. Wang, Z. Wang, D. Fan, L. Shi and J. Liu, *Chemosphere*, 2017, **171**, 142-148.
39. A. Farkas and P. F. Strohm, *Industrial & Engineering Chemistry Fundamentals*, 1965, **4**, 32-38.
40. H. Sardon, A. Pascual, D. Mecerreyes, D. Taton, H. Cramail and J. L. Hedrick, *Macromolecules*, 2015, **48**, 3153-3165.

41. X. D. Zhang, C. W. Macosko, H. T. Davis, A. D. Nikolov and D. T. Wasan, *Journal of Colloid and Interface Science*, 1999, **215**, 270-279.

CHAPTER 3 SUPPORTING INFORMATION

CARBAMATE THERMAL DECARBOXYLATION FOR THE DESIGN OF NON- ISOCYANATE POLYURETHANE FOAMS

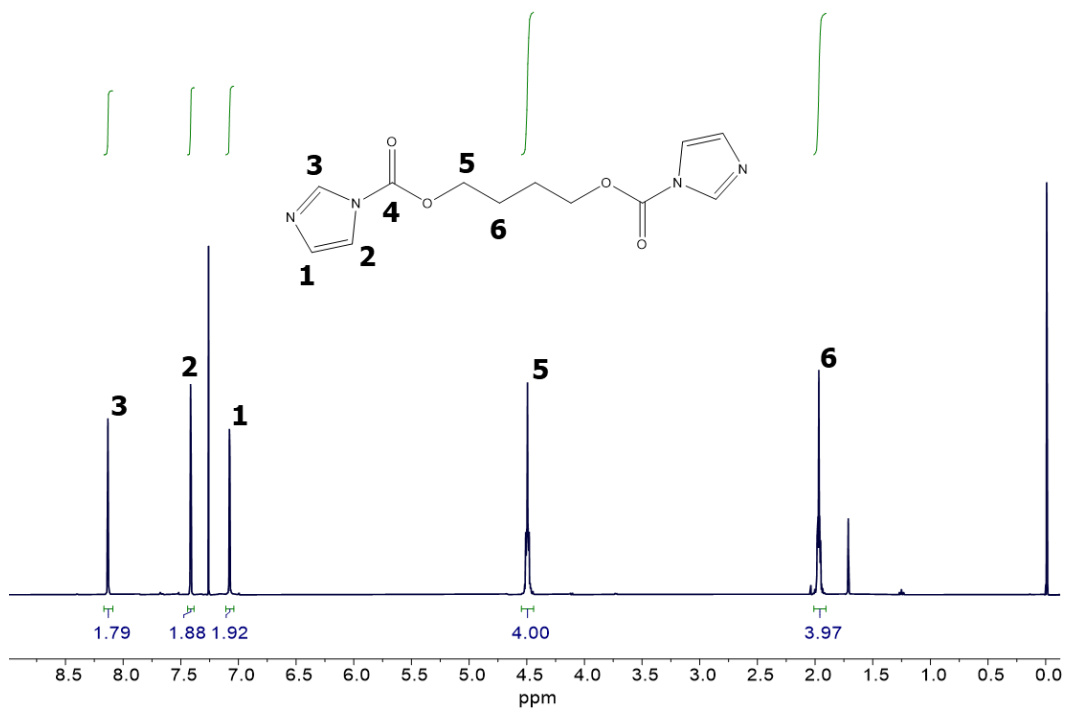


Figure S3.1. ¹H NMR, in CDCl₃, confirmed the structure and purity of the 1,4-butyl(bis-carbonylimidazolide) (1,4-BBCI).

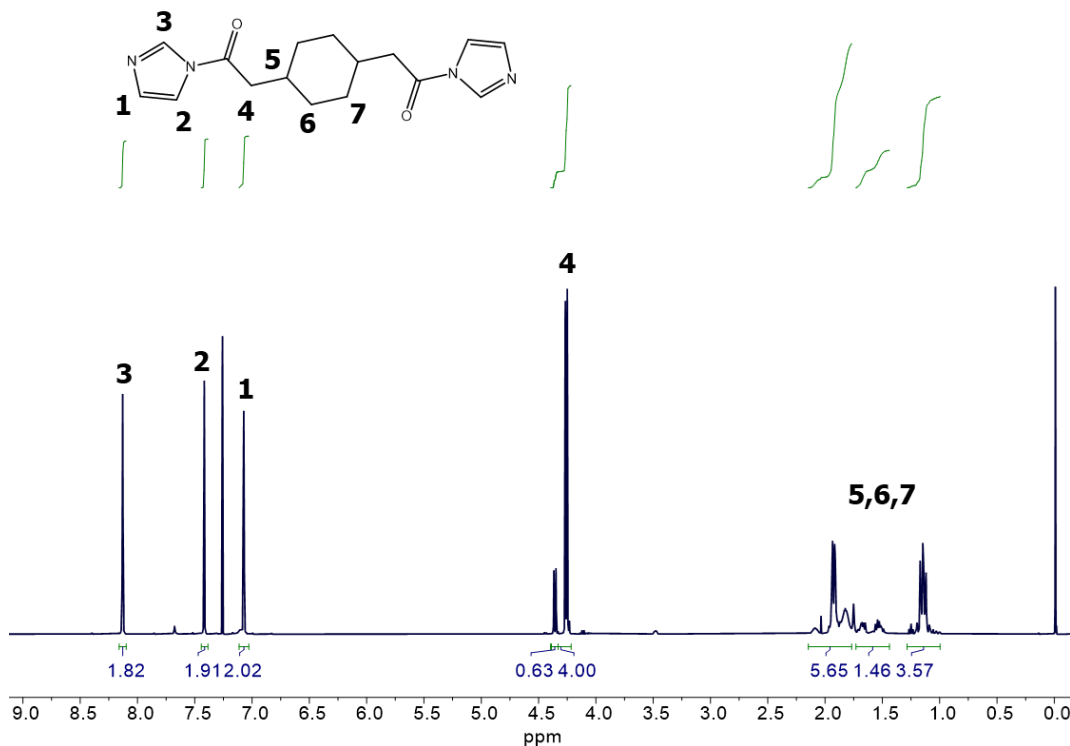


Figure S3.2. ¹H NMR, in CDCl₃, confirmed the structure and purity of the 1,4-cyclohexanedimethanol(bis-carbonylimidazolid) (1,4-CHDMBCI).

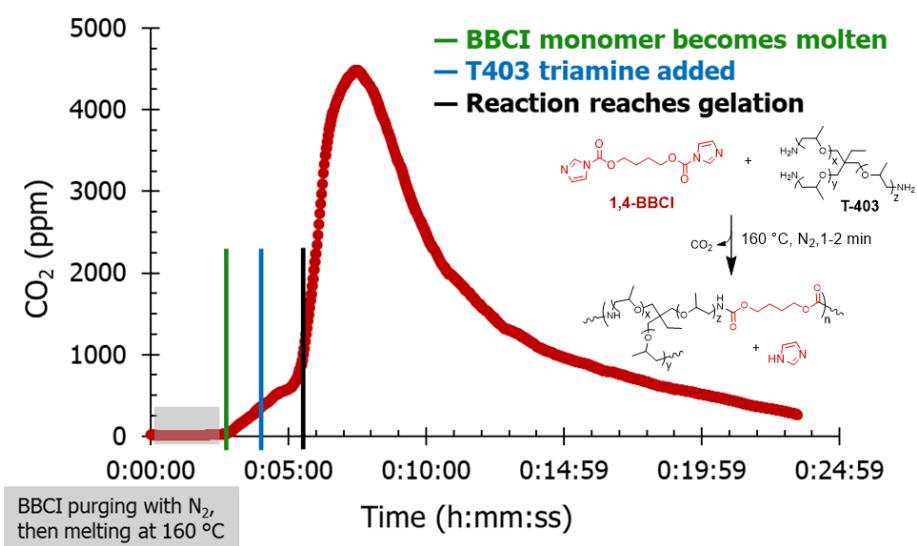


Figure S3.3. CO₂ generation occurred rapidly once monomers were in the melt-state and increased exponentially upon gelation.

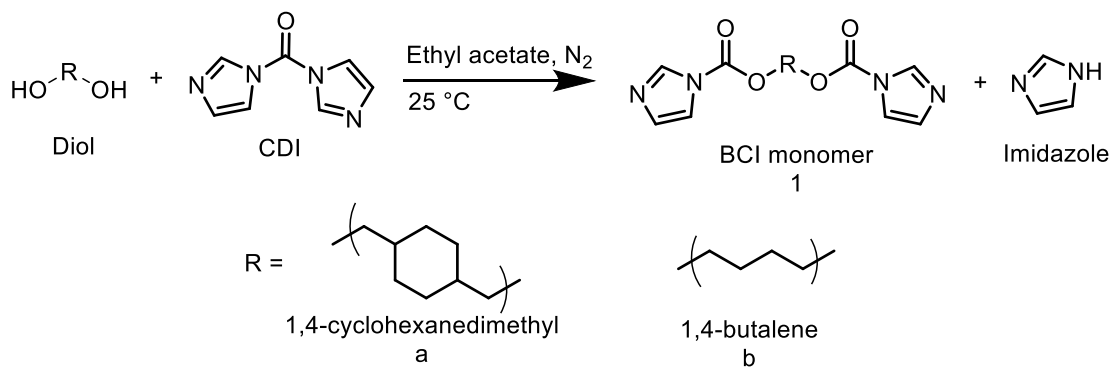


Figure S3.4. Ethyl acetate facilitated high conversion of 1,4-butanediol, **b**, and 1,4-cyclohexanedimethanol, **a**, to 1,4-butyl(bis-carbonylimidazolid) (1,4-BBCI), **1b**, and 1,4-cyclohexanedimethyl(bis-carbonylimidazolid) (1,4-CHDMBCI), **1a**, respectively.

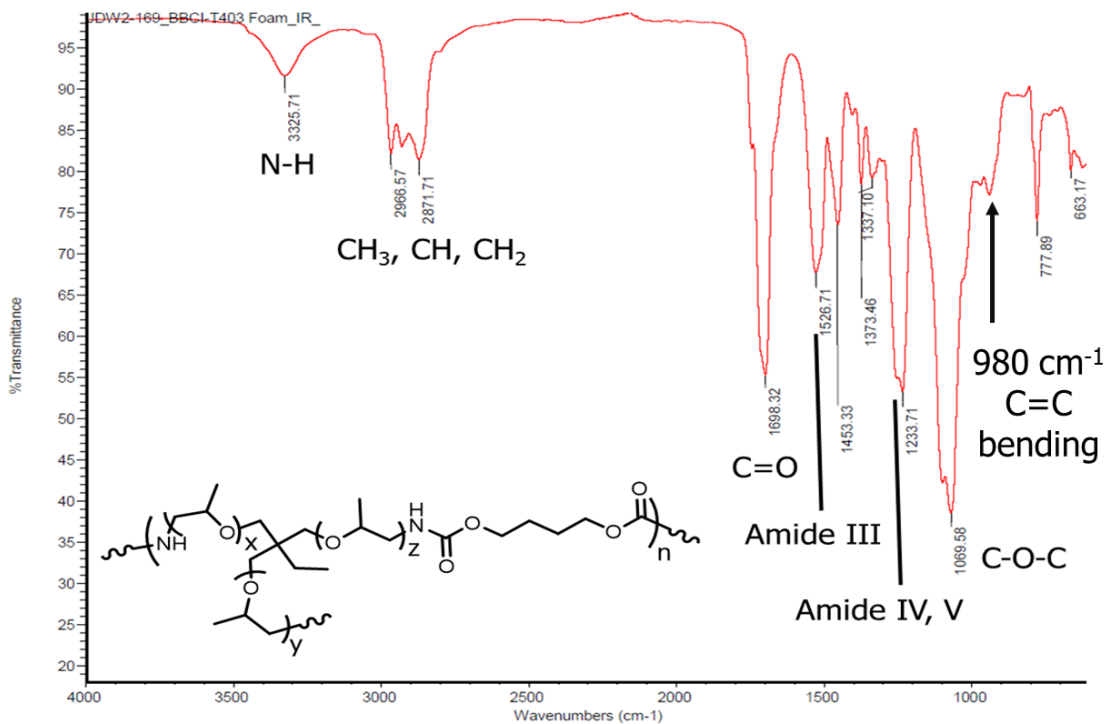


Figure S3.5. ATR-IR confirmed presence of urethane linkages and alkene moieties of PU foams.

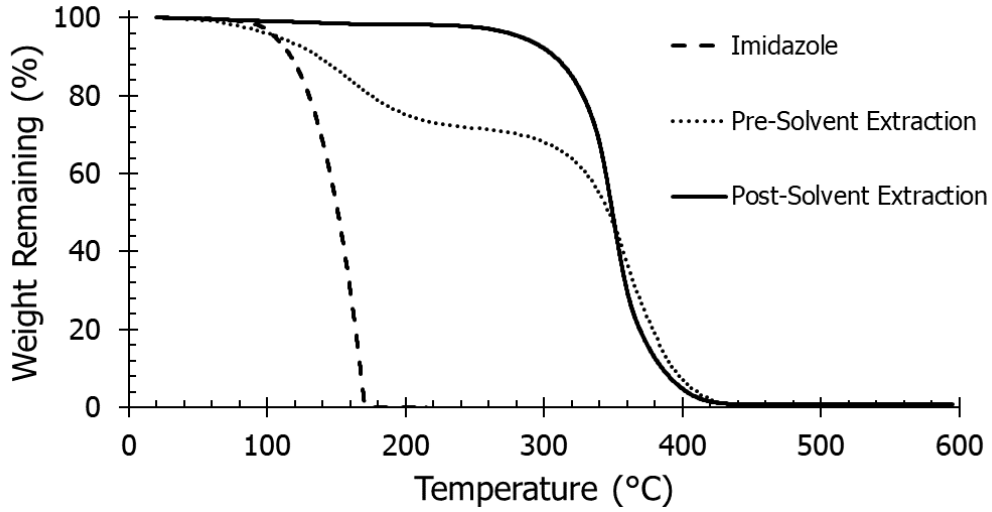


Figure S3.6. TGA temperature ramp experiment with imidazole small molecule (dashed line) and BBCI-MDA:T-403 0:100 PU foam before (dotted line) and after (solid line) solvent extraction.

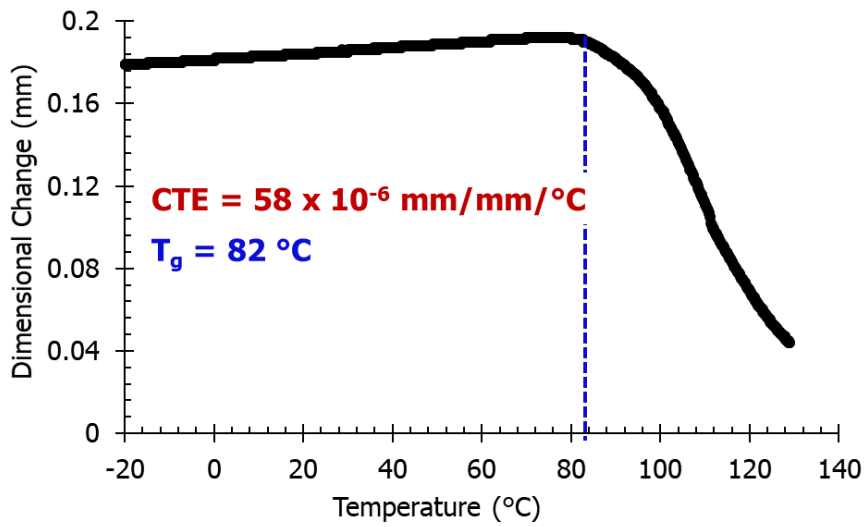


Figure S3.7. Select TMA temperature ramp of BBCI-TADE:T-403 90:10 provided CTE from slope and T_g from onset point.

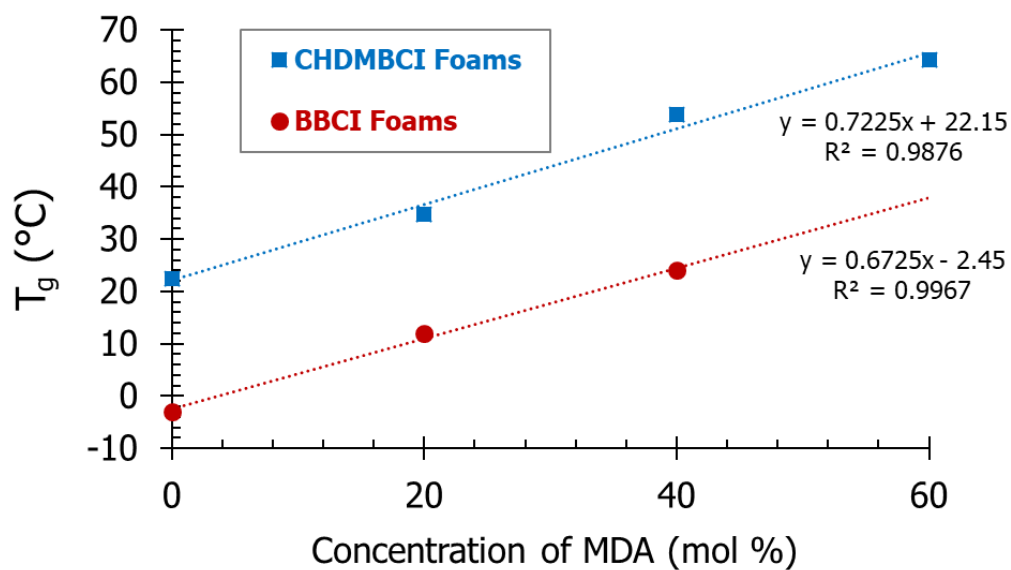


Figure S3.8. DSC analysis indicated that the addition of MDA increased the T_g of T-403-based PU foams.

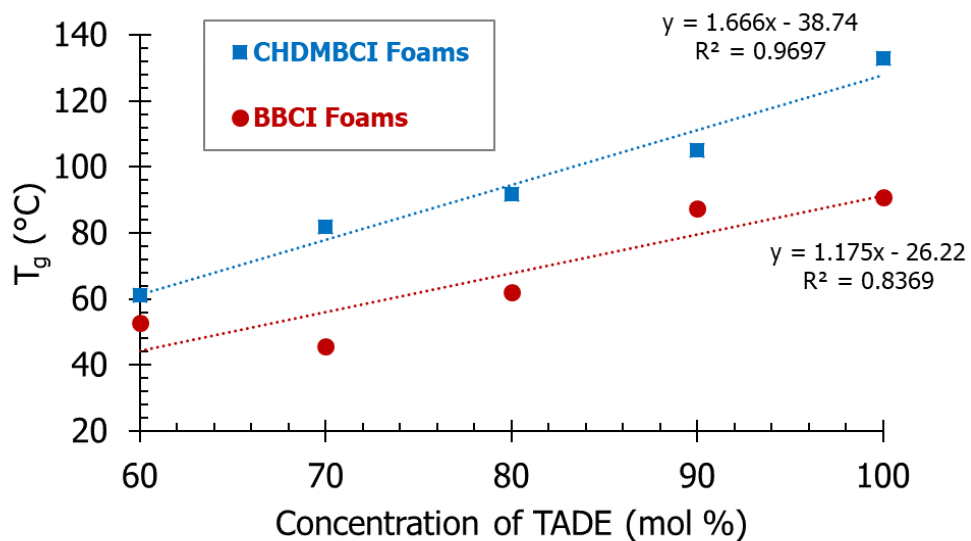


Figure S3.9. The incorporation of T-403 reduced the T_g for TADE-based PU foams according to DSC analysis.

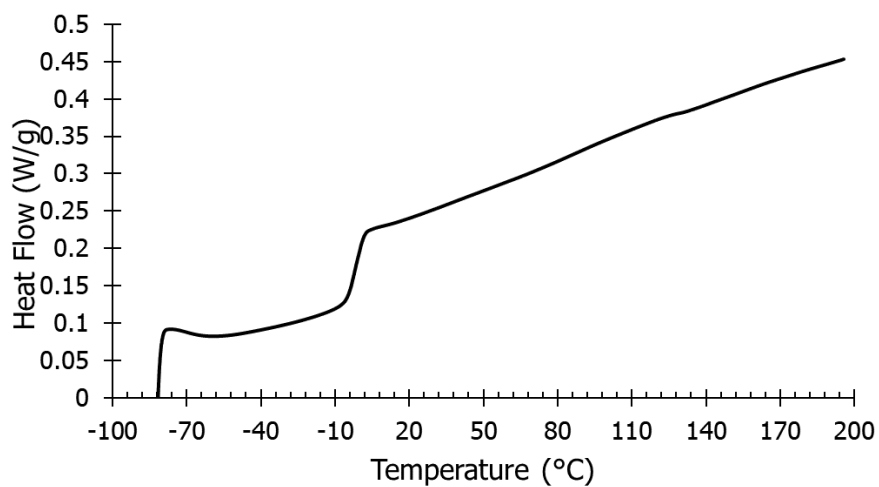


Figure S3.10. Select DSC trace of BBCI-MDA:T-403 0:100 PU foam with an observed T_g of -3 °C.

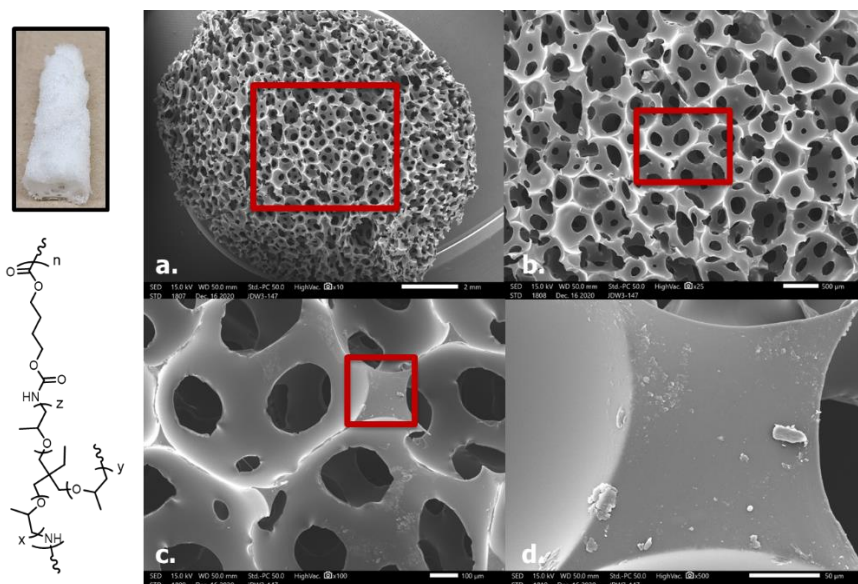


Figure S11. Introduction of surfactant (0.8 wt % Dabco[®] DC193) into BCCI-MDA:T-403 0:100 produced more open cells than without surfactant.

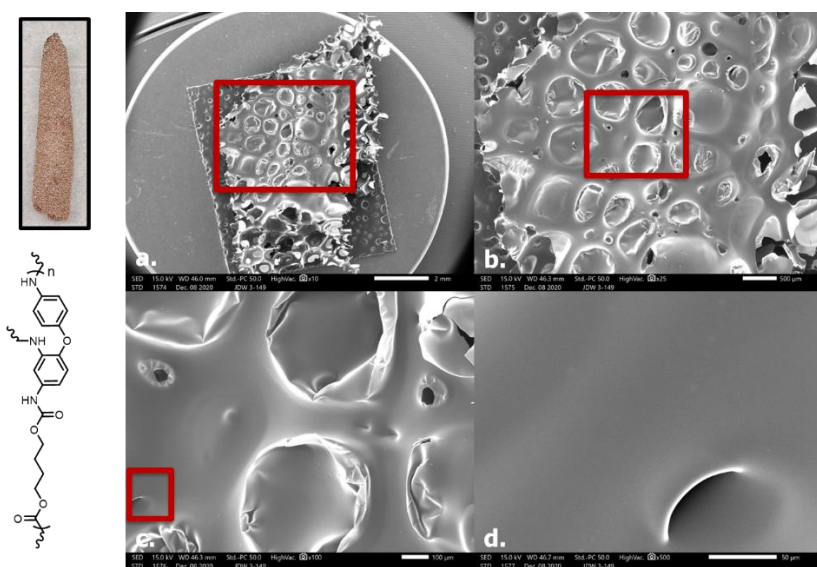


Figure S12. Introduction of surfactant (0.8 wt % Dabco[®] DC193) into BCCI-TADE:T-403 100:0 produced a more homogeneous distribution of cells than without surfactant.

CHAPTER 4

NON-ISOCYANATE POLYURETHANE SEGMENTED COPOLYMERS FROM BIS-CARBONYLIMIDAZOLIDES

4.1 Abstract

Bis-carbonylimidazolidone (BCI) functionalization enabled an efficient synthetic strategy to generate high molecular weight segmented non-isocyanate polyurethanes (NIPUs). Melt phase polymerization of ED-2003 Jeffamine[®], 4,4'-methylenebis(cyclohexylamine), and a BCI monomer that mimics a 1,4-butanediol chain extender enabled polyether NIPUs that contain varying concentrations of hard segments ranging from 40 to 80 wt. %. Dynamic mechanical analysis and differential scanning calorimetry revealed thermal transitions for soft, hard, and mixed phases. Hard segment incorporations between 40 and 60 wt. % displayed up to three distinct phases pertaining to the poly(ethylene glycol) (PEG) soft segment T_g , melting transition, and hard segment T_g , while higher hard segment concentrations prohibited soft segment crystallization, presumably due to restricted molecular mobility from the hard segment. Atomic force microscopy (AFM) allowed for visualization and size determination of nanophase-separated regimes, revealing a nanoscale rod-like assembly of HS. Small-angle x-ray scattering confirmed nanophase separation within the NIPU, characterizing both nanoscale amorphous domains and varying degrees of crystallinity. These NIPUs, which were synthesized with BCI monomers, displayed expected phase separation that is comparable to isocyanate-derived analogues. This work demonstrates nanophase separation in BCI-derived NIPUs and the feasibility of this non-isocyanate synthetic pathway for the preparation of segmented PU copolymers.

4.2 Introduction

Polyurethanes (PUs) enable various technologies due to modular molecular design that provides tunable thermomechanical properties. This modular design empowers versatile applications including coating, adhesive, insulation, textile, and additive manufacturing industries, among others.¹⁻⁴ Covalently bound nanoscale phase separated domains allow for modularity through monomer selection to yield targeted thermomechanical or adhesive properties. Traditionally, PUs leverage rapid kinetics between diverse isocyanates and alcohols in a polyaddition reaction to form urethane bonds linking hard and soft domains.⁵ Immiscibility between hard and soft segments results in nanoscale phase separated domains.^{6,7} The hard segment (HS) imparts physical crosslinking due to dimeric hydrogen bonding, which increases T_g and modulus compared to the adjacent soft segment (SS).^{8,9} Modulation of the chemical structure and concentration of the isocyanate and chain extender provides further control over thermomechanical properties with chain extenders playing a crucial role in driving phase separation.^{10,11} Chain extender symmetry, length, and composition directly correlate to phase separation behavior; critical parameters include rigidity, hydrogen bonding, and packing considerations.^{10,12-15} Conversely, flexible oligomeric polyols comprise the SS to impart flexibility, impact resistance, low temperature performance, and damping properties.¹⁶ Both of these domains are covalently bound through urethane linkages, enabling a unique combination of properties. Thus, fundamental understanding and promoting phase separation in PUs is essential for enhancing thermomechanical performance.

While the polyaddition of isocyanates allows for the efficient formation of hard and soft domains through control of reaction conditions and monomer stoichiometry, growing awareness of environmental and health considerations encouraged exploration of alternative synthetic routes for producing PUs while maintaining their desirable properties.¹⁷⁻¹⁹ The literature pervasive amine-driven ring-opening of cyclic carbonates facilitates the synthesis of linear and crosslinked hydroxy non-isocyanate polyurethanes (NIPUs).²⁰⁻²² This process offers mild reaction conditions and achieves moderate molecular weight, however, without addressing residual pendent hydroxyl groups there exists negative impacts on thermomechanical properties, i.e., increased hydrophilicity and reduced phase separation.^{23,24} Furthermore, achieving control of the pendent hydroxyl, i.e., a primary or secondary alcohol, presents a challenge. Notably, these pendent hydroxyls increase water uptake resulting in plasticization.^{25, 26} Likewise, the hydroxyls screen hydrogen bonding in the HS and increase miscibility between the HS and SS in polyether urethanes, resulting in a decrease of phase separation that produces a deviation from expected thermomechanical performance.²³ Torkelson *et. al.* demonstrated a poly(ethylene glycol) (PEG) SS led to increased phase mixing resulting from hydrogen bonding with pendant hydroxyl groups, while a poly(tetramethylene glycol) (PTMO) SS led to phase separation with a very broad interphase that improved damping, however, is not commonly desired or observed with traditional non-hydroxy PUs.^{23, 27} Several innovative chemistries serve to overcome this disadvantage through careful SS selection or introducing specialty chain extenders.^{23, 28-30} These methods proved effective in achieving nanophase separation for the cyclic carbonate NIPU system, however a facile approach that avoids pendant hydroxyl groups remains desired.

Bis-carbonylimidazolidone (BCI) functionality provides a viable strategy for synthesizing NIPUs while leveraging legacy melt polymerization conditions. This synthesis readily produces both linear and crosslinked architectures and exhibits in-situ CO₂ formation for producing NIPU foams.^{31, 32} The phase separation behavior of BCI-derived NIPU segmented copolymers has not been thoroughly investigated or reported. This manuscript demonstrates phase separation within polyether urethanes synthesized in the absence of isocyanates. Dynamic mechanical analysis (DMA) and differential scanning calorimetry (DSC) evaluated thermal transitions in phase separated NIPUs, while atomic force microscopy (AFM) allowed for surface visualization of hard and soft domain size and shape. Small-angle x-ray scattering (SAXS) enabled characterization of the bulk morphology, providing further understanding of phase separation within these NIPU systems. The results presented expand the scope of knowledge regarding phase separation within BCI-based NIPUs while maintaining traditional PU chemical compositions.

4.3 Experimental Section

4.3.1 Instruments

¹H and ¹³C nuclear magnetic resonance (NMR) spectroscopy utilized a Bruker Avance NEO 500 MHz spectrometer functioning at 500.15 MHz and 23 °C (solution concentration of 10 mg mL⁻¹). A Mel-Temp 1101D digital melting point apparatus operating at 5 °C min⁻¹ provided melting points for the monomer. A ThermoFisher Scientific Nicolet iS10 FTIR spectrometer, with a diamond cell at 25 °C, confirmed PU structure after 64 scans of melt-pressed films. A TA Instruments TGA 5500 facilitated thermogravimetric analysis (TGA) by utilizing a heating rate of 10 °C min⁻¹ from 25 to 600 °C with a steady nitrogen

purge. The $T_{d,5\%}$, or temperature where 5% of the original sample mass loss, served as an indicator for thermal stability of the sample. A TA Instruments DSC 2500 with heat/cool/heat cycles of $10\text{ }^{\circ}\text{C min}^{-1}$ provided differential scanning calorimetry data, where the sample was under a nitrogen environment throughout the experiment. DSC provided the glass transition temperatures (T_g s) from the midpoint of the endothermic transition in the second heat. Compression molding provided thin films by compressing the PU between Mylar sheets at $200\text{ }^{\circ}\text{C}$ on a PHI hydraulic press. McLube Mold Release, a silicone-based mold release agent, ensured facile removal of the PU films. A TA Instruments DMA Q800 with a temperature ramp of $3\text{ }^{\circ}\text{C min}^{-1}$ from $-90\text{ }^{\circ}\text{C}$ to $180\text{ }^{\circ}\text{C}$ at 1 Hz provided a T_g derived from the maximum of the $\tan \delta$. Liquid nitrogen cooling permitted the cryogenic temperatures required to observe the thermal transitions of the PU films. A TA Instruments TGA-SA enabled water uptake measurements between 5% and 95% relative humidity in 5% stepwise increments. A Bruker MultiMode 8-HR enabled atomic force microscopy (AFM) of melt processed NIPU films. AFM samples were prepared by heating NIPUs on an AFM stage, resulting in sample flow and a smooth surface finish upon cooling. Insolubility of these compounds prevented solvent casting or spin coating sample preparation techniques. This instrument leveraged a MikroMasch chromium and gold coated silicon AFM probe operating at 355.952 kHz with a drive amplitude of 24.4 mV. Scans were completed in a 256 by 256 raster pattern with an aspect ratio of 1 for all magnifications.

4.3.2 SAXS/WAXS Measurements

Small- and wide-angle x-ray scattering (SAXS/WAXS) measurements were performed on a Xenocs Xeuss 3.0 SAXS/WAXS instrument. A GeniX3D Cu High Flux Very Long

(HFVL) focus source was used to produce an 8 KeV Cu K alpha collimated X-ray beam with a wavelength of 1.541891 Å (generated at 50 kV and 0.6 mA). A windowless EIGER2 R 1M DECTRIS Hybrid pixel photon counting detector was used to collect the scattering signals at three sample-to-detector distances of 50 mm, 370 mm, and 900 mm (denoted as WAXS, MAXS and SAXS in the Xeuss system) to cover a broad Q range between $\sim 0.05 \text{ nm}^{-1}$ and $\sim 36.37 \text{ nm}^{-1}$ correspond to length scale range between $\sim 0.17 \text{ nm}$ and $\sim 127.61 \text{ nm}$. “High resolution” configuration was used for WAXS with a beam size of 0.4 mm. Measuring time was 30 min for the samples of 40 wt. % HS and 80 wt. % HS, and 1 h for the sample of 60 wt. % HS to account for thickness. “Standard” configuration was used for MAXS with a beam size of 0.7 mm and SAXS with a beam size of 0.5 mm. Larger beam sizes give higher flux for MAXS and SAXS which have longer sample-to-detector distances. For MAXS configuration, measuring time was 40 min for the samples of 40 wt. % HS and 80 wt. % HS, and 1 h 20 min for the sample of 60 wt. % HS. For SAXS configuration, measuring time was 1 h for the samples of 40 wt. % HS and 80 wt. % HS, and 2 h for the sample of 60 wt. % HS. Each raw 2D scattering image was reduced by azimuthal average in 360° to a 1D scattering curve considering geometrical corrections and transmitted intensity. Finally, each 1D scattering curve of sample was subtracted by the corresponding 1D scattering curve of direct beam considering sample thickness (Figure S4.5-4.9). The 2D scattering curves for the SAXS, WAXS, and MAXS display clear isotropic features, where a 5 mm gap between the two detector modules are represented as a black rectangular region.

4.3.3 Materials

1,4-butanediol (>99.0%), 1,1'-carbonyldiimidazole (CDI, >97.0%), and Jeffamine ED-2003 (ED-2003, average $M_n = 1900 \text{ g mol}^{-1}$) were purchased from Sigma Aldrich and stored in a desiccator under reduced pressure. 4,4'-methylenebis(cyclohexylamine) (HMDA, 95%, technical grade) was purchased from Sigma Aldrich and used as received. Ethyl acetate (> 99.5%, ACS grade) was purchased from Fisher Scientific and used as received. Nitrogen gas (99.999% UHP-T) and liquid nitrogen (LC240 22 PSI) were purchased from Praxair Distribution. Deuterated chloroform (CDCl_3) was purchased from Cambridge Isotope Laboratories, Inc. All reagents and solvents were used as received unless stated otherwise.

4.3.4 Synthesis of 1,4-Butyl(bis-carbonylimidazolid) (BBCI)

Synthesis adhered to our previous literature procedure.^{31, 32} 1,4-butanediol (27.04 g, 0.3 mol) was added to a three-necked, 1 L round-bottomed flask outfitted with a magnetic stir bar, nitrogen inlet, nitrogen outlet, and rubber septa. 1,4-butanediol was dissolved in ethyl acetate (600 mL) at 25 °C for 10 min under a nitrogen purge. 1,1'-carbonyldiimidazole (CDI) (121.61 g, 0.7 mol) was added to the flask in partitions to allow for even mixing and to reduce the propensity for cyclization. The initial ~60 g of CDI dissolved readily in the solvent, producing a transparent and colorless solution. CDI solution saturation and product formation resulted in a turbid, white slurry. An additional 60 mL of ethyl acetate was added to ensure reagents were well mixed. The reaction was allowed to proceed for ~2 h prior to filtration using a fritted funnel. The white powder was washed twice with ethyl acetate to remove byproducts (500 mL total) and dried at 60 °C and ~25 mmHg for 18 h. The final isolated yield was > 90% with a melting point range of 138-140 °C. $^1\text{H NMR}$ (CDCl_3 , δ)

8.13-8.14 (t, 2H, 3), 7.41-7.42 (t, 2H, 2), 7.07-7.08 (m, 2H, 1), 4.47-4.51 (t, 4H, 5) 1.95-2.00 (m, 4H, 6).

4.3.5 Synthesis of Phase Separated NIPUs

Synthesis of the phase separated NIPUs utilized melt polycondensation conditions similar to conventional polyester reactors. ED-2003, BBCI, and HMDA were degassed and dried at reduced pressure at 80 °C for 12 h prior to reacting. Stoichiometric equivalents of BBCI, ED-2003, and HMDA were added to a 100 mL round-bottomed flask with a glass t-neck adapter, metal stir rod, and glass stir rod adapter. A distillation arm was connected to collect the imidazole condensate. An overhead mechanical stirrer enabled mixing. The stoichiometry of BBCI to diamine (ED-2003 and HMDA) was maintained at a 1:1 molar ratio for all NIPU compositions. The stoichiometry of ED-2003 and HMDA were modulated to tune HS wt. % such that the final mass of BBCI after imidazole loss and HMDA comprised the HS, and ED-2003 comprised the SS. An exemplary synthetic stoichiometry for the 60 wt. % hard segment NIPU is as follows: 4.5 g (2.3 mmol) of ED-2003 Jeffamine[®], 6.27 g (22.5 mmol) of BBCI (wherein imidazole accounts for 3.07 g of the BBCI used and is therefore not included in HS calculations), and 4.23 g (20.2 mmol) are added to a round-bottomed flask. The first step of the reaction was completed under a nitrogen environment to build molecular weight and decrease reactant volatility, then vacuum was introduced to remove the imidazole condensate and promote reaction progress, as shown in **Figure 4.1**. Yields for all NIPUs ranged from 94-97 % due to transfer loss of product as it was extracted from the round bottom.

4.4 Results and Discussion

A facile, one-pot synthesis comprising of BBCI, HMDA, and ED-2003 Jeffamine® synthesized a series of phase separated NIPUs. The ED-2003 Jeffamine® contains a triblock topology where $m = 39$ repeating units and the sum of n and $l = 6$ repeating units, resulting in a majority PEG backbone. A reaction temperature of 120 °C ensured melting of all reagents for homogenous mixing in the absence of solvent. Additionally, the lower molecular weight of HMDA compared to ED-2003 resulted in the preferential reaction of BBCI and HMDA to form HS units prior to ED-2003 addition. Previous PU literature describes similar phenomenon when utilizing the “one-shot” synthetic method.⁴ Furthermore, the introduction of reduced pressure to the reaction promoted molecular weight increase due to the efficient removal of the imidazole condensate. Tuning the stoichiometry of HMDA and ED-2003 enabled control over HS and SS concentration with BBCI and HMDA comprising the HS and ED-2003 comprising the SS.

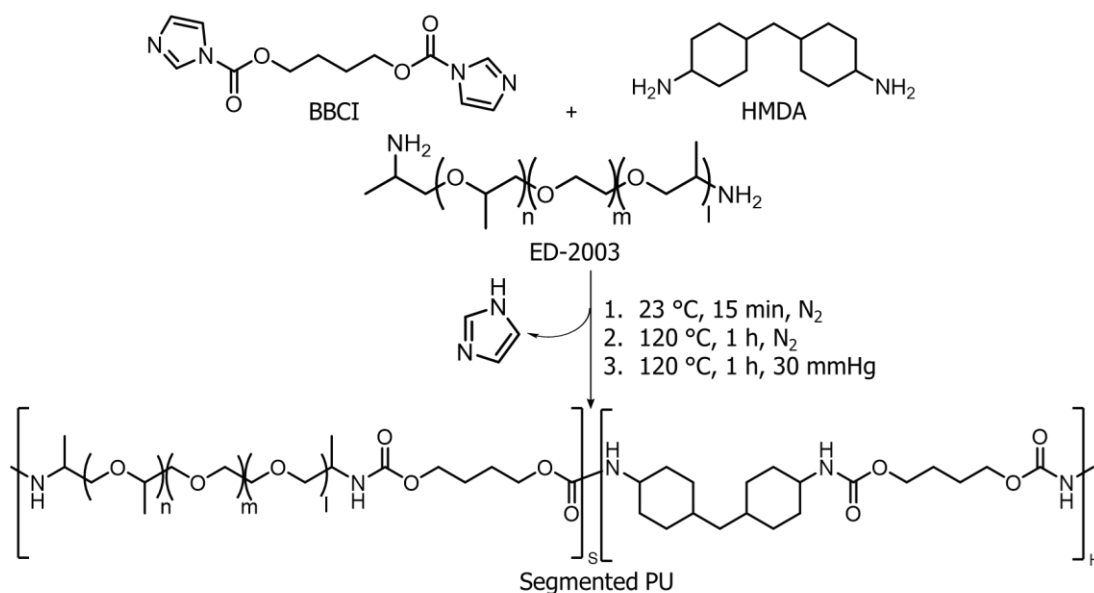


Figure 4.1. Synthetic strategy for the preparation of NIPU segmented copolymers. A one-pot synthesis comprising diverse amines with BBCI enabled efficient formation of phase separated NIPUs.

DMA probed thermal transitions present in melt-pressed NIPU films. All NIPU compositions achieved a storage modulus greater >2 GPa below the lowest T_g value, however exhibited varied transitions aligning with HS concentration upon heating, shown in **Figure 4.2**. As expected, as HS concentration increased, the storage modulus value loss attributed to the SS T_g decreased. This result aligned with expectations in nanophase-separated PU systems that contain different concentrations of structural HS. Additionally, a $\tan \delta$ maxima at 20°C present in the 40 wt. % HS (Figure S4) corresponded to melting of semi-crystalline PEG, confirmed by the presence of a sharp endothermic peak in the DSC trace. While a lower T_m than traditionally observed for PEG, propylene oxide repeating units between the PEG backbone and urethane linkage explained a lower T_m as compared to the T_m of pure PEG. Notably, this melting transition intensity decreased with increasing HS concentration, presumably due to smaller PEG domains that limit crystal formation, or a lower overall concentration of SS. The 60 wt. % HS sample displayed a melting transition with DMA that overlapped slightly with HS T_g , however possessed an independent, sharp melting endotherm in DSC data that decoupled these transitions. A lower ultimate T_g for the 60 wt. % HS sample suggested a degree of phase mixing between the HS and SS. This contrasted to the 40 wt. % sample, which displayed an elevated ultimate T_g , which was not expected due to a greater concentration of SS. However, a larger degree of phase separation that resulted in more uniform HS domains supported this elevated T_g and was further supported by SAXS scattering data that revealed a decrease in

domain size dispersity for the 40 wt. % HS sample. As expected, the 80 wt. % HS sample maintained the highest HS T_g , and additionally displayed the absence of a melting transition in both the DMA and DSC traces. $\tan \delta$ analysis of this sample indicated a small PEG T_g followed by an intense transition at 40 °C, belonging to a rigid amorphous T_g that was likely due to restricted rotation of the PEG segments adjacent to the HS. Rigid amorphous regions, which exist bound to the rigid HS, extend several nanometers into the polymer amorphous SS region.³³ This interphase size, coupled with SAXS analysis that displays interdomain spacing on the order of 6.8 nm, implies in the formation a substantial rigid amorphous region compared to the mobile amorphous domain elucidated in the -56 °C DMA transition for the 80 wt. % HS sample. SSs and HSs within the PU matrix are covalently attached, resulting in good interfacial relations between the SS and HS, further explaining the phenomenon of the rigid amorphous glass transition temperature, as the amorphous polymer is immobilized on the surface of the “filler” HS that exists below the T_g which acts as a glassy, supporting region.^{34, 35} Additional evidence for the appearance of a rigid amorphous region stems from the disappearance of PEG melting endotherms for the 80 wt. % HS sample, signaling the disappearance of PEG crystallites in the NIPU matrix. The disappearance of PEG crystallites resulting from an increase in filler concentration in PU composite systems is well-documented in prior literature, as the constraint of PEG domains results in an increase in the rigid amorphous PU fraction and decrease in PEG crystallites.³³ The distinct transitions present in all NIPU compositions arose from nanoscale phase separation, which is in sharp contrast to previously reported properties belonging to poly(hydroxyurethane) (PHU)-derived NIPUs that contain PEG SSs, where earlier literature reported T_g values below room temperature due to phase

mixing.²³ This was attributed to the absence of pendent hydroxyl groups in the HS, which presented challenges for phase separation analogous to traditional isocyanate-derived PUs. BCI monomers produce NIPUs that maintain structural similarity to conventional PUs, thus resulting in more well-defined thermomechanical properties without additional synthetic complexity.^{12, 14} Likewise, this resulted in reduced water uptake of BCI NIPUs compared to PHUs; the NIPUs in this study displayed a maximum water uptake of ~1 wt. % compared to ~8 wt. % for literature PHUs (Figure S4.2).²⁶

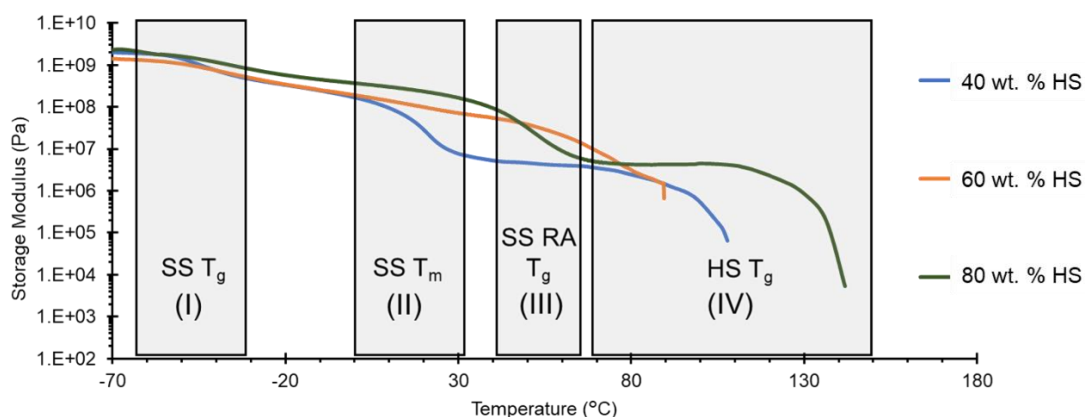


Figure 4.2. DMA reveals thermal transitions for all NIPU compositions, demonstrating the influence of HS concentration on thermomechanical behavior. Tan δ maxima provided thermal transition temperatures including SS T_g , SS T_m , SS rigid amorphous (RA) T_g , and HS T_g .

DSC traces corroborated DMA thermal transitions and provided further insight into the nature of the transitions observed, as shown in **Figure 4.3**. Melting endotherms at 22 °C in both the 40 and 60 wt. % HS NIPUs confirmed modulus loss due to melting as opposed to a phase mixed T_g . Additionally, the decrease in melt enthalpy between the 40 and 60 wt.

% HS samples correlated this melting behavior to PEG SS content, further suggesting that melting was due to PEG crystallites in the NIPU matrix. Likewise, the melting endotherm was absent in the 80 wt. % HS sample, presumably due to the decreased PEG domain size.

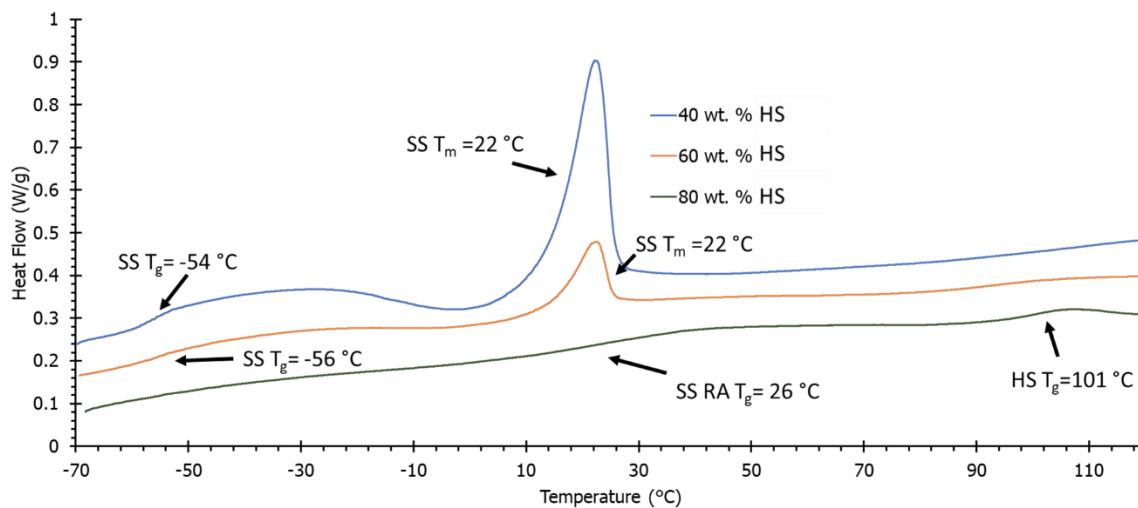


Figure 4.3 DSC traces provided further insights to DMA transitions by characterizing melting point endotherms.

ATR-FTIR spectroscopy enabled further investigations into the relative phase separation of these NIPU systems. Various investigations explore the effect of hydrogen bonding on C=O resonance frequencies within phase separated PU systems that change as a function of hydrogen bonding.³⁶⁻³⁸ “Free” urethane carbonyls without strong dimeric hydrogen bonding present at higher wavenumbers ($\sim 1730\text{-}1700\text{ cm}^{-1}$), dependent on the type of isocyanate (aliphatic or aromatic). Conversely, hydrogen-bonded carbonyls resonate at lower wavenumbers ($\sim 1700\text{-}1650\text{ cm}^{-1}$), depending on the selected isocyanate chemistry or level of carbonyl ordering. Therefore, FTIR analysis enabled a comparison between the 40, 60, and 80 wt. % HS samples. Theory predicts an increase in the relative intensities of hydrogen-bonded urethane carbonyls as HS concentration increases resulting from a

greater concentration of urethane linkages present along the polymer backbone.³⁹ Likewise, an increase in HS concentration results in a decrease in “free” carbonyls resulting from a phase mixed environment. **Figure 4.4** displays the relevant carbonyl region for all synthesized NIPUs, revealing trends that align with literature precedence. Notably, the relative intensity of hydrogen-bonded carbonyls to “free” carbonyls increased as a function of HS concentration. These results aligned with DMA data that displayed a higher plateau modulus as HS concentration increased, resulting from structural, hydrogen-bonded urethane linkages.

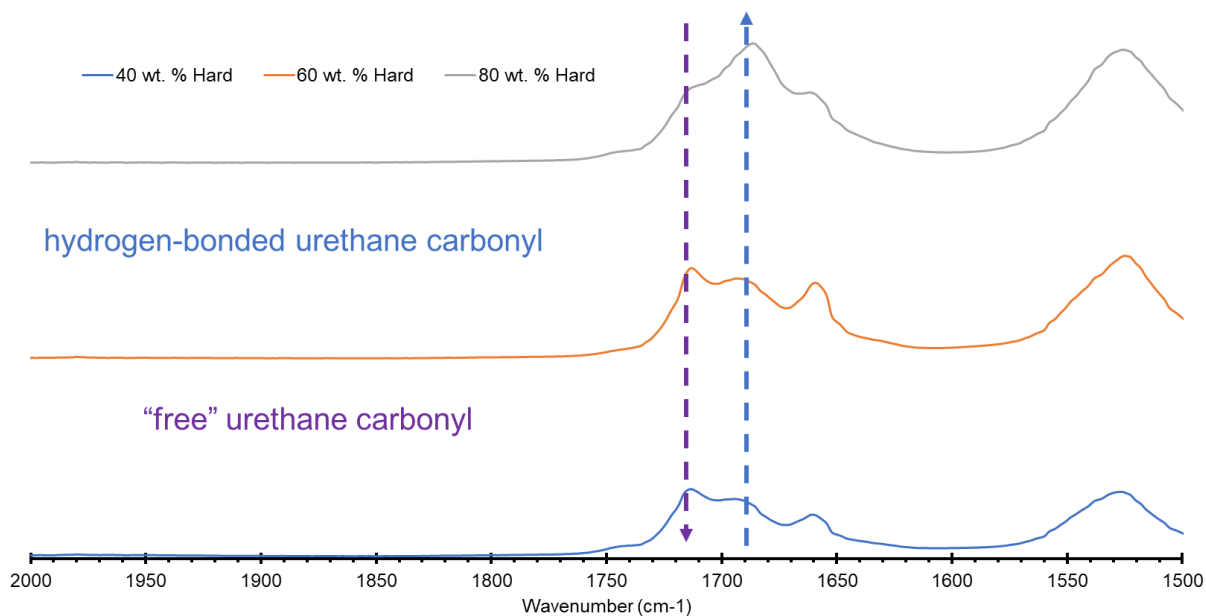


Figure 4.4 ATR-FTIR spectroscopy reveals an increase in hydrogen-bonded carbonyls as a function of HS wt. % concentration.

As previously discussed, nanoscale domains display distinct thermomechanical and chemical properties and are probed with a complement of spectroscopic and physical

characterization techniques. SAXS and WAXS allowed for measurement of the bulk morphology present in melt-pressed NIPU films.⁴⁰ **Figure 4.5** displays the SAXS scattering profiles of all NIPUs. Peaks in the scattered intensity revealed nanophase separation for all samples and Lorentzian peak fitting and power law fitting were done in the SAXS region for each sample separately. The peak center shifted from 0.63 nm^{-1} to 0.94 nm^{-1} with increasing concentration of HS, corresponding to the decrease of length scale from 9.91 nm to 6.68 nm. This indicated that the average domain size in NIPUs containing a larger concentration of HS were on average smaller. Additionally, the decrease of peak height with increasing concentration of HS revealed an increased dispersity of all domain sizes. The increase of full width half maximum (FWHM) from 0.53 nm^{-1} to 0.83 nm^{-1} showed a wider distribution of domain sizes resulting from the increase in HS concentration. The power law exponent, or the slope of the curves at low Q, displayed no significant change between samples, while the intensity at low Q was the highest for the sample with intermediate HS concentration at 60 wt. %. The enhanced complex surface scattering between HS and SS further suggested that the 60 wt. % HS sample contained the most amount of interfacial area, however was comparable with the other samples tested. While domain size dispersity increased with SS loading, the FWHM values displayed a lower dispersity as compared to previously published PHUs and are on the size order for previously reported isocyanate analogues.^{23, 27, 41} This result arises from the structural similarity between BCI NIPUs and isocyanate-derived PUs, which displayed well-understood SS and HS incompatibility leading to more well-defined phase separation. Additionally, WAXS displayed a shift in the peak towards lower Q values, indicating larger d-spacing as HS is increased (figure S5).

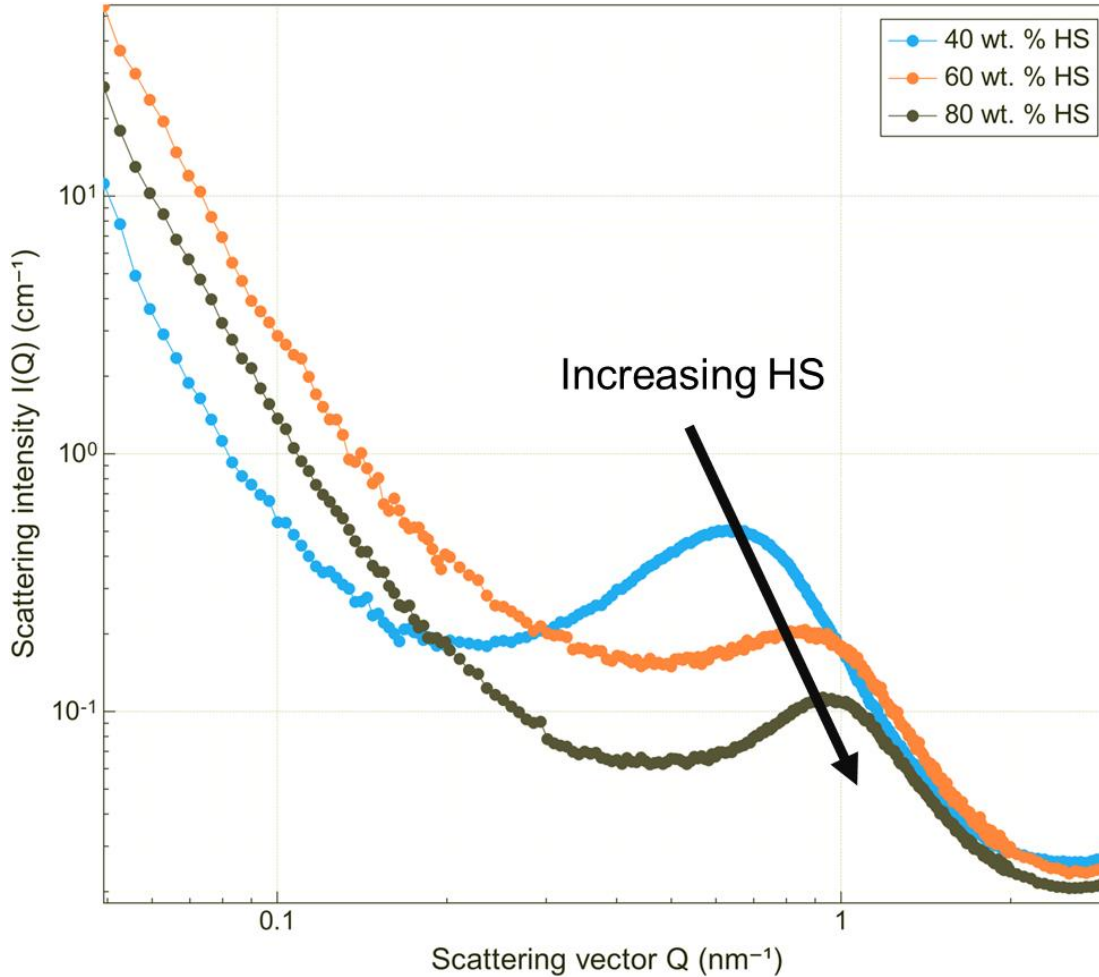


Figure 4.5 SAXS scattering patterns revealed the presence of discrete phases at the nanoscale for all NIPU compositions.

AFM analysis of PU surface phase separation provides extensive literature precedence for the visualization of this phenomenon.^{12, 15, 42} SAXS measurements also characterize domain sizing, however additional shape data from AFM analysis proves useful when visualizing these domains. Tapping mode analysis enabled phase angle measurement across the sample surface, which can be indicative of surface modulus values, however is also influenced by electrostatic interactions that may present as aberrations in the AFM

micrograph (Figure S3). SS and HS domains possess different moduli due to differing T_g values at room temperature, producing a corresponding change to phase angles across the surface. This resulted in AFM traces that clearly displayed phase separation in all samples, as depicted in **Figure 4.6**. The higher modulus HS domains appeared as linearly growing rods (lighter color), while the SS was dispersed throughout. Previous literature predicts an interconnected HS network at HS concentrations above 25 wt. % due to volume fraction considerations, apparent in all tested samples (Figure S4.3).¹⁴ Overall, AFM displayed expected nanophase separation behavior similar to traditional PUs, however, utilizing an isocyanate-free synthetic pathway. Likewise, surface characterization with AFM aligns with bulk SAXS analysis and DMA thermomechanical evaluation, strongly suggesting the appearance of nano-scale phase separated domains within all synthesized NIPUs possessing PEG SSs.

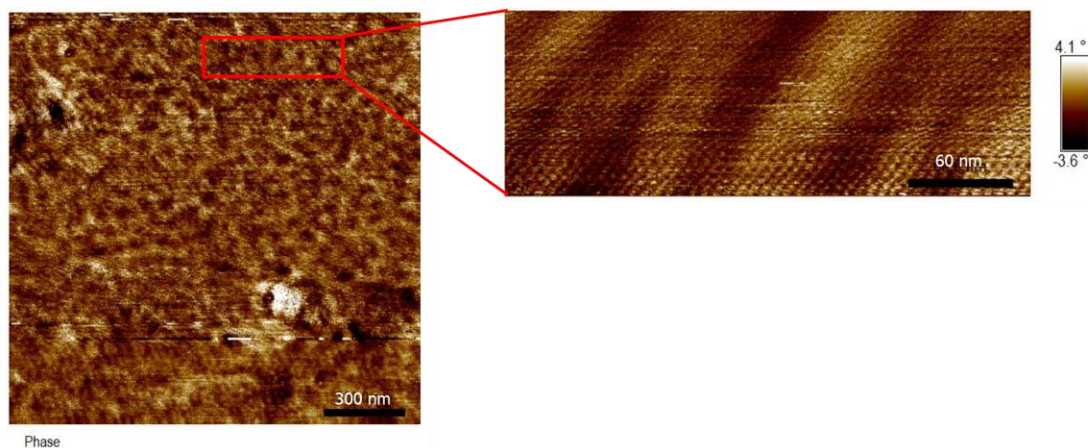


Figure 4.6 A representative AFM trace of the 60 wt. % HS sample revealed nanoscale phase separation within synthesized NIPUs. Lighter regions correspond to HS rods, while darker regimes outline the SS.

4.5 Conclusions

BCI chemistry enabled the synthesis of phase separated NIPUs utilizing a melt polycondensation reaction. The absence of pendant hydroxyl groups resulted in well-defined phase separation behavior within the investigated NIPUs. Likewise, BCI chemistry leveraged modern, isocyanate-, solvent-, and catalyst- free reaction conditions. DMA and DSC characterized thermomechanical performance, allowing for the identification of discrete segments within the NIPU matrix. Both 40 and 60 wt. % HS NIPUs displayed PEG T_g s and crystalline melting peaks, while the 80 wt. % HS sample offered increased HS T_g . AFM revealed phase separation in all compositions containing nanometer domain spacing of melt-processed film surfaces. SAXS measurements further confirmed nanometer domain sizing of the NIPU bulk. This investigation addresses concerns for the negative effects of PHU pendant hydroxyls on nanophase separation, while maintaining an isocyanate-free synthetic pathway. Further investigations into diverse SS and HS compositions will synthesize a library of phase separated NIPUs obtained without the use of isocyanates or presence of pendant hydroxyl groups.

4.6 Acknowledgements

The authors would like to acknowledge the National Science Foundation Emerging Frontiers in Research and Innovation (grant No. E3P-2132183) for funding. We would also like to acknowledge the Eyring Materials Center and ASU Biodesign Institute for their contribution to this work.

4.7 Funding

This work was funded by the ASU Biodesign Institute and NSF.

4.8 References

1. Somarathna, H. M. C. C.; Raman, S. N.; Mohotti, D.; Mutalib, A. A.; Badri, K. H., The use of polyurethane for structural and infrastructural engineering applications: A state-of-the-art review. *Construction and Building Materials* **2018**, *190*, 995-1014.
2. Akindoyo, J. O.; Beg, M. D. H.; Ghazali, S.; Islam, M. R.; Jeyaratnam, N.; Yuvaraj, A. R., Polyurethane types, synthesis and applications – a review. *RSC Advances* **2016**, *6* (115), 114453-114482.
3. Gama, N. V.; Ferreira, A.; Barros-Timmons, A., Polyurethane Foams: Past, Present, and Future. *Materials* **2018**, *11* (10), 1841.
4. Szycher, M., *Szycher's Handbook of Polyurethanes, First Edition*. Taylor & Francis: 1999.
5. Delebecq, E.; Pascault, J.-P.; Boutevin, B.; Ganachaud, F., On the Versatility of Urethane/Urea Bonds: Reversibility, Blocked Isocyanate, and Non-isocyanate Polyurethane. *Chemical Reviews* **2013**, *113* (1), 80-118.
6. Yilgör, I.; Yilgör, E.; Wilkes, G. L., Critical parameters in designing segmented polyurethanes and their effect on morphology and properties: A comprehensive review. *Polymer* **2015**, *58*, A1-A36.
7. Kwei, T. K., Phase separation in segmented polyurethanes. *Journal of Applied Polymer Science* **1982**, *27* (8), 2891-2899.
8. Miller, J. A.; Lin, S. B.; Hwang, K. K. S.; Wu, K. S.; Gibson, P. E.; Cooper, S. L., Properties of polyether-polyurethane block copolymers: effects of hard segment length distribution. *Macromolecules* **1985**, *18* (1), 32-44.
9. O'Sickey, M. J.; Lawrey, B. D.; Wilkes, G. L., Structure–property relationships of poly(urethane-urea)s with ultralow monol content poly(propylene glycol) soft

- segments. III. influence of mixed soft segments of ultralow monol poly(propylene glycol), poly(tetramethylene ether glycol), and tri(propylene glycol). *Journal of Applied Polymer Science* **2003**, 89 (13), 3520-3529.
10. Pourmohammadi-Mahunaki, M.; Haddadi-Asl, V.; Roghani-Mamaqani, H.; Koosha, M.; Yazdi, M., Effect of chain extender length and molecular architecture on phase separation and rheological properties of ether-based polyurethanes. *Polymer Bulletin* **2022**, 79 (10), 8653-8668.
11. Stribeck, A.; Pöselt, E.; Eling, B.; Jokari-Sheshdeh, F.; Hoell, A., Thermoplastic Polyurethanes with varying hard-segment components. Mechanical performance and a filler-crosslink conversion of hard domains as monitored by SAXS. *European Polymer Journal* **2017**, 94.
12. Aneja, A.; Wilkes, G. L., A systematic series of 'model' PTMO based segmented polyurethanes reinvestigated using atomic force microscopy. *Polymer* **2003**, 44 (23), 7221-7228.
13. Blackwell, J.; Nagarajan, M. R.; Hoitink, T. B., Structure of polyurethane elastomers: effect of chain extender length on the structure of MDI/diol hard segments. *Polymer* **1982**, 23 (7), 950-956.
14. Abouzahr, S.; Wilkes, G. L.; Ophir, Z., Structure-property behaviour of segmented polyether-MDI-butanediol based urethanes: effect of composition ratio. *Polymer* **1982**, 23 (7), 1077-1086.
15. Sheth, J. P.; Aneja, A.; Wilkes, G. L.; Yilgor, E.; Atilla, G. E.; Yilgor, I.; Beyer, F. L., Influence of system variables on the morphological and dynamic

- mechanical behavior of polydimethylsiloxane based segmented polyurethane and polyurea copolymers: a comparative perspective. *Polymer* **2004**, *45* (20), 6919-6932.
16. Gisselält, K.; Helgee, B., Effect of Soft Segment Length and Chain Extender Structure on Phase Separation and Morphology in Poly(urethane urea)s. *Macromolecular Materials and Engineering* **2003**, *288* (3), 265-271.
17. Zapp, J. A., Jr., Hazards of Isocyanates in Polyurethane Foam Plastic Production. *Arch. Indust. Health* **1957**, *15* (4), 324-30.
18. Liu, G.; Wu, G.; Huo, S.; Jin, C.; Kong, Z., Synthesis and properties of non-isocyanate polyurethane coatings derived from cyclic carbonate-functionalized polysiloxanes. *Progress in Organic Coatings* **2017**, *112*, 169-175.
19. Zhang, K.; Nelson, A. M.; Talley, S. J.; Chen, M.; Margareta, E.; Hudson, A. G.; Moore, R. B.; Long, T. E., Non-isocyanate poly(amide-hydroxyurethane)s from sustainable resources. *Green Chemistry* **2016**, *18* (17), 4667-4681.
20. Gomez-Lopez, A.; Elizalde, F.; Calvo, I.; Sardon, H., Trends in non-isocyanate polyurethane (NIPU) development. *Chemical Communications* **2021**, *57* (92), 12254-12265.
21. Tomita, H.; Sanda, F.; Endo, T., Model reaction for the synthesis of polyhydroxyurethanes from cyclic carbonates with amines: Substituent effect on the reactivity and selectivity of ring-opening direction in the reaction of five-membered cyclic carbonates with amine. *Journal of Polymer Science Part A: Polymer Chemistry* **2001**, *39* (21), 3678-3685.
22. Blattmann, H.; Fleischer, M.; Bähr, M.; Mülhaupt, R., Isocyanate- and Phosgene-Free Routes to Polyfunctional Cyclic Carbonates and Green Polyurethanes by

Fixation of Carbon Dioxide. *Macromolecular Rapid Communications* **2014**, 35 (14), 1238-1254.

23. Leitsch, E. K.; Beniah, G.; Liu, K.; Lan, T.; Heath, W. H.; Scheidt, K. A.; Torkelson, J. M., Nonisocyanate Thermoplastic Polyhydroxyurethane Elastomers via Cyclic Carbonate Aminolysis: Critical Role of Hydroxyl Groups in Controlling Nanophase Separation. *ACS Macro Letters* **2016**, 5 (4), 424-429.

24. Besse, V.; Camara, F.; Méchin, F.; Fleury, E.; Caillol, S.; Pascault, J.-P.; Boutevin, B., How to explain low molar masses in PolyHydroxyUrethanes (PHUs). *European Polymer Journal* **2015**, 71, 1-11.

25. Kotanen, S.; Poikelispää, M.; Efimov, A.; Harjunalanen, T.; Mills, C.; Laaksonen, T.; Sarlin, E., Hydrolytic stability of polyurethane/polyhydroxyurethane hybrid adhesives. *International Journal of Adhesion and Adhesives* **2021**, 110, 102950.

26. Frias, C. F.; Fonseca, A. C.; Coelho, J. F. J.; Serra, A. C., Crosslinked poly(hydroxyurethane) films from biobased carbonates: Structure-properties relationships and the influence of moisture in the mechanical properties. *Progress in Organic Coatings* **2024**, 187, 108100.

27. Beniah, G.; Liu, K.; Heath, W. H.; Miller, M. D.; Scheidt, K. A.; Torkelson, J. M., Novel thermoplastic polyhydroxyurethane elastomers as effective damping materials over broad temperature ranges. *European Polymer Journal* **2016**, 84, 770-783.

28. Bossion, A.; Aguirresarobe, R. H.; Irusta, L.; Taton, D.; Cramail, H.; Grau, E.; Mecerreyes, D.; Su, C.; Liu, G.; Müller, A. J.; Sardon, H., Unexpected Synthesis of Segmented Poly(hydroxyurea-urethane)s from Dicyclic Carbonates and Diamines by Organocatalysis. *Macromolecules* **2018**, 51 (15), 5556-5566.

29. Hu, S.; Chen, X.; Torkelson, J. M., Isocyanate-free, thermoplastic polyhydroxyurethane elastomers designed for cold temperatures: Influence of PDMS soft-segment chain length and hard-segment content. *Polymer* **2022**, *256*, 125251.
30. Beniah, G.; Fortman, D. J.; Heath, W. H.; Dichtel, W. R.; Torkelson, J. M., Non-Isocyanate Polyurethane Thermoplastic Elastomer: Amide-Based Chain Extender Yields Enhanced Nanophase Separation and Properties in Polyhydroxyurethane. *Macromolecules* **2017**, *50* (11), 4425-4434.
31. Wolfgang, J. D.; White, B. T.; Long, T. E., Non-isocyanate Polyurethanes from 1,1'-Carbonyldiimidazole: A Polycondensation Approach. *Macromolecular Rapid Communications* **2021**, *42* (13), 2100163.
32. Sintas, J. I.; Wolfgang, J. D.; Long, T. E., Carbamate thermal decarboxylation for the design of non-isocyanate polyurethane foams. *Polymer Chemistry* **2023**.
33. Koutsoumpis, S.; Raftopoulos, K. N.; Oguz, O.; Papadakis, C. M.; Menciloglu, Y. Z.; Pissis, P., Dynamic glass transition of the rigid amorphous fraction in polyurethane-urea/SiO₂ nanocomposites. *Soft Matter* **2017**, *13* (26), 4580-4590.
34. Füllbrandt, M.; Purohit, P. J.; Schönhals, A., Combined FTIR and Dielectric Investigation of Poly(vinyl acetate) Adsorbed on Silica Particles. *Macromolecules* **2013**, *46* (11), 4626-4632.
35. Vogiatzis, G. G.; Theodorou, D. N., Structure of Polymer Layers Grafted to Nanoparticles in Silica–Polystyrene Nanocomposites. *Macromolecules* **2013**, *46* (11), 4670-4683.
36. Pangon, A.; Dillon, G. P.; Runt, J., Influence of mixed soft segments on microphase separation of polyurea elastomers. *Polymer* **2014**, *55* (7), 1837-1844.

37. Sahebi Jouibari, I.; Haddadi-Asl, V.; Mirhosseini, M. M., A novel investigation on micro-phase separation of thermoplastic polyurethanes: simulation, theoretical, and experimental approaches. *Iranian Polymer Journal* **2019**, *28* (3), 237-250.
38. Sheth, J. P.; Klinedinst, D. B.; Pechar, T. W.; Wilkes, G. L.; Yilgor, E.; Yilgor, I., Time-Dependent Morphology Development in a Segmented Polyurethane with Monodisperse Hard Segments Based on 1,4-Phenylene Diisocyanate. *Macromolecules* **2005**, *38* (24), 10074-10079.
39. Chen, K.-S.; Leon Yu, T.; Chen, Y.-S.; Lin, T.-L.; Liu, W.-J., Soft-and hard-segment phase segregation of polyester-based polyurethane. *Journal of Polymer Research* **2001**, *8* (2), 99-109.
40. Li, Y.; Gao, T.; Chu, B., Synchrotron SAXS studies of the phase-separation kinetics in a segmented polyurethane. *Macromolecules* **1992**, *25* (6), 1737-1742.
41. Cheng, B.-X.; Gao, W.-C.; Ren, X.-M.; Ouyang, X.-Y.; Zhao, Y.; Zhao, H.; Wu, W.; Huang, C.-X.; Liu, Y.; Liu, X.-Y.; Li, H.-N.; Li, R. K. Y., A review of microphase separation of polyurethane: Characterization and applications. *Polymer Testing* **2022**, *107*, 107489.
42. Sheth, J. P.; Wilkes, G. L.; Fornof, A. R.; Long, T. E.; Yilgor, I., Probing the Hard Segment Phase Connectivity and Percolation in Model Segmented Poly(urethane urea) Copolymers. *Macromolecules* **2005**, *38* (13), 5681-5685.

CHAPTER 4

NON-ISOCYANATE POLYURETHANE SEGMENTED COPOLYMERS FROM BIS-CARBONYLIMIDAZOLIDES

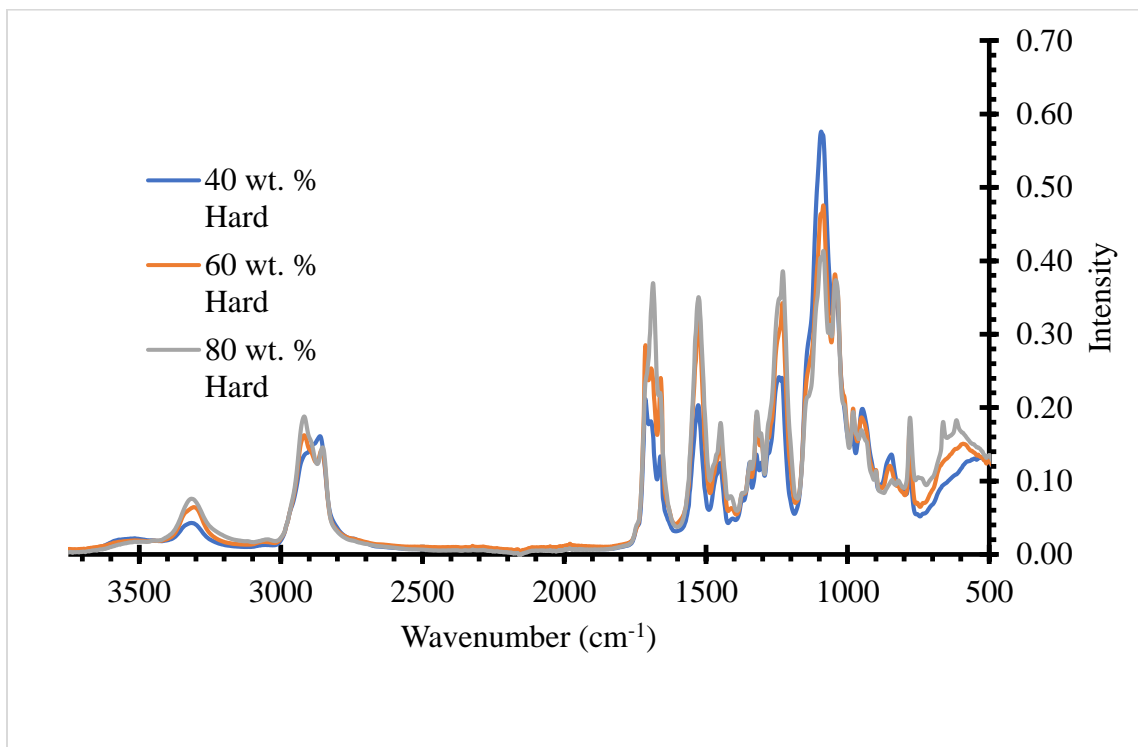


Figure S4.1 ATR-FTIR spectroscopy confirmed polyurethane structure of all synthesized compositions.

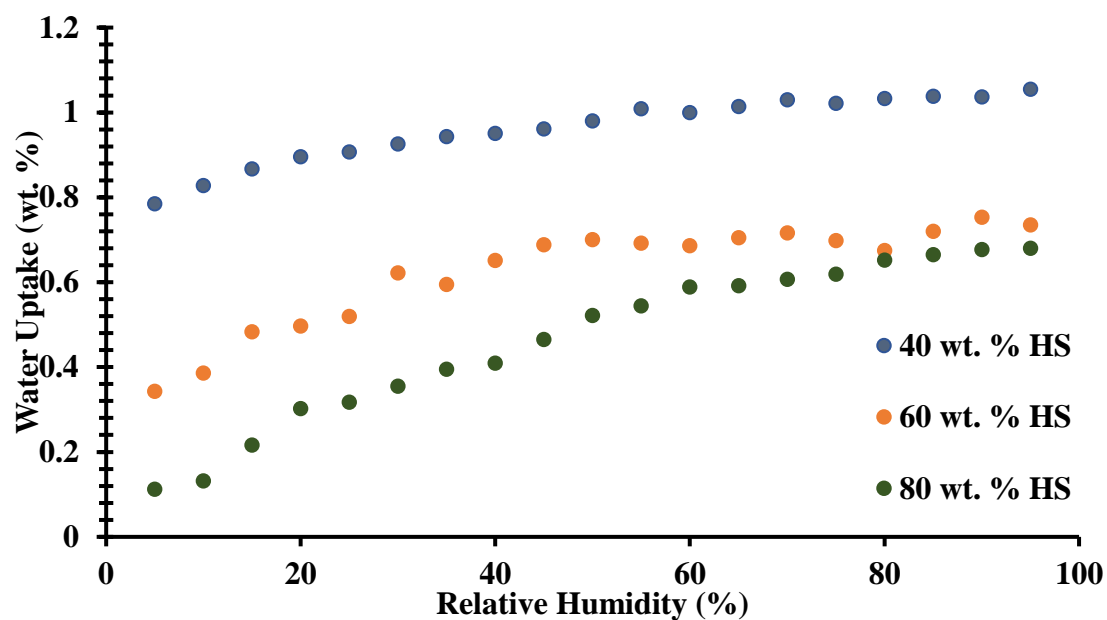


Figure S4.2: TGA-SA quantified water uptake as a function of relative humidity for all synthesized NIPUs at 25 °C.

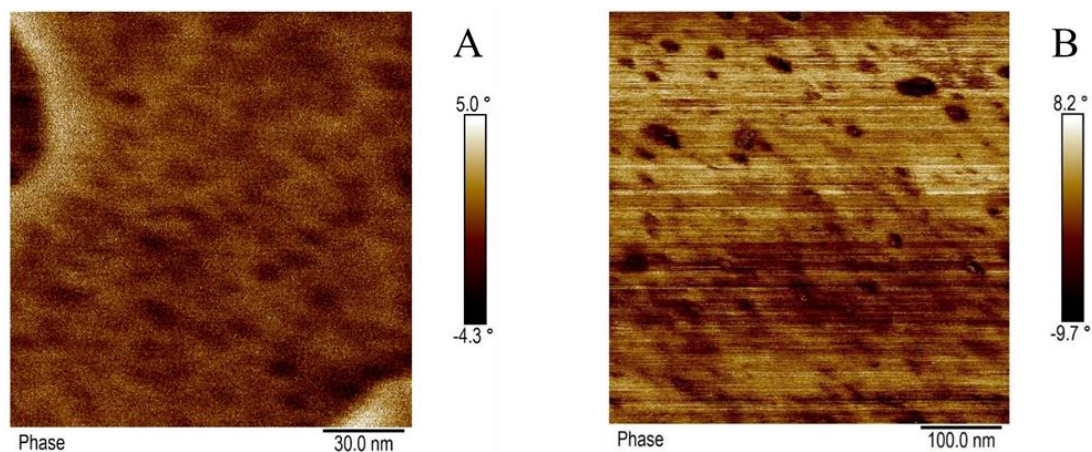


Figure S4.3: AFM of 40 (A) and 80 (B) wt. % HS NIPUs revealed nanophase separation present in all samples. Electrostatic interactions between the AFM probe and NIPU surface resulted in tip dragging at an 80 wt. % HS concentration, prohibiting small area measurements.

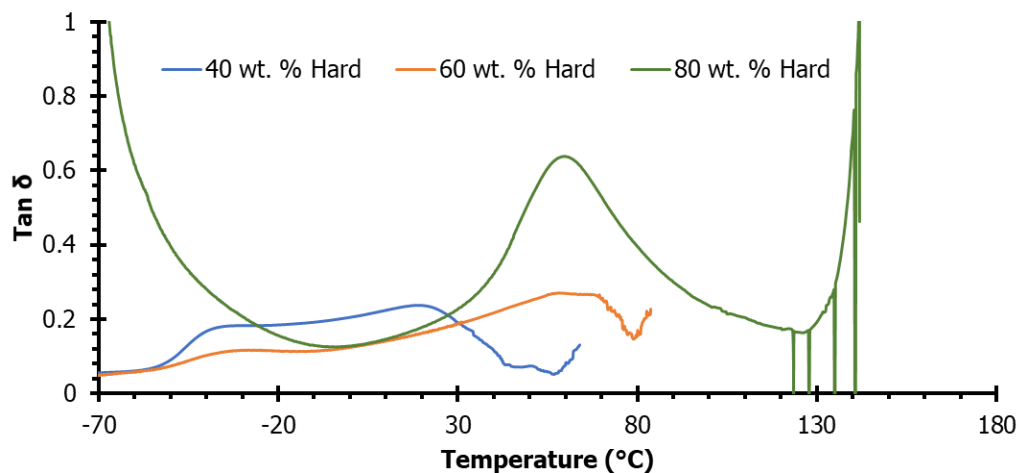


Figure S4.4: Tan δ maxima derived from DMA traces provided thermal transition temperatures for all samples.

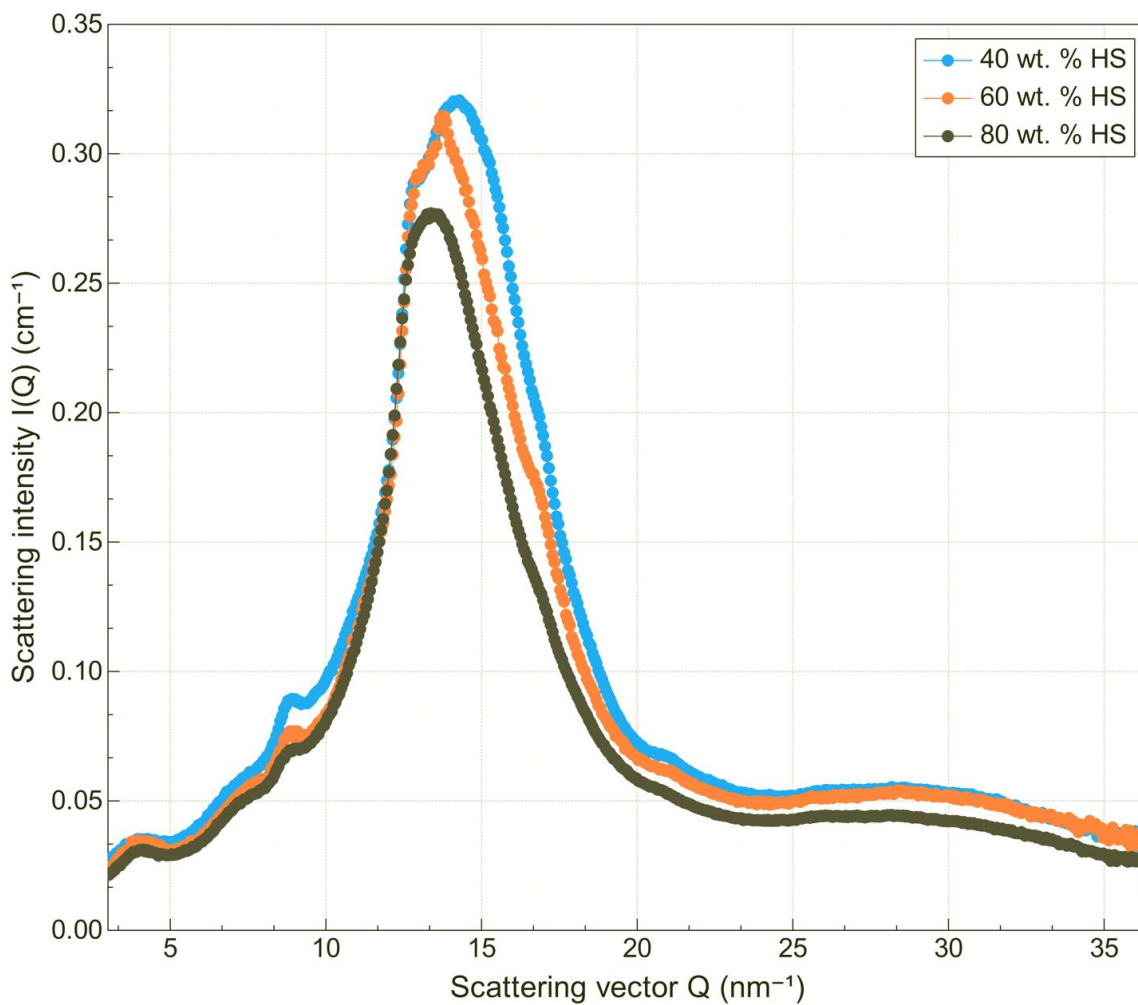


Figure S4.5: WAXS region for all synthesized NIPU compositions.

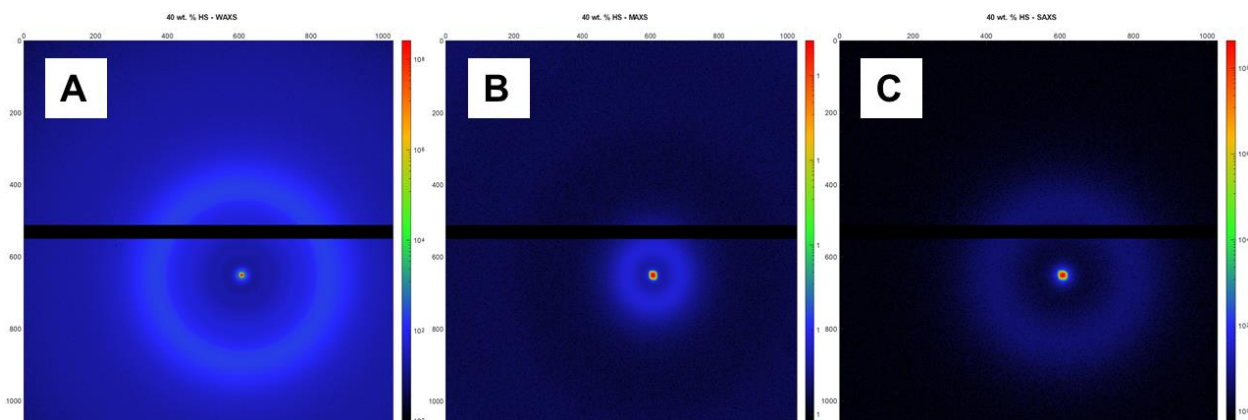


Figure S4.6: 2D graphs of 40 wt. % small (C), middle (B), and wide (A) x-ray scattering patterns.

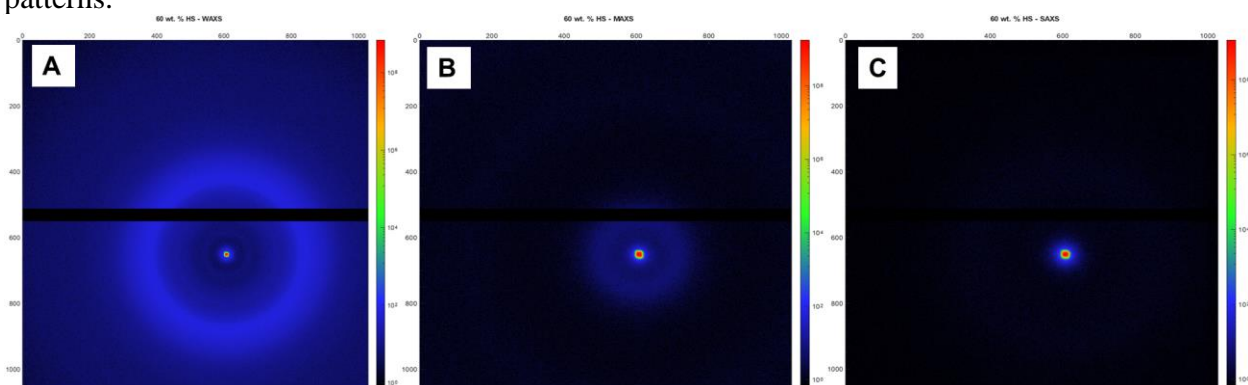


Figure S4.7: 2D graphs of 60 wt. % small (C), middle (B), and wide (A) x-ray scattering patterns.

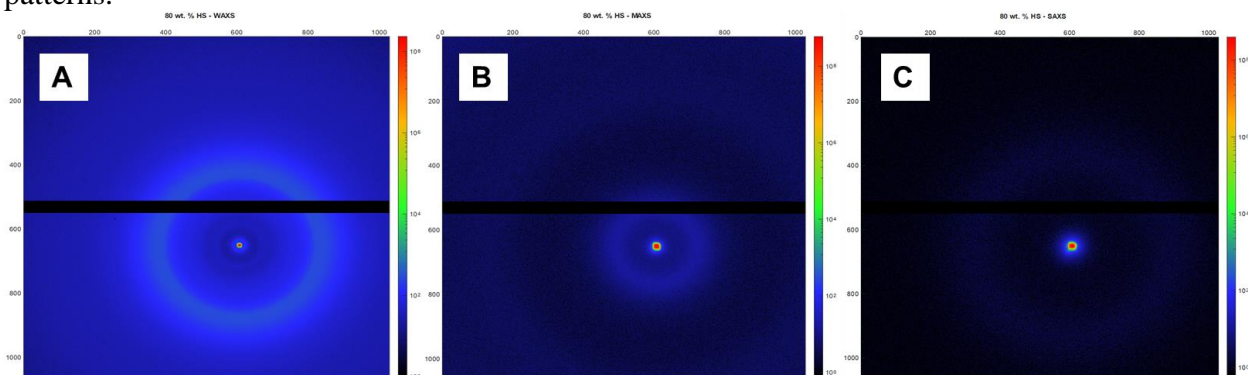


Figure S4.8: 2D graphs of 80 wt. % small (C), middle (B), and wide (A) x-ray scattering patterns.

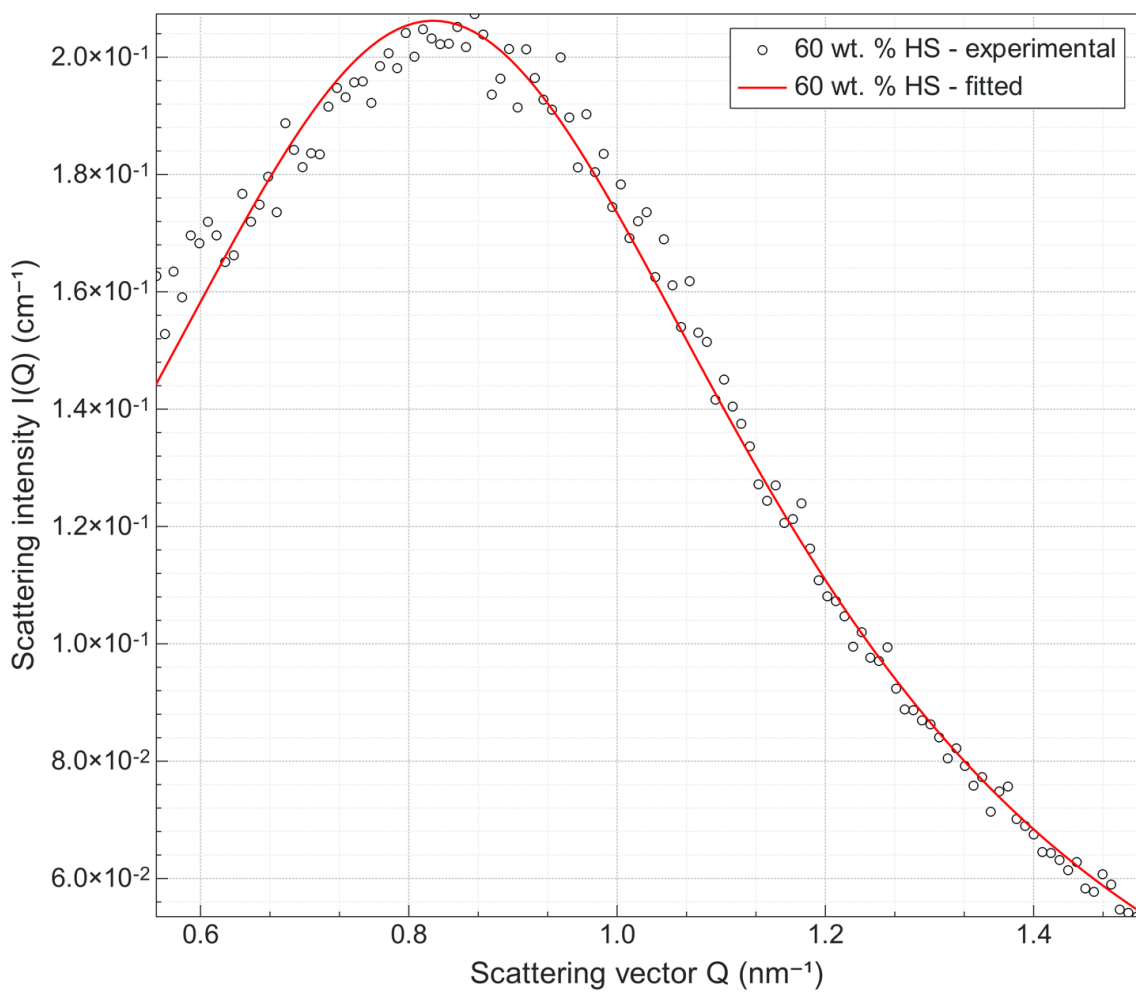


Figure S4.9: Lorentzian peak fitting of the 60 wt. % HS SAXS region. This fitting was used to analyze the FWHM, peak center, and peak height and was repeated for all samples.

	Center (nm ⁻¹)	Center_std (nm ⁻¹)	Height (cm ⁻¹)	Height_std (cm ⁻¹)	FWHM (nm ⁻¹)	FWHM_std (nm ⁻¹)	Power law exponent
40 wt. % HS	0.63389078	0.00028158666	0.514972741	0.0006091220941	0.52675283352	0.00071310024	-3.8±0.1

60 wt. % HS	0.82345707	0.00161739228	0.206213386	0.0005555464695	0.81209199857	0.00424833395	-3.6±0.1
80 wt. % HS	0.94043749	0.00065188350	0.108552673	0.00019511217439	0.83034597026	0.00270190896	-3.7±0.0

Table S4.1: Tabulated SAXS raw data for domain size and dispersity calculations.

CHAPTER 5

DIVALENT IMIDAZOLIUM IONIC LIQUIDS FROM BIS-CARBONYLIMIDAZOLIDE MONOMERS

5.1 Abstract

Reactive imidazolidine nitrogens present in biscarbonylimidazolidine (BCI) monomers enabled an S_N2 reaction with alkyl halides resulting in a novel divalent ionic liquid, BBCI IL. This novel ionic liquid possessed improved thermal stability up to 260 °C while maintaining chemical resistance to amine nucleophiles. In-situ FTIR spectroscopy coupled with ^{13}C NMR and computational modeling revealed a deactivation of the electrophilic carbonyl present in BCI monomers after conversion to the ionic liquid state. Dielectric relaxation spectroscopy revealed the temperature and frequency dependence of the ionic conductivity possessed by BBCI IL, revealing $\epsilon_s = 16$. Lastly preliminary investigations into the synthesis of conductive ionenes derived from BCI monomers provided a series of polymers capable of thermomechanical property tuning, however displaying poor air stability.

5.2 Introduction

Common descriptions of ionic liquids (ILs) classify them as salts with melting points below that of water, with some definitions requiring a molten status at ambient temperatures.¹ Unique physicochemical properties encourage their use for specialty applications that require low volatility, toxicity, flammability, high temperature stability, large thermal use window, or specialty dielectric environments.²⁻⁵ Diverse molecular structures, chemical composition, counterion selection, and molecular weight control endow these physicochemical properties throughout a large temperature range. Furthermore, the low

vapor pressure ILs possess impart environmentally friendly aspects to their use, providing green alternatives to traditional volatile solvents.⁶ Several chemical structures encompass IL formulations including imidazolium, pyridinium, ammonium, or phosphonium functionalities that possess halide, tetrafluoroborate, hexafluorophosphate, or bis-trifluoromethanesulfonimide counterions.^{7, 8} Of these various chemical compositions, imidazolium ILs have emerged as a dominant choice due to their facile synthesis and tunable properties. Furthermore, imidazolium ILs containing halide counterions found specialty use as solvents for the dissolution of cellulose and carbohydrates.⁹

Imidazolium functional groups comprise a prevalent class of small molecule and polymeric IL's due to their electrochemical stability, low toxicity, catalytic effects, and desirable thermal properties.¹⁰⁻¹² Furthermore, divalent ionic liquids (ILs with a charge of +2) offer several advantages over their monovalent counterparts exemplifying greater solvation capabilities, lower volatility, and enhanced catalytic effects.^{13, 14} These ionic liquids are based on imidazolium cations that contain two positive charges, rendering them distinct from traditional monovalent imidazolium ionic liquids. Research in this area has focused on the synthesis, characterization, and application of these ionic liquids, as well as the exploration of their fundamental properties and behavior. Despite their promise, divalent imidazolium ionic liquids also present some challenges and limitations, including the complexity of their synthesis, potential toxicity, and environmental impact. Thus, a novel synthetic method that remediates these issues is desired.

The versatility of imidazole as a reagent extends beyond IL formation, i.e. the recent use of imidazolid functionalized monomers for the synthesis of non-isocyanate polyurethane (NIPU) thermoplastic and foams.^{15, 16} Bis-carbonylimidazolid (BCI) monomers,

generated from an imidazole reagent, enabled the efficient melt polymerization of NIPUs containing various backbone chemistries and topologies. Additionally, these monomers enable the efficient synthesis of polycarbonates through careful selection of reaction conditions.^{17, 18} The pendent imidazolide functional groups BCI monomers offer an atom-efficient reaction mechanism towards a novel IL synthetic pathway, outlined in this manuscript. A facile S_N2 reaction between the nucleophilic imidzaolide nitrogen present in BCI monomers and an electrophilic alkylhalide enabled the quantitative synthesis of novel divalent imidazolium ionic liquids with carbamate functionalities. Divalent, imidazolium ionic liquids derived from BCI monomers have not been previously discussed in literature, prompting their exploration.

5.3 Materials

1,4-Butanediol (ReagentPlus[®], 99%), 1,1'-Carbonyldiimidazole (CDI, 97%), 1-iodobutane (99%), poly(ethylene glycol) (PEG, BioReagent, 400 g mol⁻¹), potassium carbonate (K₂CO₃, ACS reagent, ≥99.0%), 6-bromohexanoyl chloride (>97%), and acetonitrile (anhydrous, 99.8%) were purchased from Sigma-Aldrich and used as received. Ethyl Acetate (HPLC), anhydrous ethyl ether, ethanol (200 proof) and PEG (Bioreagent, 2,000 g mol⁻¹) were purchased from Fisher Scientific and used as received. 1,12-dibromododecane (DBD, 98%) was purchased from Sigma-Aldrich and was recrystallized from ethanol before use. N,N-dimethylformamide (DMF, extra dry, 99.8%) and dichloromethane (DCM, extra dry, 99.9%) were purchased from Acros Organics. Ultra-high purity nitrogen gas (99.999%) was purchased from Praxair

5.4 Synthesis of BBCI

The synthesis of BBCI followed the procedure reported by previous publications.¹⁹ 1,4-butanediol (10.000 g, 111 mmol) was added via powder funnel to a three-necked round bottomed flask equipped with a magnetic stir bar. Ethyl acetate (220 mL) was added to the flask and the mixture was stirred until the butanediol dissolved completely. CDI (44.981 g, 277 mmol) was added slowly to the solution to allow for easier dissolution. The reaction was allowed to proceed for 2 h at room temperature while stirring. The BBCI product precipitated from the clear solution as it was formed resulting in a white slurry. The product was filtered with a fritted filter and washed twice with additional ethyl acetate (~50 mL) to remove any unreacted reagents. The resultant white powder was dried *in vacuo* at 60 °C for 18 h to give a >95% yield. The melting point of the pure white powder measured between 135 -137 °C). ¹H NMR (CDCl₃, δ, **Figure S5.1**) 8.12-8.14 (t, 2H), 7.41-7.43 (t, 2H), 7.07-7.09 (m, 2H), 4.47-4.52 (t, 4H) 1.94-2.00 (m, 4H).

5.5 Synthesis of BBCI IL

BBCI (5 g, 18 mmol) and 1,4-iodobutane (6.61 g, 36 mmol) were added to a three-necked round bottom flask with a magnetic stir bar and dissolved in acetonitrile. The reaction was allowed to react under reflux at 80 °C for 30 hours. An in-situ FTIR probe was inserted into the reactor and was used to monitor reaction times. Acetonitrile and excess 1,4-iodobutane were removed at 120 °C under reduced pressure for 12 h.

5.6 Synthesis of Imidazolium Ionenenes

The synthesis of segmented and non-segmented ionenes were carried out using the following general procedure. For a segmented ionene containing 30 wt% HS, BBCI (2.128

g, 7.65 mmol), PEG₄₀₀ dibromide (2.518 g, 3.52 mmol), and DBD (1.353 g, 4.12 mmol) were added to a three-necked round bottomed flask equipped with a condenser and a magnetic stir bar. Anhydrous DMF was added via syringe and the flask was purged with N₂. The solution was heated at 80 °C for 48 h under constant nitrogen flow. The heterogeneous solution became homogeneous within min of heating. The polymer solution was precipitated in ether and dried *in vacuo* at 60 °C to afford a viscous pale-yellow liquid.

5.7 Analytical Methods

Nuclear magnetic resonance (NMR) spectroscopy was carried out on an Agilent U4-DD2 spectrometer operating at 400 MHz or a Bruker 500 MHz and 23 °C. All NMR samples were prepared from either a DMSO-d₆ or CDCl₃ solution at approximately 10 mg mL⁻¹. A TA instruments Q2000 facilitated differential scanning calorimetry (DSC) measurements under nitrogen flow and cooled with a refrigerated cooling system. The glass transition temperatures (T_g) were taken as the inflection point of the step transition that occurred during the second heating step. FTIR was performed on a Nicolet iS5 spectrometer equipped with an iD7 ATR stage at room temperature. A Mettler Toledo ReactIR 15 allowed for the *in-situ* monitoring of imidazolium formation. The spectra were taken 2 min apart from each other and consisted of 32 scans each. Molecular modeling of electrostatic potential was completed using WebMO.net under standard Hückel parameters.

Dielectric relaxation spectroscopy (DRS) measurements were performed using a Solartron 1260 Impedance/Gain-Phase Analyzer with a Solartron 1296A Dielectric Interface. The sample cell was a DHR rheometer accessory made by TA Instruments which utilized the

rheometer's ETC to provide temperature control and a continuous dry nitrogen atmosphere for the electrode cell. The electrodes were 25 mm in diameter, made of stainless steel, and polished to a flat, mirror finish. Inside a glovebox, liquid sample was sandwiched between two electrodes separated by 50 μm silica fibers. The test chamber was dried at 150 $^{\circ}\text{C}$ for 1 h under a continuous nitrogen flow (10 L/min) before cooling to room temperature. The sample cell was quickly transferred into the test chamber at room temperature, purged with nitrogen, and further dried under constant nitrogen flow at 100 $^{\circ}\text{C}$ for 1 h to remove any remaining moisture. The sample was then subjected to an oscillating potential of 0.1 V over a frequency range of 1-10⁶ Hz and measured at 10 points per decade using an auto-integration period \leq 10 s. This was performed at discrete temperatures from 30-0 $^{\circ}\text{C}$. DC conductivity (σ'_{DC}) was obtained by fitting horizontal lines to the plateau region of the frequency-dependent, real conductivity. Relative static permittivity (ϵ_s) values were obtained by fitting the frequency-dependent relative permittivity ($\epsilon'(\omega)$) to a sum of the real form of the Havriliak-Negami function and a power law function (i.e. $A\omega^{-n}$) to account for electrode polarization.²⁰

5.8 Results and Discussion

Previous findings revealed the facile, high-yield synthesis of non-isocyanate polyurethane precursors known as bis-carbonylimidazolidone (BCI) monomers.^{19,21} These BCI monomers readily polymerize in the presence of multifunctional amines, producing both thermoplastic and thermoset NIPUs. A base-catalyzed elimination mechanism leveraging the proton beta to the urethane carbonyl facilitated in-situ CO₂ generation for NIPU foam production. The imidazolidone nitrogen lone electron pair on BCI monomers enables the self-

catalysis of this elimination, resulting in spontaneous decarboxylation at elevated temperatures.¹⁶ This reactivity, however, enables the application of additional elementary S₂N chemistry. BBCI readily adds to 1-iodobutane to form an imidazolium ion terminated BCI monomer, **Figure 5.1**. An excess of 1-iodobutane enables the quantitative conversion of the BCI monomer to the IL form and is subsequently removed under vacuum.

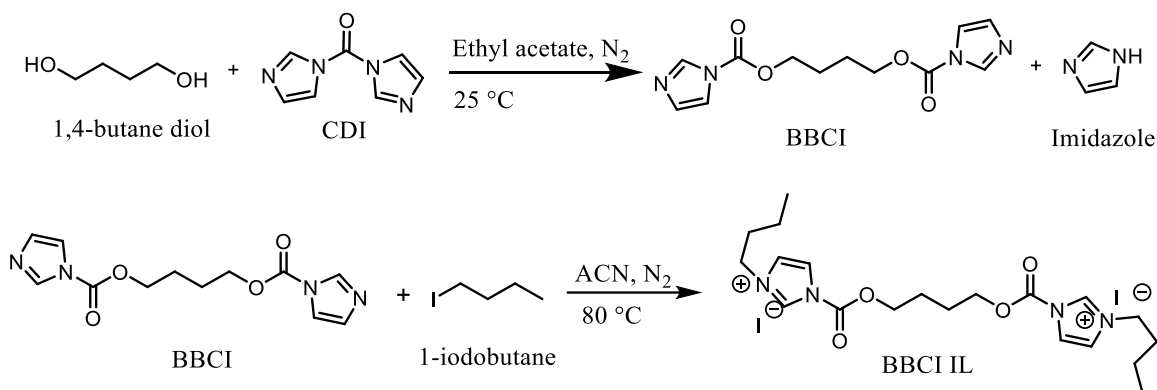


Figure 5.1 Ethyl acetate provided a medium to facilitate high conversion of 1,4-butanediol, resulting in BBCI. Reactive imidazole amine functionality enabled further reactivity to achieve a divalent ionic liquid.

In-situ FTIR spectroscopy revealed reaction kinetics for the formation of BBCI IL, **Figure 5.2**. The disappearance of the BBCI carbonyl absorbance with the formation of the imidazolium moiety allows monitoring of reaction progress. This experiment revealed complete conversion of the imidazolide unit after 25 h of reaction. The carbonyl absorbance shifted to a lower wavenumber, as expected due to the electron withdrawing nature of the adjacent imidazolium moiety. A fascinating discovery, however, is the extent of the observed carbonyl shift. Carbonyl stretches are rarely observed in the vicinity of

1564 cm^{-1} , however this novel ionic liquid structure provides additional insight on the effects of electron withdrawing substituents on carbonyl bond characteristics and stability.²²

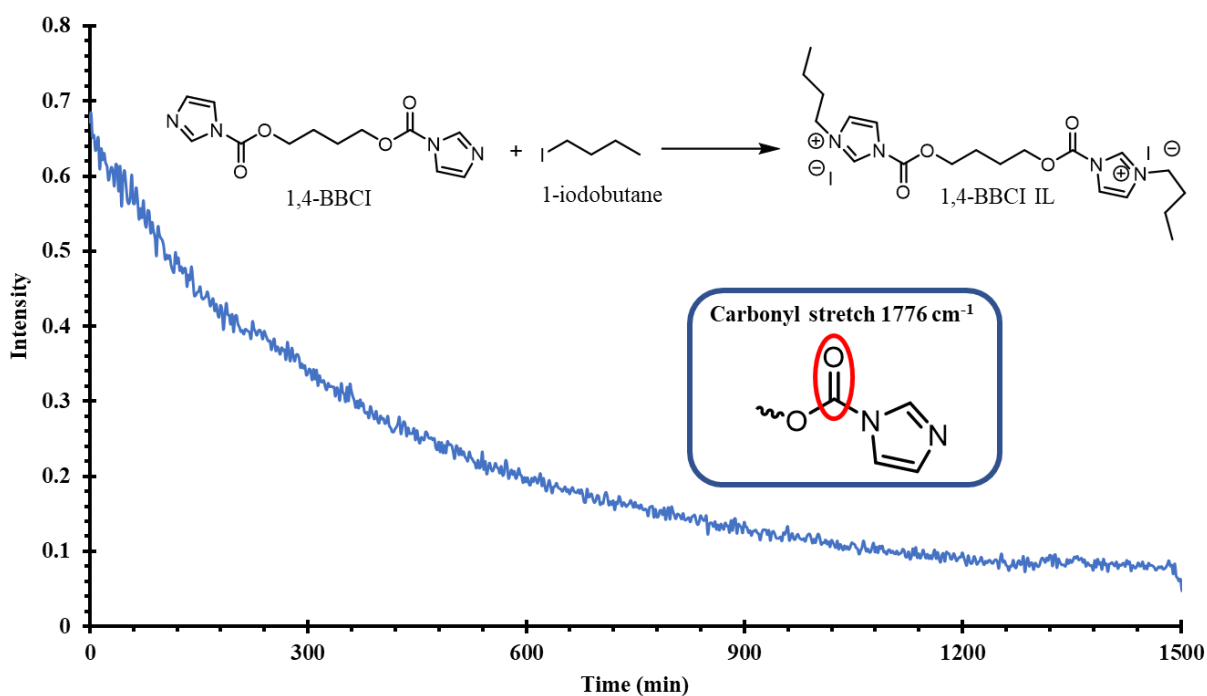


Figure 5.2 In-situ FTIR spectroscopy tracks the disappearance of the BBCI carbonyl stretch, revealing full conversion of BBCI monomer to form BBCI IL.

Non-ionic BCI monomers exhibit rapid weight loss at elevated temperatures due to a spontaneous decarboxylation event directed by the basic imidazolidine nitrogen. Earlier literature thoroughly explored this mechanism by monitoring weight loss and CO_2 release at elevated temperatures.²³ Weight loss profiles for the imidazolium functionalized ionic liquid displayed an increased $T_{d, 5\%}$ of 260 $^\circ\text{C}$, which aligns favorably for previously reported imidazolium ILs with iodide counterion literature values, **Figure 5.3**.^{24, 25} This

increase in weight loss temperature suggests the elimination of reactive imidazolidine nitrogen lone pairs due to complete functionalization with the alkyl halide. Further decarboxylation experiments revealed no CO₂ generation throughout a range of elevated temperatures, supporting this hypothesis. These results prove favorable, as functionalization removes reactivity from the final ionic liquid.

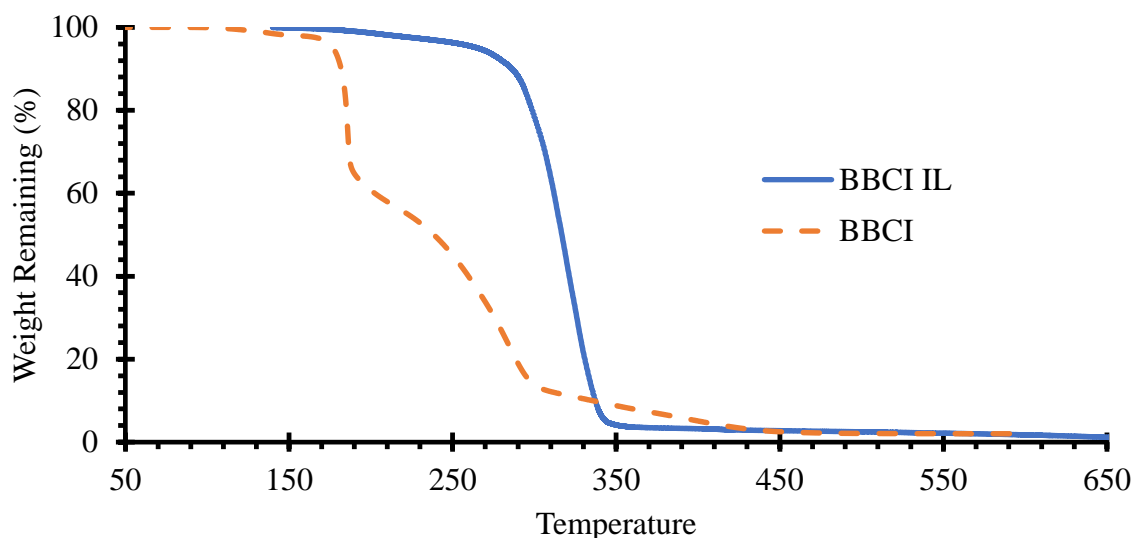


Figure 5.3 Weight loss profiles of BCCI IL reveal an increase in $T_{d, 5\%}$, suggesting full conversion of BCCI. The loss of basic imidazole amines inhibit CO₂ formation, increasing onset weight loss temperatures to values that match relevant imidazolium literature values.

In-situ FTIR spectroscopy further evaluated IL stability to carbonyl attack by a nucleophile. Unfunctionalized BCI monomers display reactivity towards amines, displacing the imidazole moiety and forming a new carbamate linkage. Transforming the imidazolidine moiety to an imidazolium fortuitously deactivates the carbonyl to nucleophilic attack. In-

situ FTIR spectroscopy, ^{13}C NMR, and elementary molecular orbital modeling explored this phenomenon. The frequency of resonance for similar IR stretches directly correlates to the polarizability and strength of the probed bond. The symmetric carbonyl stretch generally ranges from 1900 to 1600 cm^{-1} and appears as an intense and sharp peak due to its large dipole moment. Generally, aromatic carbonyl absorbances fall lower than aliphatic ones due to pi interactions that draw electron density away from the carbonyl bond. When attached to an imidazolium group, carbonyl pi electrons are drawn with a greater intensity away from that bond due to induction, resulting in an even lower stretching frequency. This is seen in the carbonyl absorbance of BBCI-IL, as the carbonyl stretch decreased from 1776 to 1564 cm^{-1} . The displacement of electron density from the carbonyl pi system, largely centered on the electronegative oxygen atom, results in an increase of electron density around the carbonyl carbon. This directly impacts reactivity, as the positive dipole moment on the carbonyl carbon directly contributes to its affinity for nucleophilic attack. To further investigate this hypothesis, ^{13}C NMR probed the change in electronic environment of the carbonyl carbon. Generally, downfield shifts in ^{13}C NMR signify a deshielded carbon environment, while higher electron density results in more upfield shifts. ^{13}C NMR spectra before and after imidazolium functionalization reveal a change in the carbonyl carbon electronic environment in a manner that suggests shielding of the carbonyl carbon (Figure S1). Molecular orbital (MO) modeling revealed expected electron density distributions within BBCI IL that further displayed this shielded environment (Figure S5.2).

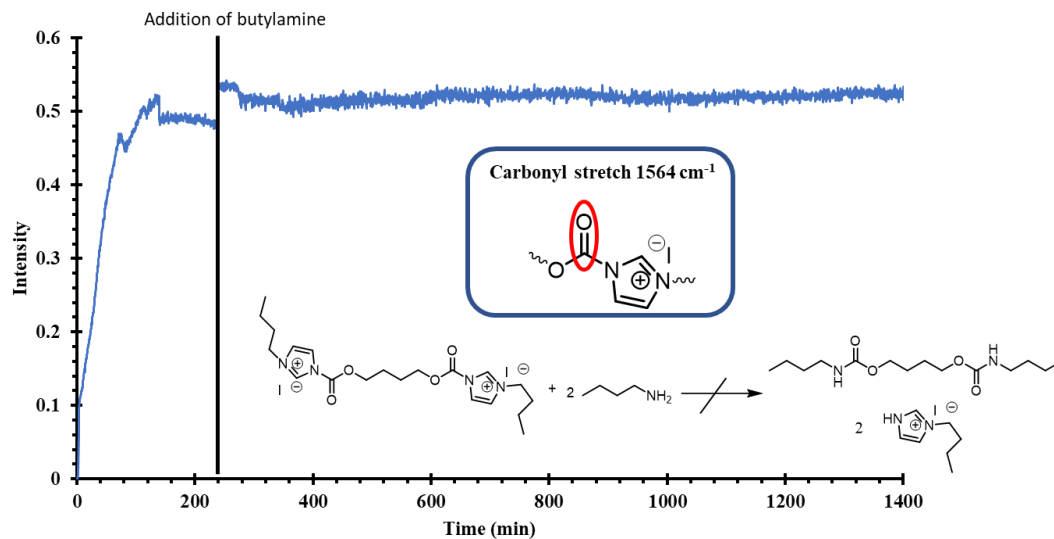


Figure 5.4 BBCI IL resists addition from primary amine, corroborated by *in situ* FTIR spectroscopy. The sample required 200 min to dissolve, producing the carbonyl plateau.

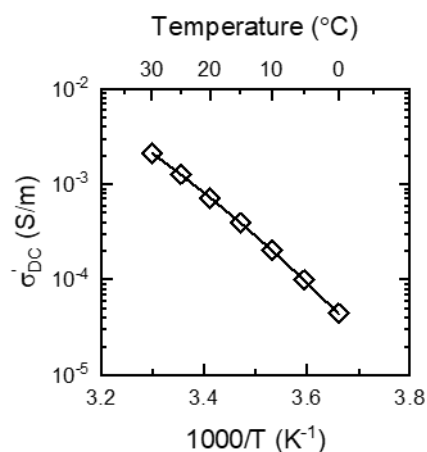


Figure 5.5: Temperature dependence of ionic conductivity for neat BBCI IL. The solid line represents fitting to the VFT equation.

The temperature-dependent ionic conductivity (σ'_{DC}) of BBCI IL, shown in **Figure 5.5**, displays the expected non-Arrhenius behavior of ILs.²⁶ The ionic conductivity of BBCI IL is comparable with other dicationic imidazolium ILs which exhibit similar glass transition temperatures.²⁷ Pitawala et al. demonstrated T_g to be the dominant factor governing

differences in ionic conductivity between five dicationic imidazolium ILs investigated, determined based on superimposing conductivity profiles on a T_g -scaled Arrhenius plot.²⁷

VFT equation: $\sigma = \sigma_{\infty} e^{-B/(T-T_0)}$		
σ_{∞} (S/m)	B (K)	T_0 (K)
631 ± 400	1608 ± 160	176 ± 6

Table 5.1: VFT equation parameters and fitting error of the ionic conductivity data for BBCI IL.

The conductivity data for BBCI IL in **Figure 5.5** were fit to the Vogel-Fulcher-Tammann (VFT) equation, listed in **Table 5.1**. The Vogel temperature, T_0 defines the theoretical or “ideal” glass transition temperature and generally lies ~ 50 K below the experimental T_g , in close agreement with that obtained here ($T_g - T_0 = 60$ K). The preexponential factor, σ_{∞} represents the high temperature limit of conductivity; B is related to dynamic activation barriers and can be useful when quantifying and comparing the extent to which conductivity depends on temperature.²⁸ The value of B obtained for BBCI IL is $> 2x$ larger than that found for similar dicationic ILs (600 vs 1600 K), implying that the ionic conductivity of BBCI IL exhibits a greater temperature dependence.²⁹ This can be interpreted as the dynamic interactions surrounding carbonylimidazolidide groups possessing greater temperature dependence than those surrounding alkyl imidazolium groups.

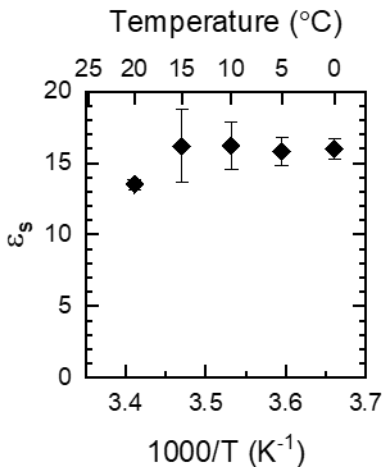


Figure 5.6: Relative static permittivity (ϵ_s) data for BBCI IL measured at discrete temperatures. Error bars denote parameter errors obtained from fitting to the Havriliak-Negami function.

Relative static permittivity (ϵ_s), or dielectric constant, values for BBCI IL were obtained by fitting the real part of the relative permittivity to the proper form of the Havriliak-Negami function, **Figure 5.6**.²⁰ The static permittivity of BBCI IL closely reflects literature values for several common alkyl imidazolium ILs, indicating that the carbonyl group does not significantly alter the capacitive properties of imidazolium-type species.³⁰ This is somewhat surprising considering the expanded resonant structures/states within carbonylimidazolidine as compared to alkyl imidazolium.

While the divalent BBCI IL displays unique chemical and electrical properties, preliminary investigations into the formation of polymeric ionenes are desired. Difunctional alkyl halides demonstrated polyaddition reactions with BBCI, resulting in linear, polyurethane ionenes demonstrated in **Scheme 2**. The facile synthesis of BBCI provided a route towards novel imidazolium ionenes with unique backbone structures. Specifically, the inclusion of a carbamate group into the imidazolium ionene structure provides a hydrogen bond

acceptor, which imparting unique thermal properties. **Figure 5.7** details the synthesis of imidazolium ionenes based on PEG dibromide and BBCI with an optional dibromide chain extender. In this case, the soft segment (SS) consists of the PEG dibromide reacted with the BBCI while the hard segment (HS) comprises of DBD reacted with BBCI. **Figure 5.8** displays the effect that HS incorporation imparts on the thermal properties of the resulting ionenes.

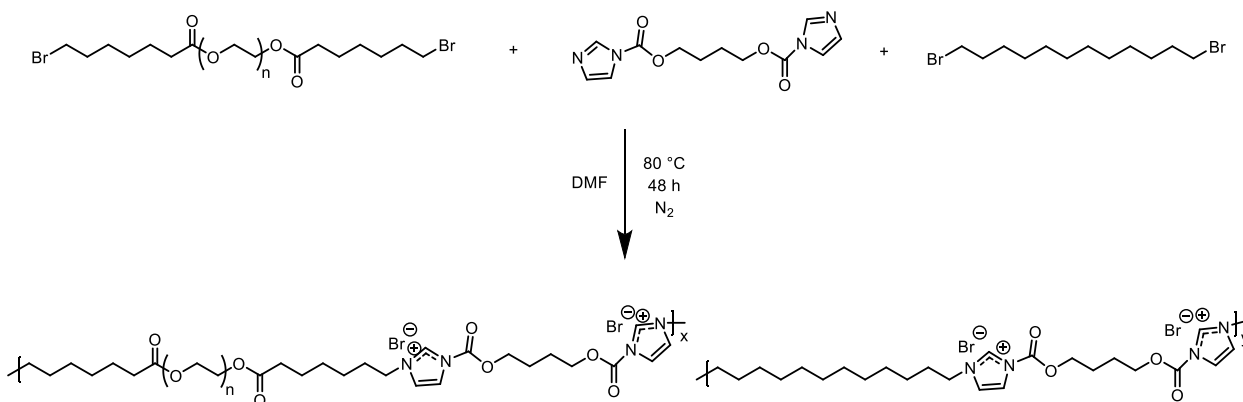


Figure 5.7: BBCI enabled a library of linear ionenes with tunable physical properties

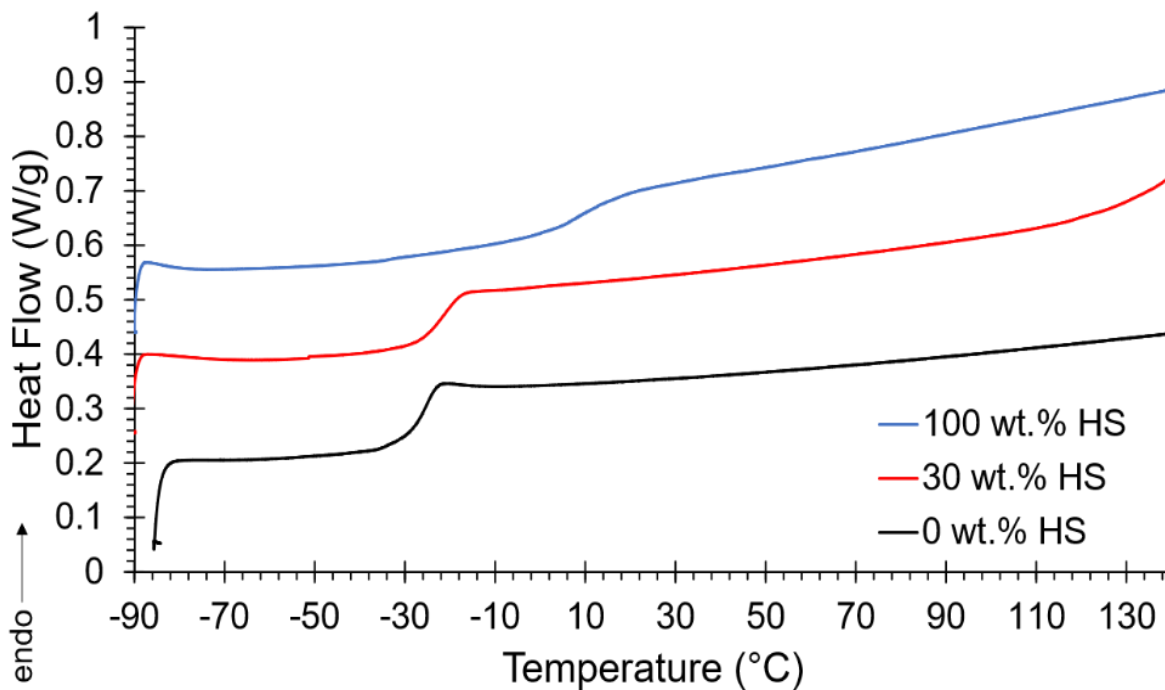


Figure 5.8: DSC thermograms of PEG₄₀₀ ionenes containing 0 (black) and 30 (red) wt.% HS compared to the 100 wt.% HS ionene (blue). Data is shifted vertically for clarity.

Prior literature demonstrated that incorporating lower molecular weight, amorphous PEG enhanced the ionic conductivity of the ionene compared to higher molecular weight, semi-crystalline PEGs.³¹ The synthesis of ionenes based on PEG₄₀₀ ($n = 9$) resulted in highly viscous liquids, which suggested the formation of polymers in both the segmented and non-segmented compositions. However, the inability of these polymers to form free-standing films suggests that their molecular weights remain below the critical molecular weight required for mechanical performance. Next, PEG_{2k} ($n = 45$) was utilized for this reaction using the rationale that starting with a higher molecular weight precursor should result in higher molecular weight polymers at similar conversions to the PEG₄₀₀ system. However, attempts to cast films of these polymers resulted in waxy, brittle solids comparable to neat PEG_{2k}. In a final attempt to achieve high molecular weight ionenes, BBCI and DBD reacted to form a homopolymer of the proposed HS. This reaction yielded a solid powder when precipitated, and solvent casting resulted in a free-standing film. Upon removing all solvent from the film in a vacuum oven, the film exhibited some flexibility, however failed when attempting to crease the film. Furthermore, exposing the film to atmosphere overnight resulted in a sticky polymer that no longer maintained mechanical integrity. This suggests that the polymer absorbed a significant amount of water from the atmosphere, which plasticized it and lowered the T_g . Water adsorption studies revealed a large affinity for water uptake, outlined in (Figure S3). Additionally, this ionene as well as all the others synthesized, displayed complete water solubility in an excess of DI water, which supports

the hypothesis of atmospheric water uptake. **Table 5.2** summarizes the compositions and thermal properties of resultant BBCI ionenes.

	Targeted HS content (wt. %)	PEG mol. %	BBCI mol. %	DBD mol%	T_g^a (°C)
PEG ₄₀₀	0	50	50	0	-25
	30	23	50	27	-21
PEG _{2k}	0	50	50	0	n/a
	30	18	50	32	n/a
DBD	100	0	50	50	4

Table 5.2: Summary of BBCI ionene compositions and resultant thermal properties

5.9 Conclusions

A BCI monomer, BBCI, provided a pathway for the efficient synthesis of divalent imidazolium ILs and ionene derivatives. In-situ FTIR spectroscopy revealed minimal reactivity of the small molecule BBCI IL to nucleophilic attack, displaying the favorable effect of imidazolium formation on the reactivity of BBCI. Furthermore, TGA suggested increased thermal stability afforded by the deactivation of reactive imidazolide nitrogens. DRS of BBCI IL displayed relatively low conductivity at a wide frequency range,

postulated to result from the high molecular weight of the compound and halide counterion. Future work including IL doping and counterion modulation may serve to remediate this issue. Reactivity of BBCI was further probed by the formation of BBCI-derived ionenes containing PEG SSs and 1,12-dibromododecane HSs that displayed additional control over T_g . However, the substantial water uptake of BBCI-derived ILs resulted in plasticization and potential degradation of the PEG containing ionenes, limiting the probing of mechanical properties.

5.10 Acknowledgements

The authors would like to thank Honeywell FM&T for their financial support

5.11

This work was funded by Honeywell FM&T

5.12 References

1. Wilkes, J. S., A short history of ionic liquids—from molten salts to neoteric solvents. *Green Chemistry* **2002**, *4* (2), 73-80.
2. Chen, M.; White, B. T.; Kasprzak, C. R.; Long, T. E., Advances in phosphonium-based ionic liquids and poly(ionic liquid)s as conductive materials. *European Polymer Journal* **2018**, *108*, 28-37.
3. Kunz, W.; Häckl, K., The hype with ionic liquids as solvents. *Chemical Physics Letters* **2016**, *661*, 6-12.
4. Noorhisham, N. A.; Amri, D.; Mohamed, A. H.; Yahaya, N.; Ahmad, N. M.; Mohamad, S.; Kamaruzaman, S.; Osman, H., Characterisation techniques for analysis of imidazolium-based ionic liquids and application in polymer preparation: A review. *Journal of Molecular Liquids* **2021**, *326*, 115340.

5. Green, M. D.; Long, T. E., Designing Imidazole-Based Ionic Liquids and Ionic Liquid Monomers for Emerging Technologies. *Polymer Reviews* **2009**, *49* (4), 291-314.
6. Earle, M. J.; Seddon, K. R., Ionic liquids. Green solvents for the future. *Pure and Applied Chemistry* **2000**, *72* (7), 1391-1398.
7. Chiappe, C.; Pomelli, C. S., Point-Functionalization of Ionic Liquids: An Overview of Synthesis and Applications. *European Journal of Organic Chemistry* **2014**, *2014* (28), 6120-6139.
8. Fraser, K. J.; MacFarlane, D. R., Phosphonium-Based Ionic Liquids: An Overview. *Australian Journal of Chemistry* **2009**, *62* (4), 309-321.
9. Ueno, K.; Tokuda, H.; Watanabe, M., Ionicity in ionic liquids: correlation with ionic structure and physicochemical properties. *Physical Chemistry Chemical Physics* **2010**, *12* (8), 1649-1658.
10. Fonseca, G. S.; Umpierre, A. P.; Fichtner, P. F. P.; Teixeira, S. R.; Dupont, J., The Use of Imidazolium Ionic Liquids for the Formation and Stabilization of Ir⁰ and Rh⁰ Nanoparticles: Efficient Catalysts for the Hydrogenation of Arenes. *Chemistry – A European Journal* **2003**, *9* (14), 3263-3269.
11. Migowski, P.; Dupont, J., Catalytic Applications of Metal Nanoparticles in Imidazolium Ionic Liquids. *Chemistry – A European Journal* **2007**, *13* (1), 32-39.
12. Baranyai, K. J.; Deacon, G. B.; MacFarlane, D. R.; Pringle, J. M.; Scott, J. L., Thermal Degradation of Ionic Liquids at Elevated Temperatures. *Australian Journal of Chemistry* **2004**, *57* (2), 145-147.
13. Bakis, E.; van den Bruinhorst, A.; Pison, L.; Palazzo, I.; Chang, T.; Kjellberg, M.; Weber, C. C.; Costa Gomes, M.; Welton, T., Mixing divalent ionic liquids: effects

of charge and side-chains. *Physical Chemistry Chemical Physics* **2021**, *23* (8), 4624-4635.

14. Avila, J.; Lepre, L. F.; Goloviznina, K.; Guazzelli, L.; Pomelli, C. S.; Chiappe, C.; Pádua, A.; Costa Gomes, M., Improved carbon dioxide absorption in double-charged ionic liquids. *Physical Chemistry Chemical Physics* **2021**, *23* (40), 23130-23140.

15. Wolfgang, J. D.; White, B. T.; Long, T. E., Non-isocyanate Polyurethanes from 1,1'-Carbonyldiimidazole: A Polycondensation Approach. *Macromolecular Rapid Communications* **2021**, *42* (13), 2100163.

16. Sintas, J. I.; Wolfgang, J. D.; Long, T. E., Carbamate thermal decarboxylation for the design of non-isocyanate polyurethane foams. *Polymer Chemistry* **2023**.

17. Olsson, J. V.; Hult, D.; García-Gallego, S.; Malkoch, M., Fluoride-promoted carbonylation polymerization: a facile step-growth technique to polycarbonates. *Chemical Science* **2017**, *8* (7), 4853-4857.

18. Houlihan, F. M.; Bouchard, F.; Frechet, J. M. J.; Willson, C. G., Thermally depolymerizable polycarbonates. 2. Synthesis of novel linear tertiary copolycarbonates by phase-transfer catalysis. *Macromolecules* **1986**, *19* (1), 13-19.

19. Wolfgang, J. D.; White, B. T.; Long, T. E., Non-Isocyanate Polyurethanes from 1,1'-Carbonyldiimidazole: An Activated Carbamate Approach. *Submitted for Publication* **2021**.

20. Schönhals, A.; Kremer, F., Analysis of Dielectric Spectra. In *Broadband Dielectric Spectroscopy*, Kremer, F.; Schönhals, A., Eds. Springer Berlin Heidelberg: Berlin, Heidelberg, 2003; pp 59-98.

21. Sintas, J. I.; Wolfgang, J. D.; Long, T. E., Carbamate thermal decarboxylation for the design of non-isocyanate polyurethane foams. *Polymer Chemistry* **2023**, *14* (13), 1497-1506.
22. Introduction to Vibrational Spectroscopy. In *Fourier Transform Infrared Spectrometry*, 2007; pp 1-18.
23. Delebecq, E.; Pascault, J.-P.; Boutevin, B.; Ganachaud, F., On the Versatility of Urethane/Urea Bonds: Reversibility, Blocked Isocyanate, and Non-isocyanate Polyurethane. *Chemical Reviews* **2013**, *113* (1), 80-118.
24. Cao, Y.; Mu, T., Comprehensive Investigation on the Thermal Stability of 66 Ionic Liquids by Thermogravimetric Analysis. *Industrial & Engineering Chemistry Research* **2014**, *53* (20), 8651-8664.
25. Haddad, B.; Kiefer, J.; Brahim, H.; Belarbi, E.-h.; Villemin, D.; Bresson, S.; Abbas, O.; Rahmouni, M.; Paolone, A.; Palumbo, O., Effects of C(2) Methylation on Thermal Behavior and Interionic Interactions in Imidazolium-Based Ionic Liquids with Highly Symmetric Anions. *Applied Sciences* **2018**, *8* (7), 1043.
26. Tokuda, H.; Ishii, K.; Susan, M. A. B. H.; Tsuzuki, S.; Hayamizu, K.; Watanabe, M., Physicochemical Properties and Structures of Room-Temperature Ionic Liquids. 3. Variation of Cationic Structures. *The Journal of Physical Chemistry B* **2006**, *110* (6), 2833-2839.
27. Pitawala, J.; Matic, A.; Martinelli, A.; Jacobsson, P.; Koch, V.; Croce, F., Thermal Properties and Ionic Conductivity of Imidazolium Bis(trifluoromethanesulfonyl)imide Dicationic Ionic Liquids. *The Journal of Physical Chemistry B* **2009**, *113* (31), 10607-10610.

28. Ikeda, M.; Aniya, M., Understanding the Vogel–Fulcher–Tammann law in terms of the bond strength–coordination number fluctuation model. *Journal of Non-Crystalline Solids* **2013**, 371-372, 53-57.
29. Moosavi, M.; Khashei, F.; Sharifi, A.; Mirzaei, M., Transport Properties of Short Alkyl Chain Length Dicationic Ionic Liquids—The Effects of Alkyl Chain Length and Temperature. *Industrial & Engineering Chemistry Research* **2016**, 55 (33), 9087-9099.
30. Huang, M.-M.; Jiang, Y.; Sasisanker, P.; Driver, G. W.; Weingärtner, H., Static Relative Dielectric Permittivities of Ionic Liquids at 25 °C. *Journal of Chemical & Engineering Data* **2011**, 56 (4), 1494-1499.
31. Lee, M.; Choi, U. H.; Salas-de la Cruz, D.; Mittal, A.; Winey, K. I.; Colby, R. H.; Gibson, H. W., Imidazolium polyesters: structure–property relationships in thermal behavior, ionic conductivity, and morphology. *Advanced Functional Materials* **2011**, 21 (4), 708-717.

CHAPTER 5 SUPPORTING INFORMATION
DIVALENT IMIDAZOLIUM IONIC LIQUIDS FROM BIS-
CARBONYLIMIDAZOLIDE MONOMERS

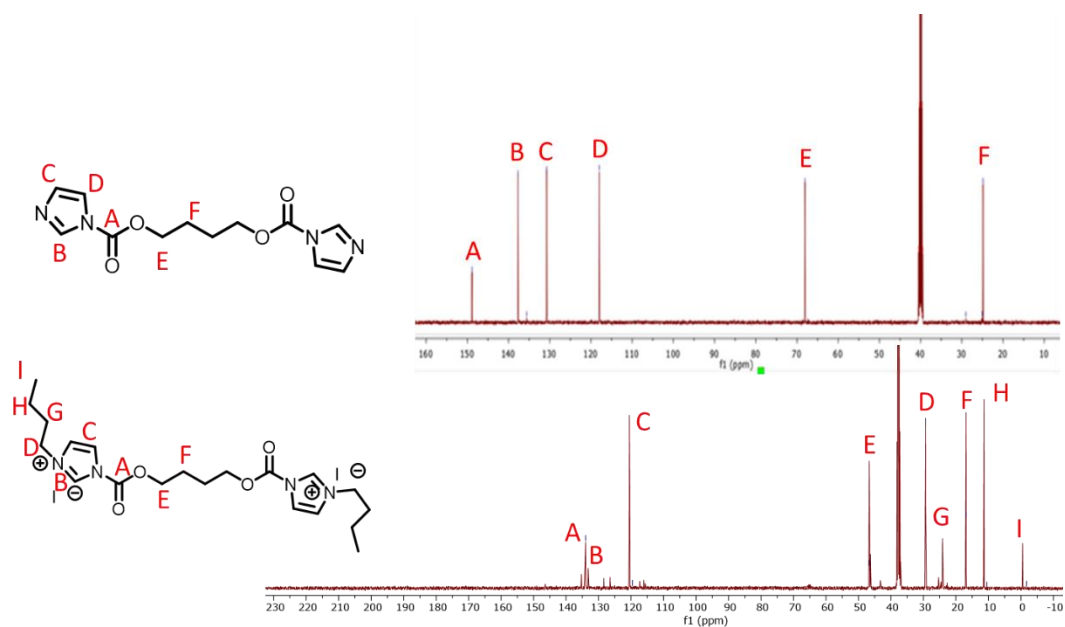


Figure S5.1 ^{13}C NMR reveals change in carbonyl carbon shift

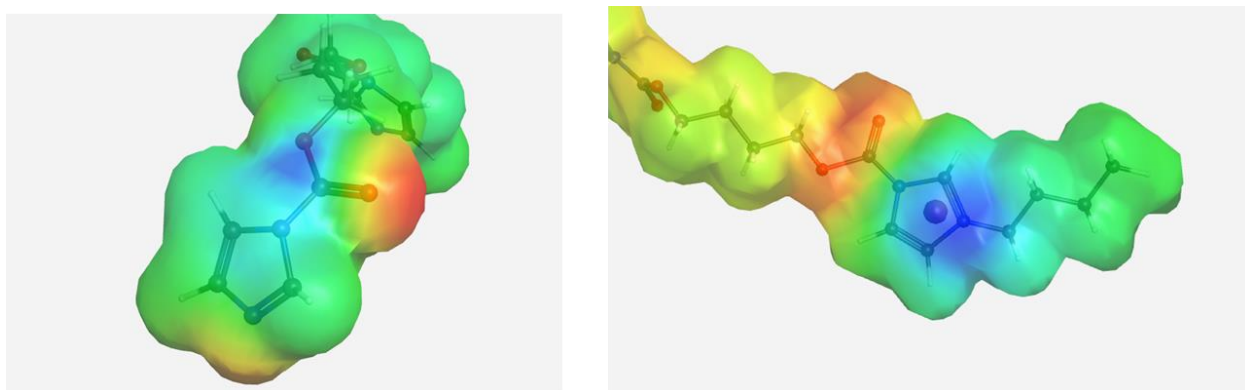


Figure S5.2 MO diagrams for BBCI and BBCIL displays shift in electron density towards carbonyl carbon

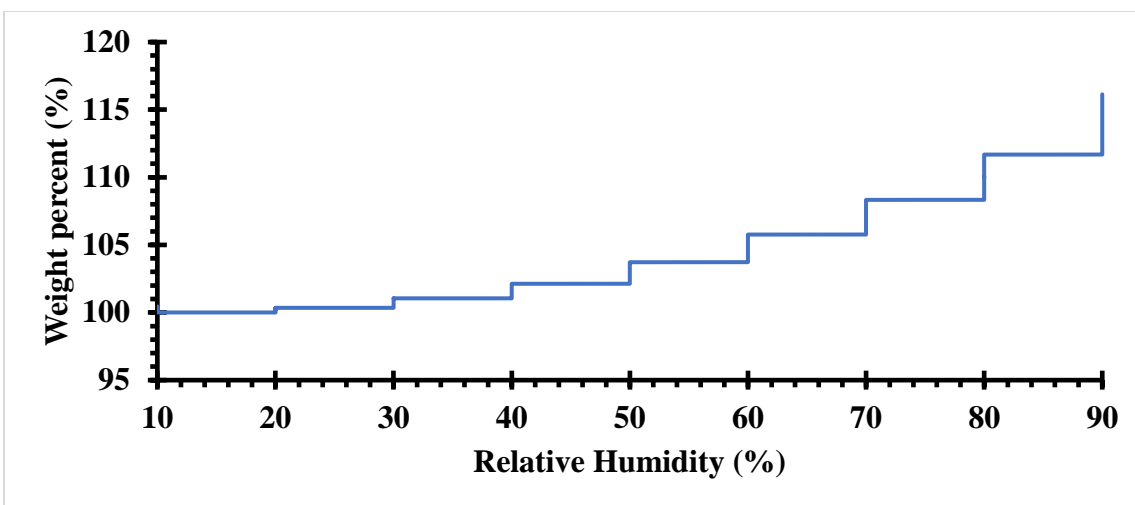


Figure S5.3: Step-wise TGA-SA curve elucidates water uptake throughout a range of humidities. This increase in water uptake likely results from installed imidazolium units.

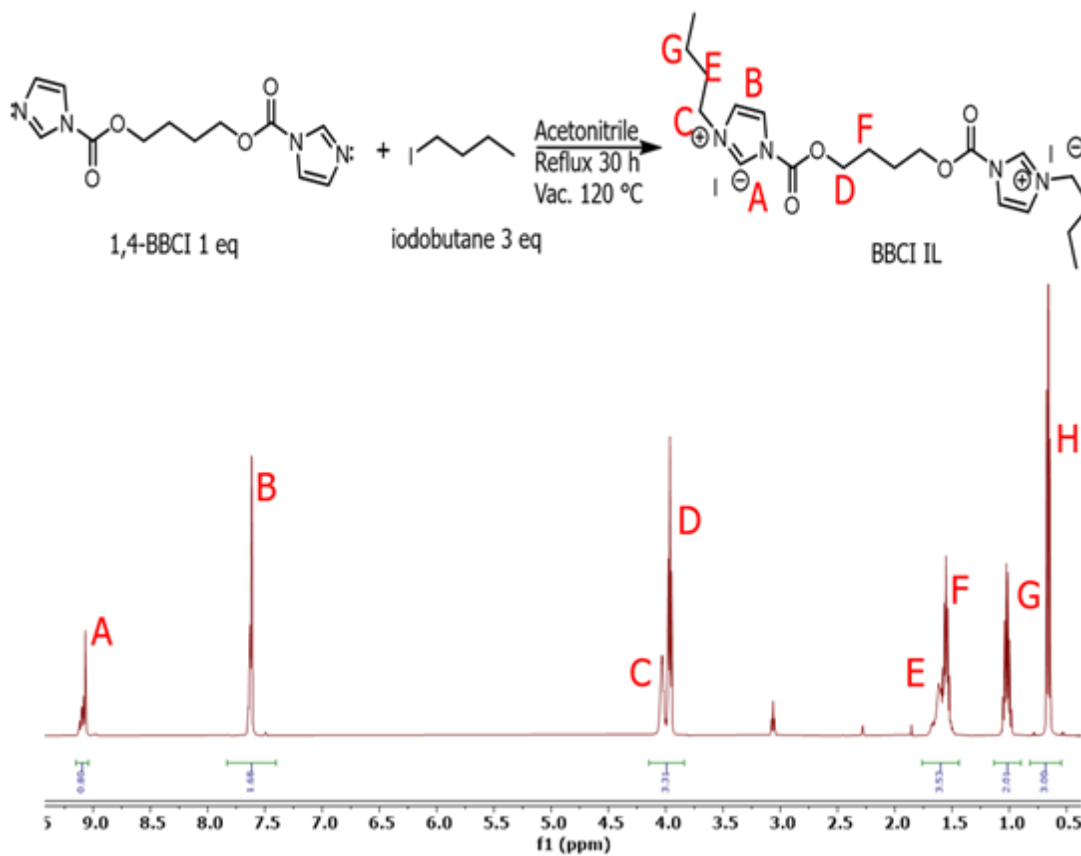


Figure S5.4 ¹H NMR of BBCI IL

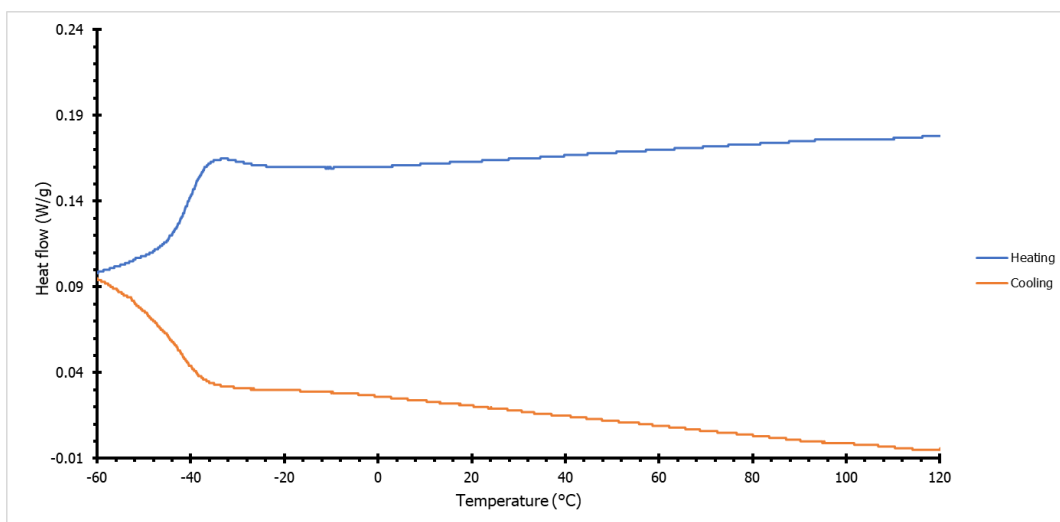


Figure S5.5 DSC of BBCI IL reveals T_g

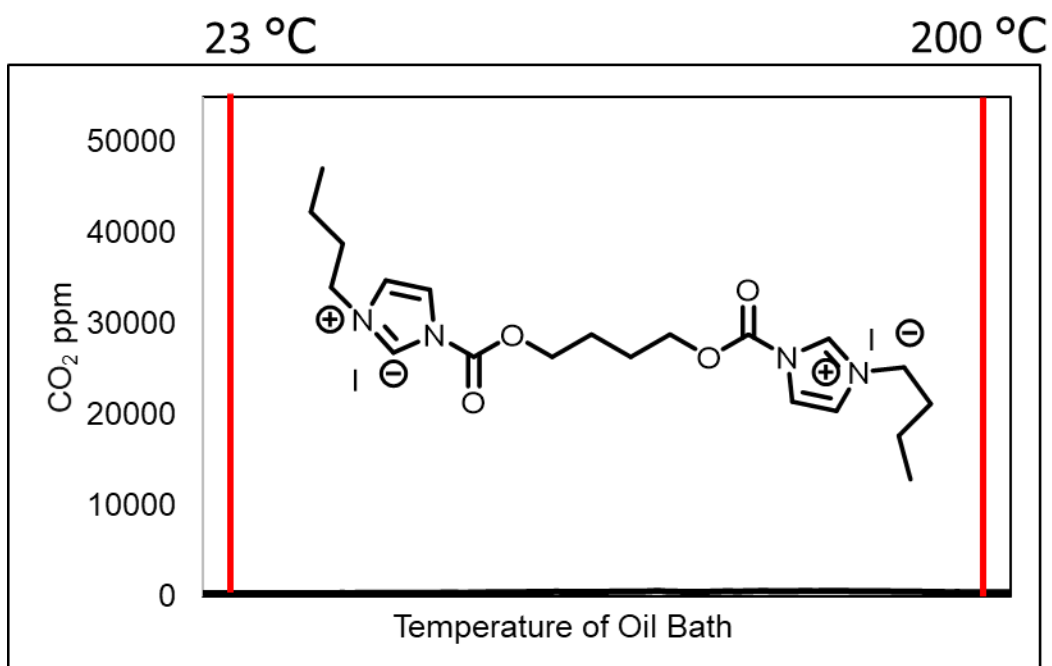


Figure S5.6 CO_2 production monitoring of BBCI IL reveals no decarboxylation after imidazolium production

CHAPTER 6

MICHAEL ACCEPTORS AS REACTIVE FILLERS IN BIS-CARBONYLIMIDAZOLIDE-DERIVED NON-ISOCYANATE POLYURETHANE FOAMS

6.1 Abstract

Previous investigations pertaining to bis-carbonylimidazolidone (BCI) monomers described a facile approach for the synthesis of non-isocyanate polyurethane (NIPU) foams with tunable thermomechanical properties. While effective at producing NIPU foams, processing difficulties arose from high melting point monomers and the need for an additional post-processing step to remove the imidazole condensate from the foam matrix. This work describes the synthesis of a novel BCI monomer that displays a melting point of $-17\text{ }^{\circ}\text{C}$, allowing for a decrease in NIPU foam reaction temperatures. Additionally, the incorporation of an acrylate- or maleimide-functionalized filler enabled efficient imidazole sequestration through a Michael addition pathway. In-situ FTIR spectroscopy validated Michael addition kinetics in a model system comprised of imidazole and butanediol diacrylate compounds, demonstrating increased kinetics at elevated temperatures. Thermogravimetric analysis confirmed imidazole sequestration within the BCI foam for both the acrylate and maleimide system. Further comparison between control BCI foams showcased an increase in thermal stability after the incorporation of the reactive filler, demonstrating the synergistic properties Michael acceptor additives have on BCI foams and further validating their use as a replacement for isocyanate-based polyurethane foam pathways.

6.3 Introduction

Polyurethane (PU) foams stand out as a high-volume product accounting for approximately 67% of global PU consumption.¹ They provide a premier solution for cushioning, construction, light weighting and transportation applications due to their tunable porous structure and modular thermomechanical properties.¹⁻⁸ The facile, high-yielding reaction between an isocyanate and alcohol enables reliable PU foam synthesis at industrial scales, while efficient water-mediated decarboxylation chemistry results in a porous structure of controlled size and shape.^{9, 10} PU foams derive their tunability from not only the diverse isocyanate and polyol chemistry available, but also from pore size and shape.^{11, 12} Thus, extensive research has been conducted to understand and control these structure-property-processing relationships.¹³⁻¹⁶ While isocyanate and polyol chemistry control phase separation and the resulting thermomechanical properties, pore geometry serves as a mechanism to instill physical damping or insulative properties. Thus, a variety of PU foams exist ranging from flexible, open-cell structures for cushioning to high T_g , closed-cell structures for light-weight structural or insulative applications.¹⁷ Likewise, the ratio of isocyanate to alcohol groups, as well as the chemical structure (aliphatic vs. aromatic) greatly contribute to foam hardness and density. Namely, 4,4'-diphenylmethane diisocyanate (MDI) and toluene diisocyanate (TDI) comprise the majority of isocyanate selection for foams where MDI produces foams with increased hardness and density compared to TDI-derived foams.¹⁸

In addition to PU chemistry considerations, additives, or fillers, offer an additional route towards achieving outstanding, tailored properties. Modern PU foams are heavily formulated to meet safety standards or property requirements for a given application.

Specifically, foams often contain added surfactants, amine and tin catalysts, flame retardants, colorants, plasticizers, and inorganic fillers among other specialized additives.^{17, 19-21} Further formulation requirements for certain applications require the additional insertion of bacteriostats for antibacterial properties, antistatic agents, UV stabilizers, compatibilizers, or auxiliary blowing agents.²²⁻²⁴ Thus, the wide-spread use of fillers for PU foams highlights the importance of additives for achieving optimal properties. While conventional isocyanate and polyol chemistry proves an effective pathway for PU foam production, the inherent toxicity of isocyanate precursors prompted the search for safer, more sustainable synthetic pathways that achieve similar thermomechanical performance.²⁵ Therefore, a wide library of research pertaining to isocyanate-free pathways for PU synthesis exists. Namely, the development of non-isocyanate polyurethanes (NIPUs) resulted in several innovative synthetic pathways for the production of PU materials, while circumventing toxic isocyanates.²⁶⁻²⁹ One such method is the ring opening of cyclic carbonates with amines producing poly(hydroxyurethane)s without the use of isocyanates.³⁰⁻³² This system proves effective at producing NIPU foam architectures, however suffers from pendant hydroxyl groups that result from the ring opening which cause increased water uptake and impedes phase separation.³³⁻³⁵ A novel synthetic approach leveraging bis-carbonylimidazolidone (BCI) monomers demonstrates a more promising route towards the production of NIPU foams that omits pendant hydroxyl groups.^{36, 37} **Figure 6.1** describes the synthesis of BCI monomers and subsequent polymerization to provide a NIPU structure. Previous investigations revealed that BCI monomers produced foams with diverse thermomechanical properties when utilizing a

basic catalyst and amine monomers with functionality >3. Likewise, careful surfactant loading successfully controlled pore architecture.

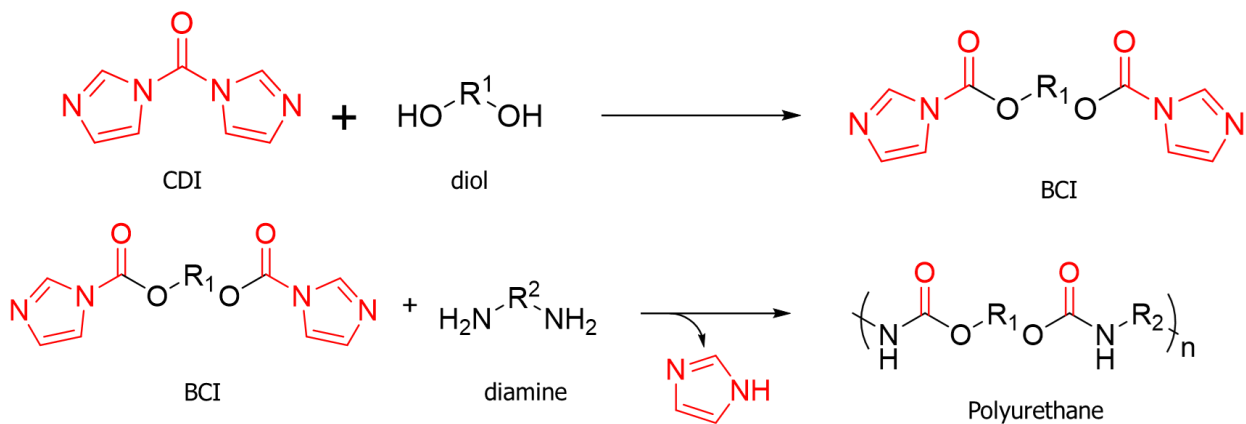


Figure 6.1: General synthetic scheme for NIPUs derived from BCI monomers. 1,1'-carbonyldiimidazole (CDI) reacts readily with diols to yield BCI monomers. These monomers undergo a polycondensation reaction in the presence of multifunctional amines to produce a high molecular weight polyurethane.

While previous literature displayed the successful formation of NIPU foams from a BCI approach, considerations regarding the imidazole byproduct were limited to solvent extractions.³⁸ The desire to reduce the number of post-processing steps prompted the exploration of a reactive filler capable of not only sequestration of the imidazole byproduct, but also the retention or enhancement of thermomechanical properties. Additionally, the successful capture of imidazole is necessary for facile adaptation of BCI chemistry to legacy foam processing techniques, i.e., molded PU foams. The nucleophilic reactivity of imidazole allowed the exploration of several Michael acceptor systems comprised of acrylate and maleimide functionalities. A Michael reaction system was chosen due to a wide temperature window for reactivity and facile incorporation into the existing BCI ecosystem.³⁹ In-situ FTIR and thermogravimetric analysis confirmed the reactivity of both

chemistries for imidazole sequestration, which proved fortuitous as this allowed for implementation into rigid and flexible NIPU foams. Previously published BCI foam formulations served as a control to evaluate the sequestration of imidazole byproduct through mass-loss measurements. This manuscript outlines the direct incorporation of reactive Michael acceptors to existing BCI foam formulations and the subsequent capture of the produced imidazole in the absence of a post-processing step.

6.3 Experimental and Methods

6.3.1 Instruments

^1H and ^{13}C nuclear magnetic resonance (NMR) spectroscopy utilized a Bruker Avance NEO 500 MHz spectrometer functioning at 500.15 MHz and 23 °C (solution concentration of 10 mg mL⁻¹). A ThermoFisher Scientific Nicolet iS5 FTIR spectrometer iD7 ATR, with a diamond cell, confirmed PU foam structure after 32 scans. A ReactIR in-situ FTIR spectrometer enabled real-time probing of Michael addition kinetics with a 2 min resolution at 64 scans per data spectrum. A TA Instruments Discovery Series TGA 5500 facilitated thermogravimetric analysis (TGA) by utilizing a heating rate of 10 °C min⁻¹ from 25 – 800 °C with a steady nitrogen purge. The $T_{d,5\%}$, or temperature where 5% of the original sample mass is lost, stands as an indicator for sample thermal stability or imidazole volatilization. Stepwise isothermal TGA followed by ramping from 25 – 800 °C at 10 °C min⁻¹ until the weight change was > 0.1 % min⁻¹, and the TGA would isotherm until the weight change was < 0.05 % min⁻¹ allowing for accurate weight loss measurements due to imidazole. A TA Instruments Discovery Series DSC 2500 with heat/cool/heat cycles of 10 °C min⁻¹, 10 °C min⁻¹, and 10 °C min⁻¹, respectively, provided differential scanning

calorimetry (DSC) data where the sample was under a nitrogen environment throughout the experiment. DSC provided the glass transition temperatures and monomer melting points from the midpoint of the endothermic transition in the 2nd heat. A TA Instruments Discovery SA (sorption analyzer) enabled water uptake measurements of foams throughout a wide range of humidity. A JEOL JSM IT500HR or JEOL 6300 scanning electron microscope coupled with a Cressington sputter coater 208HR using an Au/Pd conductive layer provided micrographs of PU foams. The 30 nm Au/Pd layer allowed for high-resolution images at 10x, 25x, 100x, and 500x magnification, and the secondary electron detector maintained 15.0 kV for all images. A Gas Lab CM-0177, S8 CO₂ sensor kit enabled the detection of CO₂ released from the foaming reaction.

6.3.2 Materials

1,4-butanediol (>99.0%), 1,1'-carbonyldiimidazole (CDI) (>97.0%), 4,8-bis(hydroxymethyl)tricyclo[5.2.1.0^{2,6}]decane (TCD) (96%), 1,4-butanediol diacrylate (BDDA) (technical grade), Dabco[®] 33LV, and dibutyltin dilaurate (95%) were purchased from Sigma Aldrich. 4,4'-dihydroxydiphenylmethane (BPF) (>99.0%), was purchased from TCI and used as received. 4-(4-aminophenoxy)benzene-1,3-diamine, or triaminodiphenylether, (TADE) (97%) was provided by SABIC and stored in a desiccator under reduced pressure. Jeffamine[®] T-403 polyetheramine was provided by Huntsman and had a number-average molecular weight of 440 g mol⁻¹. The Jeffamine[®] was dried at 60 °C under reduced pressure prior to use. Dabco[®] DC193 and 1,2-bis(2-aminophenylthio)ethane bismaleimide (APO-BMI) were provided by Honeywell NSC and used as received. Ethyl acetate (>99.5%, ACS grade), acetone (99.6% ACS reagent), and methanol (>99.8%, ACS grade) were purchased from Fisher Scientific and used as received. Nitrogen gas (99.999%

UHP-T) was purchased from Praxair Distribution. Deuterated chloroform (CDCl₃) was purchased from Cambridge Isotope Laboratories, Inc.

6.3.3 Synthesis of 1,4-butyl(bis-carbonylimidazolid) (BBCI) and 4,8-Bis(hydroxymethyl)tricyclo[5.2.1.0^{2,6}]decane(biscarbonylimidazolid) (TCDBCI)

The synthetic procedure for these monomers followed from our previous literature, with only slight modifications for TCDBCI.³⁶ 1,4-butanediol (27.04 g, 0.3 mol) was added to a three-necked, 1 L round-bottomed flask outfitted with a magnetic stir bar, nitrogen inlet, nitrogen outlet, and rubber septa. The butanediol was dissolved in ethyl acetate (600 mL) at 25 °C for 10 min under a nitrogen purge. 1,1'-Carbonyldiimidazole (CDI) (121.61 g, 0.7 mol) was added to the flask in partitions to allow for even mixing and to reduce the propensity for cyclization. The reaction was allowed to proceed for ~2 h prior to filtration using a fritted funnel. The white powder was washed twice with ethyl acetate to remove byproducts (500 mL total) and dried at 60 °C and ~1 in-Hg for 18 h. The final isolated yield was > 90% with a melting point range of 138-140 °C. ¹H NMR (CDCl₃, δ, Figure S1) 8.13-8.14 (t, 2H, 3), 7.41-7.42 (t, 2H, 2), 7.07-7.08 (m, 2H, 1), 4.47-4.51 (t, 4H, 5) 1.95-2.00 (m, 4H, 6). The synthesis for TCDBCI followed the same procedure as above, however the product was precipitated in water then centrifuged. The collected product was dried at 80 °C overnight under reduced pressure. A mixture of *cis* and *trans* isomers presents multiple peaks in NMR that split over a wide range in the aliphatic proton region. However, clear splitting of imidazole-bound protons that integrate favorably with aliphatic protons suggests complete conversion and sufficient purity.

6.3.4 Synthesis of Non-Isocyanate Polyurethane Foams

BBCI and TCDBCI were used to synthesize PU foams with varied T_g s by incorporating either aromatic or flexible aliphatic amine monomers. BBCI (5.00 g, 18.0 mmol) was added to a 50 mL single-neck round bottomed flask with a stir bar and a twin connecting hose joint to allow for nitrogen flow over the flask. The flask was purged with nitrogen for 5-10 min before lowering the flask into an oil bath at 160 °C to melt the monomer. Once the BBCI was in the melt (<5 min), the T-403 (5.17 g, 11.7 mmol) was quickly added to the reaction with a syringe. The reaction proceeded for 1-2 min before curing. The foam was extracted with 250 mL of methanol for 18 h to extract the imidazole byproduct. The foams were then placed in an oven at 80 °C for 16 h before applying reduced pressure for an additional 18 h.

An aromatic triamine was utilized to further increase the T_g of the PU foams. Following the same procedure, BBCI (1.88 g, 6.7 mmol) and TADE (0.95 g, 4.4 mmol) were added to a 50 mL single-neck round bottomed flask with a stir bar and a twin connecting hose joint to allow for nitrogen flow over the flask. The flask was purged with nitrogen for 5-10 min before lowering the flask into an oil bath at 160 °C to melt the monomers. Once the reagents were in the melt, the reaction cured in <3 min. This process was repeated for the T-403-containing foams where T-403 was added in molar ratios of 100:0, 90:10, 80:20, 70:30, and 60:40 mol:mol, TADE:T-403. A low concentration, 0.8 wt. %, of Dabco[®] DC193 was added to select PU foams to elucidate the effect on cell structure and overall homogeneity. The surfactant was added with the BCI monomer prior to the addition of the amines and surfactant-containing foams were not used for thermal characterization. Foams synthesized with TCDBCI were conducted in a similar manner, although reaction

temperatures were lowered to 120 °C to account for the lower melting point of the monomer.

6.3.5 Synthesis of Foams Containing Michael Acceptor Additives

Formulations of NIPU foams that implement imidazole capture chemistries followed similar procedures as previously stated. The addition of acrylate or maleimide chemical groups enabled the rapid and efficient capture of the imidazole byproduct, while reaching sufficient urethane conversion to form a thermoset network. The Michael acceptor compound, either BDDA or APO-BMI) was added to the BCI component of the foam mixture at a 1:1 molar ratio of functional groups, as premature introduction to the amine component results unwanted azo-Michael additions that reduce amine functionality.

6.4 Results and discussion

Previous research efforts detailed the synthesis of non-isocyanate polyurethanes from biscarbonyl imidazolide (BCI) monomers. These efforts demonstrated the efficacy of thermomechanical property control over synthesized NIPUs through the modulation of rigid and flexible BCI monomer selection. Rigid BCI and amine monomers produced high T_g foams imparted with high compressive moduli. These monomers included TADE, an aromatic triamine, and a BCI monomer derived from butanediol, butane bis-carbonylimidazolide (BBCI). While the resulting foams demonstrated favorable thermomechanical properties, elevated processing temperatures of 180 – 230 °C prevented a practical implementation of these monomers in common foam molding applications. Due to these issues, low melting monomers capable of high-performance foams was still of interest. A commercial diol, bis(hydroxymethyl)tricyclo[5.2.1.0^{2,6}]decane (TCD), was

chosen for investigation. TCD contains bulky substituents, which commonly result in decreased backbone mobility when incorporated into a polymer; this in turn raises T_g and provided an avenue to increased compressive modulus. Likewise, the mixture of isomers present in TCD results in a depression of melting point when not polymerized. Thus, the bulkiness of the BCI monomer decreased packing efficiency in the small molecule state, lowering the melting point of the monomer. To that end, a new BCI monomer was synthesized and evaluated for use in the BCI NIPU foam procedure, displayed in **Figure 6.2**.

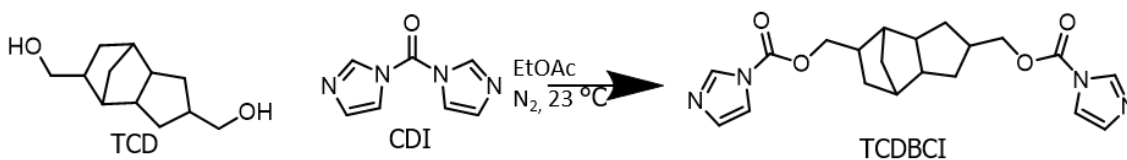


Figure 6.2. Synthesis of a novel BCI monomer for rigid foam applications. Bulky substituents enable T_g elevation of the final foam and melting point depression of the starting monomers.

Melting point evaluations for TCDBCI resulted in the selection of TCDBCI as a successful candidate for low temperature rigid foam synthesis. The low melting temperature of TCDBCI (-17 °C) enabled processing windows below 100 °C for rigid foam production while BBCI displayed melting temperatures of 140 °C. **Figure 6.3** summarizes DSC thermal performance data after reaction with either a flexible, etheric triamine (T-403), a rigid, aromatic triamine (TADE), or a mixture thereof. As predicted, an increase in the concentration of the rigid aromatic triamine resulted in an increase in T_g . Likewise,

Figure 6.3 The reaction of TCDBCI with either flexible or rigid triamines allowed for control over the final thermal properties after methanol extraction. These relations directly correlate to previously reported findings.³⁶

While solvent extraction of high performance NIPU foams resulted removal of the imidazole condensate and adequate thermomechanical properties, a facile processing procedure that circumvented this additional step remained desired. Likewise, additional fine tuning of thermomechanical properties with additives was unexplored, thus prompting investigations of a reactive filler capable of sequestering imidazole. The imidazole nitrogen provided a reactive handle for subsequent addition to an electrophile. While there exists a wide library of electrophilic moieties capable of reaction with a nucleophile, considerations regarding foam production temperatures, miscibility, and reactivity limited selection to a Michael reaction system. Compounds containing this reactivity are diverse and can be tuned for different chemistries including acrylate, maleimide, and vinyl sulfones. Likewise, the reaction is efficient, which provides high conversions. **Figure 6.4** displays a generalized reaction scheme between a nucleophile and a Michael acceptor, which reacts to high conversions to sequester the nucleophile. Tuning the chemistry of the acceptor allowed for incorporation of this filler into flexible and rigid foam systems after reacting with imidazole.

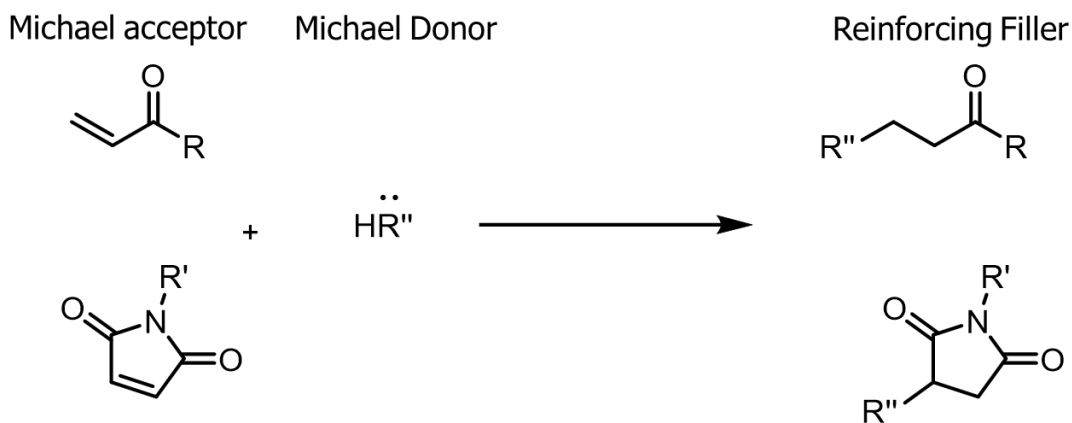


Figure 6.4 General reaction scheme for the Michael addition of a nucleophile with two common Michael acceptors, acrylate and maleimide moieties.

In-situ FTIR spectroscopy allowed probing of reaction kinetics at various temperatures for a model reaction between imidazole and a difunctional Michael acceptor, BDDA, displayed in **Figure 6.5**. Although Michael addition products undergo a reverse reaction under sufficient temperatures, elevated temperatures resulted in an increase in reaction kinetics for product formation. This proved fortuitous, since the elevated temperatures for NIPU foam synthesis served to ensure fast sequestration of imidazole. It should be noted, however, that the reaction kinetics derived from in-situ experiments required solvation of both reagents, which produces a decreased concentration of reactive groups. It is expected that melt-phase reactions involving imidazole and acrylates result in faster reaction rates on the order of foam curing rates.

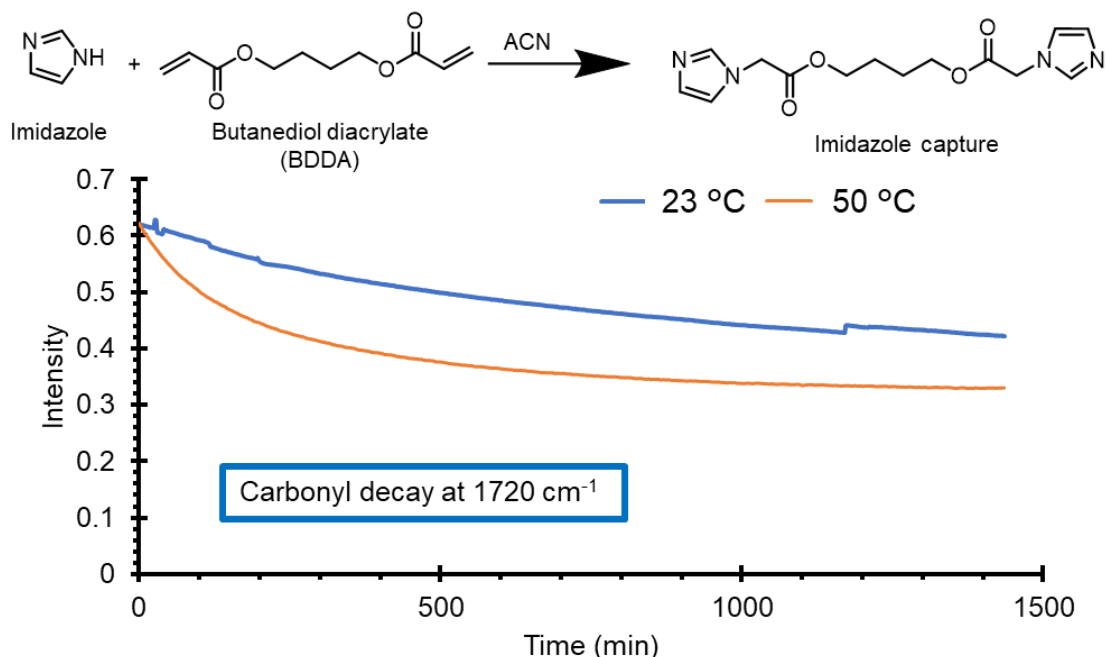


Figure 6.5: In-situ FTIR spectroscopy probed the addition of imidazole to BDDA in the absence of catalyst in acetonitrile. Disappearance of the BDDA carbonyl informed reaction extent and kinetics at different temperatures.

After In-situ FTIR spectroscopy confirmed the reactivity between imidazole and a Michael acceptor, BDDA was implemented into a conventional NIPU synthetic pathway involving BBCI and T-403. A 1:1 molar ratio of all reactive groups ensured sufficient reactivity to achieve a crosslinked foam and sequestration of any imidazole byproduct produced, shown in **Figure 6.6**. Unlike previous BBCI-T-403 NIPU foams, this product displayed increased coloration, presumably due to the acrylate additive. However, the NIPU foam containing the additive maintained flexibility expected from an open-cell architecture. This maintained flexibility was attributed to the flexible nature of BDDA, a linear aliphatic additive. It is important to highlight, however that a large mass loading of BDDA was

needed to ensure full sequestration of all produced imidazole. This may be offset by incorporating a Michael acceptor with increased functionality, such as a tri- or tetra-functional acrylate system that maintains a molar equivalent of reactive groups to the BCI monomer.

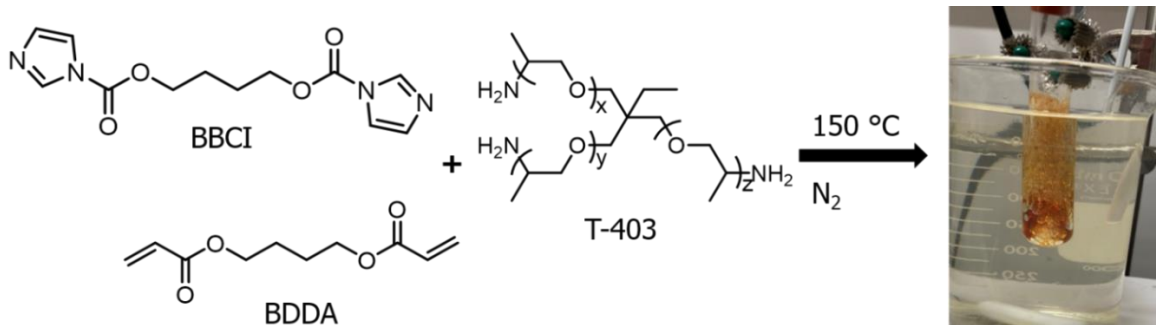


Figure 6.6: Addition of BDDA to BCI foam formulations resulted in a porous, crosslinked polyurethane foam that possessed increased coloration.

Thermogravimetric analysis provided an efficient method for monitoring residual imidazole content in a crosslinked BCI foam. A step-wise isothermal experiment, where the sample remained at a constant temperature until weight loss ceased, revealed residual imidazole content in control BCCI-T-403 and BCCI-T-403-BDDA NIPU foams. Imidazole contains a melting point of approximately 90 °C and displays an elevated vapor pressure resulting in measurable sample mass loss at this temperature. The step-wise isotherm experiment subsequently halted temperature ramping until all free imidazole in the foam sample evaporated. **Figure 6.7** highlights this phenomenon, as the control foam displays clear mass loss at 90 °C due to the thermal removal of imidazole trapped in the NIPU foam matrix. Conversely, the NIPU foam containing the BDDA additive displayed an absence of mass loss at those temperatures, instead displaying mass loss at 205 °C. This

was presumably due to a retro-Michael addition resulting in the release of imidazole and subsequent removal through evaporation.

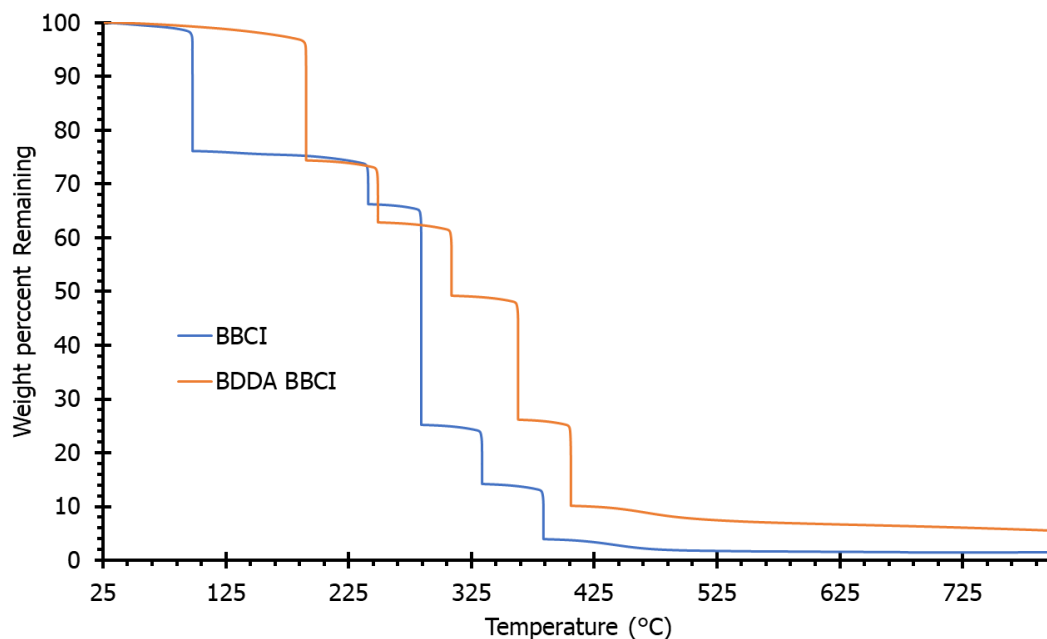


Figure 6.7 Step-wise isotherm TGA analysis provided accurate mass measurements of a flexible BBCI foam with and without the BDDA additive. An increase in weight loss onset for the BDDA BBCI foam indicates successful capture of the imidazole condensate.

Additional Michael acceptor chemistries and foam compositions allowed the investigation of this reactive additive system as a holistic solution for rigid and flexible BCI foam production. The maleimide functional group boasts impressive thermal stability while maintaining similar electrophilic reactivity as acrylates.^{40, 41} A NIPU foam formulation that leveraged monomers with restricted mobility consisting of TADE and BBCI resulted in the synthesis of a rigid BCI foam for evaluation. Subsequent incorporation of a disulfide-derived bismaleimide (APO-BMI) allowed for the retention of a high T_g while probing imidazole sequestration. TGA enabled a comparison between a control BBCI-TADE and

BBCI-TADE-APO-BMI foam to evaluate imidazole content as a function of chemical formulation and processing, shown in **Figure 6.8**. Specifically, both the neat and extracted foams were compared to rigid foam composition that contained the APO-BMI additive. As expected, the unextracted control foam displayed an earlier onset mass loss due to the evaporation of imidazole. Conversely, the NIPU foam formulation containing the APO-BMI additive displayed an increased resistance to weight loss due to the sequestration of imidazole by the reactive additive. It is interesting to note, however, that the extracted control foam displayed mass loss at lower temperatures compared the APO-BMI infused foam, presumably due to the increased thermal stability of the maleimide-imidazole sequestration product. This proved fortuitous, as not only did APO-BMI effectively trap the imidazole condensate, but it boosted thermal performance as well, providing an improvement for this rigid NIPU foam system.

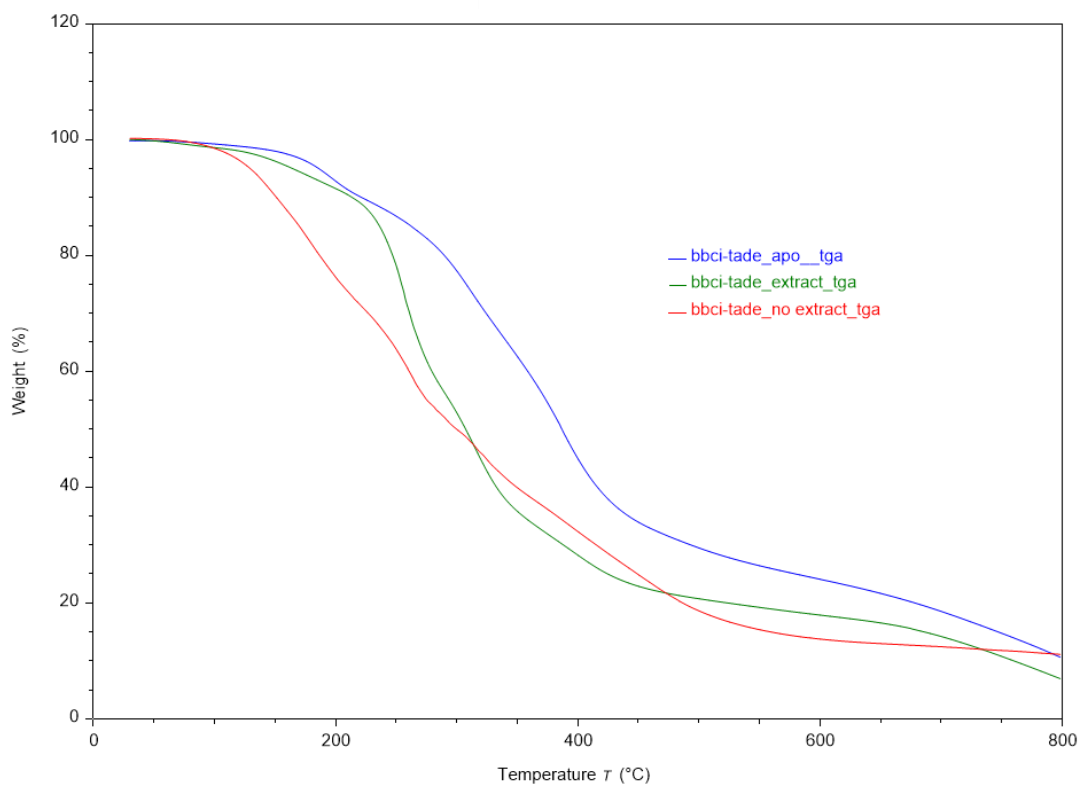
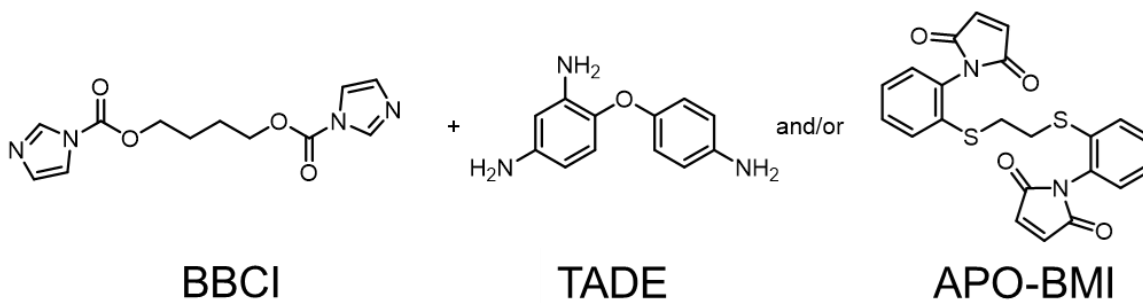


Figure 6.8 TGA weight loss traces for neat, extracted, and BMI rigid foams revealed the effects that each method has on imidazole retention and leaching. The rigid foam sample containing the maleimide additive displayed the highest degree of thermal resistance.

6.5 Conclusions

The facile synthesis of a series of novel BCI monomers derived from cyclic diols produced a series of NIPU foams with T_g s approaching 100 °C. The bulky nature of TCDBCI resulted in a low melting point monomer that enabled foam reaction temperatures of 120 °C, which is approximately 40 °C lower than previously reported. This innovation allowed successful foam production at moderate temperatures, however required additional post-processing to remove the imidazole condensate that resulted from the amine addition to BCI monomers. Thus, several Michael acceptor compounds were evaluated for their ability to capture the imidazole condensate that results from the formation of NIPU foams when utilizing BCI monomers. In-situ FTIR spectroscopy validated the aza-Michael addition of imidazole to an acrylate Michael acceptor and displayed increased reaction kinetics as a function of temperature. Incorporation of this reactive additive into flexible BCI foam formulations achieved imidazole sequestration, validated by step-wise TGA experiments, while maintaining expected T_g values. Furthermore, APO-BMI, a rigid reactive filler, enabled complete imidazole sequestration in a rigid foam system that displayed additional resistance to mass loss at elevated temperatures. The efficient imidazole sequestration shown in this work further validates the feasibility of BCI chemistry to replace isocyanates for PU foam production while providing an additional handle to tune the thermomechanical properties of the resulting foam.

6.6 Acknowledgements

I would like to thank Honeywell FM&T for guidance and funding for this work

6.7 Funding

This work was funded by Honeywell FM&T

6.8 References

1. Gama, N. V.; Ferreira, A.; Barros-Timmons, A., Polyurethane Foams: Past, Present, and Future. *Materials* **2018**, *11* (10), 1841.
2. Somarathna, H. M. C. C.; Raman, S. N.; Mohotti, D.; Mutalib, A. A.; Badri, K. H., The use of polyurethane for structural and infrastructural engineering applications: A state-of-the-art review. *Construction and Building Materials* **2018**, *190*, 995-1014.
3. Singhal, P.; Small, W.; Cosgriff-Hernandez, E.; Maitland, D. J.; Wilson, T. S., Low density biodegradable shape memory polyurethane foams for embolic biomedical applications. *Acta Biomaterialia* **2014**, *10* (1), 67-76.
4. Jin, F.-L.; Zhao, M.; Park, M.; Park, S.-J., Recent Trends of Foaming in Polymer Processing: A Review. *Polymers* **2019**, *11* (6), 953.
5. Wu, J.-W.; Sung, W.-F.; Chu, H.-S., Thermal conductivity of polyurethane foams. *International Journal of Heat and Mass Transfer* **1999**, *42* (12), 2211-2217.
6. Zhang, H.; Fang, W.-Z.; Li, Y.-M.; Tao, W.-Q., Experimental study of the thermal conductivity of polyurethane foams. *Applied Thermal Engineering* **2017**, *115*, 528-538.
7. Casati, F. M.; Herrington, R. M.; Broos, R.; Miyazaki, Y., Tailoring the Performance of Molded Flexible Polyurethane Foams for Car Seats. *Journal of Cellular Plastics* **1998**, *34* (5), 430-466.
8. Khan, T.; Acar, V.; Aydın, M. R.; Hülagü, B.; Akbulut, H.; Seydibeyoğlu, M. Ö., A review on recent advances in sandwich structures based on polyurethane foam cores. *Polymer Composites* **2020**, *41* (6), 2355-2400.

9. Delebecq, E.; Pascault, J.-P.; Boutevin, B.; Ganachaud, F., On the Versatility of Urethane/Urea Bonds: Reversibility, Blocked Isocyanate, and Non-isocyanate Polyurethane. *Chemical Reviews* **2013**, *113* (1), 80-118.
10. Yilgör, I.; Yilgör, E.; Wilkes, G. L., Critical parameters in designing segmented polyurethanes and their effect on morphology and properties: A comprehensive review. *Polymer* **2015**, *58*, A1-A36.
11. Smits, G. F., Effect of Cellsize Reduction on Polyurethane Foam Physical Properties. *Journal of Thermal Insulation and Building Envelopes* **1994**, *17* (4), 309-329.
12. Janik, H.; Marzec, M., A review: Fabrication of porous polyurethane scaffolds. *Materials Science and Engineering: C* **2015**, *48*, 586-591.
13. Blackwell, J.; Nagarajan, M. R.; Hoitink, T. B., Structure of polyurethane elastomers: effect of chain extender length on the structure of MDI/diol hard segments. *Polymer* **1982**, *23* (7), 950-956.
14. Kwei, T. K., Phase separation in segmented polyurethanes. *Journal of Applied Polymer Science* **1982**, *27* (8), 2891-2899.
15. Chu, B.; Gao, T.; Li, Y.; Wang, J.; Desper, C. R.; Byrne, C. A., Microphase separation kinetics in segmented polyurethanes: effects of soft segment length and structure. *Macromolecules* **1992**, *25* (21), 5724-5729.
16. Marciano, J. H.; Rojas, A. J.; Williams, R. J. J., Curing kinetics of a rigid polyurethane foam formulation. *Polymer* **1982**, *23* (10), 1489-1492.
17. Hansen, R., Handbook of polymeric foams and foam technology, Daniel Klempner and Kurt C. Frisch, eds., Hanser Publishers, Munich, Germany, 1992, 442 pp.

- price: \$148.00. (Distributed in the U.S. and Canada by Oxford University Press, New York.). *Journal of Polymer Science Part A: Polymer Chemistry* **1993**, *31* (5), 1344-1344.
18. Javni, I.; Zhang, W.; Petrović, Z. S., Effect of different isocyanates on the properties of soy-based polyurethanes. *Journal of Applied Polymer Science* **2003**, *88* (13), 2912-2916.
19. Lefebvre, J.; Bastin, B.; Le Bras, M.; Duquesne, S.; Paleja, R.; Delobel, R., Thermal stability and fire properties of conventional flexible polyurethane foam formulations. *Polymer Degradation and Stability* **2005**, *88* (1), 28-34.
20. Thirumal, M.; Singha, N. K.; Khastgir, D.; Manjunath, B. S.; Naik, Y. P., Halogen-free flame-retardant rigid polyurethane foams: Effect of alumina trihydrate and triphenylphosphate on the properties of polyurethane foams. *Journal of Applied Polymer Science* **2010**, *116* (4), 2260-2268.
21. Coste, G.; Negrell, C.; Caillol, S., From gas release to foam synthesis, the second breath of blowing agents. *European Polymer Journal* **2020**, *140*, 110029.
22. Sienkiewicz, N., Improvements of Polyurethane (PU) Foam's Antibacterial Properties and Bio-resistance. In *Thermal Insulation and Radiation Control Technologies for Buildings*, Kośny, J.; Yarbrough, D. W., Eds. Springer International Publishing: Cham, 2022; pp 217-240.
23. Oliviero, M.; Stanzione, M.; D'Auria, M.; Sorrentino, L.; Iannace, S.; Verdolotti, L., Vegetable Tannin as a Sustainable UV Stabilizer for Polyurethane Foams. *Polymers* **2019**, *11* (3), 480.

24. Choe, K. H.; Lee, D. S.; Seo, W. J.; Kim, W. N., Properties of Rigid Polyurethane Foams with Blowing Agents and Catalysts. *Polymer Journal* **2004**, *36* (5), 368-373.
25. Zapp, J. A., Jr., Hazards of Isocyanates in Polyurethane Foam Plastic Production. *Arch. Indust. Health* **1957**, *15* (4), 324-30.
26. Cornille, A.; Dworakowska, S.; Bogdal, D.; Boutevin, B.; Caillol, S., A new way of creating cellular polyurethane materials: NIPU foams. *European Polymer Journal* **2015**, *66*, 129-138.
27. Zhang, K.; Nelson, A. M.; Talley, S. J.; Chen, M.; Margareta, E.; Hudson, A. G.; Moore, R. B.; Long, T. E., Non-isocyanate poly(amide-hydroxyurethane)s from sustainable resources. *Green Chemistry* **2016**, *18* (17), 4667-4681.
28. Gomez-Lopez, A.; Elizalde, F.; Calvo, I.; Sardon, H., Trends in non-isocyanate polyurethane (NIPU) development. *Chemical Communications* **2021**, *57* (92), 12254-12265.
29. Khatoon, H.; Iqbal, S.; Irfan, M.; Darda, A.; Rawat, N. K., A review on the production, properties and applications of non-isocyanate polyurethane: A greener perspective. *Progress in Organic Coatings* **2021**, *154*, 106124.
30. Besse, V.; Camara, F.; Méchin, F.; Fleury, E.; Caillol, S.; Pascault, J.-P.; Boutevin, B., How to explain low molar masses in PolyHydroxyUrethanes (PHUs). *European Polymer Journal* **2015**, *71*, 1-11.
31. Tomita, H.; Sanda, F.; Endo, T., Model reaction for the synthesis of polyhydroxyurethanes from cyclic carbonates with amines: Substituent effect on the reactivity and selectivity of ring-opening direction in the reaction of five-membered

cyclic carbonates with amine. *Journal of Polymer Science Part A: Polymer Chemistry* **2001**, *39* (21), 3678-3685.

32. Bossion, A.; Aguirresarobe, R. H.; Irusta, L.; Taton, D.; Cramail, H.; Grau, E.; Mecerreyes, D.; Su, C.; Liu, G.; Müller, A. J.; Sardon, H., Unexpected Synthesis of Segmented Poly(hydroxyurea–urethane)s from Dicyclic Carbonates and Diamines by Organocatalysis. *Macromolecules* **2018**, *51* (15), 5556-5566.

33. Leitsch, E. K.; Beniah, G.; Liu, K.; Lan, T.; Heath, W. H.; Scheidt, K. A.; Torkelson, J. M., Nonisocyanate Thermoplastic Polyhydroxyurethane Elastomers via Cyclic Carbonate Aminolysis: Critical Role of Hydroxyl Groups in Controlling Nanophase Separation. *ACS Macro Letters* **2016**, *5* (4), 424-429.

34. Kotanen, S.; Poikelispää, M.; Efimov, A.; Harjunalanen, T.; Mills, C.; Laaksonen, T.; Sarlin, E., Hydrolytic stability of polyurethane/polyhydroxyurethane hybrid adhesives. *International Journal of Adhesion and Adhesives* **2021**, *110*, 102950.

35. Yu, Y.-J.; Hearon, K.; Wilson, T. S.; Maitland, D. J., The effect of moisture absorption on the physical properties of polyurethane shape memory polymer foams. *Smart Materials and Structures* **2011**, *20* (8), 085010.

36. Sintas, J. I.; Wolfgang, J. D.; Long, T. E., Carbamate thermal decarboxylation for the design of non-isocyanate polyurethane foams. *Polymer Chemistry* **2023**, *14* (13), 1497-1506.

37. Wolfgang, J. D.; White, B. T.; Long, T. E., Non-isocyanate Polyurethanes from 1,1'-Carbonyldiimidazole: A Polycondensation Approach. *Macromolecular Rapid Communications* **2021**, *42* (13), 2100163.

38. Sintas, J. I.; Wolfgang, J. D.; Long, T. E., Carbamate thermal decarboxylation for the design of non-isocyanate polyurethane foams. *Polymer Chemistry* **2023**.
39. Mather, B. D.; Viswanathan, K.; Miller, K. M.; Long, T. E., Michael addition reactions in macromolecular design for emerging technologies. *Progress in Polymer Science* **2006**, *31* (5), 487-531.
40. Brown, I. M.; Sandreczki, T. C., Cross-linking reactions in maleimide and bis(maleimide) polymers. An ESR study. *Macromolecules* **1990**, *23* (1), 94-100.
41. Daily, C.; Torres, S. M.; Robison, T. W.; Bowler, N., Dielectric and kinetic comparison of APO-BMI grades. *High Performance Polymers* **2018**, *30* (9), 1101-1113.

CHAPTER 7

A NOVEL CYCLOBUTANE BISIMIDE MONOMER FOR PHOTO-CLEAVABLE POLYURETHANE SYNTHESIS

7.1 Abstract

Innovations in the semiconductor industry require the development of novel processing methods to accommodate advanced development techniques. Temporary bond-debond (TBDB) technology represents a processing modality that requires constant innovation. Previous work illustrates the use of 1,2,3,4-cyclobutane-tetracarboxylic dianhydride (CBDA) as a pathway for photo-cleavable TBDB technology that utilizes a poly(dimethyl siloxane) backbone. This work presents the synthesis of a novel cyclobutane bisimide monomer that boasts either bisphenol or bishydroxy reactivity. The reactivity of 4-aminophenol allowed for selective addition of the aryl amine onto CBDA, producing an amic acid precursor capable of chemical and thermal imidization. FTIR and ^1H NMR spectroscopy, coupled with thermogravimetric analysis, fully characterized the synthetic pathway for this novel monomer. Subsequent polymerization with a toluenediisocyanate terminated poly(propylene glycol) monomer yielded a novel cyclobutane functionalized polyurethane for TBDB applications. Thermomechanical analysis revealed a 27 °C increase in flow temperature and 20% increase in strain after irradiation with 254 nm light. Likewise, ^1H NMR spectroscopy characterized the formation of maleimide protons resulting from cyclobutane bisimide ring cleavage after light exposure.

7.2 Introduction

As competitive innovation continues in the semiconductor industry, the development of novel materials capable of supporting technically challenging patterning processes

continue to progress. These materials must meet diverse thermomechanical and optical requirements for multi-step fabrication processes, with an emphasis on thermal expansion coefficients, thermal stability, off-gassing, and photo-activity.¹ One such use case is the temporary bonding of a substrate onto a supporting layer during the fabrication process, known as temporary bonding and debonding (TBDB).²⁻⁴ This involves an initial bonding process between a glass substrate and the wafer that subsequently undergoes development. The wafer must then be released from the substrate through a debond process that requires a release mechanism and washing of the bonding material off the wafer.³ A facile release mechanism of the TBDB process is required to ensure minimal damage to the wafer surface, as thermal debonding of the adhesive often demands elevated temperatures and heat cycling that leads to warpage or cracking of the processed device.^{5, 6} For this reason, a departure from the traditional thermal process is desired.

Light-based debonding techniques have received considerable attention due to lower processing costs and higher control.^{2, 7-9} Previous research demonstrated the potential for cyclobutane bisimide functionalities for bond/debond and patterning applications.^{9, 10} Among structural adhesives, the imide functionality displays advanced thermal stability along with low static permittivity, chemical stability, and dielectric properties that result in their prolific use in the semiconductor sector.¹¹ There exists abundant research into photo-degradable polymers for application to semiconductor patterning and processing including o-nitro benzyl or coumarin containing polymers, and 1,2,3,4-cyclobutane-tetracarboxylic dianhydride (CBDA)- derived systems.¹²⁻¹⁸ These systems may prove useful in various steps of the semiconductor packaging process due to their photo-crosslinking or photo-degradation potential.

Photo-responsive cyclobutane chemistries are widely researched for a variety of applications including coumarin, thymine, stilbene, cinnamate, and maleimide derivatives for use in photo-reversible adhesives, self-healing polymers, liquid crystals, and light harnessing.¹⁹⁻²¹ Additionally, they possess dimerization wavelengths between 350 and 270 nm and photocleavage excitations below 300 nm.^{19, 22} This broad range of photoactivity allows for careful selection of cyclobutane chemistry to match a targeted use scenario, i.e., selecting a high-energy reversal wavelength ~254 nm will allow for exposure of the system to ambient light, since that wavelength displays low intensity at ambient conditions. Thus, the selection of cyclobutane bisimide functionality enables photo-reversibility while requiring high intensities of low wavelength light for photo-cleavage. This is advantageous as it allows for orthogonal light-based processes to occur concurrently without the possibility of unwanted cyclobutane ring reversal subsequently allowing for facile integration into present packaging modalities.

Previous work describes the direct incorporation of CBDA directly into a poly(dimethyl siloxane) (PDMS) polymer backbone with concurrent polymerization and imidization process, however a technology that is readily applied to a wide variety of polymeric systems remained desired.⁹ Thus, the synthesis of a cyclobutane bisimide-containing monomer capable of photo-degradation is described in this work. The greater reactivity of the nucleophilic aryl amine of 4-aminophenol enabled a selective addition to CBDA, producing a cyclobutane-containing amic acid with bisphenol functionality. Subsequent imidization resulted in the cyclobutane-bisimide moiety with bisphenol reactivity. Furthermore, reacting this imide with ethylene carbonate resulted in the installation of hydroxy ethyl groups allowing for the selection of phenol or hydroxyl reactivity. This

expands the application space for this material, broadening the scope of this monomer to both fully aromatic and aliphatic systems. Subsequent polymerization of this monomer with diisocyanates resulted in the synthesis of a novel, cyclobutane bisimide-containing polyurethane capable of on-demand photo-degradation.

7.3 Materials and Methods

7.3.1 Materials

Cyclobutane-1,2,3,4-tetracarboxylic dianhydride (CBDA) was graciously provided by Jayhawk Fine Chemicals[®] and used as received. 4-Aminophenol (>98%), 3-aminophenol (>98%), deuterated dimethylsulfoxide-d₆ (99.95%), ethylene carbonate (98%), triethylamine (TEA) (>99.5%), poly(propylene glycol), toluene 2,4-diisocyanate terminated $M_n=2,300$ g/mol (PPG-TDI), and 1,4-diazabicyclo[2.2.2]octane (dabco) were purchased from SigmaAldrich and used as received. N,N-dimethylformamide (DMF) (>99.5%), ethyl acetate (>99.5% ACS grade), toluene (>99%), acetone (>99.5%), and 1,2-dichlorobenzene (>99%) were purchased from VWR and used as received.

7.3.2 Instruments

¹H and ¹³C nuclear magnetic resonance (NMR) spectroscopy utilized a Bruker Avance NEO 500 MHz spectrometer functioning at 500.15 MHz and 23 °C (solution concentration of 10 mg mL⁻¹). A ThermoFisher Scientific Nicolet iS10 FTIR spectrometer, with a diamond cell at 25 °C, identified key stretches for synthesized monomers and polymers. A TA Instruments TGA 5500 facilitated thermogravimetric analysis (TGA) by utilizing a heating rate of 10 °C min⁻¹ from 25 to 600 °C with a steady nitrogen purge. The $T_{d,5\%}$, or temperature where 5% of the original sample mass was lost, served as an indicator for

sample thermal stability. A TA Instruments DSC 2500 with heat/cool/heat cycles of 10 °C min⁻¹ provided differential scanning calorimetry data where the sample was under a nitrogen environment throughout the experiment. DSC provided the glass transition temperatures (T_g s) from the midpoint of the endothermic transition in the second heat. Polyurethane films were casted out of DMF at a concentration of 100 mg/mL onto a Teflon[®] petri dish at 50 °C. A TA Instruments DMA Q800 with a temperature ramp of 3 °C min⁻¹ from -90 °C to 180 °C at 1 Hz provided a T_g taken from the peak in the tan delta. Liquid nitrogen cooling permitted the cryogenic temperatures required to observe the thermal transitions of the polyurethane films. A Mineralight 254 nm 15w lamp equipped with a 254 nm filter enabled consistent irradiation of samples at an intensity of 4.8 mW/cm². A Waters ARC HPLC size exclusion chromatography system operating at a flow rate of 1 mL/min at 5mg/mL and temperature of 50 °C enabled molecular weight determination for polymeric samples. Samples were run in 0.05 M LiBr DMF and passed through a 0.45 micrometer filter before injecting. A Waters dRI detector monitored concentration change and final molecular weight was determined against a polystyrene calibration curve. An Instron 68TM-5 with a 5 kN load cell enabled tensile testing of PU films at a rate of 5 mm/min.

7.3.3 Chemical and Thermal Synthesis of CBDA-AP-I

CBDA (10.00 g, 51.0 mmol), 4-aminophenol (11.13 g, 102.0 mmol), 100 mL of toluene and 500 mL of 1,2-dichlorobenzene were added to a 3-neck round bottomed flask equipped with a magnetic stir bar, nitrogen inlet, reflux condenser, and Dean-Stark apparatus. Reagents were allowed to mix and subsequently heated to 180 °C. The reaction was allowed to progress for 18 h and remained heterogenous throughout. The toluene served to

remove any water produced throughout the imidization reaction through an azeotrope and the Dean-Stark apparatus was emptied as needed. The precipitate was filtered using a fritted funnel and allowed to dry overnight then recrystallized in DMF. The final isolated yield was > 90%. ¹H NMR (DMSO-d₆, δ, Figure S1) 9.77 (s, 2H), 7.2 (d, 4H, *J* = 8.5 Hz), 6.87 (d, 4H, *J* = 8.5 Hz), 3.62 (s, 4H).

7.3.4 Synthesis of CBDA-AP-I-HE

CBDA-AP-I (5 g, 13.21 mmol), ethylene carbonate (3.49 g, 39.64 mmol) and TEA (4.01 g, 39.64 mmol) were added to a 2-necked 1000 mL round bottomed flask equipped with a nitrogen inlet, magnetic stir bar, and reflux condenser. 500 mL of DMF was added and heated to 120 °C under nitrogen flow. The reaction was allowed to proceed for 24 h before precipitating into ethyl acetate. The precipitate was collected with a fritted funnel and dried under reduced pressure for 12 h at 120 °C. ¹H NMR (DMSO-d₆, δ, Figure S2) 7.39 (d, 4H), 7.15 (d, 4H), 4.97 (s, 2H), 4.09 (t, 4H), 3.81 (t, 4H), 3.75 (s, 4H).

7.3.5 Synthesis of CBDA-AP-I-HE PU

Dry DMF was added to a 200 mL 2-neck round bottomed flask equipped with a magnetic stir bar and purged with nitrogen. CBDA-AP-I-HE (5 g, 10.7 mmol), PPG-TDI (24.65 g, 10.7 mmol), and dabco (0.36 g, 3.2 mmol) were added to the flask and the reaction was heated to 80 °C. The reaction was allowed to progress for 12 h and then precipitated into acetone. The collected product was dried under reduced pressure at 120 °C for 12 h. CBDA-AP-I PU films were cast out of DMF at a 15 wt. % PU loading. The PU solution was placed in a Teflon[®] dish and allowed to air dry at 40 °C for 24 h. The film was then heated to 100 °C under reduced pressure for 12 h to ensure removal of DMF.

7.4 Results and Discussion

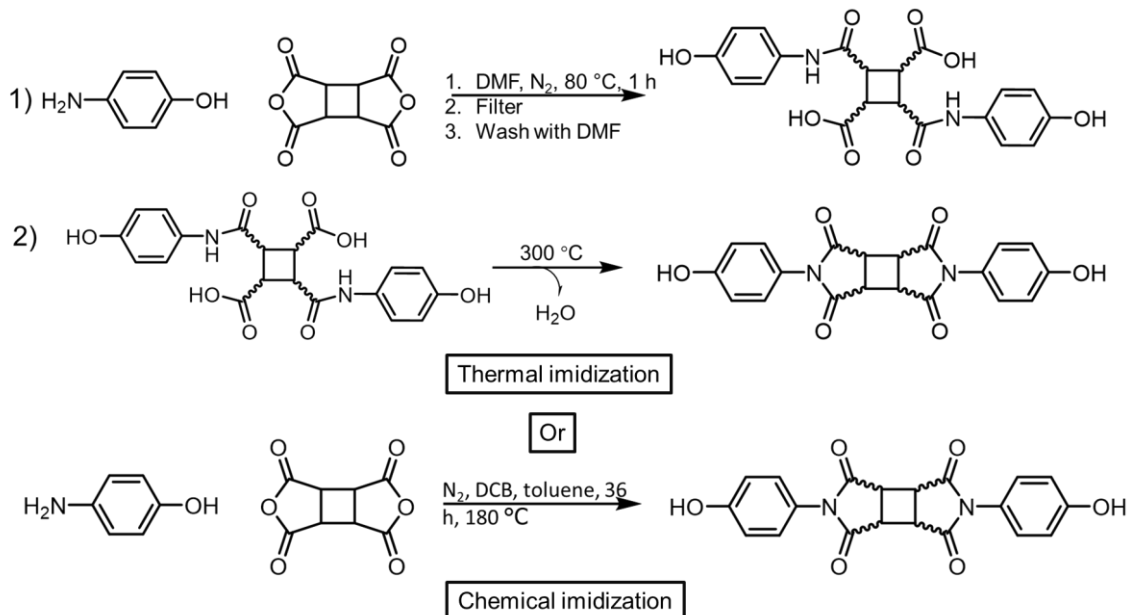


Figure 7.1 Synthetic pathway for cyclobutane bisimide monomer containing bisphenol reactivity, denoted CBDA-AP-I. Thermal and chemical imidization pathways result in a thermally stable product with a well-defined ^1H NMR spectrum.

4-aminophenol (AP) possesses both aryl amine and phenol reactivity arranged in a para configuration, however the more reactive aryl amine directed the preferential formation of an amic acid precursor. This preferential addition, confirmed with ^1H NMR analysis, provided bisphenol reactivity after either chemical or thermal imidization. The thermal imidization route required isolation of the phenol functionalized amic acid precursor followed by a thermal imidization similar to conventional imidization techniques, shown in **Figure 7.1**. It is interesting to note, however, that thermal imidization occurred at two distinct temperatures, 96 and 230 $^\circ\text{C}$, as opposed to a wide imidization window observed for polymeric imidization. FTIR, TGA, and NMR analysis of the amic acid, partially imidized, and fully imidized CBDA-AP-I compounds confirmed this phenomenon (Figures

S3-S5). This was presumably due to the small molecule nature of this compound, as opposed to a polymeric one, where various steric and chemical environments exist. While effective at achieving high conversions, the thermal imidization route resulted in severe discoloration of CBDA-AP-I due to the degradation of residual DMF bound to the amic acid precursor. This discoloration has the potential to block 254 nm light, causing a decrease in photo-cleavage efficiency. Thus, a chemical imidization process that reduced coloration of CBDA-AP-I was developed, shown in **Figure 7.1**. A one-pot reaction that leveraged a DCB and toluene mixture proved effective at achieving high purity, uncolored CBDA-AP-I. Toluene enabled the effective removal of the water condensate produced by the imide ring-closing reaction through azeotrope formation, promoting imidization.

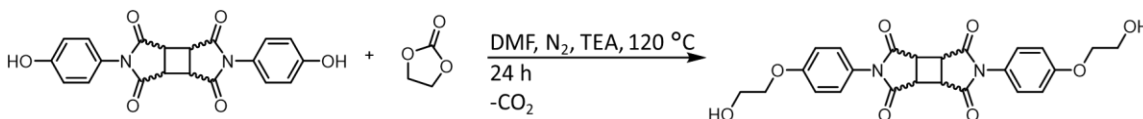


Figure 7.2 Phenolic reactive groups present on CBDA-AP-I enable the ring opening of ethylene carbonate resulting in hydroxyl functionality.

Imidization of CBDA-AP allows for a thermally stable bisphenol that readily incorporates into polymer backbones including polyesters, polycarbonates, polyurethanes, and polysulfones.^{23, 24} While versatile, phenolic linkages display reduced thermal stability within certain chemistries. Additionally, the rigid imide and aromatic structures comprising CBDA-AP-I hinder solubility, requiring temperatures above 80 °C and high-boiling polar aprotic solvents for full dissolution. The installation of hydroxyethyl functionality to phenols is well established, allowing for greater reactivity and solubility which offered an effective remediation pathway for the previously stated issues.²⁵ **Figure 7.2** portrays the

liberation of CO₂ from the reaction of CBDA-AP-I and ethylene carbonate which drove high conversions to the hydroxyethyl substituted compound, denoted CBDA-AP-I-HE. The installed hydroxy ethyl functionality subsequently increased solubility in polar aprotic solvents enabling the synthesis of a novel cyclobutane-containing PU, outlined in **Figure 7.3**.

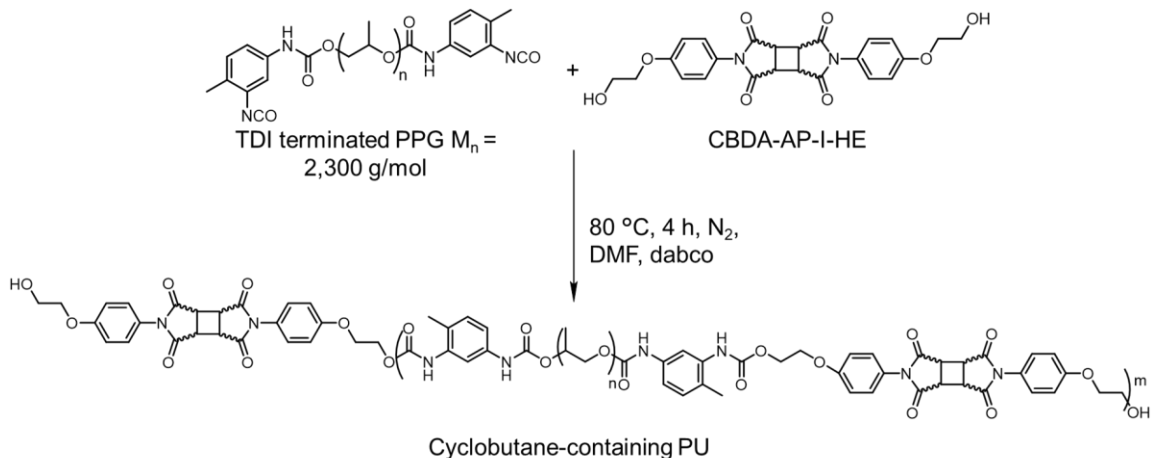


Figure 7.3 CBDA-AP-I readily reacts with isocyanate functional groups to produce a photo-responsive PU containing hydroxy end groups.

Common processing techniques for semiconductor TBDB applications include spin coating of the bonding compound followed by a thermal bake to complete the bonding process. A multi-step rheological experiment probed the efficacy of a CBDA-AP-I-HE polyurethane system for this application, exploring both the spin coating process and thermally-initiated polymerization process. A DMF solution containing both CBDA-AP-I-HE and PPG-TDI monomers underwent a steady shear experiment for 6 h to probe resin storage efficacy. Minimal viscosity increase over the 6 h period displayed the temporal stability of this monomer system. Subsequent heating mimicked a thermal bake process and demonstrated change in the storage modulus as temperature increased. A thermally

induced viscosity decrease explains the initial dip in moduli values, however a modulus increase was observed as the temperature approached sufficient values to promote molecular weight gain. Continued molecular weight increase drove a subsequent increase in moduli values. A notable crossover between storage and loss moduli signaled the formation of a polymeric system that has predominantly solid, or elastic, characteristics. A relevant bake temperature of 180 °C produced a plateau for both the storage and loss moduli, which signaled a complete bake procedure and formation of the relevant polyurethane, shown in **Figure 7.4**.

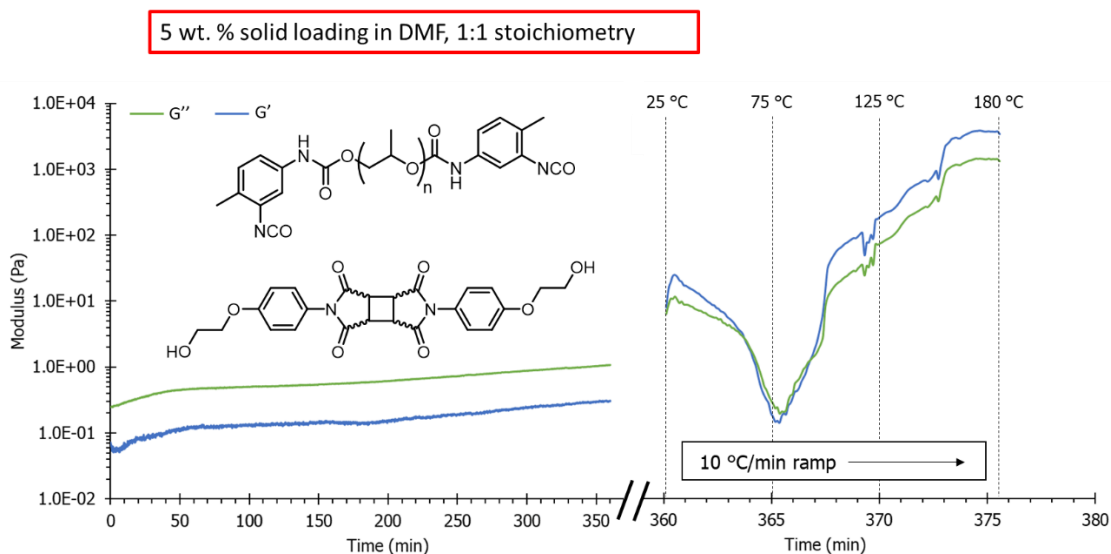


Figure 7.4 Rheological studies simulate a spin-coating application of CBDA-AP-I-HE and PPG monomers that display temporal stability at 25 °C, however polymerize when exposed to elevated temperatures.

Rheological and spectroscopy data confirmed the synthesis of a CBDA-AP-I-HE PU containing a PPG-TDI soft segment, however further thermomechanical and spectroscopic investigations allowed for evaluating cyclobutane ring cleavage after irradiation with 254

nm light. DMA measured the thermomechanical behavior of the irradiated and control PU film, shown in **Figure 7.5**. Interestingly, the DMA trace revealed the presence of a rubbery plateau, indicative of phase separation between the PPG soft segment (SS) and CBDA-AP-I-HE hard segment (HS). PU formulations often rely on chain extenders to build the molecular weight of the hard segment, resulting in the subsequent nano-scale phase separation, however the absence of chain extender in this PU formulation rendered this result surprising.^{26, 27} Both the control and irradiated PU displayed a $\tan \delta$ peak at $-27\text{ }^{\circ}\text{C}$, corresponding to the PPG soft segment. This indicated that irradiation did not affect PPG interactions contained in the SS. However, irradiation resulted in an increase in flow temperature from $62\text{ }^{\circ}\text{C}$ to $89\text{ }^{\circ}\text{C}$. HS interactions, mainly hydrogen bonding, determine the ultimate transition temperature for an amorphous PU.^{28, 29} Thus, the change in flow temperatures between the irradiated and control samples indicates a change in the chemical nature or morphology of the cyclobutane-containing HS. Presumably, cleaving of the cyclobutane bisimide linkage and subsequent maleimide formation and polymerization explains the increase in flow temperature.¹³

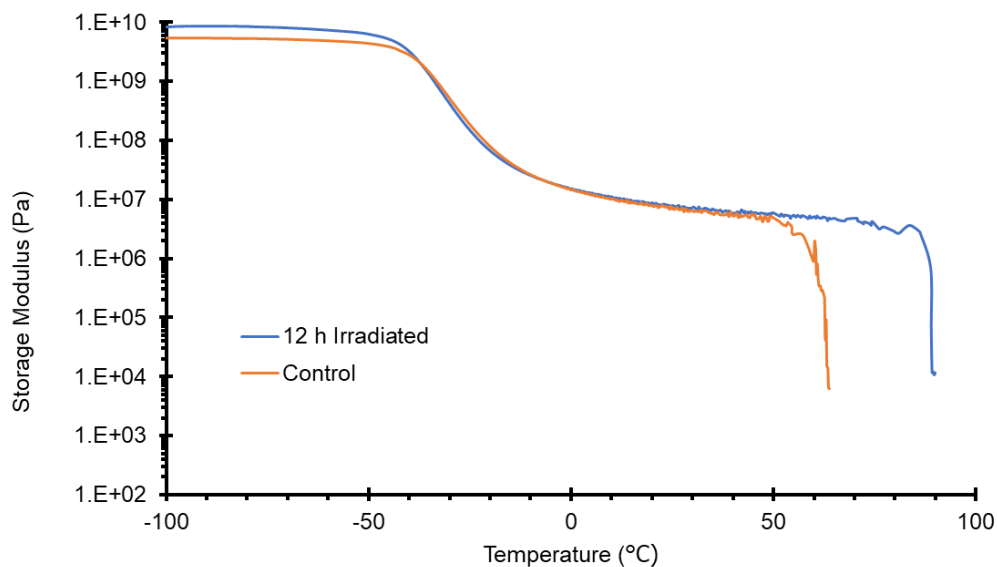


Figure 7.5: DMA suggests phase separation of the CBDA-AP-I PU homopolymer

Further probing of mechanical properties revealed a change in the tensile curves for irradiated and non-irradiated PU samples, shown in **Figure 7.6**. Stress-strain profiles for the control and irradiated sample display elastomeric properties consistent with DMA rubbery plateau moduli values. The elastomeric properties exhibited by CBDA-AP-I-HE PU provide consistent performance throughout a wide temperature range (80 °C). Possible chain extension from maleimide polymerization resulted in an increase of the strain at break after irradiation. It should be noted however, that the Young's modulus of the control film is larger due to higher molecular weight at a similar 25 °C storage modulus derived from DMA.

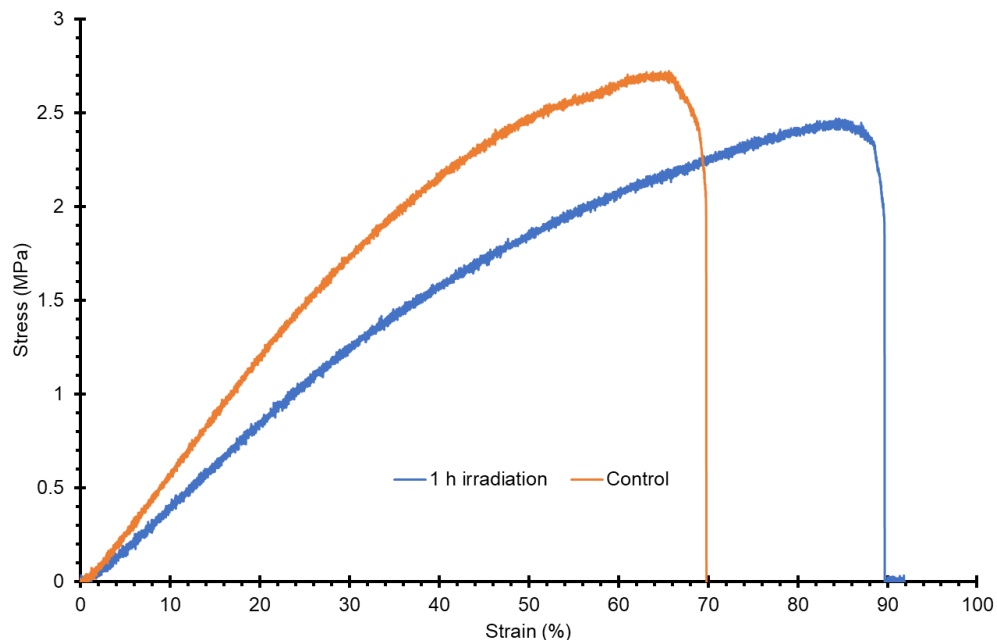


Figure 7.6: Stress-strain curves before and after irradiation demonstrates the effect of cyclobutane ring cleavage on tensile properties.

While thermomechanical measurements provided insight into the feasibility and effects of cyclobutane bisimide photo-cleavage, further probing with ^1H NMR spectroscopy enabled additional verification of this phenomenon, shown in **Figure 7.7**. The appearance of maleimide protons downfield at ~ 7 ppm indicated the successful ring opening of the cyclobutane bisimide moiety to produce alkene proton peaks. This appearance, in agreement with thermomechanical data suggested partial cleavage of the cyclobutane ring. Low signal intensity indicated that only partial cleavage was obtained, however longer irradiation times may serve to increase the yield of this reaction. Likewise, conservation of the TDI peaks adjacent to the PPG groups revealed conservation of urethane linkages and an absence of PU degradation outside of the cyclobutane linkage.

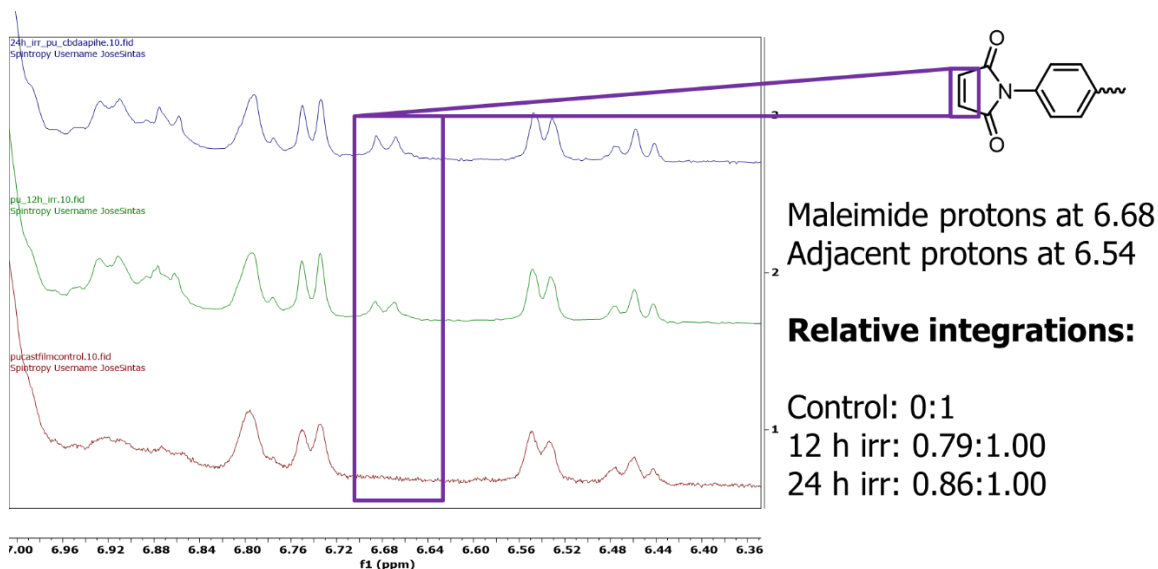


Figure 7.7 ^1H NMR spectroscopy reveals appearance of maleimide protons in CBDA-AP-I-HE PU after 254 nm irradiation.

7.5 Conclusions

Selective addition of 4-aminophenol to CBDA enabled the synthesis of a novel cyclobutane bisamic acid that underwent subsequent imidization to form a cyclobutane bisimide monomer containing bisphenol reactivity. Subsequent functionalization with ethylene carbonate yielded hydroxy ethyl functionality that allowed for the synthesis of thermally stable PUs containing cyclobutane bisimide linkages. The synthesized CBDA-AP-I-HE PU contained a PPG SS resulting in phase separation and a rubbery plateau with a storage modulus of 10^7 Pa and elastomeric properties confirmed with tensile data. Subsequent irradiation with 254 nm light resulted in a change in the HS chemistry derived from cyclobutane ring cleavage, resulting in an elevation of flow temperature and strain at break. Additionally, ^1H NMR revealed the appearance of maleimide protons after 254 nm irradiation further suggesting cyclobutane ring cleavage. Further studies that leverage a

higher intensity of 254 nm irradiation may serve to increase the yield of cyclobutane cleavage and shorten irradiation times.

7.6 Acknowledgments

I would like to thank Intel for supporting this work.

7.7 Funding

This work was funded by Intel.

7.8 References

1. Bai, Y.; Li, K.; Huang, S.; Li, J.; Liu, Q.; Li, Z.; Wang, X.; Zhang, G.; Sun, R. In *A Novel Process to Reduce the Warpage of Bond Pair for Temporary Bonding and Debonding Technique*, 2022 23rd International Conference on Electronic Packaging Technology (ICEPT), 10-13 Aug. 2022; 2022; pp 1-4.
2. Xu, D.; Wang, H. W.; Patel, J.; Brun, X. F.; Hirota, K.; Capsuto, E.; Kato, H.; Sugo, M. In *A Novel Design of Temporary Bond Debond Adhesive Technology for Wafer-Level Assembly*, 2020 IEEE 70th Electronic Components and Technology Conference (ECTC), 3-30 June 2020; 2020; pp 68-74.
3. Haq, J.; Vogt, B. D.; Howard, E.; Loy, D., Temporary bond—debond technology for high-performance transistors on flexible substrates. *Journal of the Society for Information Display* **2010**, *18* (11), 884-891.
4. Mo, Z.; Wang, F.; Li, J.; Liu, Q.; Zhang, G.; Li, W.; Yang, C.; Sun, R., Temporary Bonding and Debonding in Advanced Packaging: Recent Progress and Applications. *Electronics* **2023**, *12* (7), 1666.
5. Huang, D.; Liu, J.; Li, J.; Wang, F.; Li, K.; Liu, Q.; Yin, H.; Zhang, G.; Sun, R., Controlled Thermal Imidization of Thermoplastic Polyimide for Temporary Bonding

and Debonding in Advanced Packages. *ACS Applied Polymer Materials* **2022**, 4 (11), 8508-8519.

6. Hermanowski, J. In *Thin wafer handling — Study of temporary wafer bonding materials and processes*, 2009 IEEE International Conference on 3D System Integration, 28-30 Sept. 2009; 2009; pp 1-5.

7. Hashiguchi, H.; Fukushima, T.; Murugesan, M.; Kino, H.; Tanaka, T.; Koyanagi, M., High-Thermoresistant Temporary Bonding Technology for Multichip-to-Wafer 3-D Integration With Via-Last TSVs. *IEEE Transactions on Components, Packaging and Manufacturing Technology* **2019**, 9 (1), 181-188.

8. Lee, S.-W.; Lee, T.-H.; Park, J.-W.; Park, C.-H.; Kim, H.-J.; Kim, S.-M.; Lee, S.-H.; Song, J.-Y.; Lee, J.-H., The effect of laser irradiation on peel strength of temporary adhesives for wafer bonding. *International Journal of Adhesion and Adhesives* **2015**, 57, 9-12.

9. June, S. M.; Suga, T.; Heath, W. H.; Long, T. E.; Lin, Q.; Puligadda, R., Photo-Reactive Polyimides and Poly(siloxane imide)s as Reversible Polymeric Interfaces. *The Journal of Adhesion* **2010**, 86 (10), 1012-1028.

10. Moore, J. A.; Dasheff, A. N., An intrinsically photosensitive polyimide. *Chemistry of Materials* **1989**, 1 (1), 163-166.

11. Hergenrother, P., The Use, design, synthesis, and properties of high performance/high temperature polymers: An overview, high perform. *High Performance Polymers* **2003**, 15, 3-45.

12. Moyer, E. S.; Mohanty, D. K.; Shaw, J.; McGrath, J. E. In *Synthesis and characterization of soluble photoimageable polyimide and poly(imide siloxane) homo- and*

copolymers, International SAMPE Symposium and Exhibition (Proceedings), 1989; pp 894-904.

13. Decker, C.; Bianchi, C.; Jönsson, S., Light-induced crosslinking polymerization of a novel N-substituted bis-maleimide monomer. *Polymer* **2004**, *45* (17), 5803-5811.

14. Kang, M.; Moon, B., Synthesis of Photocleavable Poly(styrene-block-ethylene oxide) and Its Self-Assembly into Nanoporous Thin Films. *Macromolecules* **2009**, *42* (1), 455-458.

15. Piggott, A. M.; Karuso, P., Synthesis of a new hydrophilic o-nitrobenzyl photocleavable linker suitable for use in chemical proteomics. *Tetrahedron Letters* **2005**, *46* (47), 8241-8244.

16. Suzuki, H.; Abe, T.; Takaishi, K.; Narita, M.; Hamada, F., The synthesis and X-ray structure of 1,2,3,4-cyclobutane tetracarboxylic dianhydride and the preparation of a new type of polyimide showing excellent transparency and heat resistance. *Journal of Polymer Science Part A: Polymer Chemistry* **2000**, *38* (1), 108-116.

17. Trenor, S. R.; Shultz, A. R.; Love, B. J.; Long, T. E., Coumarins in Polymers: From Light Harvesting to Photo-Cross-Linkable Tissue Scaffolds. *Chemical Reviews* **2004**, *104* (6), 3059-3078.

18. Trenor, S. R.; Long, T. E.; Love, B. J., Photoreversible Chain Extension of Poly(ethylene glycol). *Macromolecular Chemistry and Physics* **2004**, *205* (6), 715-723.

19. Hughes, T.; Simon, G. P.; Saito, K., Chemistries and capabilities of photo-formable and photoreversible crosslinked polymer networks. *Materials Horizons* **2019**, *6* (9), 1762-1773.

20. Lentin, I.; Gorbunov, A.; Bezzubov, S.; Nosova, V.; Cheshkov, D.; Kovalev, V.; Vatsouro, I., Shrinkable/stretchable bis(calix[4]arenes) comprising photoreactive azobenzene or stilbene linkers. *Organic Chemistry Frontiers* **2023**, *10* (6), 1470-1484.
21. Ichimura, K.; Akita, Y.; Akiyama, H.; Kudo, K.; Hayashi, Y., Photoreactivity of Polymers with Regioisomeric Cinnamate Side Chains and Their Ability To Regulate Liquid Crystal Alignment. *Macromolecules* **1997**, *30* (4), 903-911.
22. Kaur, G.; Johnston, P.; Saito, K., Photo-reversible dimerisation reactions and their applications in polymeric systems. *Polymer Chemistry* **2014**, *5* (7), 2171-2186.
23. Dennis, J. M.; Fahs, G. B.; Moore, R. B.; Turner, S. R.; Long, T. E., Synthesis and Characterization of Polysulfone-Containing Poly(butylene terephthalate) Segmented Block Copolymers. *Macromolecules* **2014**, *47* (23), 8171-8177.
24. Sardon, H.; Pascual, A.; Mecerreyes, D.; Taton, D.; Cramail, H.; Hedrick, J. L., Synthesis of Polyurethanes Using Organocatalysis: A Perspective. *Macromolecules* **2015**, *48* (10), 3153-3165.
25. Weyhrich, C.; Will, J.; Heifferon, K.; Brown, J.; Arrington, C.; Meenakshisundaram, V.; Williams, C.; Long, T., 3D-Printing of Poly(arylene ether sulfone)s: Functional High-Performance Polymers for Vat Photopolymerization. *Macromolecular Chemistry and Physics* **2022**, *224*.
26. Aneja, A.; Wilkes, G. L., A systematic series of 'model' PTMO based segmented polyurethanes reinvestigated using atomic force microscopy. *Polymer* **2003**, *44* (23), 7221-7228.

27. Yilgör, I.; Yilgör, E.; Wilkes, G. L., Critical parameters in designing segmented polyurethanes and their effect on morphology and properties: A comprehensive review. *Polymer* **2015**, *58*, A1-A36.
28. Beniah, G.; Fortman, D. J.; Heath, W. H.; Dichtel, W. R.; Torkelson, J. M., Non-Isocyanate Polyurethane Thermoplastic Elastomer: Amide-Based Chain Extender Yields Enhanced Nanophase Separation and Properties in Polyhydroxyurethane. *Macromolecules* **2017**, *50* (11), 4425-4434.
29. Cheng, B.-X.; Gao, W.-C.; Ren, X.-M.; Ouyang, X.-Y.; Zhao, Y.; Zhao, H.; Wu, W.; Huang, C.-X.; Liu, Y.; Liu, X.-Y.; Li, H.-N.; Li, R. K. Y., A review of microphase separation of polyurethane: Characterization and applications. *Polymer Testing* **2022**, *107*, 107489.

CHAPTER 7 SUPPORTING INFORMATION
A NOVEL CYCLOBUTANE BISIMIDE MONOMER FOR PHOTO-CLEAVABLE
POLYURETHANE SYNTHESIS

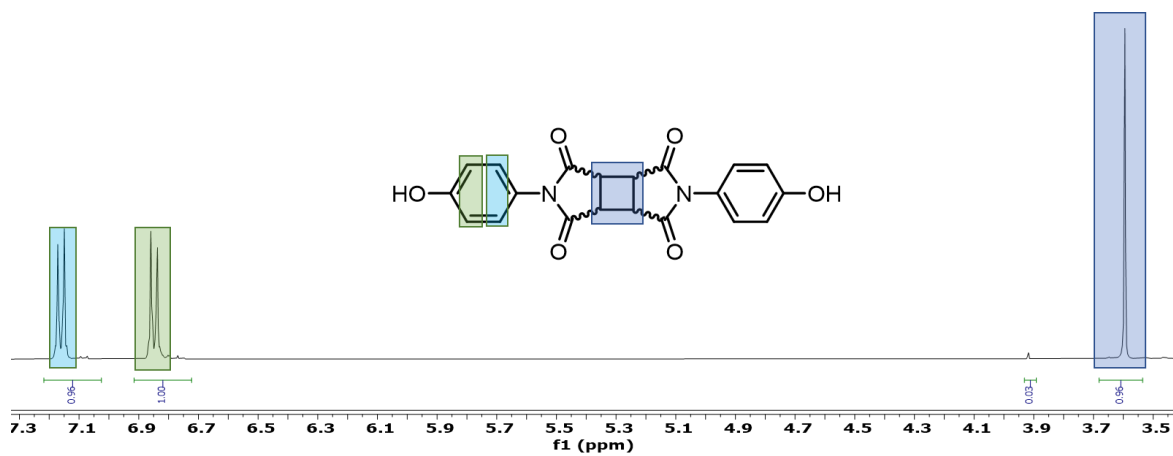


Figure S7.1: ¹H NMR spectrum of CBDA-AP-I.

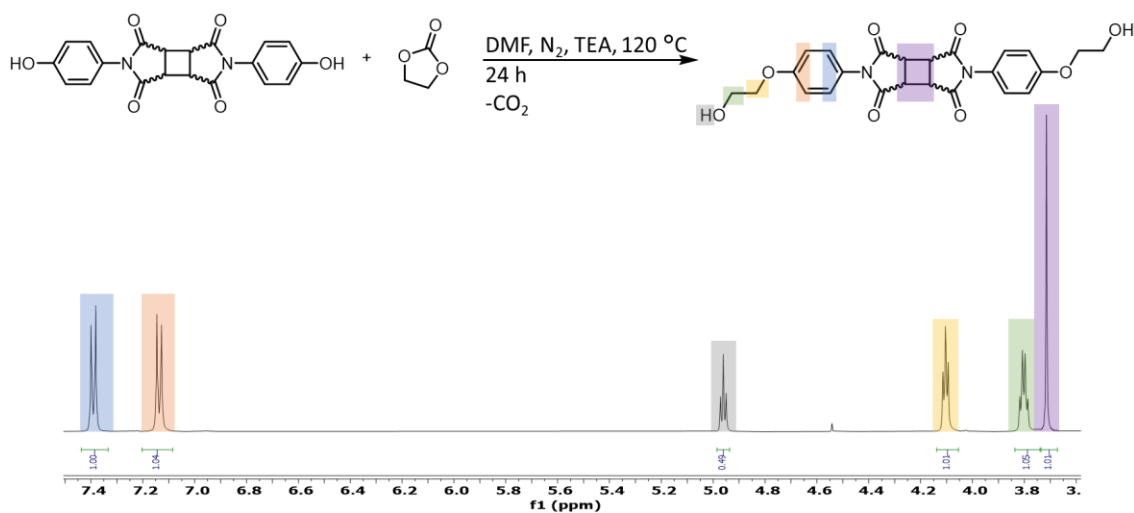


Figure S2: ¹H NMR spectrum of CBDA-AP-I-HE.

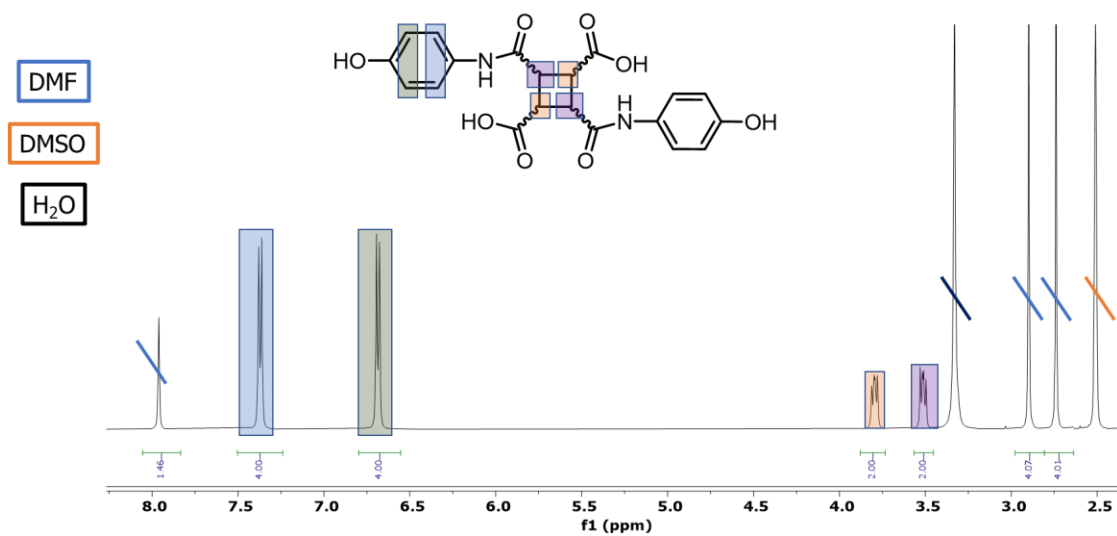


Figure S3: ¹H NMR spectrum of CBDA-AP.

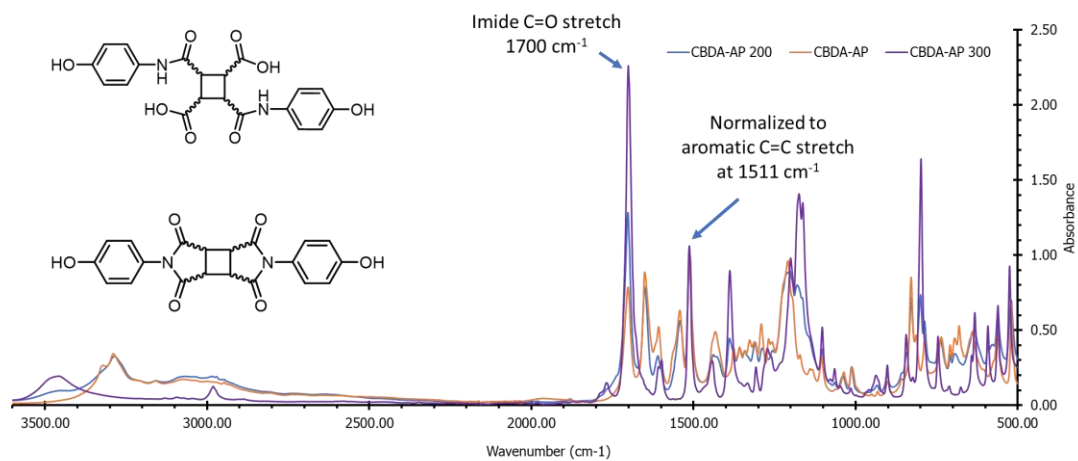


Figure S4: FTIR spectroscopy reveals complete imidization of CBDA-AP after thermal treatment to 300 °C.

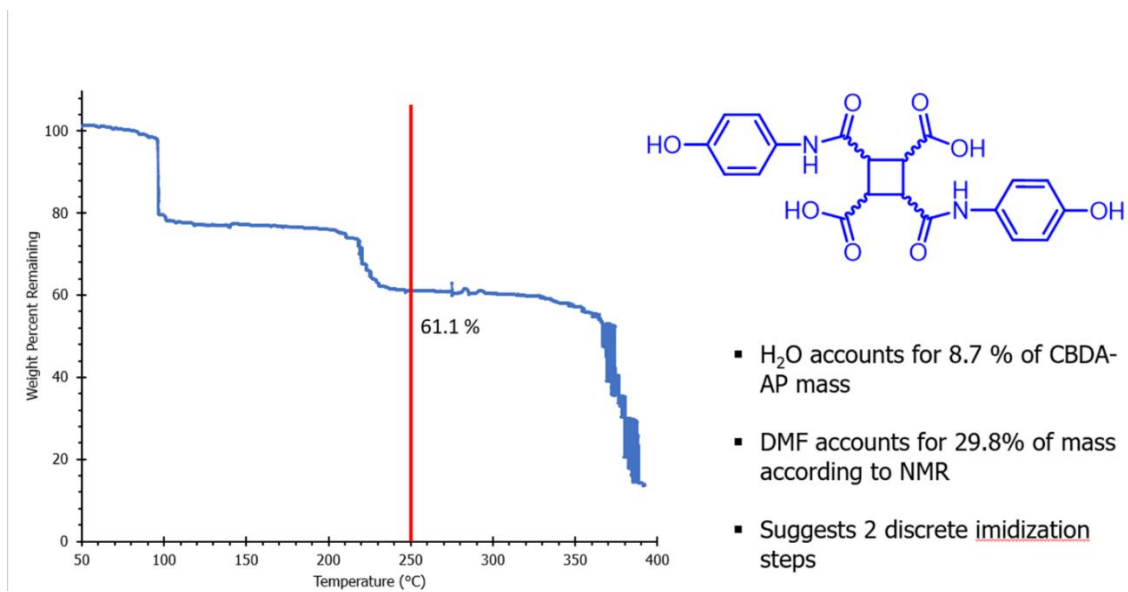


Figure S5: Step-wise TGA reveals two discrete weight-loss steps for thermal imidization of CBDA-AP.

CHAPTER 8

PHOTO-RESPONSIVE CYCLOBUTANE BISIMIDE-CONTAINING POLYSULFONES CAPABLE OF LIGHT-MEDIATED DEPOLYMERIZATION

8.1 Introduction

Polysulfones (PSUs) represent a class of high-performance engineering polymers renowned for their desirable mechanical properties and high chemical resistance, biocompatibility, and sterilizability.¹ These properties encouraged the use of PSUs in various membrane applications where anti-fouling and sterilization requirements exist.²⁻⁷ Additionally, their high strength-to-weight ratio encourages their use in automotive, aerospace, and electronic applications.^{8, 9} The aromatic structure of PSUs enables these desired engineering properties and is derived from a nucleophilic aromatic substitution reaction between bisphenol-A (BPA) and dichlorodiphenyl sulfone (DCDPS). Bulky substituents of the comprising monomers prevent crystallization, while restricting rotation along the backbone resulting in excellent optical clarity and high T_g .¹⁰ These excellent properties and wide spread use is however limited to traditional melt processing techniques and thus possesses room for innovation.

While PSUs display inherent instability to UV irradiation, installing a governable light-mediated degradation pathway remains desired for temporal control over molecular weight.¹¹ Control over these processes impacts both semi-conductor patterning and encapsulant applications, both of which stand to benefit from the thermomechanical performance and chemical resistance of PSUs. Recent literature describes the use of PSUs as encapsulants for metathesis catalysts.¹² They displayed good retention and release of

catalyst, below and above the T_g respectively, through temperature modulation. The released catalyst subsequently initiated a depolymerization process of polybutadiene rubbers that resulted in a stable trigger for tire depolymerization that is easily imbedded into the final product. Likewise, additive manufacturing benefits from controlled catalyst release. Namely, recent advancements in frontal polymerization involved the use of a PSU encapsulant for greater resin storage life, preventing spontaneous polymerization.¹³ While these innovations provide exciting avenues for future PSU research, a thermal release trigger limits these applications to high energies and poor spatial control. Thus, a photo-mediated alternative remains desired for these systems as it provides both spatial and temporal control over release in addition to orthogonality to thermal stimuli.¹⁴

Semi-conductor packaging applications leverage photo-mediated processing techniques on an industrial scale.¹⁵⁻¹⁷ Structural adhesives for bond/debond applications as well as positive photoresist for patterning benefit from photo-degradation processes.^{18, 19} The ability to cleave covalent bonds with light provides on-demand molecular weight control, which subsequently modifies mechanical properties and solubility. In addition to positive photoresist applications, photo-degradability plays an important role in next generation semiconductor processing applications including the bond/debond process where a silicon wafer is bound to a glass substrate. The release of the silicon wafer after patterning is often mediated with heat, which results in chip warpage or delamination. Thus, a photonic trigger that circumvents thermal warpage is desired.

Various [2+2] cycloaddition/cleavage modalities exist for photo-mediated molecular weight control including coumarin, thymine, cinnamic, and stilbene chemistries.²⁰ While these chemistries possess efficient photo-reversible functions, thermal stability and short,

high-energy irradiation windows are required to ensure orthogonality to other processes. Previous research demonstrated the feasibility of Cyclobutane bisimide photo-reversible chemistry for photo-cleaving semiconductor applications.^{21, 22} Outstanding thermal properties of imide and PSU chemistries allow for facile transfer of this chemistry to catalyst encapsulation applications. Thus, the facile synthesis of a cyclobutane bisimide monomer that contains bisphenol reactivity enabled the installation of photo-cleavable functionality along the PSU backbone that retains thermal stability. These novel PSUs retained thermomechanical properties expected from conventional BPA and DCDPS copolymers. Additionally, ¹H NMR analysis revealed cyclobutane bisimide end groups resulting from the decreased reactivity of the cyclobutane bisimide monomer and unfavored addition compared to BPA. This phenomenon added potential for segmented PSU block copolymers capable of selective block cleavage.²³ Lastly, irradiation with 254 nm light resulted in predictable molecular weight decrease that correlated with cyclobutane incorporation.

8.2 Materials and Methods

8.2.1 Materials

Cyclobutane-1,2,3,4-tetracarboxylic dianhydride (CBDA) was graciously provided by Jayhawk Fine Chemicals[®] and used as received. 4-Aminophenol (>98%), deuterated dimethylsulfoxide-d₆ (99.95%), deuterated chloroform CDCl₃ (99.9%), potassium carbonate (K₂CO₃) (>99%), bisphenol A (>99%), 4,4'-dichlorodiphenyl sulfone (DCDPS) (>98%), N,N-dimethylacetamide (DMAc) (anhydrous, 99.8%), and Celite[®] 545 filter agent, were purchased from SigmaAldrich and used as received. Hydrochloric acid,

chloroform (HPLC grade), 1,2-dichlorobenzene (>99%), toluene, methanol, and tetrahydrofuran (THF) were purchased from Fisher Chemical and used as received.

8.2.2 Instruments

^1H and ^{13}C nuclear magnetic resonance (NMR) spectroscopy utilized a Bruker Avance NEO 500 MHz spectrometer functioning at 500.15 MHz and 23 °C (solution concentration of 10 mg mL⁻¹). High temperature NMR was run on a Varian MR400 at 80 °C for the CBDA-AP-I monomer. A ThermoFisher Scientific Nicolet iS10 FTIR spectrometer, with a diamond cell at 25 °C, identified key stretches for synthesized monomers and polymers. A TA Instruments TGA 5500 facilitated thermogravimetric analysis (TGA) by utilizing a heating rate of 10 °C min⁻¹ from 25 to 600 °C with a steady nitrogen purge. The $T_{d,5\%}$, or temperature where 5% of the original sample mass was lost, served as an indicator for sample thermal stability. A TA Instruments DSC 2500 with heat/cool/heat cycles of 10 °C min⁻¹ provided differential scanning calorimetry data where the sample was under a nitrogen environment throughout the experiment. DSC provided the glass transition temperatures (T_g s) from the midpoint of the endothermic transition in the second heat. A TA Instruments DMA Q800 with a temperature ramp of 3 °C min⁻¹ from -90 °C to 180 °C at 1 Hz provided a T_g taken from the peak in the tan delta. Liquid nitrogen cooling permitted the cryogenic temperatures required to observe the thermal transitions of the PSU films. A Mineralight 254 nm 15w lamp equipped with a 254 nm filter enabled consistent irradiation of samples at an intensity of 4.8 mW/cm². A Waters ARC HPLC size exclusion chromatography system operating at a flow rate of 1 mL/min at 5 mg/mL and temperature of 50 °C enabled molecular weight determination for polymeric samples. Samples were run in 0.05 M LiBr DMF and passed through a 0.45 micrometer filter before injecting. A

Waters dRI detector monitored concentration change and final molecular weight was determined against a polystyrene calibration curve.

8.2.3 Synthesis of CBDA-AP-I

CBDA (10.00 g, 51.0 mmol), 4-aminophenol (11.13 g, 102.0 mmol), 100 mL of toluene and 500 mL of 1,2-dichlorobenzene were added to a 3-neck round bottomed flask equipped with a magnetic stir bar, nitrogen inlet, reflux condenser, and Dean-Stark apparatus. Reagents were allowed to mix and subsequently heated to 180 °C. The reaction was allowed to progress for 18 h and remained heterogenous throughout. The toluene served to remove any water produced throughout the imidization reaction through an azeotrope and the Dean-Stark apparatus was emptied as needed. The precipitate was filtered using a fritted funnel and allowed to dry overnight then recrystallized in DMF. The final isolated yield was > 90%. ¹H NMR (DMSO-d₆, 80 °C, δ, Figure S1) 9.77 (s, 2H), 7.2 (d, 4H, *J* = 8.5 Hz), 6.87 (d, 4H, *J* = 8.5 Hz), 3.62 (s, 4H).

8.2.4 Synthesis of Phenol-terminated PSU 1, 2, and 3

Phenol-terminated polysulfones (PSUs) were synthesized using an established procedure, illustrated in **Figure 8.1**.^{11, 24} In order to achieve phenolic ends (preferred over DCDPS end groups for stability), a slight excess of phenol monomer was employed. PSU 1 is a homopolymer of BPA and DCDPS and thus only utilized those two monomers. However, PSU 2 and 3 contained either 5 mol. % or 10 mol. % respectively of CBDA-AP-I relative to the total moles of bisphenol incorporated. BPA, or a combination of BPA and CBDA-AP-I at either a 95:5 or 90:10 molar ratio respectively (0.2300 mol), 4,4'-dichlorodiphenyl sulfone (64.89 g, 0.2260 mol), and potassium carbonate (40.35, 0.2919 mol) were added to anhydrous N,N-dimethylacetamide (400 mL) and toluene (200 mL) in a three-necked,

round-bottomed flask fitted with a nitrogen adapter, Dean-Stark trap with a condenser, and a glass mechanical stir rod with a Teflon[®] paddle. The heterogenous solution was purged with nitrogen for 20 min then heated to 160 °C. The reaction was refluxed for 5 h, the toluene/water azeotrope was removed periodically, then the reaction was heated to 180 °C for 18 h. The resulting solution was filtered through a Celite[®] earth plug, neutralized with 1 M HCl solution in THF, and then precipitated into methanol. The resulting white powder was dried *in vacuo* at 190 °C for 18 h. For PSU 1, ¹H NMR spectroscopy elucidated molecular weight through end group analysis. ¹H NMR (500 MHz, CDCl₃) δ 7.86-7.83 (d, 56H, *J* = 8.89 Hz), 7.25-7.23 (d, 56H, *J* = 8.75 Hz), 7.10-7.07 (d, 4H, *J* = 8.67 Hz), 7.01-6.99 (d, 56H, *J* = 8.87 Hz), 6.95-6.92 (d, 56H, *J* = 8.71 Hz), 6.77-6.74 (d, 4H, *J* = 8.71 Hz), 1.69 (s, 76H), 1.65 (s, 12H).

8.3 Results and Discussion

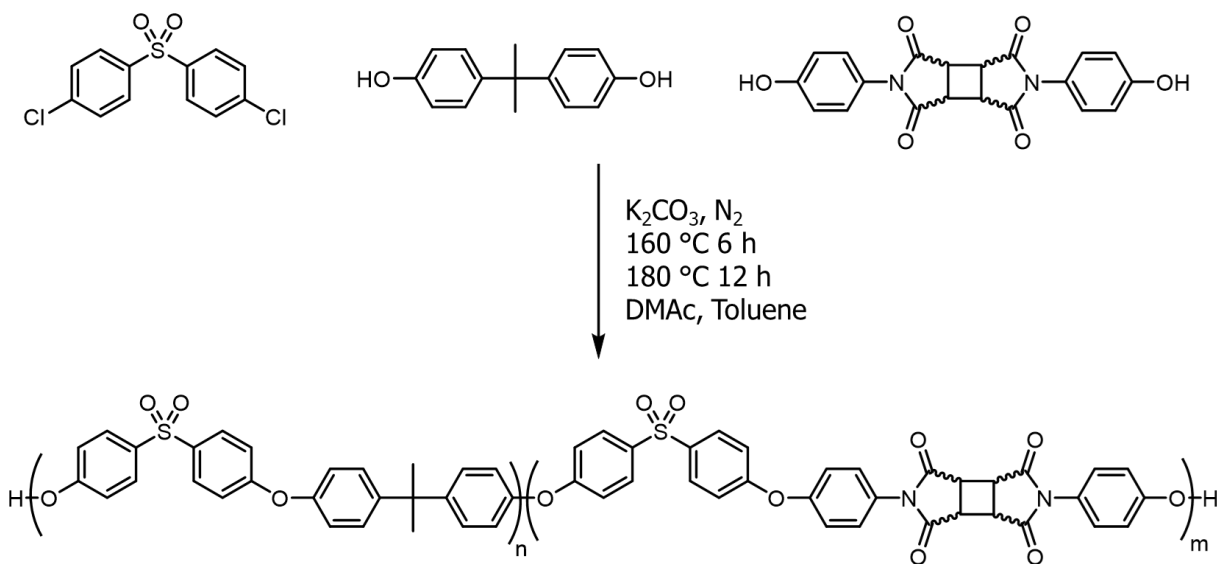


Figure 8.1 The electron withdrawing nature of DCDPS promotes a nucleophilic aromatic substitution with phenolic nucleophiles, resulting in a polycondensation polymerization

mechanism. Systematic incorporation of CBDA-AP-I produced a series of novel polysulfone copolymers.

The favorable solubility of CBDA-AP-I in DMAc allowed for the retention of reaction conditions used to synthesize PSU 1. This proved fortuitous, as it eliminated deviations in reaction setups between all PSUs with consistent reaction setups. The phenolic reactivity of CBDA-AP-I enabled seamless incorporation of a cyclobutane bisimide into PSUs alongside BPA, a common PSU monomer. Furthermore, incorporation of varying concentrations of CBDA-AP-I, 5 mol. % for PSU 2 and 10 mol. % for PSU 3, allowed for systematic probing of structure-property relationships that arise due to the incorporation of this novel monomer. A DMAc-toluene solvent selection provided both effective removal of water throughout the reaction facilitated by a toluene-water azeotrope as well as complete solubility of the growing polymer. A non-nucleophilic base enabled efficient trapping of the HCl condensate, driving the reaction towards high conversion. A silica plug and methanol precipitation removed impurities and provided high molecular weight PSUs capable of producing creasible films after melt-processing.

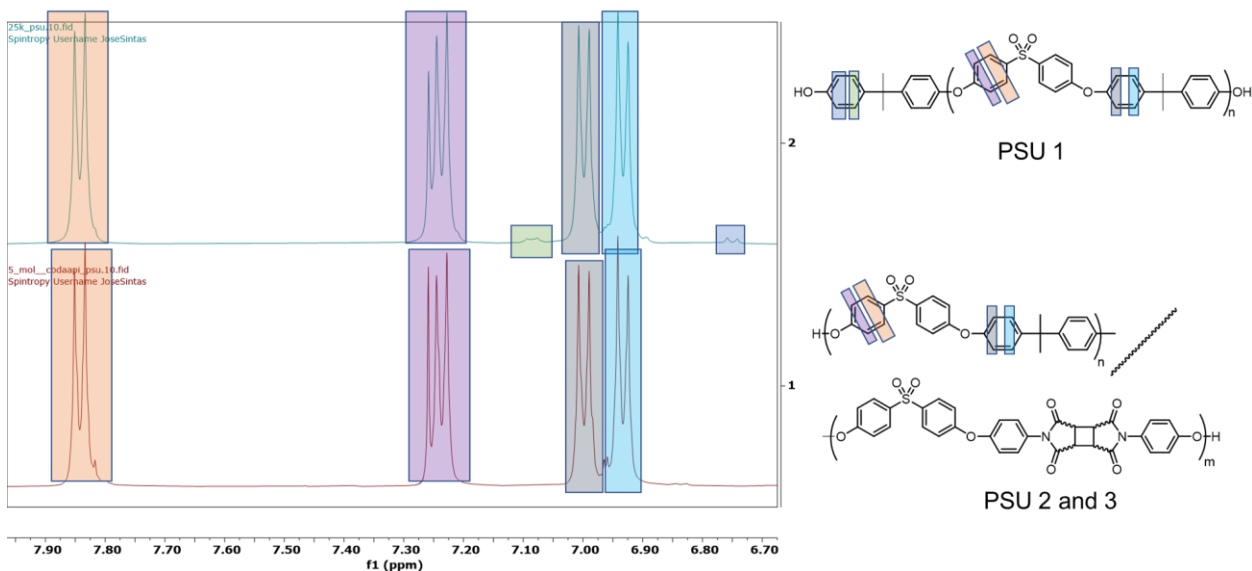


Figure 8.2 ^1H NMR end group analysis displayed a disappearance of BPA end groups across all PSU compositions that contained CBDA-AP-I. This not only convoluted molecular weight determination for PSU 2 and 3, but also suggests that they contain CBDA-AP-I end groups.

End group analysis is a well-established method for determining molecular weight of polymers.²⁵ Commonly, the proton integration of a known polymer terminal functionality is compared to known backbone proton integration, providing a degree of polymerization that is then converted to molecular weight. For PSU 1, which does not contain CBDA-AP-I, this method was effective at determining the molecular weight and agreed favorably with SEC analysis. PSU 2 and 3, however, did not display any discernable end group protons from either the BPA or CBDA-AP-I end groups, displayed in **Figure 8.2**. This was surprising, as an excess of phenol was leveraged to target phenolic end groups. Likewise, the high molecular weight of the resulting polymer suggests large degrees of conversion that would allow for these end groups to exist. Thus, it is theorized that not only are the

end groups of PSU 2 and 3 CBDA-AP-I, but also that those end group protons overlap with backbone protons resulting in a peak convolution that prohibits molecular weight determination with NMR. This theory is further bolstered by the comparatively lower reactivity of CBDA-AP-I compared to BPA. Namely, BPA does not possess any electron withdrawing character that affects the reactive phenol moiety, while CBDA-AP-I possesses an electron withdrawing imide linkage that decreases reactivity. For these reasons, it is likely that PSU 2 and 3 are gradient block copolymer, with the less reactive CBDA-AP-I monomers located in increasing concentration closer to the end groups of the polymer.

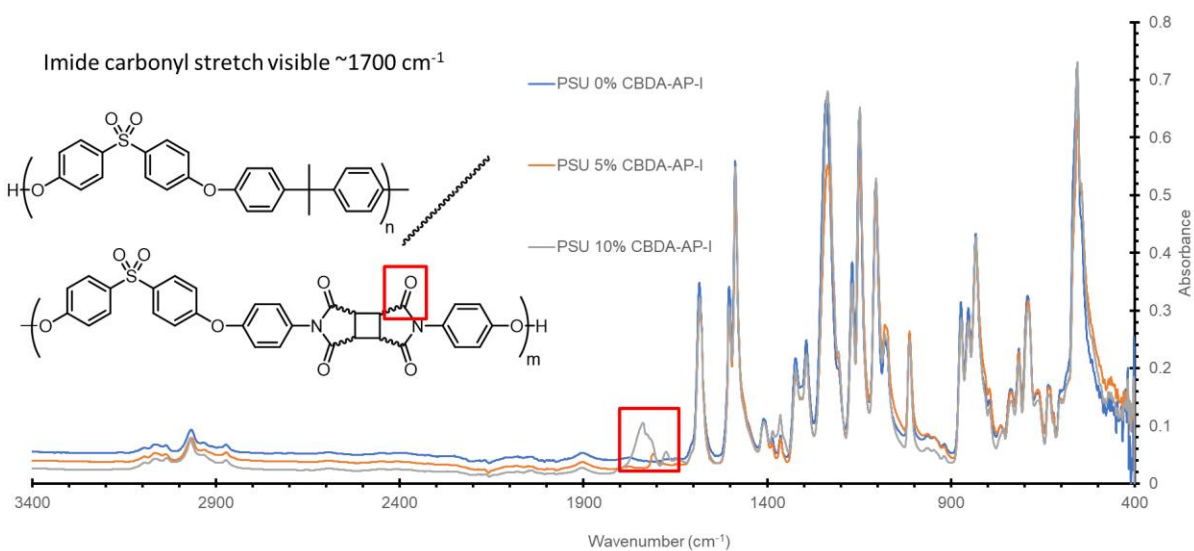


Figure 8.3 ATR FTIR spectroscopy probed incorporation of CBDA-AP-I into the PSU backbone through absorbances in the newly introduced imide carbonyl stretch.

While NMR is effective at determining chemical structure, additional spectroscopic methods serve to bolster molecular structure analysis. FTIR enabled further probing of CBDA-AP-I incorporation, shown in **Figure 8.3**. The distinct bisimide chemical group introduces a new C=O stretching mode that is distinct from the sulfone carbonyl system.

As expected, PSU 1 did not display any imide symmetric or asymmetric carbonyl stretching modes, however PSU 2 and 3 possessed a carbonyl peak in the expected region. Furthermore, the stretch intensity increased from PSU 2 to PSU 3 as a result of the greater CBDA-AP-I incorporation. This data, coupled with NMR analysis, concludes that not only was CBDA-AP-I systematically incorporated into the PSU backbone, but is also less reactive than its BPA counterpart thus directing its position near the PSU end groups. This claim is further supported by thermogravimetric analysis (TGA). The stability of the polymer backbone, largely due to its restricted mobility, results in the majority of polymer thermal degradation to originate in the more mobile chain ends. TGA analysis of the CBDA-AP-I monomer demonstrates a thermal degradation temperature of 400 °C, shown in **Figure 8.4**. This may be counter intuitive, however the cyclobutane bisimide moiety is thermally robust. A systematic study on the weight loss profiles for all PSUs allowed further exploration of the effects CBDA-AP-I concentration had on the final polymer. PSU 2 and 3 displayed an earlier onset of weight loss, perhaps due to the electron withdrawing character of the bisimide linkage resulting in a weaker backbone linkage and premature degradation of the PSU backbone. It should be noted that the low quantity of weight loss does not directly correlate to wt. % CBDA-AP-I incorporation, however. Overall, the change in weight loss profile, loss of BPA chain ends on NMR, and appearance of imide stretching absorbances on FTIR strongly suggests controlled incorporation of CBDA-AP-I into the PSU backbone.

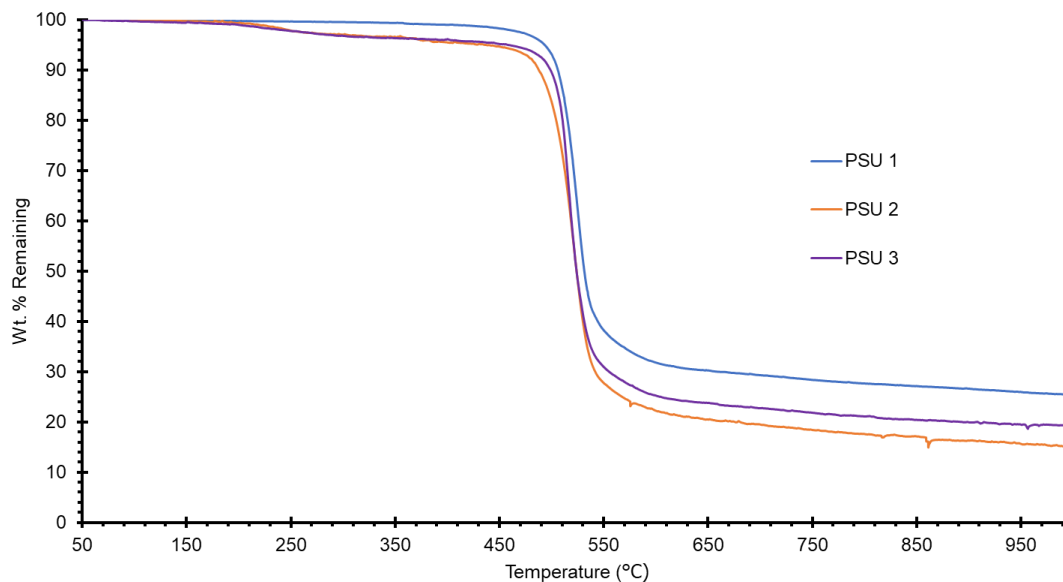


Figure 8.4 TGA of all PSUs reveals an earlier onset weight loss for CBDA-AP-I containing PSUs.

Differential scanning calorimetry (DSC) provided insight into the thermal properties CBDA-AP-I endows PSUs, shown in **Figure 8.5**. PSU 1 possess a T_g at an expected temperature range (182 °C) when compared to literature values. Interestingly, however, the incorporation of rigid CBDA-AP-I did not raise T_g as expected, but lowered it considerably. This phenomenon trends with the concentration of CBDA-AP-I incorporated with PSU 2 having a higher T_g than PSU 3. While counterintuitive, polymer physics theories help explain this behavior. PSUs are commonly viewed as rigid rod, amorphous polymers and derive high T_g s from intermolecular entanglements that come from their helical structure.^{26, 27} These well-defined helical structures produce a very short entanglement molecular weight, however require a regular repeating chemical structure to produce this property. The addition of CBDA-AP-I in PSU 2 and 3 disrupt this helical structure, thus decreasing the beneficial entanglement interactions PSU 1 enjoys. As

previously discussed, the CBDA-AP-I monomer is located near the end of the PSU chains. This directly affects T_g because chain mobility is theorized to start at the less sterically hindered chain ends. The lower T_g of PSU 2 and 3 suggests that CBDA-AP-I packs less efficiently than its BPA counterpart.

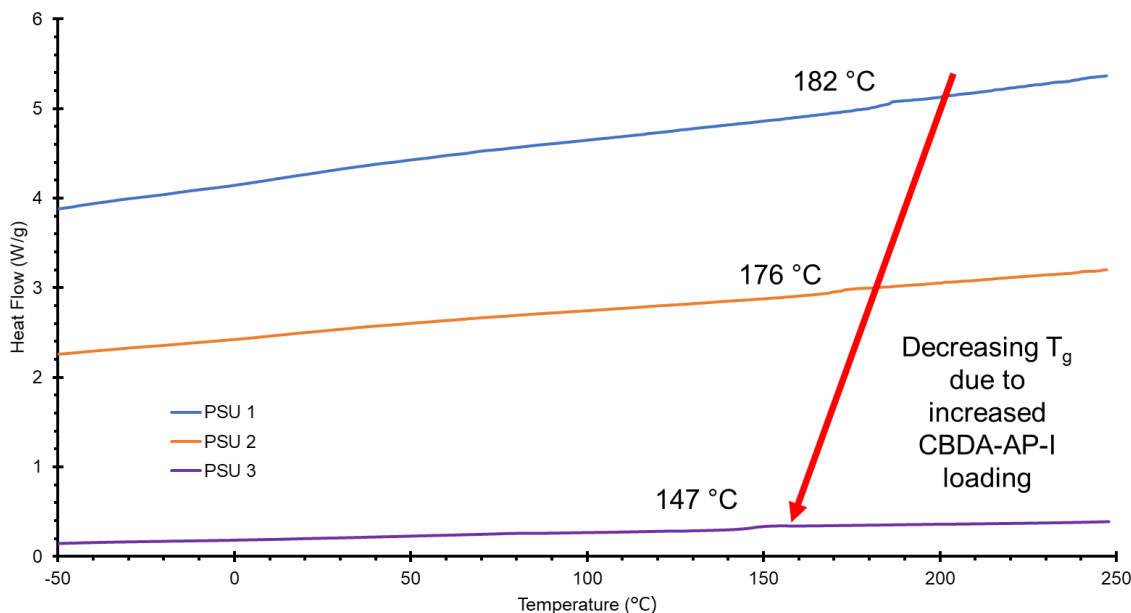


Figure 8.5 DSC displays the effect of increased CBDA-AP-I loading on T_g .

Dynamic mechanical analysis allows for deeper exploration into the effects CBDA-AP-I concentration has on thermomechanical properties, displayed in **Figure 8.6**. PSU 1 displayed a possess an expected thermomechanical behavior of an amorphous, high T_g polymer with a $\tan \delta$ peak at 200 °C. PSU 1 also displays a storage modulus value > 1 Gpa, characteristic of a glassy polymer. PSU 2 and 3, however, displayed lower modulus values suggesting a low temperature transition not captured in this DMA experiment. Likewise, the decrease in T_g observed in DSC experiments is reflected in the DMA traces with $\tan \delta$ peaks for PSU 2 and 3 T_g s at 198 and 188 °C respectively. Additionally, PSU 3 which

contains a 10 mol. % concentration of CBDA-AP-I displays an additional $\tan \delta$ peak at 111 °C. DSC analysis does not display this transition; however, a faster scanning rate may help resolve this. This DMA curve supports previous claims that the incorporation of a rigid cyclobutane bisimide comonomer may serve to decrease chain entanglements, thus lowering thermal properties. Furthermore, the possibility of a gradient copolymer topology with CBDA-AP-I located near the chain ends may result in some degree of phase separation, leading to two independent T_g s at higher concentrations of the cyclobutane monomer.

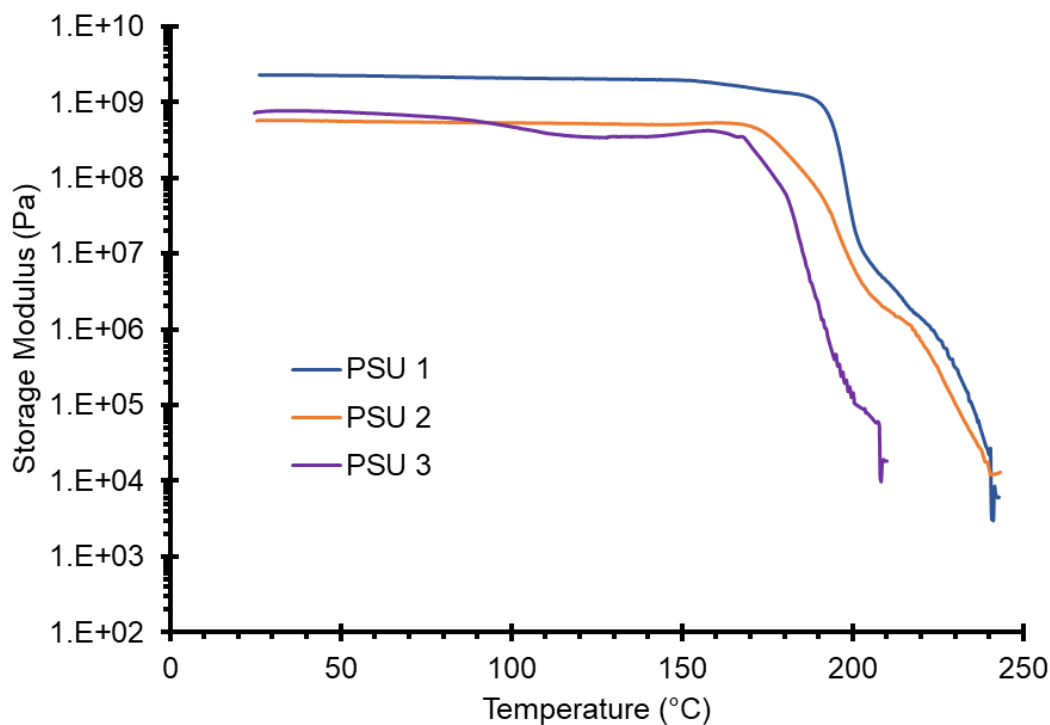


Figure 8.6 DMA displays thermal transitions of all synthesized PSUs. Incorporation of CBDA-AP-I results in decreased thermal performance that correlates with mol. % concentration.

Lastly, these PSUs were evaluated for their ability to photocleave under 254 nm irradiation. The incorporated cyclobutane bisimide moiety endows photo-reactivity when exposed to certain wavelengths, namely the photocleavage of the cyclobutane ring under 254 nm irradiation to form 2 maleimide end groups. A 254 nm filter attached to a broadband UV light source and size exclusion chromatography (SEC) provided an evaluation of PSU molecular weight before and after irradiation for all samples. Even in the absence of cyclobutane bisimide monomers, PSUs react with UV light to undergo several chain scission events through the formation of radicals.²⁸ Another result of radical formation commonly experienced in PSUs is the coupling reaction of several radicals to provide chain extension after UV irradiation. These oxidation events lead to a decrease in material properties, namely toughness. UV irradiation of PSU 1 revealed a chain coupling degradation pathway, seen by the increase in molecular weight after narrow 254 nm irradiation of a melt pressed thin film, **Table 8.1**. Interestingly, the addition of CBDA-AP-I in PSU 2 and 3 resulted in a noticeable decrease in M_n after 254 nm irradiation. This is due to the incorporation of the cyclobutane bisimide functional group along the polymer backbone that underwent photocleavage. As expected, the change in molecular weight increased with increasing CBDA-AP-I loading (27% for PSU 2 and 34% for PSU 3).

Polymer	M_n (g/mol)	M_w (g/mol)	\bar{D}
PSU 1 (0 mol. %)	14,600	27,600	1.88
PSU 2 (5 mol. %)	31,500	57,200	1.63
PSU 3 (10 mol. %)	24,800	31,000	1.25
PSU 1 L (0 mol. %)	19,800	33,100	1.68
PSU 2 L (5 mol. %)	23,000	20,700	1.77
PSU 3 L (10 mol. %)	16,300	22,100	1.36
Polymer	ΔM_n (g/mol)	ΔM_n (%)	$\Delta \bar{D}$
PSU 1 (0 mol. %)	+5,200	+36%	-0.20
PSU 2 (5 mol. %)	-8500	-27%	+0.14
PSU 3 (10 mol. %)	-8500	-34%	+0.11

Table 8.1 SEC reveals change in molecular weight after irradiation with 254 nm light. The decrease in molecular weight in PSU 1 and 2 is attributed to the introduction of controlled photo-cleaving of cyclobutane bisimide linkages.

8.4 Conclusions

A traditional polycondensation synthetic strategy afforded a series of novel PSUs containing photoreactive cyclobutane bisimide linkages. The incorporation of a novel monomer, CBDA-AP-I, provided insight into new structure-property relationships for PSUs, evaluated with DSC, DMA, FTIR, and NMR analysis. Spectroscopy revealed the successful installation of CBDA-AP-I into the polymer backbone, with NMR suggesting an increase in CBDA-AP-I concentration towards the end groups of the polymer. Electron withdrawing imide linkages in resonance with the reactive phenols of this compound explained this phenomenon, which likely resulted in BPA outcompeting CBDA-AP-I with

respect to nucleophilicity. This presumably produced a gradient copolymer topology where CBDA-AP-I reacts after BPA yielding CBDA-AP-I end groups, although additional time dependent reaction kinetic studies are needed to fully validate this claim. Likewise, the incorporation of CBDA-AP-I resulted in a trend of decreasing T_g with increasing concentration. DMA also suggested the possibility of phase separation at an adequate concentration of the CBDA-AP-I monomer, as noted by the two $\tan \delta$ peaks present in PSU 3. Further experiments that utilize X-ray scattering are needed to explore this phenomenon, however. Lastly, irradiation with 254 nm light showed a clear decrease in molecular weight within PSU 2 and 3, confirming photocleavage of the incorporated cyclobutane bisimide linkage.

8.5 Acknowledgements

I would like to thank Sandia National Labs for sponsoring this work.

8.6 Funding

This work was funded by Sandia National Labs.

8.7 References

1. Deberdeev, T. R.; Akhmetshina, A. I.; Karimova, L. K.; Ignat'eva, E. K.; Galikhmanov, N. R.; Grishin, S. V.; Berlin, A. A.; Deberdeev, R. Y., Aromatic Polysulfones: Strategies of Synthesis, Properties, and Application. *Polymer Science, Series D* **2020**, *13* (3), 320-328.
2. Serbanescu, O. S.; Voicu, S. I.; Thakur, V. K., Polysulfone functionalized membranes: Properties and challenges. *Materials Today Chemistry* **2020**, *17*, 100302.

3. Tan, X.; Rodrigue, D., A Review on Porous Polymeric Membrane Preparation. Part I: Production Techniques with Polysulfone and Poly (Vinylidene Fluoride). *Polymers* **2019**, *11* (7), 1160.
4. Abdelrasoul, A.; Doan, H.; Lohi, A.; Cheng, C.-H., Morphology Control of Polysulfone Membranes in Filtration Processes: a Critical Review. *ChemBioEng Reviews* **2015**, *2* (1), 22-43.
5. Kheirieh, S.; Asghari, M.; Afsari, M., Application and modification of polysulfone membranes. *Reviews in Chemical Engineering* **2018**, *34* (5), 657-693.
6. Chen, Y.; Lin, B.; Qiu, Y., Modification of polysulfone and the biomedical application of modified polysulfone. *International Journal of Polymeric Materials and Polymeric Biomaterials* **2023**, *72* (3), 224-242.
7. Hoseinpour, V.; Noori, L.; Mahmoodpour, S.; Shariatinia, Z., A review on surface modification methods of poly(arylsulfone) membranes for biomedical applications. *Journal of Biomaterials Science, Polymer Edition* **2021**, *32* (7), 906-965.
8. Yu, L.; Zhao, D.; Wang, W., Mechanical properties and long-term durability of recycled polysulfone plastic. *Waste Management* **2019**, *84*, 402-412.
9. Andrady, A. L.; Neal, M. A., Applications and societal benefits of plastics. *Philos Trans R Soc Lond B Biol Sci* **2009**, *364* (1526), 1977-84.
10. Hergenrother, P., The Use, design, synthesis, and properties of high performance/high temperature polymers: An overview, high perform. *High Performance Polymers* **2003**, *15*, 3-45.
11. Weyhrich, C.; Will, J.; Heifferon, K.; Brown, J.; Arrington, C.; Meenakshisundaram, V.; Williams, C.; Long, T., 3D-Printing of Poly(arylene ether

sulfone)s: Functional High-Performance Polymers for Vat Photopolymerization. *Macromolecular Chemistry and Physics* **2022**, 224.

12. Warner, M. J.; Lassa, J. P.; Narcross, H.; Commisso, A.; Ghosh, K.; Romero, M.; Schwartz, J. M.; Engler, A. C.; Kohl, P. A.; Leguizamon, S. C.; Jones, B. H., Chemical Recycling of Polybutadiene Rubber with Tailored Depolymerization Enabled by Microencapsulated Metathesis Catalysts. *ACS Sustainable Chemistry & Engineering* **2023**, 11 (39), 14538-14548.

13. Davydovich, O.; Greenlee, A. J.; Root, H. D.; Jansen, A. L.; Gallegos, S. C.; Warner, M. J.; Kent, M. S.; Cardenas, J. A.; Appelhans, L. N.; Roach, D. J.; Jones, B. H.; Leguizamon, S. C., Encapsulated Transition Metal Catalysts Enable Long-term Stability in Frontal Polymerization Resins. *Macromolecules* **2023**, 56 (18), 7543-7550.

14. Yoon, T. P.; Ischay, M. A.; Du, J., Visible light photocatalysis as a greener approach to photochemical synthesis. *Nature Chemistry* **2010**, 2 (7), 527-532.

15. Moreau, W. M., *Semiconductor Lithography: Principles, Practices, and Materials*. Springer US: 2012.

16. Costner, E. A.; Lin, M. W.; Jen, W.-L.; Willson, C. G., Nanoimprint Lithography Materials Development for Semiconductor Device Fabrication. *Annual Review of Materials Research* **2009**, 39 (1), 155-180.

17. Lin, B.-J., Immersion lithography and its impact on semiconductor manufacturing. *Journal of Micro/Nanolithography, MEMS, and MOEMS* **2004**, 3 (3).

18. Haq, J.; Vogt, B. D.; Howard, E.; Loy, D., Temporary bond—debond technology for high-performance transistors on flexible substrates. *Journal of the Society for Information Display* **2010**, 18 (11), 884-891.

19. Ober, C. K.; Käfer, F.; Yuan, C., Recent developments in photoresists for extreme-ultraviolet lithography. *Polymer* **2023**, *280*, 126020.
20. Hughes, T.; Simon, G. P.; Saito, K., Chemistries and capabilities of photo-formable and photoreversible crosslinked polymer networks. *Materials Horizons* **2019**, *6* (9), 1762-1773.
21. June, S. M.; Suga, T.; Heath, W. H.; Long, T. E.; Lin, Q.; Puligadda, R., Photo-Reactive Polyimides and Poly(siloxane imide)s as Reversible Polymeric Interfaces. *The Journal of Adhesion* **2010**, *86* (10), 1012-1028.
22. Moore, J. A.; Dasheff, A. N., An intrinsically photosensitive polyimide. *Chemistry of Materials* **1989**, *1* (1), 163-166.
23. Dennis, J. M.; Fahs, G. B.; Moore, R. B.; Turner, S. R.; Long, T. E., Synthesis and Characterization of Polysulfone-Containing Poly(butylene terephthalate) Segmented Block Copolymers. *Macromolecules* **2014**, *47* (23), 8171-8177.
24. Dennis, J. M.; Fahs, G. B.; Moon, N. G.; Mondschein, R. J.; Moore, R. B.; Wilkes, G. L.; Long, T. E., Synthesis of Polysulfone-Containing Poly(butylene terephthalate) Segmented Block Copolymers: Influence of Segment Length on Thermomechanical Performance. *Macromolecules* **2017**, *50* (13), 5107-5113.
25. Coleman, M. M., *Fundamentals of Polymer Science: An Introductory Text, Second Edition*. CRC Press: 2019.
26. Yang, H.; Wu, X.; Li, S., A compatibilizer for a blend of polysulfone with a liquid crystalline polyester. *Polymer Engineering & Science* **1996**, *36* (22), 2781-2784.
27. Shaw, M. T.; Miller, J. C., The rheology of polysulfone. *Polymer Engineering & Science* **1978**, *18* (5), 372-377.

28. Yamashita, T.; Tomitaka, H.; Kudo, T.; Horie, K.; Mita, I., Degradation of sulfur-containing aromatic polymers: Photodegradation of polyethersulfone and polysulfone. *Polymer Degradation and Stability* **1993**, 39 (1), 47-54.

CHAPTER 8 SUPPORTING INFORMATION

PHOTO-RESPONSIVE CYCLOBUTANE BISIMIDE-CONTAINING
POLYSULFONES CAPABLE OF LIGHT-MEDIATED DEPOLYMERIZATION

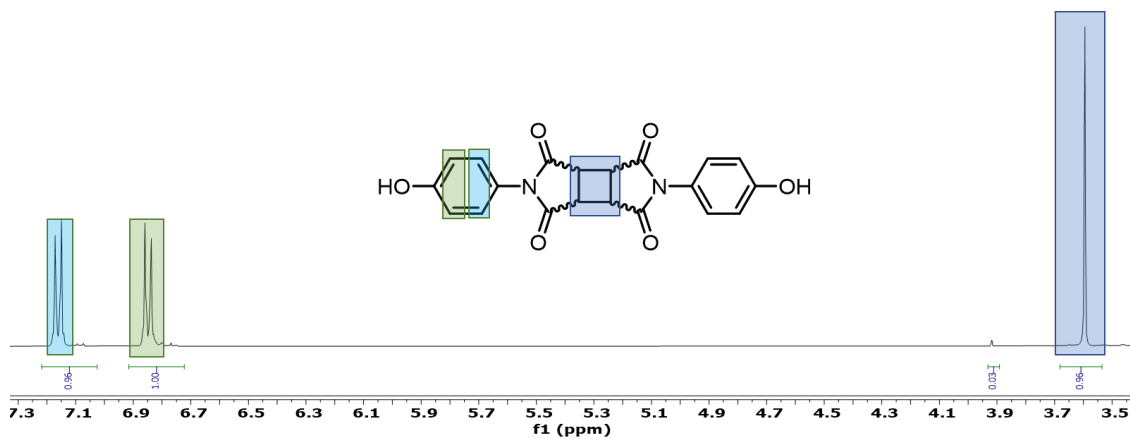


Figure S1: ¹H NMR displays purity of CBDA-AP-I.

CHAPTER 9

FUTURE WORK

9.1 Injection Molding of Non-Isocyanate Polyurethane Structural Foam Composites

A library of BCI monomers enabled the synthesis of rigid and flexible NIPU foams.^{1, 2} Subsequent catalyst and surfactant optimization provided control over pore geometry and Michael acceptor reactive fillers resolved the issue of residual imidazole in the foam matrix. These results marked a substantial advancement in the field of NIPU foam chemistry, however applying this technology to commercially relevant processing modalities remains undiscussed. PU foam processing is largely divided into slabstock and molded modalities. Slabstock foams are produced by a continuous production pathway where isocyanates and polyols are mixed continuously to produce slabs of PU foams.³ Conversely, direct injection molding of isocyanate and polyol into a specially designed mold comprises molded PU foams.^{3, 4} Each processing modality contains specific benefits and drawbacks, i.e., the facile production, but post-processing required for slabstock foams compared to the cost-intensive, however specialized molded foam process. The tunability of BCI monomers for rigid, structural foam applications renders this chemistry compatible with molded foam applications. Thus, the adaptation of this chemistry to a molded foam processing modality remains feasible and desired. Advancements described in chapter six of this document remediated the issue of residual imidazole, which represented the final hurdle in achieving facile processing of BCI NIPU foams for structural applications and enables the next step for the BCI platform.

Several BCI monomers that impart restricted rotation along the NIPU backbone serve as ideal candidates for foam molding applications, as sufficient modulus values are required

for mold release. TCD, outlined in chapter six allowed for the synthesis of such monomers, allowing for subsequent processing, shown in **Figure 9.1**. As discussed in chapter 6, TCDBCI produces high T_g NIPU foams when reacted with the triaryl amine monomer, TADE. However, this rigid monomer selection resulted in the embrittlement of the final foam part, necessitating a flexible chain spacer to maintain part toughness.

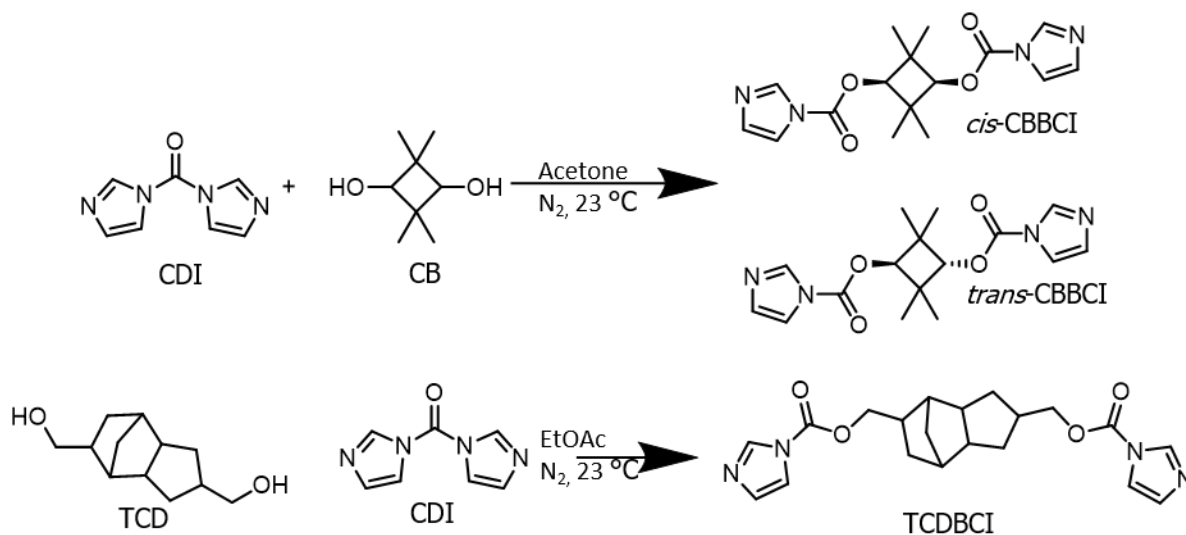


Figure 9.1: CDI readily reacts with cyclic diols to produce BCI monomers that restrict backbone movement after polymerization.

As previously mentioned, the addition of a Jeffamine[®] to the TCDBCI-TADE foam formulation resulted in a NIPU foam with decreased brittleness that maintained a relatively high T_g value of 74 °C, **Figure 9.2**. Synthetic procedures followed that of chapter three, with all reagents mixed in the melt to produce a cylindrical foam after extraction from a test tube.

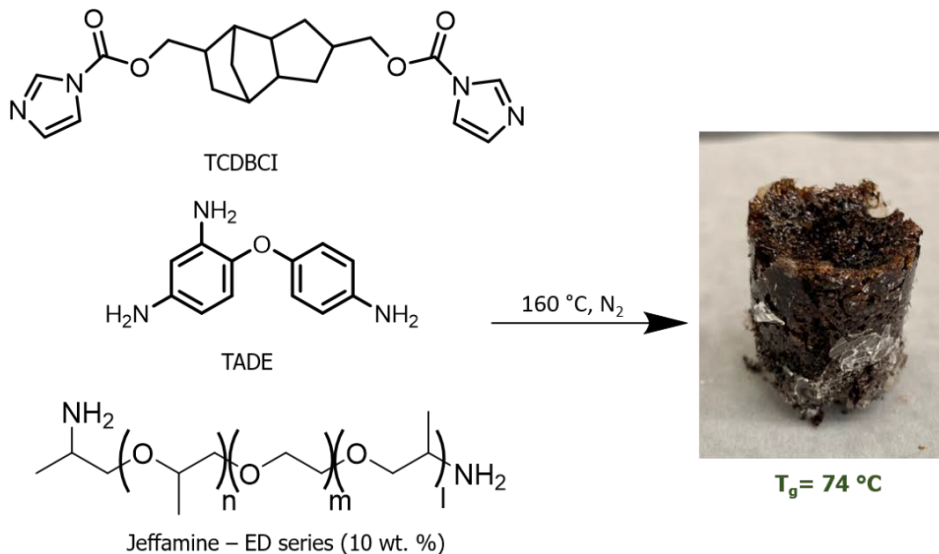


Figure 9.2: TCDBCI reacts with TADA and an etheric Jeffamine[®] to produce a tough NIPU foam.

The design of a specialized foam mold allowed for initial explorations into foam molding processing routes with BCI monomers, displayed in **Figure 9.3**. The foam mold utilized for these experiments underwent several iterations to account for pressure increases caused by CO₂ and imidazole production, as well as sufficient monomer loading to target foam density. Foam density was targeted by utilizing the known volume of the foam mold, as well as the monomer mass loading deducting the mass of the imidazole condensate. For systems incorporating a bis-maleimide Michael acceptor, APO-BMI, the mass of imidazole was retained, as TGA demonstrated efficient capture and no weight loss after curing. The mold was constructed out of aluminum to ensure efficient heat transfer throughout the rising foam, and a 0.01 mm vent hole allowed for depressurization during foam blowing. Initial BCI foam molding experiments consisted of the Jeffamine[®]-doped TCDBCI-TADE structural foam and yielded a square specimen that displayed adequate shape retention after removal from the foam mold.

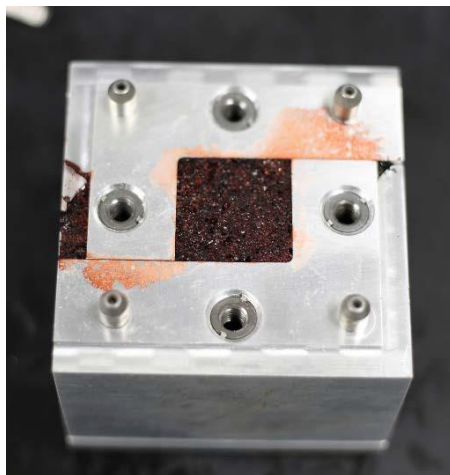


Figure 9.3: The top of a molded foam rectangle. This foam piece released from the mold, resulting in minimal damage to the outside surface. A diamond saw was used to further shape this foam into test specimens

Incorporation of the reactive filler (APO-BMI) described in chapter 6 resulted in a visual change of the molded foam. Microscopy images of initial molded parts display smooth edges, however cross-sectional analysis revealed uneven pore structure, shown in **Figure 9.4**. This result highlights the importance of surfactants during the foaming process, and represents a vital area for innovation. While bismaleimides successfully capture the imidazole condensate and boast mechanical properties, surfactant effects on cell geometry remains unexplored. Investigations into surfactant chemistries and concentration serve to further improve BCI foam molding processes.



Figure 9.4: Microscopy of molded foam cross sections reveal good shape retention and closed cell structure. The addition of a Michael acceptor to the BCI formulation resulted in increased gloss of the final part.

The process outlined above produces molded foam parts without the need for post-processing considerations, however improvements relating to monomer loading still serve to streamline this process. Future work in this area pertains to the reactive twin-screw extrusion of BCI monomers in the presence of multifunctional amines, chain spacers, reactive fillers, surfactants, and catalysts. Careful tuning of recycle times, influenced by catalyst loading, and monomer selection, will enable the realization of a continuous injection molded foam process. In this process, all reagents are mixed for homogeneously, then injected into a predetermined mold shape to yield a final NIPU foam part. Catalyst loading and amine reactivity tune working times, which allow for successful mold filling, while surfactant loading will control pore geometry. Lastly, the incorporation of reactive maleimide additives, outlined in chapter 6, will eliminate any post-processing needs by incorporating the imidazole condensate as functional filler in the final foam part. Careful control over mold temperatures and foam modulus will serve to optimize delamination of the final foam from the mold surface, allowing for smooth finishes shown in **Figure 9.4**.

The effects of carefully curated BCI foam formulations on thermomechanical properties is of great interest, as achieving optimal properties serves to further validate BCI chemistry as a viable alternative to isocyanate-derived PUs.

9.2 Enhanced Phase Separation of Non-Isocyanate Polyurethane Thermoplastic Elastomers

Previous investigations in chapter four outlined the synthesis of NIPUs derived from a polycondensation approach that utilized BCI monomers. This synthetic method utilized Le Chatelier's principle to actively drive molecular weight increase, which contrasts to the polyaddition mechanism leveraged by traditional isocyanate derived PUs. While a primary benefit of BCI chemistry is the green aspect of safer monomers, fully utilizing the imidazole condensate to achieve unique PU structures of high molecular weight provides an additional outstanding benefit. Additionally, chapter 3 highlighted a decarboxylation mechanism for BCI monomers, which increases in reaction rate at elevated temperatures.⁵ This was useful for NIPU foam synthesis, however required careful considerations during thermoplastic NIPU synthesis, where careful control over monomer stoichiometry is essential for achieving high molecular weight. The synthesis of high T_g NIPUs, however, requires elevated reaction temperatures to prevent the vitrification of the growing polymer chain, thus a method to inhibit this decarboxylation pathway was developed. As demonstrated throughout this work, informed monomer design allows for such control. 2,2'-4,4'-tetramethyl-1,3-cyclobutanediol (CB) is a commercial diol used for the synthesis of Tritan[®] polycarbonates (PCs), and imparts impact resistance and high T_g into the final PC. Interestingly, CB displays an absence of β -hydrogens, which eliminates the

decarboxylation pathway for BCI monomers. Thus, CB was reacted with CDI to produce a novel BCI monomer, CBBCI, described in **Figure 9.5**.

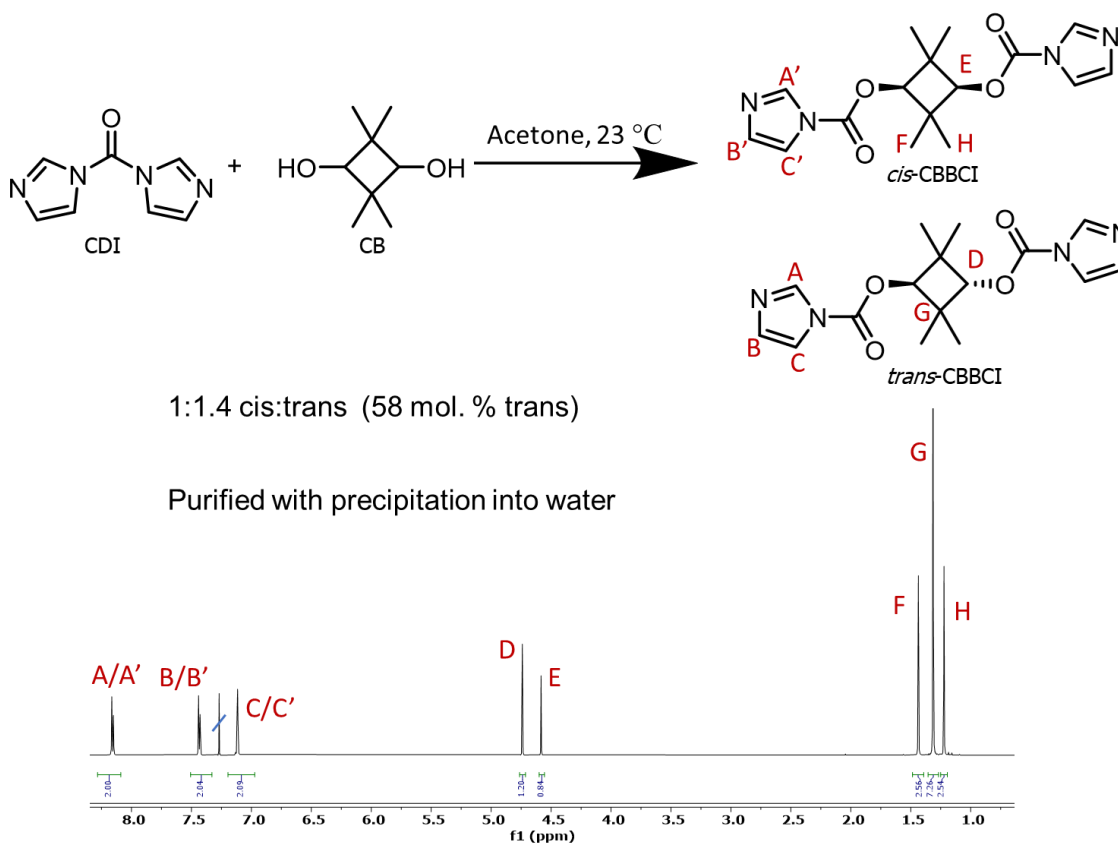


Figure 9.5: CB readily reacts with CDI to form CBBCI at high yields and purity.

As predicted, this monomer displays no CO₂ generation at elevated temperature, which contrasts other BCI monomers outlined in chapter 3. This was confirmed with a CO₂ detector and multiple heating cycles, shown in **Figure 9.6**. The unique thermal stability that CBBCI possesses allows for future work in the synthesis of high T_g or high T_m NIPUs, without the need for decarboxylation considerations. Thus, focus can be shifted towards the synthesis of high-performance, thermally robust NIPUs of various chemical compositions.

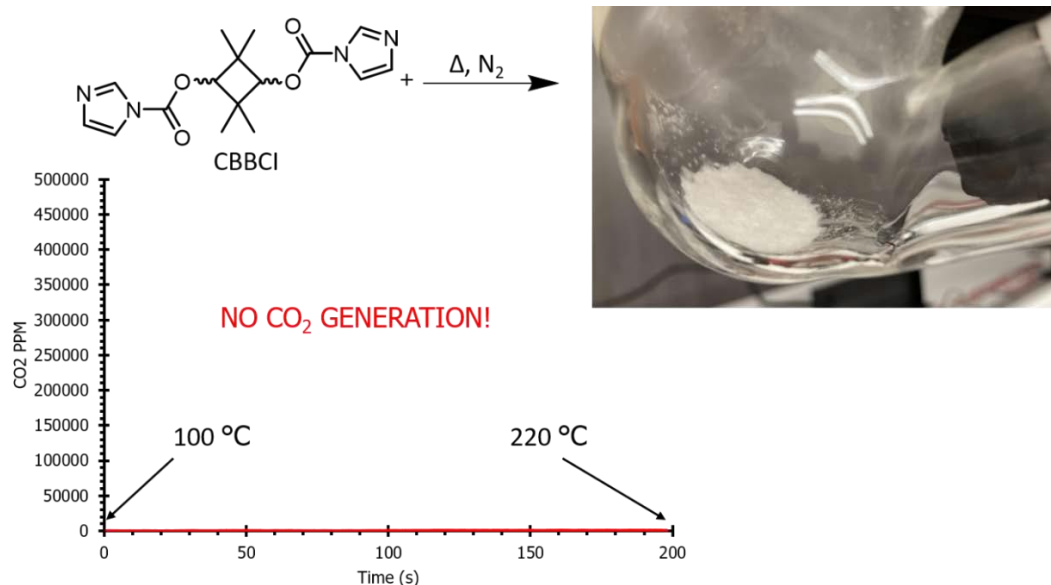


Figure 9.6: Decarboxylation experiments utilizing CBBCI display no CO₂ generation throughout a wide temperature range.

One such composition is the incorporation of poly(dimethyl siloxane) (PDMS) into the backbone of high-performance BCI NIPUs. As discussed in chapter 2, PDMS urethanes readily adapt to specialty applications including the biomedical device and coatings space.^{6, 7} This is due to the unique properties PDMS instills, namely low surface energy, the introduction of large temperature windows for operation, and high oxidation resistance.⁸ The low T_g of PDMS, -125 °C (reported as low as -150 °C), enables this large performance window.^{9, 10} Logically, pairing this low temperature performance with a high ultimate thermal transitions serves to lengthen the thermal performance window of PDMS-based PUs. Thus, combining amine-functionalized PDMS with CBBCI and an amine chain extender will enable the synthesis of a novel, high-performance NIPU, displayed in **Figure 9.7**.

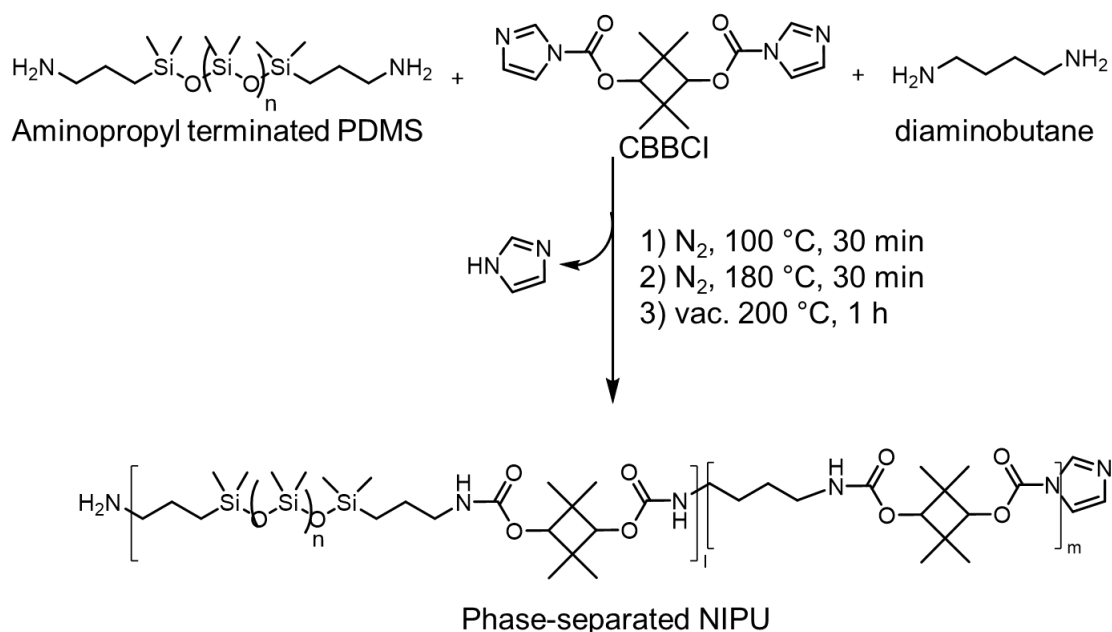


Figure 9.7: CBBCI reacts with amine functionalized monomers in a one-shot process to produce a nanoscale phase-separated NIPU.

The preparation of a PDMS-containing NIPU that possesses impact-resistance CB linkages has potential use for coating applications, where thermal and damping properties are critical.^{11, 12} However, CBBCI is not limited to reactivity with PDMS soft segments. Conversely, it serves as a thermally stable, difunctional monomer capable of coupling with any amine-functionalized reactant. Likewise, the selection of chain extender can be tuned for increased T_g through selection of a rigid, cycloaliphatic amine. Additionally, evaluation of the phase separation behaviour with differing selections of chain extenders and soft segments enables further analysis of structure-property relationships of polyurethanes with novel structures. Furthermore, the lack of CO₂ generation present in CBBCI enables the production of BCI NIPU foams that possess tunable pore structures. This can be done through utilizing CBBCI in conjunction with a CO₂-producing BCI monomer, such as

BBCI, to control the extent of decarboxylation, providing an additional handle for tuning foam density.

9.3 High performance Cyclobutane bisimide-containing polyesters

Chapters seven and eight utilize a novel, cyclobutane bisimide-containing bisphenol monomer for the production of photo-active PUs and PSUs. The tunable reactivity of CBDA-AP-I enabled these systems, as it provided a mechanism for packaging cyclobutane bisimide functionality into both bisphenol and hydroxy functionalities, shown in **Figure 9.8**. While PSUs, and to a greater extent PUs, encompass a large share of polymer production, the large global production of polyesters renders them an important member of the plastics family. Thus, adapting this versatile monomer to polyesters is desired.

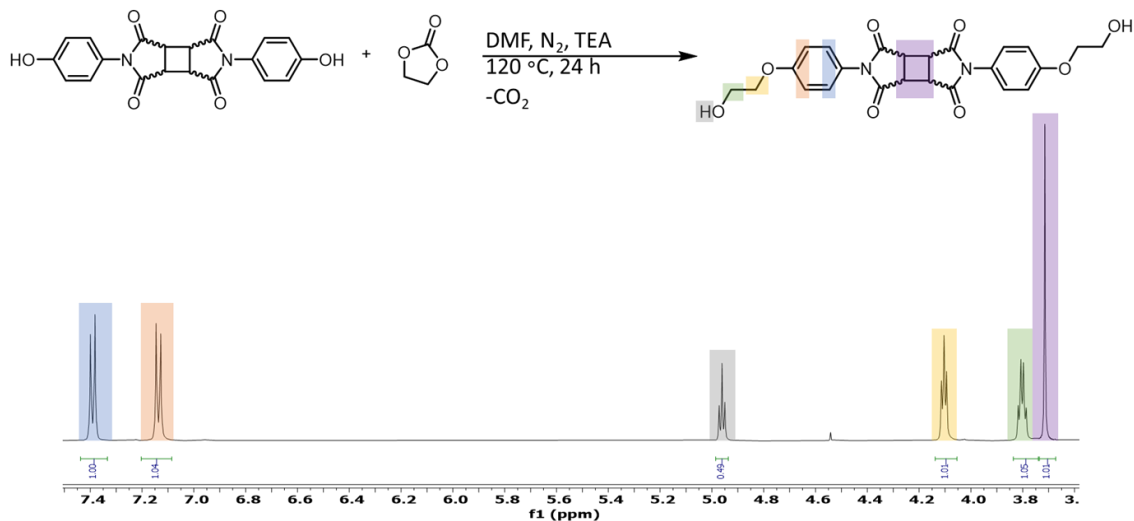


Figure 9.8: Ethylene carbonate reacts with CBDA-AP-I to install hydroxyethyl functionality.

The polycondensation between CBDA-AP-I-HE and terephthalic acid will synthesize a novel polyester containing a photo-sensitive trigger placed along the polymer backbone, described in **Figure 9.9**. This proves advantageous, as polyesters already possess

sustainable aspects including facile depolymerization and repolymerization.¹³⁻¹⁵ Likewise, the rise of bio-derived polyester monomers further solidifies polyesters as a sustainable platform for the future.¹⁴ The addition of a thermally robust, photo-reversible monomer to the polyester library only serves to further increase sustainability within the field.

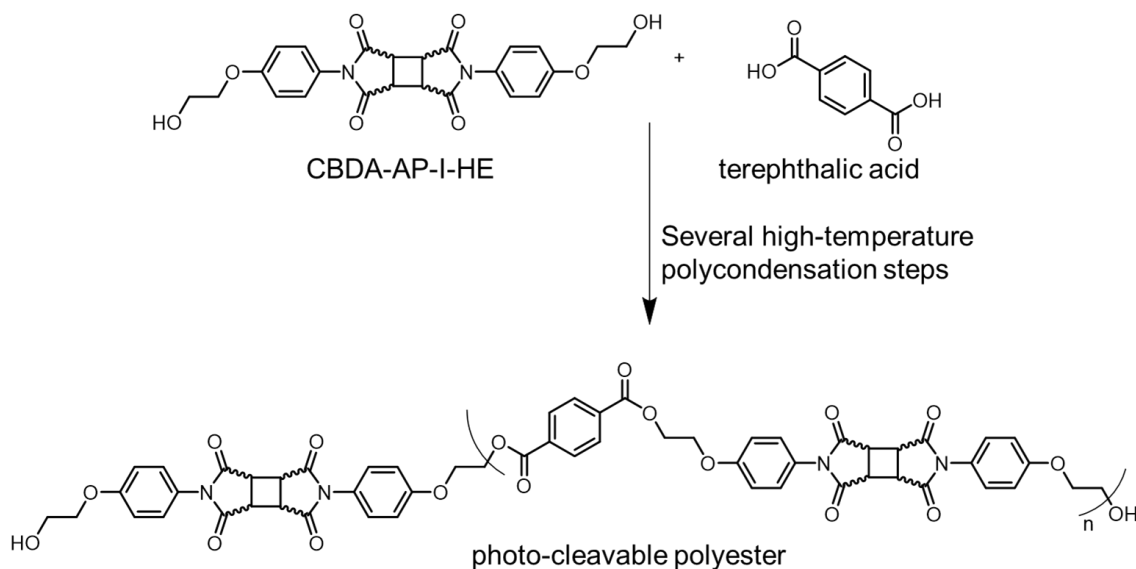


Figure 9.9: A polycondensation reaction between CBDA-AP-I-HE and terephthalic acid provides a high-performance, photo-cleavable polyester.

9.4 Coumarin Containing Photo-Reversible Polymeric Systems

While there is literature and experimental precedence for the photo-cleavage of cyclobutane bisimide systems, the desire for additional platforms for photo-stimulated polymeric systems prompts the exploration of coumarin-containing polymers.¹⁶ Similar to work discussed in chapters seven and eight, a method where the photo-cleavable unit is installed in the backbone of the polymeric systems holds several benefits. Namely, increased molecular weight decrease from lower dosages of UV irradiation. Additionally, the selection of phenol or hydroxy reactivity remains desired for incorporation into fully aromatic or aliphatic systems. Previously published research describes the use of coumarin

functionality in photo-reversible polymeric systems for reversible adhesives, tissue scaffolds, or light harvesting applications.¹⁷⁻¹⁹ Largely, the use of coumarins for these applications were limited to pendant groups that underwent photo-reversibility under photo-irradiation. Thus, future work focuses on the synthesis of a coumarin dimer that readily incorporates into the polymer backbone, outlined in **Figure 9.10**. Initial reactions leveraged broadband UV irradiation, resulting in low conversions to the dimer state, however the use of a photosensitizer such as benzophenone may serve to increase dimerization yields. Prominent factors that influence coumarin dimer formation include UV dosage, solvent selection, and solution concentration.²⁰ The impacts of these factors on isomerization serve as an additional handle when addressing the structure-property relationships of the resulting materials.

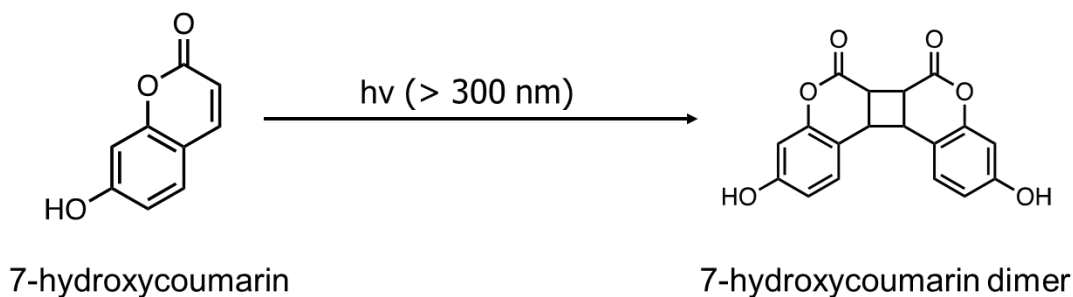


Figure 9.10: Proposed reaction for the dimerization of 7-hydroxycoumarin.

The bisphenol reactivity of the 7-hydroxycoumarin dimer allows for integration into PSU systems, as well as the synthesis of fully aromatic polyesters.²¹ However, aromatic alcohols often suffer from decreased reactivity that interferes with polyester synthesis resulting in low molecular weight. Thus, the subsequent installation of hydroxyethyl functionality onto the 7-hydroxycoumarin dimer provides an avenue for broadening the participation of this compound into various polymeric systems, i.e., polyesters, PUs, polycarbonates, and epoxy

systems. Previously reported ethylene carbonate, as well as 2-bromoethanol, serve as pathways for this installation, described in **Figure 9.11**. Subsequent reaction of the hydroxyethyl functionalized 7-hydroxycoumarin dimer with isocyanates or diacids will enable the formation of photo-responsive PUs and polyesters for efficient reversible adhesive or depolymerization applications.²²⁻²⁴

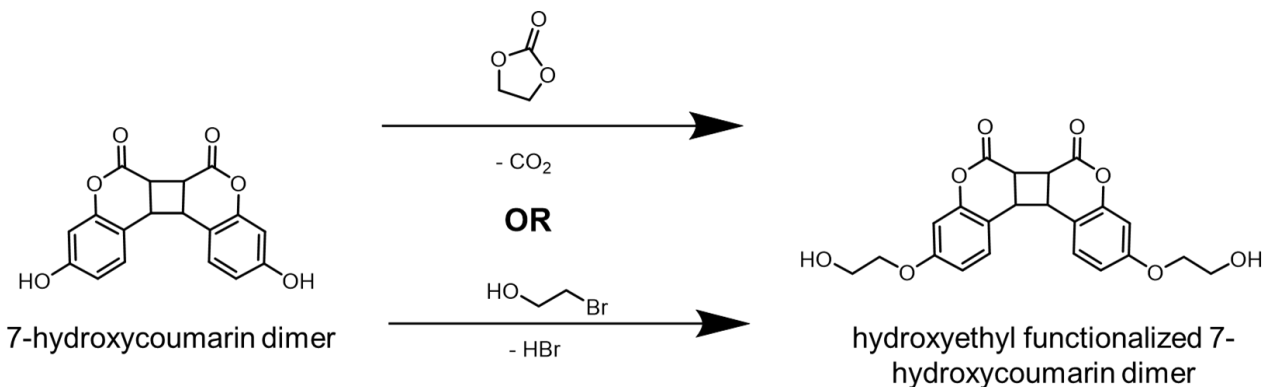


Figure 9.11: Either ethylene carbonate or bromoethanol can install hydroxyethyl functionality to the proposed 7-hydroxycoumarin dimer.

9.5 References:

1. Sintas, J. I.; Wolfgang, J. D.; Long, T. E., Carbamate thermal decarboxylation for the design of non-isocyanate polyurethane foams. *Polymer Chemistry* **2023**.
2. Wolfgang, J. D.; White, B. T.; Long, T. E., Non-isocyanate Polyurethanes from 1,1'-Carbonyldiimidazole: A Polycondensation Approach. *Macromolecular Rapid Communications* **2021**, 42 (13), 2100163.
3. Dounis, D. V.; Wilkes, G. L., Structure-property relationships of flexible polyurethane foams. *Polymer* **1997**, 38 (11), 2819-2828.

4. Moreland, J. C.; Wilkes, G. L.; Turner, R. B., Viscoelastic behavior of flexible slabstock polyurethane foam as a function of temperature and relative humidity. II. Compressive creep behavior. *Journal of Applied Polymer Science* **1994**, *52* (4), 569-576.
5. Delebecq, E.; Pascault, J.-P.; Boutevin, B.; Ganachaud, F., On the Versatility of Urethane/Urea Bonds: Reversibility, Blocked Isocyanate, and Non-isocyanate Polyurethane. *Chemical Reviews* **2013**, *113* (1), 80-118.
6. Miranda, I.; Souza, A.; Sousa, P.; Ribeiro, J.; Castanheira, E. M. S.; Lima, R.; Minas, G., Properties and Applications of PDMS for Biomedical Engineering: A Review. *Journal of Functional Biomaterials* **2022**, *13* (1), 2.
7. Eduok, U.; Faye, O.; Szpunar, J., Recent developments and applications of protective silicone coatings: A review of PDMS functional materials. *Progress in Organic Coatings* **2017**, *111*, 124-163.
8. Ji, X.; Wang, H.; Ma, X.; Hou, C.; Ma, G., Progress in polydimethylsiloxane-modified waterborne polyurethanes. *RSC Advances* **2017**, *7* (54), 34086-34095.
9. Volkov, A., Polydimethylsiloxane (PDMS). In *Encyclopedia of Membranes*, Drioli, E.; Giorno, L., Eds. Springer Berlin Heidelberg: Berlin, Heidelberg, 2015; pp 1-2.
10. Coleman, M. M., *Fundamentals of Polymer Science: An Introductory Text, Second Edition*. CRC Press: 2019.
11. Iqbal, N.; Sharma, P. K.; Kumar, D.; Roy, P. K., Protective polyurea coatings for enhanced blast survivability of concrete. *Construction and Building Materials* **2018**, *175*, 682-690.

12. Chattopadhyay, D. K.; Raju, K. V. S. N., Structural engineering of polyurethane coatings for high performance applications. *Progress in Polymer Science* **2007**, *32* (3), 352-418.
13. Allen, R. D.; James, M. I., Chemical Recycling of PET. In *Circular Economy of Polymers: Topics in Recycling Technologies*, American Chemical Society: 2021; Vol. 1391, pp 61-80.
14. Vilela, C.; Sousa, A. F.; Fonseca, A. C.; Serra, A. C.; Coelho, J. F. J.; Freire, C. S. R.; Silvestre, A. J. D., The quest for sustainable polyesters – insights into the future. *Polymer Chemistry* **2014**, *5* (9), 3119-3141.
15. Ikada, Y.; Tsuji, H., Biodegradable polyesters for medical and ecological applications. *Macromolecular Rapid Communications* **2000**, *21* (3), 117-132.
16. June, S. M.; Suga, T.; Heath, W. H.; Long, T. E.; Lin, Q.; Puligadda, R., Photo-Reactive Polyimides and Poly(siloxane imide)s as Reversible Polymeric Interfaces. *The Journal of Adhesion* **2010**, *86* (10), 1012-1028.
17. Trenor, S. R.; Long, T. E.; Love, B. J., Photoreversible Chain Extension of Poly(ethylene glycol). *Macromolecular Chemistry and Physics* **2004**, *205* (6), 715-723.
18. Trenor, S. R.; Long, T. E.; Love, B. J., Development of a Light-Deactivatable PSA Via Photodimerization. *The Journal of Adhesion* **2005**, *81* (2), 213-229.
19. Palmans, A. R. A.; Smith, P.; Weder, C., Polarizing Energy Transfer in Photoluminescent Conjugated Polymers with Covalently Attached Sensitizers. *Macromolecules* **1999**, *32* (14), 4677-4685.

20. Trenor, S. R.; Shultz, A. R.; Love, B. J.; Long, T. E., Coumarins in Polymers: From Light Harvesting to Photo-Cross-Linkable Tissue Scaffolds. *Chemical Reviews* **2004**, *104* (6), 3059-3078.
21. Dennis, J. M.; Fahs, G. B.; Moore, R. B.; Turner, S. R.; Long, T. E., Synthesis and Characterization of Polysulfone-Containing Poly(butylene terephthalate) Segmented Block Copolymers. *Macromolecules* **2014**, *47* (23), 8171-8177.
22. Boga, K.; Patti, A. F.; Warner, J. C.; Simon, G. P.; Saito, K., Eco-Friendly Photoreversible Adhesives Derived from Coumarin-Functionalized Epoxy Soybean Oil. *ACS Applied Polymer Materials* **2023**, *5* (7), 4644-4653.
23. Hohl, D. K.; Weder, C., (De)bonding on Demand with Optically Switchable Adhesives. *Advanced Optical Materials* **2019**, *7* (16), 1900230.
24. Takahashi, H.; Sakuragi, M.; Hasegawa, M.; Takahashi, H., Photodegradable polyamides. *Journal of Polymer Science Part A-1: Polymer Chemistry* **1972**, *10* (5), 1399-1409.

CHAPTER 10

SUMMARY AND CONCLUSIONS

Green chemistry advancements in polymer science holds a prominent position with regards to modern concerns over plastic impacts on human health and the environment, especially apparent when considering the increased interest in this field as plastics infiltrate national and global news. The widespread use of and society's dependence on polymer chemistry prevents a departure from their continued use, further justifying the search for harmony between plastic materials and global health. Chapter two outlines the pursuit for better materials that enable an increase in the quality of human health at the human-polymer interface. Various biomedical devices rely on polymers for their unique performance parameters including biocompatibility, insulation, softness, and toughness, however the extreme environments of the human body subject these materials to long-term degradation. While these devices are heavily formulated for optimal performance, emerging insights into structure-property relationships between polyurethanes (PUs) and the human body allow for further optimization. Notably, the increasing awareness of the effect of hydrophilicity on biofilm formation serves to inform on the design of next-generation biomedical devices, i.e., increasing hydrophilicity decreases bacterial binding. Likewise, the development of new coatings capable of low surface energy (diamond-like carbon) and the integration of antibiotics into a degradable PU coating serve to further alleviate this issue. Lastly, understanding oxidation pathways that arise from reactive oxygen species in the blood or from trace metal impurities in biomedical wiring informed soft segment design towards poly(dimethyl siloxane) platforms.

Chapters three through six represent advancements pertaining to the green synthesis of PUs. Isocyanates readily react with hydroxyls to form urethane linkages, producing PUs with highly tailored properties for engineering applications. Likewise, the efficient reaction is amenable to various processing modalities including reactive extrusion, spray coating, and foam molding, which enables the widespread use of PUs in everyday applications. However, this efficient reactivity comes at a cost of increased toxicity to humans, causing asthma or death upon repeated contact. Thus, various investigations into a platform that maintains traditional PU properties while circumventing isocyanates served to alleviate this issue. Namely, the development of non-isocyanate polyurethane (NIPU) systems outlined in this work serve as a next step for the evolution of PU technology. Bis-carbonylimidazolide (BCI) chemistry enabled the synthesis of a library of NIPUs for both thermoplastic and thermoset applications. Conversely to traditional PU synthesis, BCI chemistry results in a polycondensation approach for NIPUs, as opposed to a polyaddition one. The polycondensation approach produces an imidazole byproduct, which leads to both positive and negative impacts; removal of the byproduct serves to ensure high reaction conversions that result in high molecular weight, however the presence of residual imidazole byproducts in thermoset applications proved unfavorable.

Thus, thermoplastic NIPU applications utilized a melt-phase polycondensation reaction similar to that of traditional polyester reactors, where the monomers remained in the melt under inert conditions. Generation of sufficient molecular weight allowed for the introduction of vacuum to the system without reagent loss, subsequently removing the imidazole byproduct and achieving high molecular weight. Further melt processing allowed for the generation of phase-separated NIPU films that underwent

thermomechanical and spectroscopic analysis. This project highlighted a major innovation in the field of NIPU chemistry, as NIPUs synthesized with this method alleviated a major issue in this field, namely the exclusion of pendant hydroxyl groups present on NIPUs derived from other isocyanate-free chemistries, i.e., the cyclic carbonate route. Pendant hydroxyl groups present in cyclic carbonate NIPUs impede phase separation in polyether soft segment systems and vastly increase the water uptake. However, BCI-derived NIPUs showcased in chapter four displayed excellent nano-scale phase separation with a poly(ethylene glycol) soft segment and minimal water uptake, confirmed with SAXS and AFM measurements.

When considering a greener pathway for a PUs, it is important to consider the diverse topologies required for their wide-spread use. Considerations for topology, processing methods, and final properties increase viability for the adoption of a new, greener synthetic platform, thus prompting the exploration in to crosslinked NIPU systems. Multifunctional monomers enabled the exploration of thermosetting NIPU systems in chapters three and six. The discovery of a novel decarboxylation pathway for BCI monomers enabled concurrent CO₂ generation with NIPU curing, resulting in the production of NIPU foams. BCI monomer structure dictated foam T_g values, covering rigid and flexible foam systems. Specifically, flexible etheric triamines coupled with aliphatic BCI monomers enabled low T_g foams with open-cell structures conducive to cushioning applications. Conversely a selection of rigid, aromatic triamines and cyclic BCI monomers allowed for production of structural, closed-cell foams and a combination of flexible and rigid monomers allowed for tuning of thermal transition temperatures.

Heavy formulation of commercial PU foams prompted the exploration of catalyst and surfactant effects on the BCI NIPU system. Catalyst screening identified Dabco[®] 33-LV as a versatile selection for BCI systems, as control over catalyst concentration allowed for tuning of reaction times, which is essential for foam molding applications. Additionally, control over surfactant type, a poly(dimethyl siloxane)-Poly(ethylene glycol) derivative, and concentration effectively programmed cell architecture into the final NIPU foam. Larger surfactant concentrations yielded closed-cell foam systems, ideal for structural and insulative applications, while moderate loadings resulted in an open-cell structure conducive to cushioning. While BCI NIPU foams displayed ideal properties and facile synthetic routes, the need for post processing steps to remove the trapped imidazole condensate required innovation. As outlined in chapter six, the introduction of an orthogonal curing agent equipped with Michael acceptor reactivity remediated this issue. Careful selection of the reactive filler ensured retention of the targeted thermomechanical properties for each NIPU foam formulation. Insight into structure-property relationships resulted in the selection of a flexible butanediol diacrylate filler for flexible foam systems and rigid, aromatic maleimide additives for structural foam applications. In-situ FTIR confirmed a temperature-dependent reactivity of imidazole with Michael acceptor systems and weight loss measurements confirmed successful sequestration of the imidazole byproduct at elevated temperatures.

This work highlights advancements in developing a greener synthetic method for the production of PUs, positively impacting human-plastic relationships. Chapters seven and eight outline further advancements into polymer sustainability. Previous understandings of photo-induced cleavage of polymeric structures informed the next step in light-based

polymeric processing. Light serves as a sustainable stimuli source for functional polymeric materials and provides an alternative to thermal processes, which are energy-intensive. Furthermore, light-based processes hold unique advantages in the semiconductor space, as thermal process produce warpage during chip manufacturing which leads to defective products. The synthesis of a novel cyclobutane bisimide monomer (CBDA-AP-I) containing bisphenol reactivity enabled the incorporation of sustainable photo-processing to PU and polysulfone (PSU) modalities. Namely, the development of a novel photo-cleavable PU that displayed phase separation and a subsequent change in thermomechanical properties upon irradiation with 254 nm light. Likewise, CBDA-AP-I introduced controlled photo-cleavage when incorporated into a BPA-based PSU system. Chapter eight highlights this feat with molecular weight traces that indicated PSU photo-cleavage correlating to CBDA-AP-I incorporation. These two investigations serve to highlight the advantage of a monomeric solution for photo-cleavage applications, as a photocleavable monomer can be directly incorporated into a variety of polymeric systems.

Key Takeaways:

- A library of bis-carbonylimidazolide (BCI) monomers enabled the synthesis of non-isocyanate polyurethane (NIPU) foams with controlled thermomechanical properties
- Discovery and mechanistic understanding of a decarboxylation pathway for BCI monomers enabled in-situ CO₂ formation in NIPU thermoset systems resulting in foam production
- Explorations into surfactant and catalyst effects on BCI NIPU foams resulted in control over pore structure and shape, as well as predictable control over cure times.

- BCI monomers mediated the synthesis of linear, nanophase separated NIPUs containing poly(ethylene glycol) soft segments without any additional post-processing steps.
- Michael acceptors were shown to successfully sequester the imidazole byproduct produced during BCI foam curing, resulting in the elimination of the solvent extraction post processing step.
- 4-aminophenol (AP) and 1,2,3,4-cyclobutane-tetracarboxylic dianhydride (CBDA) enabled the synthesis of a novel bisphenol monomer that contained cyclobutane bisimide functionality. Subsequent functionalization with ethylene carbonate produced telechelic hydroxyethyl reactivity.
- Hydroxyethyl functionality on CBDA-AP-I-HE allowed for the synthesis of a poly(propylene glycol)-based polyurethane containing cyclobutane bisimide functionality. Subsequent measurements of thermomechanical properties displayed elastomeric behavior as well as light-dependent properties.
- Phenol reactivity present on CBDA-AP-I allowed for facile incorporation of cyclobutane bisimide chemistry into a bisphenol-A derived polysulfone system. Effects of CBDA-AP-I concentration on thermomechanical properties were evaluated and irradiation with 254 nm light resulted in a predictable decrease in molecular weight.

REFERENCES

Chapter 1

1. Staudinger, H., Über Polymerisation. Berichte der deutschen chemischen Gesellschaft (A and B Series) 1920, 53 (6), 1073-1085.
2. Andradý, A. L.; Neal, M. A., Applications and societal benefits of plastics. Philos Trans R Soc Lond B Biol Sci 2009, 364 (1526), 1977-84.
3. Szycher, M., Szycher's Handbook of Polyurethanes, First Edition. Taylor & Francis: 1999.
4. Hydrogen Bonding in Polymeric Materials. In Hydrogen Bonding in Polymeric Materials, 2018; pp 1-8.
5. Paul C. Painter, M. M. C., Fundamentals of Polymer Science Second ed.; CRC Press LLC: 1997.
6. Bayer, O. A Process for the Production of Polyurethanes and Polyureas. 1937.
7. Prisacariu, C., Polyurethane Elastomers: From Morphology to Mechanical Aspects. Springer Vienna: 2011.
8. Kaushiva, B. D.; McCartney, S. R.; Rossmý, G. R.; Wilkes, G. L., Surfactant level influences on structure and properties of flexible slabstock polyurethane foams. Polymer 2000, 41 (1), 285-310.
9. Hyun, M. E.; Kim, S. C., A study on the reactive extrusion process of polyurethane. Polymer Engineering & Science 1988, 28 (11), 743-757.
10. Yilgör, I.; Yilgör, E.; Wilkes, G. L., Critical parameters in designing segmented polyurethanes and their effect on morphology and properties: A comprehensive review. Polymer 2015, 58, A1-A36.
11. Stoffel, N. C.; Kramer, E. J.; Volksen, W.; Russell, T. P., Solvent and isomer effects on the imidization of pyromellitic dianhydride-oxydianiline-based poly(amic ethyl ester)s. Polymer 1993, 34 (21), 4524-4530.
12. Hergenrother, P., The Use, design, synthesis, and properties of high performance/high temperature polymers: An overview, high perform. High Performance Polymers 2003, 15, 3-45.

13. Hegde, M.; Meenakshisundaram, V.; Chartrain, N.; Sekhar, S.; Tafti, D.; Williams, C. B.; Long, T. E., 3D Printing All-Aromatic Polyimides using Mask-Projection Stereolithography: Processing the Nonprocessable. *Advanced Materials* 2017, 29 (31), 1701240.
14. Arrington, C. B.; Hegde, M.; Meenakshisundaram, V.; Dennis, J. M.; Williams, C. B.; Long, T. E., Supramolecular Salts for Additive Manufacturing of Polyimides. *ACS Applied Materials & Interfaces* 2021, 13 (40), 48061-48070.
15. June, S. M.; Suga, T.; Heath, W. H.; Long, T. E.; Lin, Q.; Puligadda, R., Photo-Reactive Polyimides and Poly(siloxane imide)s as Reversible Polymeric Interfaces. *The Journal of Adhesion* 2010, 86 (10), 1012-1028.

Chapter 2

1. Akindoyo, J. O.; Beg, M. D. H.; Ghazali, S.; Islam, M. R.; Jeyaratnam, N.; Yuvaraj, A. R., Polyurethane types, synthesis and applications – a review. *RSC Advances* 2016, 6 (115), 114453-114482.
2. Xie, F.; Zhang, T.; Bryant, P.; Kurusingal, V.; Colwell, J. M.; Laycock, B., Degradation and stabilization of polyurethane elastomers. *Progress in Polymer Science* 2019, 90, 211-268.
3. Gama, N. V.; Ferreira, A.; Barros-Timmons, A., Polyurethane Foams: Past, Present, and Future. *Materials* 2018, 11 (10), 1841.
4. Delebecq, E.; Pascault, J.-P.; Boutevin, B.; Ganachaud, F., On the Versatility of Urethane/Urea Bonds: Reversibility, Blocked Isocyanate, and Non-isocyanate Polyurethane. *Chemical Reviews* 2013, 113 (1), 80-118.
5. Yilgör, I.; Yilgör, E.; Wilkes, G. L., Critical parameters in designing segmented polyurethanes and their effect on morphology and properties: A comprehensive review. *Polymer* 2015, 58, A1-A36.
6. Abouzahr, S.; Wilkes, G. L.; Ophir, Z., Structure-property behaviour of segmented polyether-MDI-butanediol based urethanes: effect of composition ratio. *Polymer* 1982, 23 (7), 1077-1086.
7. Aneja, A.; Wilkes, G. L., A systematic series of 'model' PTMO based segmented polyurethanes reinvestigated using atomic force microscopy. *Polymer* 2003, 44 (23), 7221-7228.

8. Rusu, L.-C.; Ardelean, L. C.; Jitariu, A.-A.; Miu, C. A.; Streian, C. G., An Insight into the Structural Diversity and Clinical Applicability of Polyurethanes in Biomedicine. *Polymers* 2020, 12 (5), 1197.
9. Joseph, J.; Patel, R. M.; Wenham, A.; Smith, J. R., Biomedical applications of polyurethane materials and coatings. *Transactions of the IMF* 2018, 96 (3), 121-129.
10. Wendels, S.; Avérous, L., Biobased polyurethanes for biomedical applications. *Bioactive Materials* 2021, 6 (4), 1083-1106.
11. Griesser, H. J., Degradation of polyurethanes in biomedical applications—A review. *Polymer Degradation and Stability* 1991, 33 (3), 329-354.
12. Król, P., Synthesis methods, chemical structures and phase structures of linear polyurethanes. Properties and applications of linear polyurethanes in polyurethane elastomers, copolymers and ionomers. *Progress in Materials Science* 2007, 52 (6), 915-1015.
13. Polymers as Ureteral Stents. *Journal of Endourology* 2010, 24 (2), 191-198.
14. Gunatillake, P. A.; Martin, D. J.; Meijs, G. F.; McCarthy, S. J.; Adhikari, R., Designing Biostable Polyurethane Elastomers for Biomedical Implants. *Australian Journal of Chemistry* 2003, 56 (6), 545-557.
15. Zawadzak, E.; Bil, M.; Ryszkowska, J.; Nazhat, S. N.; Cho, J.; Bretcanu, O.; Roether, J. A.; Boccaccini, A. R., Polyurethane foams electrophoretically coated with carbon nanotubes for tissue engineering scaffolds. *Biomed Mater* 2009, 4 (1), 015008.
16. Singhal, P.; Small, W.; Cosgriff-Hernandez, E.; Maitland, D. J.; Wilson, T. S., Low density biodegradable shape memory polyurethane foams for embolic biomedical applications. *Acta Biomaterialia* 2014, 10 (1), 67-76.
17. Adhikari, R.; Gunatillake, P. A.; Griffiths, I.; Tatai, L.; Wickramaratna, M.; Houshyar, S.; Moore, T.; Mayadunne, R. T. M.; Field, J.; McGee, M.; Carbone, T., Biodegradable injectable polyurethanes: Synthesis and evaluation for orthopaedic applications. *Biomaterials* 2008, 29 (28), 3762-3770.
18. Guelcher, S.; Srinivasan, A.; Hafeman, A.; Gallagher, K.; Doctor, J.; Khetan, S.; McBride, S.; Hollinger, J., Synthesis, in vitro degradation, and mechanical properties of two-component poly(ester urethane)urea scaffolds: effects of water and polyol composition. *Tissue Eng* 2007, 13 (9), 2321-33.
19. Zdrahala, R. J.; Zdrahala, I. J., Biomedical Applications of Polyurethanes: A Review of Past Promises, Present Realities, and a Vibrant Future. *Journal of Biomaterials Applications* 1999, 14 (1), 67-90.

20. Synthesis, In Vitro Degradation, and Mechanical Properties of Two-Component Poly(Ester Urethane)Urea Scaffolds: Effects of Water and Polyol Composition. *Tissue Engineering* 2007, 13 (9), 2321-2333.
21. Lyu, S.; Untereker, D., Degradability of Polymers for Implantable Biomedical Devices. *International Journal of Molecular Sciences* 2009, 10 (9), 4033-4065.
22. Sobczak, M., Biodegradable Polyurethane Elastomers for Biomedical Applications – Synthesis Methods and Properties. *Polymer-Plastics Technology and Engineering* 2015, 54 (2), 155-172.
23. Pedersen, D. D.; Kim, S.; Wagner, W. R., Biodegradable polyurethane scaffolds in regenerative medicine: Clinical translation review. *Journal of Biomedical Materials Research Part A* 2022, 110 (8), 1460-1487.
24. Szycher, M., *Szycher's Handbook of Polyurethanes*, First Edition. Taylor & Francis: 1999.
25. Mathur, A. B.; Collier, T. O.; Kao, W. J.; Wiggins, M.; Schubert, M. A.; Hiltner, A.; Anderson, J. M., In vivo biocompatibility and biostability of modified polyurethanes. *J Biomed Mater Res* 1997, 36 (2), 246-57.
26. NIOSH Publication No. 2008-109.
[https://www.cdc.gov/niosh/topics/isocyanates/default.html#:~:text=The%20most%20commonly%20used%20diisocyanates,and%20isophorone%20diisocyanate%20\(IPDI](https://www.cdc.gov/niosh/topics/isocyanates/default.html#:~:text=The%20most%20commonly%20used%20diisocyanates,and%20isophorone%20diisocyanate%20(IPDI)
(accessed 09/07/2020).
27. Seefried Jr, C. G.; Koleske, J. V.; Critchfield, F. E., Thermoplastic urethane elastomers. II. Effects of variations in hard-segment concentration. *Journal of Applied Polymer Science* 1975, 19 (9), 2503-2513.
28. Allan, D.; Daly, J. H.; Liggat, J. J., Oxidative and non-oxidative degradation of a TDI-based polyurethane foam: Volatile product and condensed phase characterisation by FTIR and solid state ¹³C NMR spectroscopy. *Polymer Degradation and Stability* 2019, 161, 57-73.
29. Juan V. Cauich-Rodríguez, L. H. C.-C., Fernando Hernandez-Sánchez and José M. Cervantes-Uc, Degradation of Polyurethanes for Cardiovascular Applications. *Advances in Biomaterials Science and Biomedical Applications*, Rosario Pignatello, IntechOpen 2013, 51-82.
30. Bardaweel, S. K.; Gul, M.; Alzweiri, M.; Ishaqat, A.; HA, A. L.; Bashatwah, R. M., Reactive Oxygen Species: the Dual Role in Physiological and Pathological Conditions of the Human Body. *Eurasian J Med* 2018, 50 (3), 193-201.

31. Ulbricht, J.; Jordan, R.; Luxenhofer, R., On the biodegradability of polyethylene glycol, polypeptoids and poly(2-oxazoline)s. *Biomaterials* 2014, 35 (17), 4848-4861.
32. Korotkova, E. I.; Misini, B.; Dorozhko, E. V.; Bukkel, M. V.; Plotnikov, E. V.; Linert, W., Study of OH● Radicals in Human Serum Blood of Healthy Individuals and Those with Pathological Schizophrenia. *International Journal of Molecular Sciences* 2011, 12 (1), 401-409.
33. Stevenson, J. S.; Kusy, R. P., Structural degradation of polyurethane-based elastomeric modules. *Journal of Materials Science: Materials in Medicine* 1995, 6 (7), 377-384.
34. Anderson, J. M.; Hiltner, A.; Wiggins, M. J.; Schubert, M. A.; Collier, T. O.; Kao, W. J.; Mathur, A. B., Recent advances in biomedical polyurethane biostability and biodegradation. *Polymer International* 1998, 46 (3), 163-171.
35. Stokes, K.; McVenes, R.; Anderson, J. M., Polyurethane Elastomer Biostability. *Journal of Biomaterials Applications* 1995, 9 (4), 321-354.
36. Zweifel, H., *Stabilization of Polymeric Materials*. 1 ed.; Springer-Verlag Berlin Heidelberg: 1998; p 219.
37. Ward, B.; Anderson, J.; Ebert, M.; McVenes, R.; Stokes, K., In vivo biostability of polysiloxane polyether polyurethanes: Resistance to metal ion oxidation. *Journal of Biomedical Materials Research Part A* 2006, 77A (2), 380-389.
38. Stokes, K.; Urbanski, P.; Upton, J., The in vivo auto-oxidation of polyether polyurethane by metal ions. *Journal of Biomaterials Science, Polymer Edition* 1989, 1 (3), 207-230.
39. Wiggins, M. J.; Wilkoff, B.; Anderson, J. M.; Hiltner, A., Biodegradation of polyether polyurethane inner insulation in bipolar pacemaker leads. *Journal of Biomedical Materials Research* 2001, 58 (3), 302-307.
40. Stokes, K.; Coury, A.; Urbanski, P., Autooxidative Degradation of Implanted Polyether Polyurethane Devices. *Journal of Biomaterials Applications* 1986, 1 (3), 411-448.
41. Navas-Gómez, K.; Valero, M. F., Why Polyurethanes Have Been Used in the Manufacture and Design of Cardiovascular Devices: A Systematic Review. *Materials* 2020, 13 (15), 3250.
42. Meijs, G. F.; McCarthy, S. J.; Rizzardo, E.; Chen, Y.-C.; Chatelier, R. C.; Brandwood, A.; Schindhelm, K., Degradation of medical-grade polyurethane elastomers:

The effect of hydrogen peroxide in vitro. *Journal of Biomedical Materials Research* 1993, 27 (3), 345-356.

43. Christenson, E. M.; Anderson, J. M.; Hiltner, A., Antioxidant inhibition of poly(carbonate urethane) in vivo biodegradation. *Journal of Biomedical Materials Research Part A* 2006, 76A (3), 480-490.
44. Nouman, M.; Saunier, J.; Jubeli, E.; Marlière, C.; Yagoubi, N., Impact of sterilization and oxidation processes on the additive blooming observed on the surface of polyurethane. *European Polymer Journal* 2017, 90, 37-53.
45. Gallagher, G.; Padsalgikar, A.; Tkatchouk, E.; Jenney, C.; Iacob, C.; Runt, J., Environmental stress cracking performance of polyether and PDMS-based polyurethanes in an in vitro oxidation model. *Journal of Biomedical Materials Research Part B: Applied Biomaterials* 2017, 105 (6), 1544-1558.
46. Ducom, G.; Laubie, B.; Ohannessian, A.; Chottier, C.; Germain, P.; Chatain, V., Hydrolysis of polydimethylsiloxane fluids in controlled aqueous solutions. *Water Science and Technology* 2013, 68 (4), 813-820.
47. Wu, H.; Dai, T.; Ao, W.; Shao, S.; Li, Z.; Luo, F.; Li, J.; Zhao, D.; Lan, W.; Zhang, H.; Tan, H., The role of segmental mixing on the mechanical properties and oxidative stability of polydimethylsiloxane-based polyetherurethane. *Polymer* 2022, 261, 125401.
48. Tang, L.; Long, X.; He, X.; Ding, M.; Zhao, D.; Luo, F.; Li, J.; Li, Z.; Tan, H.; Zhang, H., Improved in vivo stability of silicon-containing polyurethane by fluorocarbon side chain modulation of the surface structure. *Journal of Materials Chemistry B* 2021, 9 (14), 3210-3223.
49. Kim, S.; Ye, S.-h.; Adamo, A.; Orizondo, R. A.; Jo, J.; Cho, S. K.; Wagner, W. R., A biostable, anti-fouling zwitterionic polyurethane-urea based on PDMS for use in blood-contacting medical devices. *Journal of Materials Chemistry B* 2020, 8 (36), 8305-8314.
50. KEANE, P. F.; BONNER, M. C.; JOHNSTON, S. R.; ZAFAR, A.; GORMAN, S. P., Characterization of biofilm and encrustation on ureteric stents in vivo. *British Journal of Urology* 1994, 73 (6), 687-691.
51. Kram, W.; Buchholz, N.; Hakenberg, O. W., Ureteral stent encrustation. *Pathophysiology. Arch Esp Urol* 2016, 69 (8), 485-493.
52. Scotland, K. B.; Lo, J.; Grgic, T.; Lange, D., Ureteral stent-associated infection and sepsis: pathogenesis and prevention: a review. *Biofouling* 2019, 35 (1), 117-127.

53. Vladkova, T. G.; Staneva, A. D.; Gospodinova, D. N., Surface engineered biomaterials and ureteral stents inhibiting biofilm formation and encrustation. *Surface and Coatings Technology* 2020, 404, 126424.
54. Lange, D.; Bidnur, S.; Hoag, N.; Chew, B. H., Ureteral stent-associated complications—where we are and where we are going. *Nature Reviews Urology* 2015, 12 (1), 17-25.
55. Penna, M. J.; Mijajlovic, M.; Tamerler, C.; Biggs, M. J., Molecular-level understanding of the adsorption mechanism of a graphite-binding peptide at the water/graphite interface. *Soft Matter* 2015, 11 (26), 5192-5203.
56. Zander, Z. K.; Becker, M. L., Antimicrobial and Antifouling Strategies for Polymeric Medical Devices. *ACS Macro Letters* 2018, 7 (1), 16-25.
57. Ostuni, E.; Chapman, R. G.; Holmlin, R. E.; Takayama, S.; Whitesides, G. M., A Survey of Structure–Property Relationships of Surfaces that Resist the Adsorption of Protein. *Langmuir* 2001, 17 (18), 5605-5620.
58. MacKintosh, E. E.; Patel, J. D.; Marchant, R. E.; Anderson, J. M., Effects of biomaterial surface chemistry on the adhesion and biofilm formation of *Staphylococcus epidermidis* in vitro. *Journal of Biomedical Materials Research Part A* 2006, 78A (4), 836-842.
59. TIESZER, C.; REID, G.; DENSTEDT, J., CONDITIONING FILM DEPOSITION ON URETERAL STENTS AFTER IMPLANTATION. *Journal of Urology* 1998, 160 (3 Part 1), 876-881.
60. Zhang, H.; Chiao, M., Anti-fouling Coatings of Poly(dimethylsiloxane) Devices for Biological and Biomedical Applications. *Journal of Medical and Biological Engineering* 2015, 35 (2), 143-155.
61. Laube, N.; Kleinen, L.; Bradenahl, J.; Meissner, A., Diamond-Like Carbon Coatings on Ureteral Stents—A New Strategy for Decreasing the Formation of Crystalline Bacterial Biofilms? *Journal of Urology* 2007, 177 (5), 1923-1927.
62. Kram, W.; Rebl, H.; de la Cruz, J. E.; Haag, A.; Renner, J.; Epting, T.; Springer, A.; Soria, F.; Wienecke, M.; Hakenberg, O. W., Interactive Effects of Copper-Doped Urological Implants with Tissue in the Urinary Tract for the Inhibition of Cell Adhesion and Encrustation in the Animal Model Rat. *Polymers* 2022, 14 (16), 3324.
63. Wang, B.; Jin, T.; Xu, Q.; Liu, H.; Ye, Z.; Chen, H., Direct Loading and Tunable Release of Antibiotics from Polyelectrolyte Multilayers To Reduce Bacterial Adhesion and Biofilm Formation. *Bioconjugate Chemistry* 2016, 27 (5), 1305-1313.

64. Dirk Lange, K. S., *The Role of Bacteria in Urology*. Springer International Publishing, 2019; p 193.
65. Tomer, N.; Garden, E.; Small, A.; Palese, M., Ureteral Stent Encrustation: Epidemiology, Pathophysiology, Management and Current Technology. *Journal of Urology* 2021, 205 (1), 68-77.
66. Grases, F.; Söhnel, O.; Costa-Bauzá, A.; Ramis, M.; Wang, Z., Study on concretions developed around urinary catheters and mechanisms of renal calculi development. *Nephron* 2001, 88 (4), 320-8.
67. Broomfield, R. J.; Morgan, S. D.; Khan, A.; Stickler, D. J., Crystalline bacterial biofilm formation on urinary catheters by urease-producing urinary tract pathogens: a simple method of control. *J Med Microbiol* 2009, 58 (Pt 10), 1367-1375.
68. Jones, D. S.; Bonner, M. C.; Gorman, S. P.; Akay, M.; Keane, P. F., Sequential polyurethane–poly(methylmethacrylate) interpenetrating polymer networks as ureteral biomaterials: mechanical properties and comparative resistance to urinary encrustation. *Journal of Materials Science: Materials in Medicine* 1997, 8 (11), 713-717.
69. McBane, J. E.; Santerre, J. P.; Labow, R. S., The interaction between hydrolytic and oxidative pathways in macrophage-mediated polyurethane degradation. *Journal of Biomedical Materials Research Part A* 2007, 82A (4), 984-994.
70. Barghouthy, Y.; Wiseman, O.; Ventimiglia, E.; Letendre, J.; Cloutier, J.; Daudon, M.; Kleinclauss, F.; Doizi, S.; Corrales, M.; Traxer, O., Silicone-hydrocoated ureteral stents encrustation and biofilm formation after 3-week dwell time: results of a prospective randomized multicenter clinical study. *World J Urol* 2021, 39 (9), 3623-3629.
71. Mathias, S.; Wiseman, O., Silicone vs. Polyurethane Stent: The Final Countdown. *J Clin Med* 2022, 11 (10).
72. Gadzhiev, N.; Gorelov, D.; Malkhasyan, V.; Akopyan, G.; Harchelava, R.; Mazurenko, D.; Kosmala, C.; Okhunov, Z.; Petrov, S., Comparison of silicone versus polyurethane ureteral stents: a prospective controlled study. *BMC Urology* 2020, 20 (1), 10.
73. Chaffin, K. A.; Chen, X.; McNamara, L.; Bates, F. S.; Hillmyer, M. A., Polyether Urethane Hydrolytic Stability after Exposure to Deoxygenated Water. *Macromolecules* 2014, 47 (15), 5220-5226.
74. Takahara, A.; Hergenrother, R. W.; Coury, A. J.; Cooper, S. L., Effect of soft segment chemistry on the biostability of segmented polyurethanes. II. In vitro hydrolytic degradation and lipod sorption. *Journal of Biomedical Materials Research* 1992, 26 (6), 801-818.

75. Sheikh, Z.; Brooks, P. J.; Barzilay, O.; Fine, N.; Glogauer, M., Macrophages, Foreign Body Giant Cells and Their Response to Implantable Biomaterials. *Materials* 2015, 8 (9), 5671-5701.
76. Stefanović, I. S.; Špírková, M.; Poręba, R.; Steinhart, M.; Ostojić, S.; Tešević, V.; Pergal, M. V., Study of the Properties of Urethane–Siloxane Copolymers Based on Poly(propylene oxide)-b-poly(dimethylsiloxane)-b-poly(propylene oxide) Soft Segments. *Industrial & Engineering Chemistry Research* 2016, 55 (14), 3960-3973.
77. Jayabalan, M.; Shunmuga Kumar, N.; Rathinam, K.; Kumari, T. V., In vivo biocompatibility of an aliphatic crosslinked polyurethane in rabbit. *Journal of Biomedical Materials Research* 1991, 25 (12), 1431-1442.
78. Ward, R.; Anderson, J.; McVenes, R.; Stokes, K., In vivo biostability of polysiloxane polyether polyurethanes: Resistance to biologic oxidation and stress cracking. *Journal of Biomedical Materials Research Part A* 2006, 77A (3), 580-589.

Chapter 3

1. H. M. C. C. Somarathna, S. N. Raman, D. Mohotti, A. A. Mutalib and K. H. Badri, *Construction and Building Materials*, 2018, 190, 995-1014.
2. N. V. Gama, A. Ferreira and A. Barros-Timmons, *Materials*, 2018, 11, 1841.
3. P. Singhal, W. Small, E. Cosgriff-Hernandez, D. J. Maitland and T. S. Wilson, *Acta Biomaterialia*, 2014, 10, 67-76.
4. F.-L. Jin, M. Zhao, M. Park and S.-J. Park, *Polymers*, 2019, 11, 953.
5. J.-W. Wu, W.-F. Sung and H.-S. Chu, *International Journal of Heat and Mass Transfer*, 1999, 42, 2211-2217.
6. H. Zhang, W.-Z. Fang, Y.-M. Li and W.-Q. Tao, *Applied Thermal Engineering*, 2017, 115, 528-538.
7. F. M. Casati, R. M. Herrington, R. Broos and Y. Miyazaki, *Journal of Cellular Plastics*, 1998, 34, 430-466.
8. T. Khan, V. Acar, M. R. Aydin, B. Hülagü, H. Akbulut and M. Ö. Seydibeyoğlu, *Polymer Composites*, 2020, 41, 2355-2400.

9. G. F. Smits, *Journal of Thermal Insulation and Building Envelopes*, 1994, 17, 309-329.
10. M. Thirumal, D. Khastgir, N. K. Singha, B. S. Manjunath and Y. P. Naik, *Journal of Applied Polymer Science*, 2008, 108, 1810-1817.
11. M. Thirumal, N. K. Singha, D. Khastgir, B. S. Manjunath and Y. P. Naik, *Journal of Applied Polymer Science*, 2010, 116, 2260-2268.
12. R. Hansen, *Journal of Polymer Science Part A: Polymer Chemistry*, 1993, 31, 1344-1344.
13. J. P. Sheth, S. Unal, E. Yilgor, I. Yilgor, F. L. Beyer, T. E. Long and G. L. Wilkes, *Polymer*, 2005, 46, 10180-10190.
14. I. Yilgör, E. Yilgör and G. L. Wilkes, *Polymer*, 2015, 58, A1-A36.
15. A. Aneja and G. L. Wilkes, *Polymer*, 2003, 44, 7221-7228.
16. E. Burgaz, *Polyurethane Insulation Foams for Energy and Sustainability*, Springer Cham, 2019.
17. E. Delebecq, J.-P. Pascault, B. Boutevin and F. Ganachaud, *Chemical Reviews*, 2013, 113, 80-118.
18. V. S. Daniel Klempner, *Handbook of Polymeric Foams and Foam Technology* Hanser Gardner Publications Inc. , Cincinnati, Ohio, 2nd edn., 2004.
19. H. Khatoon, S. Iqbal, M. Irfan, A. Darda and N. K. Rawat, *Progress in Organic Coatings*, 2021, 154, 106124.
20. J. W. McAuley, *Environmental Science & Technology*, 2003, 37, 5414-5416.
21. A. T. Mayyas, A. Qattawi, A. R. Mayyas and M. Omar, *Journal of Cleaner Production*, 2013, 40, 177-189.
22. M. Fadzil, A. B. Abdullah, Z. Samad, F. Yusof and Y. H. P. Manurung, in *Design for Sustainability*, eds. S. M. Sapuan and M. R. Mansor, Elsevier, 2021, DOI: <https://doi.org/10.1016/B978-0-12-819482-9.00006-X>, pp. 435-463.
23. H. Blattmann, M. Fleischer, M. Bähr and R. Mülhaupt, *Macromolecular Rapid Communications*, 2014, 35, 1238-1254.
24. E. K. Leitsch, G. Beniah, K. Liu, T. Lan, W. H. Heath, K. A. Scheidt and J. M. Torkelson, *ACS Macro Letters*, 2016, 5, 424-429.

25. Y.-J. Yu, K. Hearon, T. S. Wilson and D. J. Maitland, *Smart Materials and Structures*, 2011, 20, 085010.
26. H. Blattmann, M. Lauth and R. Mülhaupt, *Macromolecular Materials and Engineering*, 2016, 301, 944-952.
27. F. Monie, B. Grignard, J.-M. Thomassin, R. Mereau, T. Tassaing, C. Jerome and C. Detrembleur, *Angewandte Chemie International Edition*, 2020, 59, 17033-17041.
28. J. D. Wolfgang, B. T. White and T. E. Long, *Macromolecular Rapid Communications*, 2021, 42, 2100163.
29. E. B. Anderson and T. E. Long, *Polymer*, 2010, 51, 2447-2454.
30. R. Gao, M. Zhang, S.-W. Wang, R. B. Moore, R. H. Colby and T. E. Long, *Macromolecular Chemistry and Physics*, 2013, 214, 1027-1036.
31. K. Zhang, A. M. Nelson, S. J. Talley, M. Chen, E. Margareta, A. G. Hudson, R. B. Moore and T. E. Long, *Green Chemistry*, 2016, 18, 4667-4681.
32. J. M. Dennis, L. I. Steinberg, A. M. Pekkanen, J. Maiz, M. Hegde, A. J. Müller and T. E. Long, *Green Chemistry*, 2018, 20, 243-249.
33. R. A. Sheldon, *Chemical Society Reviews*, 2012, 41, 1437-1451.
34. M. Ravey and E. M. Pearce, *Journal of Applied Polymer Science*, 1997, 63, 47-74.
35. N. Yoshitake and M. Furukawa, *Journal of Analytical and Applied Pyrolysis*, 1995, 33, 269-281.
36. J. O. Akindoyo, M. D. H. Beg, S. Ghazali, M. R. Islam, N. Jeyaratnam and A. R. Yuvaraj, *RSC Advances*, 2016, 6, 114453-114482.
37. F. A. Milton, M. G. Lacerda, S. B. P. Sinoti, P. G. Mesquita, D. Prakasan, M. S. Coelho, C. L. de Lima, A. G. Martini, G. T. Pazzine, M. d. F. Borin, A. A. Amato and F. d. A. R. Neves, *Frontiers in Pharmacology*, 2017, 8.
38. S. Zhang, L. Wang, Z. Wang, D. Fan, L. Shi and J. Liu, *Chemosphere*, 2017, 171, 142-148.
39. A. Farkas and P. F. Strohm, *Industrial & Engineering Chemistry Fundamentals*, 1965, 4, 32-38.
40. H. Sardon, A. Pascual, D. Mecerreyes, D. Taton, H. Cramail and J. L. Hedrick, *Macromolecules*, 2015, 48, 3153-3165.

41. X. D. Zhang, C. W. Macosko, H. T. Davis, A. D. Nikolov and D. T. Wasan, *Journal of Colloid and Interface Science*, 1999, 215, 270-279.

Chapter 4

1. Somarathna, H. M. C. C.; Raman, S. N.; Mohotti, D.; Mutalib, A. A.; Badri, K. H., The use of polyurethane for structural and infrastructural engineering applications: A state-of-the-art review. *Construction and Building Materials* 2018, 190, 995-1014.
2. Akindoyo, J. O.; Beg, M. D. H.; Ghazali, S.; Islam, M. R.; Jeyaratnam, N.; Yuvaraj, A. R., Polyurethane types, synthesis and applications – a review. *RSC Advances* 2016, 6 (115), 114453-114482.
3. Gama, N. V.; Ferreira, A.; Barros-Timmons, A., Polyurethane Foams: Past, Present, and Future. *Materials* 2018, 11 (10), 1841.
4. Szycher, M., *Szycher's Handbook of Polyurethanes*, First Edition. Taylor & Francis: 1999.
5. Delebecq, E.; Pascault, J.-P.; Boutevin, B.; Ganachaud, F., On the Versatility of Urethane/Urea Bonds: Reversibility, Blocked Isocyanate, and Non-isocyanate Polyurethane. *Chemical Reviews* 2013, 113 (1), 80-118.
6. Yilgör, I.; Yilgör, E.; Wilkes, G. L., Critical parameters in designing segmented polyurethanes and their effect on morphology and properties: A comprehensive review. *Polymer* 2015, 58, A1-A36.
7. Kwei, T. K., Phase separation in segmented polyurethanes. *Journal of Applied Polymer Science* 1982, 27 (8), 2891-2899.
8. Miller, J. A.; Lin, S. B.; Hwang, K. K. S.; Wu, K. S.; Gibson, P. E.; Cooper, S. L., Properties of polyether-polyurethane block copolymers: effects of hard segment length distribution. *Macromolecules* 1985, 18 (1), 32-44.
9. O'Sickey, M. J.; Lawrey, B. D.; Wilkes, G. L., Structure–property relationships of poly(urethane-urea)s with ultralow monol content poly(propylene glycol) soft segments. III. influence of mixed soft segments of ultralow monol poly(propylene glycol), poly(tetramethylene ether glycol), and tri(propylene glycol). *Journal of Applied Polymer Science* 2003, 89 (13), 3520-3529.
10. Pourmohammadi-Mahunaki, M.; Haddadi-Asl, V.; Roghani-Mamaqani, H.; Koosha, M.; Yazdi, M., Effect of chain extender length and molecular architecture on

phase separation and rheological properties of ether-based polyurethanes. *Polymer Bulletin* 2022, 79 (10), 8653-8668.

11. Stribeck, A.; Pöselt, E.; Eling, B.; Jokari-Sheshdeh, F.; Hoell, A., Thermoplastic Polyurethanes with varying hard-segment components. Mechanical performance and a filler-crosslink conversion of hard domains as monitored by SAXS. *European Polymer Journal* 2017, 94.

12. Aneja, A.; Wilkes, G. L., A systematic series of 'model' PTMO based segmented polyurethanes reinvestigated using atomic force microscopy. *Polymer* 2003, 44 (23), 7221-7228.

13. Blackwell, J.; Nagarajan, M. R.; Hoitink, T. B., Structure of polyurethane elastomers: effect of chain extender length on the structure of MDI/diol hard segments. *Polymer* 1982, 23 (7), 950-956.

14. Abouzahr, S.; Wilkes, G. L.; Ophir, Z., Structure-property behaviour of segmented polyether-MDI-butanediol based urethanes: effect of composition ratio. *Polymer* 1982, 23 (7), 1077-1086.

15. Sheth, J. P.; Aneja, A.; Wilkes, G. L.; Yilgor, E.; Atilla, G. E.; Yilgor, I.; Beyer, F. L., Influence of system variables on the morphological and dynamic mechanical behavior of polydimethylsiloxane based segmented polyurethane and polyurea copolymers: a comparative perspective. *Polymer* 2004, 45 (20), 6919-6932.

16. Gissselfält, K.; Helgee, B., Effect of Soft Segment Length and Chain Extender Structure on Phase Separation and Morphology in Poly(urethane urea)s. *Macromolecular Materials and Engineering* 2003, 288 (3), 265-271.

17. Zapp, J. A., Jr., Hazards of Isocyanates in Polyurethane Foam Plastic Production. *Arch. Indust. Health* 1957, 15 (4), 324-30.

18. Liu, G.; Wu, G.; Huo, S.; Jin, C.; Kong, Z., Synthesis and properties of non-isocyanate polyurethane coatings derived from cyclic carbonate-functionalized polysiloxanes. *Progress in Organic Coatings* 2017, 112, 169-175.

19. Zhang, K.; Nelson, A. M.; Talley, S. J.; Chen, M.; Margareta, E.; Hudson, A. G.; Moore, R. B.; Long, T. E., Non-isocyanate poly(amide-hydroxyurethane)s from sustainable resources. *Green Chemistry* 2016, 18 (17), 4667-4681.

20. Gomez-Lopez, A.; Elizalde, F.; Calvo, I.; Sardon, H., Trends in non-isocyanate polyurethane (NIPU) development. *Chemical Communications* 2021, 57 (92), 12254-12265.

21. Tomita, H.; Sanda, F.; Endo, T., Model reaction for the synthesis of polyhydroxyurethanes from cyclic carbonates with amines: Substituent effect on the

reactivity and selectivity of ring-opening direction in the reaction of five-membered cyclic carbonates with amine. *Journal of Polymer Science Part A: Polymer Chemistry* 2001, 39 (21), 3678-3685.

22. Blattmann, H.; Fleischer, M.; Bähr, M.; Mülhaupt, R., Isocyanate- and Phosgene-Free Routes to Polyfunctional Cyclic Carbonates and Green Polyurethanes by Fixation of Carbon Dioxide. *Macromolecular Rapid Communications* 2014, 35 (14), 1238-1254.

23. Leitsch, E. K.; Beniah, G.; Liu, K.; Lan, T.; Heath, W. H.; Scheidt, K. A.; Torkelson, J. M., Nonisocyanate Thermoplastic Polyhydroxyurethane Elastomers via Cyclic Carbonate Aminolysis: Critical Role of Hydroxyl Groups in Controlling Nanophase Separation. *ACS Macro Letters* 2016, 5 (4), 424-429.

24. Besse, V.; Camara, F.; Méchin, F.; Fleury, E.; Caillol, S.; Pascault, J.-P.; Boutevin, B., How to explain low molar masses in PolyHydroxyUrethanes (PHUs). *European Polymer Journal* 2015, 71, 1-11.

25. Kotanen, S.; Poikelispää, M.; Efimov, A.; Harjunalanen, T.; Mills, C.; Laaksonen, T.; Sarlin, E., Hydrolytic stability of polyurethane/polyhydroxyurethane hybrid adhesives. *International Journal of Adhesion and Adhesives* 2021, 110, 102950.

26. Frias, C. F.; Fonseca, A. C.; Coelho, J. F. J.; Serra, A. C., Crosslinked poly(hydroxyurethane) films from biobased carbonates: Structure-properties relationships and the influence of moisture in the mechanical properties. *Progress in Organic Coatings* 2024, 187, 108100.

27. Beniah, G.; Liu, K.; Heath, W. H.; Miller, M. D.; Scheidt, K. A.; Torkelson, J. M., Novel thermoplastic polyhydroxyurethane elastomers as effective damping materials over broad temperature ranges. *European Polymer Journal* 2016, 84, 770-783.

28. Bossion, A.; Aguirresarobe, R. H.; Irusta, L.; Taton, D.; Cramail, H.; Grau, E.; Mecerreyes, D.; Su, C.; Liu, G.; Müller, A. J.; Sardon, H., Unexpected Synthesis of Segmented Poly(hydroxyurea-urethane)s from Dicyclic Carbonates and Diamines by Organocatalysis. *Macromolecules* 2018, 51 (15), 5556-5566.

29. Hu, S.; Chen, X.; Torkelson, J. M., Isocyanate-free, thermoplastic polyhydroxyurethane elastomers designed for cold temperatures: Influence of PDMS soft-segment chain length and hard-segment content. *Polymer* 2022, 256, 125251.

30. Beniah, G.; Fortman, D. J.; Heath, W. H.; Dichtel, W. R.; Torkelson, J. M., Non-Isocyanate Polyurethane Thermoplastic Elastomer: Amide-Based Chain Extender Yields Enhanced Nanophase Separation and Properties in Polyhydroxyurethane. *Macromolecules* 2017, 50 (11), 4425-4434.

31. Wolfgang, J. D.; White, B. T.; Long, T. E., Non-isocyanate Polyurethanes from 1,1'-Carbonyldiimidazole: A Polycondensation Approach. *Macromolecular Rapid Communications* 2021, 42 (13), 2100163.
32. Sintas, J. I.; Wolfgang, J. D.; Long, T. E., Carbamate thermal decarboxylation for the design of non-isocyanate polyurethane foams. *Polymer Chemistry* 2023.
33. Li, Y.; Gao, T.; Chu, B., Synchrotron SAXS studies of the phase-separation kinetics in a segmented polyurethane. *Macromolecules* 1992, 25 (6), 1737-1742.
34. Cheng, B.-X.; Gao, W.-C.; Ren, X.-M.; Ouyang, X.-Y.; Zhao, Y.; Zhao, H.; Wu, W.; Huang, C.-X.; Liu, Y.; Liu, X.-Y.; Li, H.-N.; Li, R. K. Y., A review of microphase separation of polyurethane: Characterization and applications. *Polymer Testing* 2022, 107, 107489.
35. Sheth, J. P.; Wilkes, G. L.; Fornof, A. R.; Long, T. E.; Yilgor, I., Probing the Hard Segment Phase Connectivity and Percolation in Model Segmented Poly(urethane urea) Copolymers. *Macromolecules* 2005, 38 (13), 5681-5685.

Chapter 5

1. Wilkes, J. S., A short history of ionic liquids—from molten salts to neoteric solvents. *Green Chemistry* 2002, 4 (2), 73-80.
2. Chen, M.; White, B. T.; Kasprzak, C. R.; Long, T. E., Advances in phosphonium-based ionic liquids and poly(ionic liquid)s as conductive materials. *European Polymer Journal* 2018, 108, 28-37.
3. Kunz, W.; Häckl, K., The hype with ionic liquids as solvents. *Chemical Physics Letters* 2016, 661, 6-12.
4. Noorhisham, N. A.; Amri, D.; Mohamed, A. H.; Yahaya, N.; Ahmad, N. M.; Mohamad, S.; Kamaruzaman, S.; Osman, H., Characterisation techniques for analysis of imidazolium-based ionic liquids and application in polymer preparation: A review. *Journal of Molecular Liquids* 2021, 326, 115340.
5. Green, M. D.; Long, T. E., Designing Imidazole-Based Ionic Liquids and Ionic Liquid Monomers for Emerging Technologies. *Polymer Reviews* 2009, 49 (4), 291-314.
6. Earle, M. J.; Seddon, K. R., Ionic liquids. Green solvents for the future. *Pure and Applied Chemistry* 2000, 72 (7), 1391-1398.

7. Chiappe, C.; Pomelli, C. S., Point-Functionalization of Ionic Liquids: An Overview of Synthesis and Applications. *European Journal of Organic Chemistry* 2014, 2014 (28), 6120-6139.
8. Fraser, K. J.; MacFarlane, D. R., Phosphonium-Based Ionic Liquids: An Overview. *Australian Journal of Chemistry* 2009, 62 (4), 309-321.
9. Ueno, K.; Tokuda, H.; Watanabe, M., Ionicity in ionic liquids: correlation with ionic structure and physicochemical properties. *Physical Chemistry Chemical Physics* 2010, 12 (8), 1649-1658.
10. Fonseca, G. S.; Umpierre, A. P.; Fichtner, P. F. P.; Teixeira, S. R.; Dupont, J., The Use of Imidazolium Ionic Liquids for the Formation and Stabilization of Ir⁰ and Rh⁰ Nanoparticles: Efficient Catalysts for the Hydrogenation of Arenes. *Chemistry – A European Journal* 2003, 9 (14), 3263-3269.
11. Migowski, P.; Dupont, J., Catalytic Applications of Metal Nanoparticles in Imidazolium Ionic Liquids. *Chemistry – A European Journal* 2007, 13 (1), 32-39.
12. Baranyai, K. J.; Deacon, G. B.; MacFarlane, D. R.; Pringle, J. M.; Scott, J. L., Thermal Degradation of Ionic Liquids at Elevated Temperatures. *Australian Journal of Chemistry* 2004, 57 (2), 145-147.
13. Bakis, E.; van den Bruinhorst, A.; Pison, L.; Palazzo, I.; Chang, T.; Kjellberg, M.; Weber, C. C.; Costa Gomes, M.; Welton, T., Mixing divalent ionic liquids: effects of charge and side-chains. *Physical Chemistry Chemical Physics* 2021, 23 (8), 4624-4635.
14. Avila, J.; Lepre, L. F.; Goloviznina, K.; Guazzelli, L.; Pomelli, C. S.; Chiappe, C.; Pádua, A.; Costa Gomes, M., Improved carbon dioxide absorption in double-charged ionic liquids. *Physical Chemistry Chemical Physics* 2021, 23 (40), 23130-23140.
15. Wolfgang, J. D.; White, B. T.; Long, T. E., Non-isocyanate Polyurethanes from 1,1'-Carbonyldiimidazole: A Polycondensation Approach. *Macromolecular Rapid Communications* 2021, 42 (13), 2100163.
16. Sintas, J. I.; Wolfgang, J. D.; Long, T. E., Carbamate thermal decarboxylation for the design of non-isocyanate polyurethane foams. *Polymer Chemistry* 2023.
17. Olsson, J. V.; Hult, D.; García-Gallego, S.; Malkoch, M., Fluoride-promoted carbonylation polymerization: a facile step-growth technique to polycarbonates. *Chemical Science* 2017, 8 (7), 4853-4857.
18. Houlihan, F. M.; Bouchard, F.; Frechet, J. M. J.; Willson, C. G., Thermally depolymerizable polycarbonates. 2. Synthesis of novel linear tertiary copolycarbonates by phase-transfer catalysis. *Macromolecules* 1986, 19 (1), 13-19.

19. Wolfgang, J. D.; White, B. T.; Long, T. E., Non-Isocyanate Polyurethanes from 1,1'-Carbonyldiimidazole: An Activated Carbamate Approach. Submitted for Publication 2021.
20. Schönhals, A.; Kremer, F., Analysis of Dielectric Spectra. In *Broadband Dielectric Spectroscopy*, Kremer, F.; Schönhals, A., Eds. Springer Berlin Heidelberg: Berlin, Heidelberg, 2003; pp 59-98.
21. Sintas, J. I.; Wolfgang, J. D.; Long, T. E., Carbamate thermal decarboxylation for the design of non-isocyanate polyurethane foams. *Polymer Chemistry* 2023, 14 (13), 1497-1506.
22. Introduction to Vibrational Spectroscopy. In *Fourier Transform Infrared Spectrometry*, 2007; pp 1-18.
23. Delebecq, E.; Pascault, J.-P.; Boutevin, B.; Ganachaud, F., On the Versatility of Urethane/Urea Bonds: Reversibility, Blocked Isocyanate, and Non-isocyanate Polyurethane. *Chemical Reviews* 2013, 113 (1), 80-118.
24. Cao, Y.; Mu, T., Comprehensive Investigation on the Thermal Stability of 66 Ionic Liquids by Thermogravimetric Analysis. *Industrial & Engineering Chemistry Research* 2014, 53 (20), 8651-8664.
25. Haddad, B.; Kiefer, J.; Brahim, H.; Belarbi, E.-h.; Villemin, D.; Bresson, S.; Abbas, O.; Rahmouni, M.; Paolone, A.; Palumbo, O., Effects of C(2) Methylation on Thermal Behavior and Interionic Interactions in Imidazolium-Based Ionic Liquids with Highly Symmetric Anions. *Applied Sciences* 2018, 8 (7), 1043.
26. Tokuda, H.; Ishii, K.; Susan, M. A. B. H.; Tsuzuki, S.; Hayamizu, K.; Watanabe, M., Physicochemical Properties and Structures of Room-Temperature Ionic Liquids. 3. Variation of Cationic Structures. *The Journal of Physical Chemistry B* 2006, 110 (6), 2833-2839.
27. Pitawala, J.; Matic, A.; Martinelli, A.; Jacobsson, P.; Koch, V.; Croce, F., Thermal Properties and Ionic Conductivity of Imidazolium Bis(trifluoromethanesulfonyl)imide Dicationic Ionic Liquids. *The Journal of Physical Chemistry B* 2009, 113 (31), 10607-10610.
28. Ikeda, M.; Aniya, M., Understanding the Vogel–Fulcher–Tammann law in terms of the bond strength–coordination number fluctuation model. *Journal of Non-Crystalline Solids* 2013, 371-372, 53-57.
29. Moosavi, M.; Khashei, F.; Sharifi, A.; Mirzaei, M., Transport Properties of Short Alkyl Chain Length Dicationic Ionic Liquids—The Effects of Alkyl Chain Length and Temperature. *Industrial & Engineering Chemistry Research* 2016, 55 (33), 9087-9099.

30. Huang, M.-M.; Jiang, Y.; Sasisanker, P.; Driver, G. W.; Weingärtner, H., Static Relative Dielectric Permittivities of Ionic Liquids at 25 °C. *Journal of Chemical & Engineering Data* 2011, 56 (4), 1494-1499.
31. Lee, M.; Choi, U. H.; Salas-de la Cruz, D.; Mittal, A.; Winey, K. I.; Colby, R. H.; Gibson, H. W., Imidazolium polyesters: structure–property relationships in thermal behavior, ionic conductivity, and morphology. *Advanced Functional Materials* 2011, 21 (4), 708-717.

Chapter 6

1. Gama, N. V.; Ferreira, A.; Barros-Timmons, A., Polyurethane Foams: Past, Present, and Future. *Materials* 2018, 11 (10), 1841.
2. Somarathna, H. M. C. C.; Raman, S. N.; Mohotti, D.; Mutalib, A. A.; Badri, K. H., The use of polyurethane for structural and infrastructural engineering applications: A state-of-the-art review. *Construction and Building Materials* 2018, 190, 995-1014.
3. Singhal, P.; Small, W.; Cosgriff-Hernandez, E.; Maitland, D. J.; Wilson, T. S., Low density biodegradable shape memory polyurethane foams for embolic biomedical applications. *Acta Biomaterialia* 2014, 10 (1), 67-76.
4. Jin, F.-L.; Zhao, M.; Park, M.; Park, S.-J., Recent Trends of Foaming in Polymer Processing: A Review. *Polymers* 2019, 11 (6), 953.
5. Wu, J.-W.; Sung, W.-F.; Chu, H.-S., Thermal conductivity of polyurethane foams. *International Journal of Heat and Mass Transfer* 1999, 42 (12), 2211-2217.
6. Zhang, H.; Fang, W.-Z.; Li, Y.-M.; Tao, W.-Q., Experimental study of the thermal conductivity of polyurethane foams. *Applied Thermal Engineering* 2017, 115, 528-538.
7. Casati, F. M.; Herrington, R. M.; Broos, R.; Miyazaki, Y., Tailoring the Performance of Molded Flexible Polyurethane Foams for Car Seats. *Journal of Cellular Plastics* 1998, 34 (5), 430-466.
8. Khan, T.; Acar, V.; Aydin, M. R.; Hülägü, B.; Akbulut, H.; Seydibeyoğlu, M. Ö., A review on recent advances in sandwich structures based on polyurethane foam cores. *Polymer Composites* 2020, 41 (6), 2355-2400.
9. Delebecq, E.; Pascault, J.-P.; Boutevin, B.; Ganachaud, F., On the Versatility of Urethane/Urea Bonds: Reversibility, Blocked Isocyanate, and Non-isocyanate Polyurethane. *Chemical Reviews* 2013, 113 (1), 80-118.

10. Yilgör, I.; Yilgör, E.; Wilkes, G. L., Critical parameters in designing segmented polyurethanes and their effect on morphology and properties: A comprehensive review. *Polymer* 2015, 58, A1-A36.
11. Smits, G. F., Effect of Cellsize Reduction on Polyurethane Foam Physical Properties. *Journal of Thermal Insulation and Building Envelopes* 1994, 17 (4), 309-329.
12. Janik, H.; Marzec, M., A review: Fabrication of porous polyurethane scaffolds. *Materials Science and Engineering: C* 2015, 48, 586-591.
13. Blackwell, J.; Nagarajan, M. R.; Hoitink, T. B., Structure of polyurethane elastomers: effect of chain extender length on the structure of MDI/diol hard segments. *Polymer* 1982, 23 (7), 950-956.
14. Kwei, T. K., Phase separation in segmented polyurethanes. *Journal of Applied Polymer Science* 1982, 27 (8), 2891-2899.
15. Chu, B.; Gao, T.; Li, Y.; Wang, J.; Desper, C. R.; Byrne, C. A., Microphase separation kinetics in segmented polyurethanes: effects of soft segment length and structure. *Macromolecules* 1992, 25 (21), 5724-5729.
16. Marciano, J. H.; Rojas, A. J.; Williams, R. J. J., Curing kinetics of a rigid polyurethane foam formulation. *Polymer* 1982, 23 (10), 1489-1492.
17. Hansen, R., Handbook of polymeric foams and foam technology, Daniel Klempner and Kurt C. Frisch, eds., Hanser Publishers, Munich, Germany, 1992, 442 pp. price: \$148.00. (Distributed in the U.S. and Canada by Oxford University Press, New York.). *Journal of Polymer Science Part A: Polymer Chemistry* 1993, 31 (5), 1344-1344.
18. Javni, I.; Zhang, W.; Petrović, Z. S., Effect of different isocyanates on the properties of soy-based polyurethanes. *Journal of Applied Polymer Science* 2003, 88 (13), 2912-2916.
19. Lefebvre, J.; Bastin, B.; Le Bras, M.; Duquesne, S.; Paleja, R.; Delobel, R., Thermal stability and fire properties of conventional flexible polyurethane foam formulations. *Polymer Degradation and Stability* 2005, 88 (1), 28-34.
20. Thirumal, M.; Singha, N. K.; Khastgir, D.; Manjunath, B. S.; Naik, Y. P., Halogen-free flame-retardant rigid polyurethane foams: Effect of alumina trihydrate and triphenylphosphate on the properties of polyurethane foams. *Journal of Applied Polymer Science* 2010, 116 (4), 2260-2268.
21. Coste, G.; Negrell, C.; Caillol, S., From gas release to foam synthesis, the second breath of blowing agents. *European Polymer Journal* 2020, 140, 110029.

22. Sienkiewicz, N., Improvements of Polyurethane (PU) Foam's Antibacterial Properties and Bio-resistance. In *Thermal Insulation and Radiation Control Technologies for Buildings*, Kośny, J.; Yarbrough, D. W., Eds. Springer International Publishing: Cham, 2022; pp 217-240.
23. Oliviero, M.; Stanzione, M.; D'Auria, M.; Sorrentino, L.; Iannace, S.; Verdolotti, L., Vegetable Tannin as a Sustainable UV Stabilizer for Polyurethane Foams. *Polymers* 2019, 11 (3), 480.
24. Choe, K. H.; Lee, D. S.; Seo, W. J.; Kim, W. N., Properties of Rigid Polyurethane Foams with Blowing Agents and Catalysts. *Polymer Journal* 2004, 36 (5), 368-373.
25. Zapp, J. A., Jr., Hazards of Isocyanates in Polyurethane Foam Plastic Production. *Arch. Indust. Health* 1957, 15 (4), 324-30.
26. Cornille, A.; Dworakowska, S.; Bogdal, D.; Boutevin, B.; Caillol, S., A new way of creating cellular polyurethane materials: NIPU foams. *European Polymer Journal* 2015, 66, 129-138.
27. Zhang, K.; Nelson, A. M.; Talley, S. J.; Chen, M.; Margareta, E.; Hudson, A. G.; Moore, R. B.; Long, T. E., Non-isocyanate poly(amide-hydroxyurethane)s from sustainable resources. *Green Chemistry* 2016, 18 (17), 4667-4681.
28. Gomez-Lopez, A.; Elizalde, F.; Calvo, I.; Sardon, H., Trends in non-isocyanate polyurethane (NIPU) development. *Chemical Communications* 2021, 57 (92), 12254-12265.
29. Khatoon, H.; Iqbal, S.; Irfan, M.; Darda, A.; Rawat, N. K., A review on the production, properties and applications of non-isocyanate polyurethane: A greener perspective. *Progress in Organic Coatings* 2021, 154, 106124.
30. Besse, V.; Camara, F.; Méchin, F.; Fleury, E.; Caillol, S.; Pascault, J.-P.; Boutevin, B., How to explain low molar masses in PolyHydroxyUrethanes (PHUs). *European Polymer Journal* 2015, 71, 1-11.
31. Tomita, H.; Sanda, F.; Endo, T., Model reaction for the synthesis of polyhydroxyurethanes from cyclic carbonates with amines: Substituent effect on the reactivity and selectivity of ring-opening direction in the reaction of five-membered cyclic carbonates with amine. *Journal of Polymer Science Part A: Polymer Chemistry* 2001, 39 (21), 3678-3685.
32. Bossion, A.; Aguirresarobe, R. H.; Irusta, L.; Taton, D.; Cramail, H.; Grau, E.; Mecerreyes, D.; Su, C.; Liu, G.; Müller, A. J.; Sardon, H., Unexpected Synthesis of

Segmented Poly(hydroxyurea–urethane)s from Dicyclic Carbonates and Diamines by Organocatalysis. *Macromolecules* 2018, 51 (15), 5556-5566.

33. Leitsch, E. K.; Beniah, G.; Liu, K.; Lan, T.; Heath, W. H.; Scheidt, K. A.; Torkelson, J. M., Nonisocyanate Thermoplastic Polyhydroxyurethane Elastomers via Cyclic Carbonate Aminolysis: Critical Role of Hydroxyl Groups in Controlling Nanophase Separation. *ACS Macro Letters* 2016, 5 (4), 424-429.

34. Kotanen, S.; Poikelispää, M.; Efimov, A.; Harjunalanen, T.; Mills, C.; Laaksonen, T.; Sarlin, E., Hydrolytic stability of polyurethane/polyhydroxyurethane hybrid adhesives. *International Journal of Adhesion and Adhesives* 2021, 110, 102950.

35. Yu, Y.-J.; Hearon, K.; Wilson, T. S.; Maitland, D. J., The effect of moisture absorption on the physical properties of polyurethane shape memory polymer foams. *Smart Materials and Structures* 2011, 20 (8), 085010.

36. Sintas, J. I.; Wolfgang, J. D.; Long, T. E., Carbamate thermal decarboxylation for the design of non-isocyanate polyurethane foams. *Polymer Chemistry* 2023, 14 (13), 1497-1506.

37. Wolfgang, J. D.; White, B. T.; Long, T. E., Non-isocyanate Polyurethanes from 1,1'-Carbonyldiimidazole: A Polycondensation Approach. *Macromolecular Rapid Communications* 2021, 42 (13), 2100163.

38. Sintas, J. I.; Wolfgang, J. D.; Long, T. E., Carbamate thermal decarboxylation for the design of non-isocyanate polyurethane foams. *Polymer Chemistry* 2023.

39. Mather, B. D.; Viswanathan, K.; Miller, K. M.; Long, T. E., Michael addition reactions in macromolecular design for emerging technologies. *Progress in Polymer Science* 2006, 31 (5), 487-531.

40. Brown, I. M.; Sandreczki, T. C., Cross-linking reactions in maleimide and bis(maleimide) polymers. An ESR study. *Macromolecules* 1990, 23 (1), 94-100.

41. Daily, C.; Torres, S. M.; Robison, T. W.; Bowler, N., Dielectric and kinetic comparison of APO-BMI grades. *High Performance Polymers* 2018, 30 (9), 1101-1113.

Chapter 7

1. Bai, Y.; Li, K.; Huang, S.; Li, J.; Liu, Q.; Li, Z.; Wang, X.; Zhang, G.; Sun, R. In A Novel Process to Reduce the Warpage of Bond Pair for Temporary Bonding and De-bonding Technique, 2022 23rd International Conference on Electronic Packaging Technology (ICEPT), 10-13 Aug. 2022; 2022; pp 1-4.
2. Xu, D.; Wang, H. W.; Patel, J.; Brun, X. F.; Hirota, K.; Capsuto, E.; Kato, H.; Sugo, M. In A Novel Design of Temporary Bond Debond Adhesive Technology for Wafer-Level Assembly, 2020 IEEE 70th Electronic Components and Technology Conference (ECTC), 3-30 June 2020; 2020; pp 68-74.
3. Haq, J.; Vogt, B. D.; Howard, E.; Loy, D., Temporary bond—debond technology for high-performance transistors on flexible substrates. *Journal of the Society for Information Display* 2010, 18 (11), 884-891.
4. Mo, Z.; Wang, F.; Li, J.; Liu, Q.; Zhang, G.; Li, W.; Yang, C.; Sun, R., Temporary Bonding and Debonding in Advanced Packaging: Recent Progress and Applications. *Electronics* 2023, 12 (7), 1666.
5. Huang, D.; Liu, J.; Li, J.; Wang, F.; Li, K.; Liu, Q.; Yin, H.; Zhang, G.; Sun, R., Controlled Thermal Imidization of Thermoplastic Polyimide for Temporary Bonding and Debonding in Advanced Packages. *ACS Applied Polymer Materials* 2022, 4 (11), 8508-8519.
6. Hermanowski, J. In Thin wafer handling — Study of temporary wafer bonding materials and processes, 2009 IEEE International Conference on 3D System Integration, 28-30 Sept. 2009; 2009; pp 1-5.
7. Hashiguchi, H.; Fukushima, T.; Murugesan, M.; Kino, H.; Tanaka, T.; Koyanagi, M., High-Thermoresistant Temporary Bonding Technology for Multichip-to-Wafer 3-D Integration With Via-Last TSVs. *IEEE Transactions on Components, Packaging and Manufacturing Technology* 2019, 9 (1), 181-188.
8. Lee, S.-W.; Lee, T.-H.; Park, J.-W.; Park, C.-H.; Kim, H.-J.; Kim, S.-M.; Lee, S.-H.; Song, J.-Y.; Lee, J.-H., The effect of laser irradiation on peel strength of temporary adhesives for wafer bonding. *International Journal of Adhesion and Adhesives* 2015, 57, 9-12.
9. June, S. M.; Suga, T.; Heath, W. H.; Long, T. E.; Lin, Q.; Puligadda, R., Photo-Reactive Polyimides and Poly(siloxane imide)s as Reversible Polymeric Interfaces. *The Journal of Adhesion* 2010, 86 (10), 1012-1028.
10. Moore, J. A.; Dasheff, A. N., An intrinsically photosensitive polyimide. *Chemistry of Materials* 1989, 1 (1), 163-166.

11. Hergenrother, P., The Use, design, synthesis, and properties of high performance/high temperature polymers: An overview, high perform. High Performance Polymers 2003, 15, 3-45.
12. Moyer, E. S.; Mohanty, D. K.; Shaw, J.; McGrath, J. E. In Synthesis and characterization of soluble photoimageable polyimide and poly(imide siloxane) homo- and copolymers, International SAMPE Symposium and Exhibition (Proceedings), 1989; pp 894-904.
13. Decker, C.; Bianchi, C.; Jönsson, S., Light-induced crosslinking polymerization of a novel N-substituted bis-maleimide monomer. Polymer 2004, 45 (17), 5803-5811.
14. Kang, M.; Moon, B., Synthesis of Photocleavable Poly(styrene-block-ethylene oxide) and Its Self-Assembly into Nanoporous Thin Films. Macromolecules 2009, 42 (1), 455-458.
15. Piggott, A. M.; Karuso, P., Synthesis of a new hydrophilic o-nitrobenzyl photocleavable linker suitable for use in chemical proteomics. Tetrahedron Letters 2005, 46 (47), 8241-8244.
16. Suzuki, H.; Abe, T.; Takaishi, K.; Narita, M.; Hamada, F., The synthesis and X-ray structure of 1,2,3,4-cyclobutane tetracarboxylic dianhydride and the preparation of a new type of polyimide showing excellent transparency and heat resistance. Journal of Polymer Science Part A: Polymer Chemistry 2000, 38 (1), 108-116.
17. Trenor, S. R.; Shultz, A. R.; Love, B. J.; Long, T. E., Coumarins in Polymers: From Light Harvesting to Photo-Cross-Linkable Tissue Scaffolds. Chemical Reviews 2004, 104 (6), 3059-3078.
18. Trenor, S. R.; Long, T. E.; Love, B. J., Photoreversible Chain Extension of Poly(ethylene glycol). Macromolecular Chemistry and Physics 2004, 205 (6), 715-723.
19. Hughes, T.; Simon, G. P.; Saito, K., Chemistries and capabilities of photo-formable and photoreversible crosslinked polymer networks. Materials Horizons 2019, 6 (9), 1762-1773.
20. Lentin, I.; Gorbunov, A.; Bezzubov, S.; Nosova, V.; Cheshkov, D.; Kovalev, V.; Vatsouro, I., Shrinkable/stretchable bis(calix[4]arenes) comprising photoreactive azobenzene or stilbene linkers. Organic Chemistry Frontiers 2023, 10 (6), 1470-1484.
21. Ichimura, K.; Akita, Y.; Akiyama, H.; Kudo, K.; Hayashi, Y., Photoreactivity of Polymers with Regioisomeric Cinnamate Side Chains and Their Ability To Regulate Liquid Crystal Alignment. Macromolecules 1997, 30 (4), 903-911.
22. Kaur, G.; Johnston, P.; Saito, K., Photo-reversible dimerisation reactions and their applications in polymeric systems. Polymer Chemistry 2014, 5 (7), 2171-2186.

23. Dennis, J. M.; Fahs, G. B.; Moore, R. B.; Turner, S. R.; Long, T. E., Synthesis and Characterization of Polysulfone-Containing Poly(butylene terephthalate) Segmented Block Copolymers. *Macromolecules* 2014, 47 (23), 8171-8177.
24. Sardon, H.; Pascual, A.; Mecerreyes, D.; Taton, D.; Cramail, H.; Hedrick, J. L., Synthesis of Polyurethanes Using Organocatalysis: A Perspective. *Macromolecules* 2015, 48 (10), 3153-3165.
25. Weyhrich, C.; Will, J.; Heifferon, K.; Brown, J.; Arrington, C.; Meenakshisundaram, V.; Williams, C.; Long, T., 3D-Printing of Poly(arylene ether sulfone)s: Functional High-Performance Polymers for Vat Photopolymerization. *Macromolecular Chemistry and Physics* 2022, 224.
26. Aneja, A.; Wilkes, G. L., A systematic series of 'model' PTMO based segmented polyurethanes reinvestigated using atomic force microscopy. *Polymer* 2003, 44 (23), 7221-7228.
27. Yilgör, I.; Yilgör, E.; Wilkes, G. L., Critical parameters in designing segmented polyurethanes and their effect on morphology and properties: A comprehensive review. *Polymer* 2015, 58, A1-A36.
28. Beniah, G.; Fortman, D. J.; Heath, W. H.; Dichtel, W. R.; Torkelson, J. M., Non-Isocyanate Polyurethane Thermoplastic Elastomer: Amide-Based Chain Extender Yields Enhanced Nanophase Separation and Properties in Polyhydroxyurethane. *Macromolecules* 2017, 50 (11), 4425-4434.
29. Cheng, B.-X.; Gao, W.-C.; Ren, X.-M.; Ouyang, X.-Y.; Zhao, Y.; Zhao, H.; Wu, W.; Huang, C.-X.; Liu, Y.; Liu, X.-Y.; Li, H.-N.; Li, R. K. Y., A review of microphase separation of polyurethane: Characterization and applications. *Polymer Testing* 2022, 107, 107489.

Chapter 8

1. Deberdeev, T. R.; Akhmetshina, A. I.; Karimova, L. K.; Ignat'eva, E. K.; Galikhmanov, N. R.; Grishin, S. V.; Berlin, A. A.; Deberdeev, R. Y., Aromatic Polysulfones: Strategies of Synthesis, Properties, and Application. *Polymer Science, Series D* 2020, 13 (3), 320-328.
2. Serbanescu, O. S.; Voicu, S. I.; Thakur, V. K., Polysulfone functionalized membranes: Properties and challenges. *Materials Today Chemistry* 2020, 17, 100302.
3. Tan, X.; Rodrigue, D., A Review on Porous Polymeric Membrane Preparation. Part I: Production Techniques with Polysulfone and Poly (Vinylidene Fluoride). *Polymers* 2019, 11 (7), 1160.

4. Abdelrasoul, A.; Doan, H.; Lohi, A.; Cheng, C.-H., Morphology Control of Polysulfone Membranes in Filtration Processes: a Critical Review. *ChemBioEng Reviews* 2015, 2 (1), 22-43.
5. Kheirieh, S.; Asghari, M.; Afsari, M., Application and modification of polysulfone membranes. *Reviews in Chemical Engineering* 2018, 34 (5), 657-693.
6. Chen, Y.; Lin, B.; Qiu, Y., Modification of polysulfone and the biomedical application of modified polysulfone. *International Journal of Polymeric Materials and Polymeric Biomaterials* 2023, 72 (3), 224-242.
7. Hoseinpour, V.; Noori, L.; Mahmoodpour, S.; Shariatnia, Z., A review on surface modification methods of poly(arylsulfone) membranes for biomedical applications. *Journal of Biomaterials Science, Polymer Edition* 2021, 32 (7), 906-965.
8. Yu, L.; Zhao, D.; Wang, W., Mechanical properties and long-term durability of recycled polysulfone plastic. *Waste Management* 2019, 84, 402-412.
9. Andrady, A. L.; Neal, M. A., Applications and societal benefits of plastics. *Philos Trans R Soc Lond B Biol Sci* 2009, 364 (1526), 1977-84.
10. Hergenrother, P., The Use, design, synthesis, and properties of high performance/high temperature polymers: An overview, high perform. *High Performance Polymers* 2003, 15, 3-45.
11. Weyhrich, C.; Will, J.; Heifferon, K.; Brown, J.; Arrington, C.; Meenakshisundaram, V.; Williams, C.; Long, T., 3D-Printing of Poly(arylene ether sulfone)s: Functional High-Performance Polymers for Vat Photopolymerization. *Macromolecular Chemistry and Physics* 2022, 224.
12. Warner, M. J.; Lassa, J. P.; Narcross, H.; Commisso, A.; Ghosh, K.; Romero, M.; Schwartz, J. M.; Engler, A. C.; Kohl, P. A.; Leguizamon, S. C.; Jones, B. H., Chemical Recycling of Polybutadiene Rubber with Tailored Depolymerization Enabled by Microencapsulated Metathesis Catalysts. *ACS Sustainable Chemistry & Engineering* 2023, 11 (39), 14538-14548.
13. Davydovich, O.; Greenlee, A. J.; Root, H. D.; Jansen, A. L.; Gallegos, S. C.; Warner, M. J.; Kent, M. S.; Cardenas, J. A.; Appelhans, L. N.; Roach, D. J.; Jones, B. H.; Leguizamon, S. C., Encapsulated Transition Metal Catalysts Enable Long-term Stability in Frontal Polymerization Resins. *Macromolecules* 2023, 56 (18), 7543-7550.
14. Yoon, T. P.; Ischay, M. A.; Du, J., Visible light photocatalysis as a greener approach to photochemical synthesis. *Nature Chemistry* 2010, 2 (7), 527-532.
15. Moreau, W. M., *Semiconductor Lithography: Principles, Practices, and Materials*. Springer US: 2012.

16. Costner, E. A.; Lin, M. W.; Jen, W.-L.; Willson, C. G., Nanoimprint Lithography Materials Development for Semiconductor Device Fabrication. *Annual Review of Materials Research* 2009, 39 (1), 155-180.
17. Lin, B.-J., Immersion lithography and its impact on semiconductor manufacturing. *Journal of Micro/Nanolithography, MEMS, and MOEMS* 2004, 3 (3).
18. Haq, J.; Vogt, B. D.; Howard, E.; Loy, D., Temporary bond—debond technology for high-performance transistors on flexible substrates. *Journal of the Society for Information Display* 2010, 18 (11), 884-891.
19. Ober, C. K.; Käfer, F.; Yuan, C., Recent developments in photoresists for extreme-ultraviolet lithography. *Polymer* 2023, 280, 126020.
20. Hughes, T.; Simon, G. P.; Saito, K., Chemistries and capabilities of photoformable and photoreversible crosslinked polymer networks. *Materials Horizons* 2019, 6 (9), 1762-1773.
21. June, S. M.; Suga, T.; Heath, W. H.; Long, T. E.; Lin, Q.; Puligadda, R., Photo-Reactive Polyimides and Poly(siloxane imide)s as Reversible Polymeric Interfaces. *The Journal of Adhesion* 2010, 86 (10), 1012-1028.
22. Moore, J. A.; Dasheff, A. N., An intrinsically photosensitive polyimide. *Chemistry of Materials* 1989, 1 (1), 163-166.
23. Dennis, J. M.; Fahs, G. B.; Moore, R. B.; Turner, S. R.; Long, T. E., Synthesis and Characterization of Polysulfone-Containing Poly(butylene terephthalate) Segmented Block Copolymers. *Macromolecules* 2014, 47 (23), 8171-8177.
24. Dennis, J. M.; Fahs, G. B.; Moon, N. G.; Mondschein, R. J.; Moore, R. B.; Wilkes, G. L.; Long, T. E., Synthesis of Polysulfone-Containing Poly(butylene terephthalate) Segmented Block Copolymers: Influence of Segment Length on Thermomechanical Performance. *Macromolecules* 2017, 50 (13), 5107-5113.
25. Coleman, M. M., *Fundamentals of Polymer Science: An Introductory Text*, Second Edition. CRC Press: 2019.
26. Yang, H.; Wu, X.; Li, S., A compatibilizer for a blend of polysulfone with a liquid crystalline polyester. *Polymer Engineering & Science* 1996, 36 (22), 2781-2784.
27. Shaw, M. T.; Miller, J. C., The rheology of polysulfone. *Polymer Engineering & Science* 1978, 18 (5), 372-377.

28. Yamashita, T.; Tomitaka, H.; Kudo, T.; Horie, K.; Mita, I., Degradation of sulfur-containing aromatic polymers: Photodegradation of polyethersulfone and polysulfone. *Polymer Degradation and Stability* **1993**, *39* (1), 47-54.

Chapter 9

1. Sintas, J. I.; Wolfgang, J. D.; Long, T. E., Carbamate thermal decarboxylation for the design of non-isocyanate polyurethane foams. *Polymer Chemistry* **2023**.
2. Wolfgang, J. D.; White, B. T.; Long, T. E., Non-isocyanate Polyurethanes from 1,1'-Carbonyldiimidazole: A Polycondensation Approach. *Macromolecular Rapid Communications* **2021**, *42* (13), 2100163.
3. Dounis, D. V.; Wilkes, G. L., Structure-property relationships of flexible polyurethane foams. *Polymer* **1997**, *38* (11), 2819-2828.
4. Moreland, J. C.; Wilkes, G. L.; Turner, R. B., Viscoelastic behavior of flexible slabstock polyurethane foam as a function of temperature and relative humidity. II. Compressive creep behavior. *Journal of Applied Polymer Science* **1994**, *52* (4), 569-576.
5. Delebecq, E.; Pascault, J.-P.; Boutevin, B.; Ganachaud, F., On the Versatility of Urethane/Urea Bonds: Reversibility, Blocked Isocyanate, and Non-isocyanate Polyurethane. *Chemical Reviews* **2013**, *113* (1), 80-118.
6. Miranda, I.; Souza, A.; Sousa, P.; Ribeiro, J.; Castanheira, E. M. S.; Lima, R.; Minas, G., Properties and Applications of PDMS for Biomedical Engineering: A Review. *Journal of Functional Biomaterials* **2022**, *13* (1), 2.
7. Eduok, U.; Faye, O.; Szpunar, J., Recent developments and applications of protective silicone coatings: A review of PDMS functional materials. *Progress in Organic Coatings* **2017**, *111*, 124-163.
8. Ji, X.; Wang, H.; Ma, X.; Hou, C.; Ma, G., Progress in polydimethylsiloxane-modified waterborne polyurethanes. *RSC Advances* **2017**, *7* (54), 34086-34095.
9. Volkov, A., Polydimethylsiloxane (PDMS). In *Encyclopedia of Membranes*, Drioli, E.; Giorno, L., Eds. Springer Berlin Heidelberg: Berlin, Heidelberg, 2015; pp 1-2.
10. Coleman, M. M., *Fundamentals of Polymer Science: An Introductory Text, Second Edition*. CRC Press: 2019.
11. Iqbal, N.; Sharma, P. K.; Kumar, D.; Roy, P. K., Protective polyurea coatings for enhanced blast survivability of concrete. *Construction and Building Materials* **2018**, *175*, 682-690.

12. Chattopadhyay, D. K.; Raju, K. V. S. N., Structural engineering of polyurethane coatings for high performance applications. *Progress in Polymer Science* **2007**, *32* (3), 352-418.
13. Allen, R. D.; James, M. I., Chemical Recycling of PET. In *Circular Economy of Polymers: Topics in Recycling Technologies*, American Chemical Society: 2021; Vol. 1391, pp 61-80.
14. Vilela, C.; Sousa, A. F.; Fonseca, A. C.; Serra, A. C.; Coelho, J. F. J.; Freire, C. S. R.; Silvestre, A. J. D., The quest for sustainable polyesters – insights into the future. *Polymer Chemistry* **2014**, *5* (9), 3119-3141.
15. Ikada, Y.; Tsuji, H., Biodegradable polyesters for medical and ecological applications. *Macromolecular Rapid Communications* **2000**, *21* (3), 117-132.
16. June, S. M.; Suga, T.; Heath, W. H.; Long, T. E.; Lin, Q.; Puligadda, R., Photo-Reactive Polyimides and Poly(siloxane imide)s as Reversible Polymeric Interfaces. *The Journal of Adhesion* **2010**, *86* (10), 1012-1028.
17. Trenor, S. R.; Long, T. E.; Love, B. J., Photoreversible Chain Extension of Poly(ethylene glycol). *Macromolecular Chemistry and Physics* **2004**, *205* (6), 715-723.
18. Trenor, S. R.; Long, T. E.; Love, B. J., Development of a Light-Deactivatable PSA Via Photodimerization. *The Journal of Adhesion* **2005**, *81* (2), 213-229.
19. Palmans, A. R. A.; Smith, P.; Weder, C., Polarizing Energy Transfer in Photoluminescent Conjugated Polymers with Covalently Attached Sensitizers. *Macromolecules* **1999**, *32* (14), 4677-4685.
20. Trenor, S. R.; Shultz, A. R.; Love, B. J.; Long, T. E., Coumarins in Polymers: From Light Harvesting to Photo-Cross-Linkable Tissue Scaffolds. *Chemical Reviews* **2004**, *104* (6), 3059-3078.
21. Dennis, J. M.; Fahs, G. B.; Moore, R. B.; Turner, S. R.; Long, T. E., Synthesis and Characterization of Polysulfone-Containing Poly(butylene terephthalate) Segmented Block Copolymers. *Macromolecules* **2014**, *47* (23), 8171-8177.
22. Boga, K.; Patti, A. F.; Warner, J. C.; Simon, G. P.; Saito, K., Eco-Friendly Photoreversible Adhesives Derived from Coumarin-Functionalized Epoxy Soybean Oil. *ACS Applied Polymer Materials* **2023**, *5* (7), 4644-4653.
23. Hohl, D. K.; Weder, C., (De)bonding on Demand with Optically Switchable Adhesives. *Advanced Optical Materials* **2019**, *7* (16), 1900230.

24. Takahashi, H.; Sakuragi, M.; Hasegawa, M.; Takahashi, H., Photodegradable polyamides. *Journal of Polymer Science Part A-1: Polymer Chemistry* **1972**, *10* (5), 1399-1409.

APPENDIX A

PUBLISHED PORTIONS OF THIS DISSERTATION

Portions of the data presented in this dissertation have been previously published, submitted for publication, or will be submitted for publication in the following journals. The published materials were included with permission from all co-authors.

CHAPTER 3

Sintas, J. I.; Wolfgang, J. D.; Long, T. E., Carbamate thermal decarboxylation for the design of non-isocyanate polyurethane foams. *Polymer Chemistry* **2023**, *14* (13), 1497-1506.

CHAPTER 4

Sintas, J. I.; Bean, R. H.; Zhang, R.; Long, T. E., Non-Isocyanate Polyurethane Segmented Copolymers from Bis-Carbonylimidazolides. *Macromolecular Rapid Communications*. **2024** (Submitted Feb 2024)

CHAPTER 5

Sintas, J. I.; White, T. B.; Grim, B. J.; Green M. D.; Long, T. E., Divalent Imidazolium Ionic Liquids from Bis-Carbonylimidazolidone Monomers. (Planned for 2024 submission)

APPENDIX B

PERMISSIONS

Figure 2.2 and 2.3 reprinted from Ulbricht, J.; Jordan, R.; Luxenhofer, R., On the biodegradability of polyethylene glycol, polypeptoids and poly(2-oxazoline)s.

Biomaterials **2014**, *35* (17), 4848-4861. With permission from Elsevier.

Figure 2.4 reprinted from Zander, Z. K.; Becker, M. L., Antimicrobial and Antifouling Strategies for Polymeric Medical Devices. *ACS Macro Letters* **2018**, *7* (1), 16-25. With permission from American Chemical Society

Figure 2.5 reprinted from Dakkak, Y.; Janane, A.; Ould-Ismail, T.; Ghadouane, M.; Ameer, A.; Abbar, M., Management of encrusted ureteral stents. *African Journal of Urology* **2012**, *18* (3), 131-134. With permission from Elsevier under a creative common license.